

POLITECNICO DI MILANO

Scuola di Ingegneria Industriale e dell'Informazione

Corso di Laurea Magistrale in
Mechanical Engineering



**Human-Structure Interaction:
three approaches to account for the presence of moving
pedestrians for the estimation of the vibration levels**

Supervisor: Prof. Stefano Manzoni

Advisors: Ing. Marta Berardengo

Prof. Marcello Vanali

Degree Thesis of:

Loris Drago Matr. 836847

Academic Year 2015/2016

Acknowledgments

I would like to thank the campus of Lecco of Politecnico di Milano, which have helped in the realization of a fundamental measurement step of this research project.

Index

Chapter 1 Introduction to Human-Structure Interaction.....	1
1.1 State of Art	1
1.1.1 Literature Review	2
1.1.2 Lateral Vibration	3
1.1.3 Parametric Study	3
1.1.4 Guidelines.....	3
1.1.5 Comparison of Base Models	7
1.1.6 Posture & Degrees of Freedoms.....	8
1.1.7 Other Modeling Approaches	9
1.2 Previous Contributions.....	9
1.2.1 Passive People Effect	9
1.2.2 Active Pedestrian Effect.....	12
Chapter 2 Modeling of HSI	15
2.1 Pedestrian Interaction.....	15
2.1.1 Pedestrian Description.....	16
2.2 Background of the Models	20
2.3 Model 1	21
2.3.1 Single Pedestrian–1DOF Structure	21
2.3.2 Multi Pedestrians-Multi DOF Structure	24
2.3.3 Apparent Mass.....	29
2.3.4 Active Force	30
2.4 Model 2	31
2.4.1 Overlap Study.....	32
2.4.2 Apparent Mass.....	33
2.4.3 Active Force	34
2.4.4 Mathematical Model	34
2.5 Model 3	36
Chapter 3 Inputs to the Models: Experiments & Discussion	39
3.1 Active Force Experiments.....	39
3.1.1 Experimental Set-up.....	40
3.1.2 Tests	41
3.1.3 Results	41
3.2 Passive Force Experiments.....	43
3.2.1 2DOF Transfer Function	44
3.2.2 Experimental Set-Up	47
3.2.3 Tests	48
3.2.4 Apparent Mass Curves	51
3.3 Structural Modal Analysis.....	60

3.3.1 Description of the Structure.....	60
3.3.2 Discretization of the structure.....	61
3.3.3 Structure Analysis.....	62
3.3.4 Post-Processing.....	64
Chapter 4 Numerical Simulations & Experimental Campaign.....	67
4.1 Numerical Simulations	69
4.1.1 Input Data	69
4.1.2 Working Principle.....	69
4.1.3 Number of Simulations & Computational Effort.....	72
4.1.4 Simulations	73
4.1.5 Post-Processing.....	73
4.2 Experimental Campaign	83
Chapter 5 Results & Discussion	89
5.1 Summary Tables	91
5.2 Whole Results.....	95
5.3 Other Tests.....	127
5.4 Summary Tables (Mode Filtered Results).....	135
5.5 Frequency Response Functions (FRFs)	138
Chapter 6 Conclusions.....	145

Introduction

“Prevention is better than cure”, this statement could be applied in many fields, but none of them can be considered as expensive as the building one. Not only for the costs of the structure itself, but also for the post-built in adjustments. Indeed, in presence of a low stiff structure, due to its material and/or geometry, it is nowadays common practice the addition of Tuned-Mass-Dampers (TMD) after the construction, for serviceability reasons. Their implementation requires a deep analysis of the completed structure, leading to consistent additional costs. This procedure is not always a choice, but, sometimes, it is necessary. One of the most unpleasant case is the closure of the London Millennium Bridge, during its opening, due to an unexpected lively dynamic behaviour. Countermeasures required almost a year of study and additional costs of 5 million pounds. It wasn't a design error due to a mere account, but it was a design error due to a deep lack of knowledge concerning the interaction between Humans and Structure. Since that moment, engineers have definitely acknowledged the Human-Structure-Interaction (HSI) as a serious problem to be addressed urgently.

This work proposes a contribution to the HSI modelization, as a pursuance of previous works [1,2], by means of the development, application and validation of three new HSI Models. In the first one, Model 1, a local modelization of the pedestrian, with respect to his/her position on the structure, is adopted. This represents a great improvement, if compared with the approach adopted by the previous work [2]. As for Model 2 and 3, in each of them a different additional complexity is treated and modeled, for a more detailed description of the HSI, starting by Model 1 as background. An experimental campaign was performed to acquire a series of pedestrian information required to correctly replicate the people and their effects on the occupied structure. Not only, also the structure must to be analysed (a staircase was taken as reference), to properly reproduce it during the numerical application of the Models too. Finally, a series of different HSI scenarios were reproduced both numerically and experimentally, in order to validate the Models. The pedestrian situations were thought to test different aspects of the Models and so to assess their behavior, through the vibration levels estimated by each of them. The experimental tests were performed with the cooperation of five subjects, the same ones for which the pedestrian parameters were acquired, over the aforementioned staircase.

The aim was to verify if a more realistic representation of the pedestrians-structure coupling (i.e. HSI), and so a greater complexity involved, could produce significant improvement in the estimation of the serviceability of the structure. This, through a correct prediction of the vibration levels undertaken by the structure itself.

At first, in Chapter 1, the topic is introduced by the State of Art about the HSI, and a short presentation of the previous contribution to the HSI modeling is presented as well. In Chapter 2, a deep description of the three advanced Models, along with an explanation of their working principle, is reported. Instead, a description of the procedures used for the experimental acquisition of the necessary pedestrian information and their storage in databases, followed by the Experimental Modal Analysis of the structure, is illustrated in Chapter 3. Then, in Chapter 4, the application of the proposed Models, for the numerical simulation of the scheduled pedestrian scenarios, and the post-processing analysis of the simulation results are explained.

They are followed by the description of the experimental campaign of the scheduled pedestrian scenarios. Finally, in Chapter 5, all the results obtained by the experimental and numerical simulations of each tested pedestrian scenario are reported, and conclusions about the performed work are drawn.

Chapter 1

Introduction to

Human-Structure Interaction

1.1 State of Art

In the last decades, engineering experience and knowledge, allied with the use of newly developed materials and technologies, have allowed to build up always more complex structures. Of these, pedestrian infrastructures, like footbridges, resulted in slender, longer and lighter configurations. The con was that in this way, also small exiting components, like pedestrian walking action, were found to be able to make the structure dynamically respond. Even if such response most of the time doesn't involve structural failures, an unsustainable vibration level for the human being sensibility was observed. In response to the issue, design criteria started to account for the problem. Historically, the British Standard BS 5400 [3] was the first code that, more than 35 years ago, was concerned to footbridge vibration problem. Despite it was followed by others, this wasn't enough to fix the matter. Indeed a number of problems with vibration serviceability continued to be reported. None of them as widely discussed as the closures of both the Pont de Solferino bridge in Paris in 1999 (Sétra [4]) and then the London Millennium Bridge in 2000 (Dallard et al. [5]), during their inaugurations. This last can be consider as the most prominent case, which once and for all drew the scientific attention on the infrastructural problem.

The vibration serviceability issue doesn't refer only to "small" structures, but also to huge ones. Indeed, different publications dealt with buildings and structures for public events. For example, Reynolds et al. [6] monitored the vibration response of a stadium. The observations were made when the structure was empty, and in the meanwhile of different events/activities. For the occupied stadium, the modal properties were extracted, and the configurations of the crowd were monitored by correlating vibration response data with synchronised video images. The observations showed that seated crowd led to a decrease in natural frequencies and an increase in damping ratios. Further decreases in natural frequencies were observed when the crowd stood and/or jumped, highlighting in this way the influence of different postures.

As just introduced, another important matter in the field of the HSI is the position/activity performed by the crowd that occupied the structure. This is due to a change of stiffness and damping of the human contribution as a function of the posture. Therefore, great attention was and is paid to the body configuration in the different analysed scenarios. A contribution in this direction was carried out by Van Nimmen et al. [7]. In her work, the dynamical characteristics of people in the normal standing, two legs bent postures and postures corresponding to the single and double stance

phase of the walking cycle were identified experimentally and compared with other researches. An experimental study on a footbridge in laboratory conditions showed a decrease of the natural frequencies and an increase in structural damping. Similar observations were obtained on an in situ footbridge analysis. A simulation stage was then performed in which the human occupants were represented by Single Degree Of Freedom (SDOF) systems, since the body response, at low frequencies, was found well approximated by a highly damped SDOF system. Such human-bridge model was able to predict the experimentally identified dynamic behaviour of the occupied structure.

In the following, a literature review is presented. At first, a gathering of the publications of the last years are reported, to provide some of the most comprehensive references. Then, a series of paragraphs to illustrate the main aspects of the Human-Structure Interaction (HSI) problem are introduced: (i) the lateral vibration interaction issue, since it was the first direction of interaction to be deeply studied, as it was discovered to be the main responsible for the London Millennium Bridge troubles; (ii) the first studies based on parametric analyses, which tried to connect the multiple variables involved in the HSI with the observed structural behaviours, to show how little it was understood until the beginning of the 2000; (iii) the discussion on the design guidelines suggested by the regulations and (iv) a comparison of the simplest models utilized to reproduce the human-structure interaction. Finally, the study of the human's apparent mass, with its usual (v) and unusual (vi) approaches to account for it, are treated.

1.1.1 Literature Review

As a new phenomenon to be studied, the publication on the topic have been several, with different approaches and methodologies. Some well-made literature reviews, which can be useful to have a whole view on the research already done in this field, are presented by Sachse et al. [8], Zivanovic et al.[9] and Racic et al. [10].

Sachse et al. [8], in 2003, released a literature review, with more than 130 pieces, concerning the problem of Human-Structure dynamic Interaction applied to the design of civil engineering structures. Firstly, the paper dealt with how structural movement affects human induced dynamic forces, and then, how humans change the dynamic properties of structure they occupy. The literature dealing with the first aspect was found quite limited. Several Single Degree Of Freedom models of standing people were discovered. However, all these models were found based on unwarranted assumptions in respect to damping and/or the lumped mass of the occupant model. Furthermore, the experimental data used to derive the properties of human occupant models were declared often incomplete and unreliable.

In 2005, Zivanovic et al. [9] published a review of about 200 references, referred to the vibration serviceability of footbridges under human-induced excitation. The sources of vibration, mechanical parameters of the footbridges and the receiver of the vibrations, the pedestrian, were the main key points. From it was concluded that the influence of walking people on footbridge vibration properties, such as the natural frequencies and damping, was not well understood, let alone quantified. In fact, a single national or international design guidance, which covers all the aspects of the problem, was not found. The authors ended stating: *"the overdue update of the current codes will be a great challenge for the next 10 years"*.

A great comprehensive review of publications up to 2009, with 270 references dealing with different experimental and analytical characterizations of human walking load, was presented by Racic et al. [10]. Basing on the review, the authors provided a consistent background and indicated the major gaps for future researches. More than the traditional force measurements utilizing a force plate, methods were introduced for indirect measurement of time-varying records via combination of visual motion tracking and known body mass distribution. A considerable uncertainty about how

structural vibrations modify walking, and hence affect the pedestrian-induced forces, was underlined as a main challenge.

1.1.2 Lateral Vibration

Since the most significant event of this topic (the aforementioned London Millennium Bridge in 2000) was discovered to be caused by a non-linear interaction between pedestrians and lateral vibrations, at this specific vibration direction was dedicated most of the initial literature. Here, two different approaches to the study of the problem, which was advanced in the past years, are reported.

Venuti et al. [11] proposed a mathematical model and a computational approach to study the interaction between the lateral vibrations of footbridges and the pedestrians who walk on them. The method is based on the decomposition of the coupled system into two subsystems and on the interaction between them. In particular, the dynamics of the crowd was modelled in analogy to a compressible flow. However, the model was tested with a lack of experimental data, therefore it was used only to qualitative considerations.

The other completely different approach reported is the one of Ingólfsson et al. [12]. A stochastic load model was used from them to model the frequency and amplitude dependency of the pedestrian-induced lateral forces. It was made by the sum of the “simple” lateral induced force and the ones due to the interaction with the structure, which were quantified through equivalent pedestrian damping and mass coefficients. The selection of parameters was shown affects the critical number of pedestrians needed to trigger excessive lateral vibrations.

1.1.3 Parametric Study

To approach the Human-Structure Interaction problem, parametric studies were also conducted. Such methodology is generally chosen to handle a problem that is again at its initial understanding, to help to highlight the main correlations among the inputs and the outputs of the studied phenomenon. In this perspective, two valid works which bring their contribution at five years of the new millennium are reported.

Sachse et al. [13] attempted to explain observed changes in modal characteristics made by other researchers, when the considered structures were occupied by people. Natural frequencies, mode shapes, modal masses and damping ratios were examined parametrically for ranges of mass, stiffness and damping coefficients of two SDOF systems connected in series. One SDOF represents a pedestrian and the other one the relevant mode of the empty structure. It was found that such a model can explain (1) the damping increase, (2) additional modes and (3) the increases as well as the decreases of natural frequencies as a function of resonant frequency considered, high and low respectively.

Alexander [14] advanced a theoretical treatment for the modeling of the crowd-structure interaction. The model was built up in plane, with a continuous crowd mass spread over the structure. Using a mathematical approach, each mode of the structure was done interact with the corresponding crowd mode only. This allowed to treat the problem as a series of 2 Degrees Of Freedom (2DOF) systems, one per mode. Given the uncertainty in the values of biomechanical and structural parameters, an extensive parametric study was conducted. As a result, a series of loci plots were obtained. From them, a set of crucial parameters was showed exist, at which a sudden drop in natural frequencies, for small increase in crowd mass, takes place.

1.1.4 Guidelines

Although along the time different regulations were set by authorities, in order to account for Human-Structure Interaction during the design stage of new structures, these guidelines were and

are discussed by a lot of authors. The contestations are due to the type of models used, which are considered as non-physically representative of the phenomena considered. Consequent incorrect vibration levels are estimated. To find more reliable approaches, a lot of publications compare new ideas with the in-force regulations.

Figueiredo et al. [15], with the purpose to obtain a reliable model for the dynamic behavior of composite footbridges (i.e. concrete slab laid on a steel truss structure), performed extensive parametric studies on eleven one-span structures. Four different load models were considered to incorporate the dynamical effects induced by people walking. In the first one, only the Fourier's harmonic of the pedestrian walking load that matched the first natural frequency of the structure was applied. In the second one, the individual weight and the first fourth harmonics of the Fourier series of the walking load was used, with always one matching resonant condition. The first two models were applied at the midspan of the footbridges. The third model was set equal to the second, with the difference that the dynamical load position was changed accordingly to the individual position. A number of six forces to model one single step were set and applied accordingly in time and space. To obtain the fourth walking load model, the human heel effect was added to the third model. To do that, a modified Fourier series, to incorporate the heel impact effect, was adopted. A parametric analysis considering footbridge span variation was conducted. The structure model was made with three-dimensional beam elements, for the steel girders, and shell elements, for the concrete slab. The footbridge maximum acceleration values were calculated for the four load models and compared with the American Institute of Steel Construction (AISC) [16] regulation and the ISO 2631-2 [17]. The acceleration peak values showed that the load model II produces acceleration values always higher than load model I, underling the effect of the load harmonic components. Even more high values were observed with the load models III and IV. This fact emphasizes that when the individual position is changed, there is a substantial increase in the structure dynamical response. As result, the acceleration peaks of the load model III and IV crossed the AISC [16] and ISO [17] limit values. Whereby, the authors [15] stated that the actuals design standards could produce unsafe threshold values, since they are based on excessively simplified load models.

Also Setarh et al. [18] analysed the effect of walking force models coming from widely used sources, applied on a long-cantilevered building structures. It was made by a 34 m long steel trusses part, cantilevered from a concrete core. The walking tests were conducted by the same male individual, walking along corridors which cover the length of the structure. To measure the response, accelerometers were placed at the extremity of the cantilever. By using a metronome to synchronize the steps, the individual walked at the first three measured resonance frequencies. A computer model of the structure was created and updated by the modal test results. Also for the simulations, only walking at the first three modes were considered. Six walking forces were used. Four Fourier series based models, since they were/are generally adopted, taking the Dynamic Load Factors (DLF) from sources (Bachmann et al. [19], Smith et al. [20], ISO 10137 [21], Murray et al. [16]). Plus, other two measured walking force functions were used, as they were recommended by Bachmann et al. [19] and by Khoncarly [22]. These last two were used to find the best representative step force way. To do that, numerical and measured accelerance FRFs were computed and compared per mode. By using their ratio, the first harmonics of the forcing functions were adjusted. The subsequent application of these two walking force functions were made by applying each step at the corresponding time and location, with the appropriate overlap time, with the three resonant step frequencies in turn. Discrepancies with the used of the Fourier series models were reported. In most cases an overestimation, while in a few cases an underestimated. A good match was observed for the measured force functions after the adjustments. The explanation proposed by the authors [18] involved the fact that the Fourier series-based force functions were applied on the model by using the combination of the two steps at each step contact point. While using the measured force functions, the correct spatial and temporal sequence of steps was used. Hence, they concluded that

the way in which the step force functions are applied can have a large effect on the response. Also for the Fourier series based models it was proposed an adjustment, changing the DLFs. It was found that to have a good match, substantially different coefficients could be required. This depends on how the walk forcing function are applied on the structure. As last, because most design guides that use the Fourier series approach recommend to place it steadily at the most critical position, the authors compared also the response resulting from in-place marching and from walking along the cantilever. In-place marching seemed to overestimated the structural response.

Another noteworthy work, is the one conducted by Mashaly et al. [23], in which the authors used a response spectrum approach to predict the vertical acceleration peak. In it, five footbridges were taken into account. The pedestrian walking force was modelled as a Fourier series, using the first four harmonics. This was applied steadily at the midspan and as a moving walking load (case V1 and V2). A walking frequency was chosen such that it or its harmonics coincide with the bridge fundamental frequency. Two types of structural models were used. A Multi-Degrees Of Freedom (MDOF) model made by two-dimensional beam elements. The second model was a Generalized Single Degree Of Freedom (GSDOF), in which the footbridge excitation was filtered by a half sine shape function and the fundamental frequency was the same of an equivalent free bending pinned-pinned beam. The fundamental frequencies, of the five footbridges, calculated using the MDOF and the GSDOF models, were found almost identical. The maximum acceleration at midspan for each model was obtained, using also the American Institute for Steel Constructions (AISC) standards (i.e. with the Allen and Murray's equation [16]). The data showed that the accelerations obtained by the GSDOF model for load cases V1 and V2 were almost identical to the ones obtained by the MDOF model. This was attributed to the fact that the bridge dynamic response, during the resonance, was totally governed by the response of the fundamental mode. Moreover, the accelerations obtained for load case V2 were always found lower than those of load case V1. For what concern the acceleration calculated with the Allen and Murray's equation [16], it tended to be higher than the one of the V2 case, but more close to the one of the V1 case. Looking at the case V2, as opposed to V1, the acceleration response was found to increase, as the pedestrian walked closer to the midspan, and then to decrease, as he walked away from the midspan. Going forward, to study the effect of the bridge dynamic properties on the vibration response, the peak value of a response quantity, as a function of the natural frequency of the structure, was investigated. As response quantity was considered a pseudo force, defined as the GSDOF maximum acceleration times the GSDOF mass. In this way, all the GSDOF systems that have different masses but constant frequency and damping ratio will have the same pseudo force. The response spectra were developed for different damping ratios. This approach implies that the pedestrian dynamic load is considered stationary at the midspan of the footbridge. At the end, the GSDOF maximum acceleration was/can be calculated as the pseudo force, divided by the GSDOF mass. This equation indicates the effect induced by the mass of the footbridg, as it increases, the maximum acceleration decreases. The results showed that the response spectrum predictions were very close to those of the MDOF approach, and more accurate than the results obtained by the Allen and Murra method [16]. This capability to catch the maximum acceleration responses was attributed to the fundamental vibration mode, as main responsible of the dynamic response. Therefore, this can be assumed to be a useful tool to evaluate the maximum vibration level of a structure, as long as the structure can be approximated as a SDOF. It requires just the fundamental frequency, damping ratio and modal mass.

Instead, Van Nimmen et al. [24] evaluated the European HiVoSS [25] and the French Sétra [4] guideline, which are widely applied in practice. In them, the human induced loads by a stream of pedestrians are simplified as a uniform load applied from an equivalent number of N perfectly synchronised pedestrians. Among the parameters, a coefficient is present to account for the probability to match the frequency of the considered mode. Looking at the reference structure, the guidelines classify a footbridge based on the expected pedestrian traffic, i.e. pedestrian density.

They also suggest minimum and mean values for the damping ratio as a function of the accounted type of structure. Vibration assessment is performed by maximum acceleration level in a specific direction, which is calculated considering resonant conditions for the investigated mode. The outcomes are classified in four levels, with the corresponding comfort indexes. To test the rules, they were applied to eight footbridges, “before and after” their construction. With the information available at the design stage, the vibration assessments were carried out for different pedestrian densities. Due to the strong variations of the aforementioned coefficient, the acceleration predictions were found highly sensitive to small variations in natural frequency prediction. Hence, Van Nimmen et al. [24] pointed out that the present form of the two guidelines could be exploited by designers to pass the vibration serviceability check. Just small adjustments, to shift the predicted natural frequencies in a low value zone of such coefficient, would require. To fix this issue, the authors [24] proposed a modified coefficient to adopt in the design stage. Going forward, it was put in evidence that only the force component in the considered direction were taken into account. This would be not true if modes with significant modal displacements in more than one direction are present. A more reliable prediction was obtained by using the experimental natural frequencies and damping ratios. A deviation up to 10 % in natural frequency and a good prediction of the mode shapes were observed. Therefore, high sensitivity to small variations in the predicted natural frequencies and the corroboration for the recommended damping values were concluded for the checked guidelines.

Toso et al. [26] performed an extensive parameter study for the identification of reliable force and biodynamic walking pedestrian models, as alternatives to the ones suggested by the regulations (i.e. S etra [4], ISO 10137 [27] and Young [28]). Moreover, they compared the vibration levels reached with the comfort classes indicated from the UK-NA to ENI code [29] and the S etra guidelines [4]. Going in details, the biodynamic model was set as a SDOF system, moving along the structure, with the corresponding ground reaction force. This last was only applied on the structure, since it was obtained from walking on a rigid surface. While the force model was composed by only the ground reaction force. The biodynamic model parameters (i.e. mass, damping and stiffness) were obtained for every pedestrian by solving a system of three non-linear equations, which were the expression of the acceleration Frequency Response Function (FRF) of the SDOF model. The required information were the first three harmonics of the ground reaction force and of the acceleration at the waist level. In addition, data of pedestrians (weight, height and step frequency) were statistically processed, with correlation and regression functions, with both the biodynamic and force model parameters (mass, damping, stiffness / Dynamic Load Factors). Not only, regression functions were evaluated also for several combinations of the variables, and the best correlations were used to propose new ways to evaluate the biodynamic and force model parameters. An Artificial Neural Network (ANN) was implemented too. The proposed regression models were compared with those obtained by other authors and with the original non-linear system. Toso et al. [26] conducted the experimental stage using a prototype footbridge, subjected to three pedestrian densities. A closed walking path, in which the test subjects crossed the structure, was adopted. An accelerometer was placed at midspan. In the Finite Element Model (FEM) model, the SDOFs were placed along all the structure deck and activated/deactivated when was required to “moving” the pedestrians along the structure. The force models were moved with the SDOF one. The Correlation Vector Index (CVI) was used to indicate the degree of consistency between the experimental and numerical accelerations. It was found that the models can predict the reduction of natural frequency due to the increase of the mass, for high pedestrian densities. However, such shifts were not observed when the force-only model was used. Looking at the damping, the results from the biodynamic model showed a better match with the experiments. The authors [26] concluded claiming the better performance of the ANN, compared to the regression approach, and supporting the proposed models as a valid alternative to the viewed guidelines.

Going on, given the lack of reliable models and adequate design guidelines pertinent to vibration serviceability of light and slender structures, Venuti et al. [30] proposed a their approach to handle the problem, using as comparison some of the most relevant design guidelines, e.g. the French Sétra guideline [4], the European HIVoSS [25] and ISO 10-137 [21]. In their work, they proposed a model that comprises also crowd dynamics (positions and velocities of each pedestrian), in addition to the HSI model. Indeed, the speed of a pedestrian is modified by the interaction with neighbouring pedestrians and environment. To account for that, a frontal pedestrian field of interaction was used, which triggers an as high repulsive force as the proximity of the obstacles is. After a sensitivity analysis, executed to calibrate the input parameters of the crowd model, the crowd model was able to predict the expected decrease of speeds as the density of pedestrian increased. It is to highlight that such model was used separately from the vibration analysis, since “no experimental evidence was found that vertical structural vibration alters walking velocity of pedestrians”, stated the authors [30]. For what concern the HSI, the structure was modeled as a SDOF, representing the first mode, and moving SDOFs were used to represent the pedestrians. As a consequence, separated simulation was conducted. For what concern pedestrian mechanical parameters, they were taken from published studies, and randomly assigned during the simulations. Along with the pedestrian dynamic model, an external force was applied to the structure only. To account for the inter and intra subject variability, the vertical walking force was obtained by a stochastic generator. It was divided per pacing frequency. The key input parameters of the generator are the mean step frequency and durations of successive footfalls, which are derived from position and velocity given by the crowd model. A test stage was performed on four virtual footbridges, all of them with the same size, natural frequency, damping ratio and mode-shape, but different modal masses. Simulations with light, medium and dense pedestrian traffic were carried out on each footbridge. For each structure-density pair, the structural response was evaluated with: (i) HSI model, without the crowd dynamics; pedestrians were done walk along straight lines and equally spaced, at same velocity. (ii) Pedestrians modelled just as forces moving at the velocity obtained from the crowd model. (iii) All sub-models together. The results showed that neglecting the crowd dynamics the structural response was underestimated with respect to with it, since synchronisation of pace rate with the footbridge natural frequency couldn't take place. While neglecting the pedestrian dynamic model, the response was found 30 times higher than the one with it. This was concluded due to the damping added by the pedestrians, up to 5 % was claimed in the paper. Venuti et al. [30] analysed also the acceleration probability density function, finding the best match with a Weibull distribution. Thereby, they suggested that having a prior knowledge of daily traffic and the properties of the footbridge, the likelihood to exceed a given acceleration limit could be evaluated by means of such distribution.

1.1.5 Comparison of Base Models

In the following is reported a comparison about the most common base models utilized at the beginning of the HSI modeling. They are presented together with a critical analysis of the discrepancy of the results obtained with each of them. This useful contribution is due to Caprani et al. [31]. Indeed, after a deep literature review, the authors chose three different models to compare. The treatment was argued with a well-posed mathematical background. The pedestrian was in turn reduced to a Moving Force (MF), Moving Mass (MM) + MF and moving Spring-Mass-Damper (SMD) + MF. The pedestrian models were then extended to crowd models by superimposition. The pedestrian and force parameters were taken by the reviewed literature. The walking was described by spatially continuous footfall forces. The considered structure was an arbitrary footbridge, a pinned-pinned continuous beam, that was modelled using both modal coordinates (MA), with 10 modes, and Finite Elements (FE) method. The bridge damping ratio was taken as a constant (0.5 %) for each mode in the MA cases, and changed following the Rayleigh damping in the FE cases.

For the FE description, one-dimensional elements were used with two DOF per node, and shape functions were used to allow continuous walking. The three models were tested in different scenarios (single pedestrian, deterministic crowd, and random crowd), for both the FE and MA analyses. A noteworthy work is the tracking of the change of the dynamic properties of the structure, frequency and damping ratio, as pedestrians cross the structure. Moving forward, in the single pedestrian case the pacing frequency was taken equal to the empty bridge natural frequency. For the deterministic crowd simulation, 100 pedestrians with deterministic characteristics were generated. However, a normal distribution for pacing frequency was assumed and arrival gap of 1 m was used. In the random crowd case, 100 pedestrians were generated too, for 100 times, but using different distributions for pedestrian and walking parameters. Pedestrian arrival was considered as a Poisson process, and pedestrians with differing velocities were free to overtake each other. The differences in bridge response, among the different pedestrian models, were found to be more pronounced when subjected to crowd cases. While results from FE and MA simulations were found close. Looking at the results, the MF pedestrian model was observed overestimating the vibration response. In the MM and SMD models, the bridge frequency reached its minimum value when the pedestrian reached the midspan, while the mode damping experienced its maximum. For MM model, approximately half magnitude for the change in frequencies, and an order less with opposite sign for the damping, with respect to the SMD model, were observed. A further contribution of this work are the shapes of the change of frequency vs pedestrian density and change of damping vs pedestrian density. These two were not found uniform for the random crowd as they were for the deterministic crowd. Therefore, prediction of frequency and damping shifts, under random crowd, are not straightforward. On this, requirement of further study was stated by the authors.

1.1.6 Posture & Degrees of Freedoms

Great attention was paid to the human body mechanical schematization, in particular to its passive effect on the occupied structure. On this matter, a determinant role is played by the posture and the activity that the people undertake during the analysed case scenario. For these reasons, a lot of the published literature dealt and deal with this problem. In the following, some of the main contributions in this sense are reported.

A study conducted by Matsumoto et al. [32] was aimed to determine the influence of the posture and the vibration magnitude on the dynamic response of the standing human body. Motion was measured along the whole body. Twelve subjects took part at the experiment with three leg postures (normal, legs bent and one leg), and five magnitudes of random vibrations, in the frequency range of 0.5–30 Hz, were considered. The main resonance frequencies of the apparent masses were found to differ with the posture. When the legs were bent, the resonance frequency of the apparent mass decreased. The same was observed for the one leg posture, but no other distinguishable peaks at frequencies below 30 Hz were present. The main resonances were found to slightly decrease, as the vibration magnitude increased. Going on with the work, Matsumoto et al., in [33], searched mathematical models, based on lumped parameters, to model the human body apparent masses. SDOF and 2DOF systems, both in series and in parallel, with and without support mass, were considered. The model parameters were optimised using the mean apparent masses taken from the previous study [32], for three different standing postures and four vibration magnitudes. The calculated responses of the 2DOF models, with a massless support, showed the best agreement with the measured apparent mass and phase. The model parameters obtained by fitting the mean measured apparent masses of all subjects were similar to the means of all sets of parameters obtained by fitting the individual apparent masses.

Sim et al. [34] analysed the frequency response of a joint crowd-structure system in which the structure was treated as a SDOF system and the seated and standing crowds were both modelled as a 2DOF system. In a subsequent work, Sim et al. [35] investigated the HSI by two equivalent

reduced systems, a SDOF and 3DOF system. The two were compared with their previous work [34]. The results showed that a full model exhibits the behaviour of a SDOF system for structures with natural frequencies less than 4 Hz (when empty), whereas for structures with natural frequencies above 4 Hz, the equivalent 3DOF system provided a better fitting.

Kim et al [36] gave their own contribution on the human body modeling too, by utilizing a 2DOF model. Comparison with the dynamic responses using the time-domain force and experimental data were performed. Unexpectedly, the dynamic responses using the human body model was found to be larger than the time-domain force model. It was also found, as expected, that the synchronization of walking produces larger dynamic responses than those from the random walking. However, for low density walking stream, synchronization of walking and random walking showed similar results.

1.1.7 Other Modeling Approaches

As can be understood by the previous Section (1.1.6), the Human-Structure Interaction is all but a simple issue to deal with. Therefore, unconventional methods (e.g. spectral models [37], control theory [38] or 3D inertia tracking [39]) with respect to the previous (and most common) ones have been proposed to face the problem too. Some of the most particular ones are in the following showed.

Based on pedestrian traffic, modeled probabilistically and with non-dimensional parameters, a spectral model for the modal force induced by pedestrian groups, was proposed by Piccardo et al. [37]. It was based on the assumption that pedestrians can be schematized as a stationary random process. This requires a minimum time of pedestrian flow to approximate as stationary the loading process. Based on it, a simple evaluation scheme was introduced to evaluate the maximum of the dynamic response.

In the wake of recent proposed models based on the control theory, Caicedo et al. [38] suggested closed loop control models (PD and PID) to model the Human Structure Interaction. A comparison with two traditional models, using a SDOF and a 2DOF, was performed. The experimental data used for the comparison were obtained from a laboratory test structure, that was modeled as a SDOF. The 2DOF model showed a better agreement than the SDOF, to represent the experimental Transfer Function (TF): force - acceleration. However, models based on closed loop control theory present more agreement, with the advantage of less parameters required.

Instead, Van Nimmen et al. [39] tried to characterize walking loads by a 3D inertial motion tracking technique. A first laboratory stage was conducted. The registered motion allowed for a stride-to-stride variation identification, which is usually disregarded in the simulation of walking forces. This allowed to identify the average step frequency of the tested subject, which was implemented in the simulation by means of a generalised force model, providing a good approximation of the imperfect real walking force. A subsequent application on a real footbridge was executed, which was followed by the calibration of its numerical model. Accounting for the walking variabilities led to a significant improvement of agreement between the measured and the simulated responses. While perfectly periodic forces led to a significant overestimation of the structural response. The remaining discrepancies were explained through the structural changes caused by the presence of pedestrians.

1.2 Previous Contributions

1.2.1 Passive People Effect

One of the previous publications [1] analysed the influence of the presence of passive people on the modal properties of a structure, and proposed a method to predict such changes. The approach

was able to provide a mathematical justification to the observed phenomenon. In fact, the effect of each human subject on the structure was evaluated locally. To do that, two elements were required:

- (i) a dynamical model of the empty structure;
- (ii) a description of the dynamic behaviour of each person standing on the structure.

As for point (i), a modal model of the structure was employed (i.e. natural frequencies, damping ratios and mode shapes). It can be obtained either from experimental data or from a FE model. As for point (ii), the quantity used to represent the dynamic behaviour of the human body was the *apparent mass* [40]. It is the transfer function between the force exerted by the person on the structure f^{Human} at the contact point, Fig. 1, the Ground Reaction Force (GRF), and the corresponding acceleration \ddot{x} , in the frequency domain

$$M_a(j\omega) = \frac{f^{Human}(j\omega)}{\ddot{x}(j\omega)} \quad (1)$$

Obviously, $M_a(j\omega)$ is a complex function and the GRF of each person on the structure depends on his/her body dynamic properties (i.e. mass, stiffness, damping).

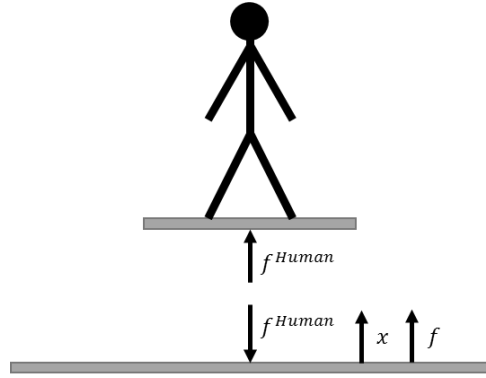


Fig. 1: Connection passive person-structure through f^{Human} (GRF).

The approach proposed by Krenk [41] was employed to account for presence of people on the structure. Krenk's model was originally developed for the introduction of dampers on discretised structural systems. The effect of each damper is introduced through the force exerted by the damper on the structure. In the frequency domain, this force may be expressed as the product between the FRF of the damper and the displacement of the point where the damper is located. This model was extended to the case of passive people by the authors [1]. One of the advantages of this model is the possibility to introduce each subject and evaluate the corresponding effect individually.

The basic steps of the approach used to obtain the transfer function of the joint HS system are reported below.

Since the eigenvectors were measured at discrete points (nodes), the FRFs of the empty structure, expressed as forces over displacements, were a finite number and stored in the matrix $\mathbf{G}(j\omega)$, which expression is [41]

$$\mathbf{G}(j\omega) = \sum_{i=1}^N \frac{\boldsymbol{\phi}_i \boldsymbol{\phi}_i^T}{-\omega^2 + j2\xi_i \omega_i \omega + \omega_i^2} \quad (2)$$

where $\boldsymbol{\phi}_i$ is the i -th mode shape vector, normalized by the square root of the unit modal mass, ω_i is the i -th natural frequency of the structure, ξ_i is the non-dimensional damping ratio of the i -th mode, N is the number of modes taken into consideration. Therefore, the dynamic response of the structure, in terms of displacements, can be obtained by

$$\mathbf{x}(j\omega) = \mathbf{G}(j\omega)\mathbf{f}(j\omega) \quad (3)$$

Accordingly, $\mathbf{x}(j\omega)$ is the vector that contains the displacement responses at the nodes of the structure, while $\mathbf{f}(j\omega)$ is a generic force vector containing the forces applied to the nodes.

People contribution remained to be added. According to the definition of apparent mass, each person, fixed to a node of the structure, introduce a force in agreement with the structure acceleration \ddot{x} of the specific point of contact. Therefore, the GRF for a passive subject (i.e. a stationary one) connected to the k-th point of the structure is

$$f_k^{Human}(j\omega) = M_a(j\omega)\ddot{x}_k(j\omega) = -M_a(j\omega)\omega^2 x(j\omega) = H(j\omega)x_k(j\omega) \quad (4)$$

In terms of full vectors, Eq. (4) can be expressed in matrix form as

$$\mathbf{f}^{Human}(j\omega) = H(j\omega)\mathbf{w}_k\mathbf{w}_k^T\mathbf{x}(j\omega) \quad (5)$$

thanks to \mathbf{w}_k , which identifies the connection of the person with the k-th node of the structure, as it is shown in Fig. 2. Extending the procedure to m people present on the structure:

$$\mathbf{f}^{Human}(j\omega) = \mathbf{W}\mathbf{H}(j\omega)\mathbf{W}^T\mathbf{x}(j\omega) \quad (6)$$

where $\mathbf{W} = [\mathbf{w}_1, \dots, \mathbf{w}_m]$ contains m \mathbf{w}_k vectors, and so the information about the connection of each of the m subjects with the structure. While $\mathbf{H}(j\omega)$ is the diagonal transfer function matrix containing the m $H(j\omega)$ functions of the subjects.

Joining the two contributions, that are Eq. (3) and (6), and keeping Fig. 1 as reference:

$$\mathbf{G}^{-1}(j\omega)\mathbf{x}(j\omega) = \mathbf{f}(j\omega) - \mathbf{f}^{Human}(j\omega) = \mathbf{f}(j\omega) - \mathbf{W}\mathbf{H}(j\omega)\mathbf{W}^T\mathbf{x}(j\omega) \quad (7)$$

$$[\mathbf{G}^{-1}(j\omega) + \mathbf{W}\mathbf{H}(j\omega)\mathbf{W}^T]\mathbf{x}(j\omega) = \mathbf{G}_H^{-1}(j\omega)\mathbf{x}(j\omega) = \mathbf{f}(j\omega) \quad (8)$$

Thus, in Eq. (8) $\mathbf{G}_H(j\omega)$ represents the new transfer functions of the HS system. The new FRFs can be expressed explicitly in $\mathbf{G}(j\omega)$ by the Woodbury matrix identity [42]:

$$[\mathbf{A} + \mathbf{UCV}]^{-1} = \mathbf{A}^{-1} - \mathbf{A}^{-1}\mathbf{U}[\mathbf{C}^{-1} + \mathbf{VA}^{-1}\mathbf{U}]^{-1}\mathbf{VA}^{-1} \quad (9)$$

$$\mathbf{G}_H = [\mathbf{G}^{-1} + \mathbf{W}\mathbf{H}\mathbf{W}^T] = \mathbf{G} - \mathbf{G}\mathbf{W}[\mathbf{H}^{-1} + \mathbf{W}^T\mathbf{G}\mathbf{W}]^{-1}\mathbf{W}^T\mathbf{G} \quad (10)$$

This approach allowed to evaluate separately the effect of each subject by means of his/her apparent mass, which is contained in $\mathbf{H}(j\omega)$ and just scaled by $-\omega^2$. This effect is a function of the characteristics of the subject and posture, but also of his/her position on the structure, which is accounted through \mathbf{w}_k in the matrix \mathbf{W} .

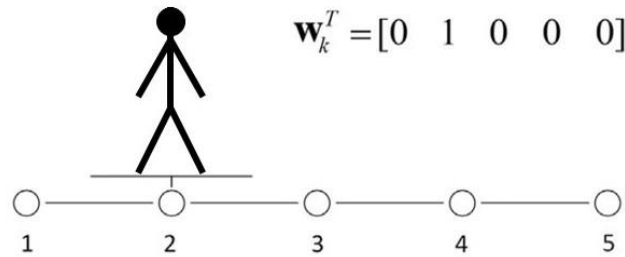


Fig. 2: Connection of a subject with the 2nd node of the structure.

The procedure was tested by using different models of apparent mass and the effect of using apparent masses obtained with different levels of vibration was analysed too.

1.2.2 Active Pedestrian Effect

In case of occupied structure, the use of the dynamic properties of the empty one to estimate the structural response induced by the effect of active pedestrians can lead to an erroneous prediction of the vibration amplitudes. On this problem, the latest contribution [2] proposed an approach to improve the estimation of the response, basing on the previous methodology [1] (Section 1.2.1).

A distinction between active and passive effect was first of all introduced. Since in [1] only the passive effect was present, since only standing people were accounted. Thereby, the force f^{Human} induced by the pedestrian was implicitly equal to the Passive Ground Reaction Force (PGRF) f^{PGR} . Conversely, in presence of a moving pedestrian, both the PGRF and the Active Ground Reaction Force (AGRF) must be considered. Therefore, the force f^{Human} , induced by the pedestrian, comprises both the contributions:

$$f^{Human} = f^{PGR} + f^{act} \quad (11)$$

This split of contributions was allowed since f^{act} was considered as the active force exerted on an infinite stiff surface (i.e. no ground displacement and so no PGRF involvement), while f^{PGR} accounted only for the ground vibration and the consequent body response. In this way, the problem of estimating the response of the occupied structure by moving people was decoupled into two main tasks, i.e. the identification of the PGRFs of moving people and their AGRFs. Accordingly, the PGRF of each subject was modelled through his/her equivalent apparent mass. They were then added to the empty structure $\mathbf{G}(j\omega)$, as shown in Eq.(7), in order to obtain the FRFs of the occupied structure (i.e. $\mathbf{G}_H(j\omega)$, Eq. (10)). Hence, the dynamic model of the occupied structure is given by the empty structure one plus the passive pedestrian contributions. On such model, the active forces were then easily applied, adding their contribution to the right-hand side of Eq. (8)

$$[\mathbf{G}^{-1}(j\omega) + \mathbf{W}\mathbf{H}(j\omega)\mathbf{W}^T]\mathbf{x}(j\omega) = \mathbf{G}_H^{-1}(j\omega)\mathbf{x}(j\omega) = \mathbf{f}(j\omega) - \mathbf{f}^{act}(j\omega) \quad (12)$$

Unlike to still people, the passive contribution (i.e. PGRF) of a moving person significantly changes with time because of the change of posture. Indeed, the apparent mass of a person strongly depends on his/her body configuration. The approach proposed in [2] assumed that a mean PGRFs can be used to represent the average behavior of the human body during the walking. To do that, the subsequent steps were followed:

- I. identification of the cycle time T (i.e. the elapsing time between two subsequent touches of the same foot with the ground);
- II. divide the cycle into an appropriate number of postures P (which must be representative of the overall motion);
- III. identify an average apparent mass $M_{a,i}(j\omega)$, for each posture i , to accounts for different people (inter-subject variability);
- IV. define an equivalent apparent mass $M_{eq}(j\omega)$ as the weighted average of the posture apparent masses $M_{a,i}(j\omega)$:

$$M_{eq}(j\omega) = \sum_{i=1}^P \alpha_i M_{a,i}(j\omega) \quad (13)$$

where the coefficients α_i are the weights such that: $0 \leq \alpha_i \leq 1$ and $\sum_{i=1}^P \alpha_i = 1$.

Three postures were used, and so three weight coefficients, because they were found enough to describe the main walking postures: one leg (left), standing on two legs and one leg (right).

At this point, two ways were proposed to apply the PGRF contribution:

- I. Each f^{PGR} is considered as a moving component. Hence, the $\mathbf{G}_h(j\omega)$ changes with time due to the matrix \mathbf{W} , which accounts for the pedestrian positions (Eq. (7) and (8)).
- II. A fractional apparent mass $m_{fr}(j\omega)$ is assessed:

$$m_{fr}(j\omega) = \frac{m}{n} M_{eq}(j\omega) \quad (14)$$

with m the number of people on the structure, and n the number of points in which the structure is discretised. Then $m_{fr}(j\omega)$ is applied to each node of the structure. Thus, $\mathbf{H}(j\omega)$ becomes a diagonal matrix of only scaled $m_{fr}(j\omega)$ (i.e. $\mathbf{H}(j\omega) = -\omega^2 m_{fr}(j\omega) \mathbf{I}$, with \mathbf{I} identity matrix) and the PGRF for each point $k \in [1, \dots, n]$ becomes as follow

$$f_k^{PGR}(j\omega) = m_{fr}(j\omega) \ddot{x}_k(j\omega) = -\omega^2 m_{fr}(j\omega) x(j\omega) \quad (15)$$

Collecting all of them in full vectors, Eq.(15) becomes

$$\mathbf{f}^{PGR}(j\omega) = \mathbf{W}\mathbf{H}(j\omega)\mathbf{W}^T \mathbf{x}(j\omega) = -\omega^2 m_{fr}(j\omega) \mathbf{W}\mathbf{I}\mathbf{W}^T \mathbf{x}(j\omega) \quad (16)$$

where, under the current assumptions, both \mathbf{I} and $\mathbf{W}\mathbf{I}\mathbf{W}^T$ are $n \times n$ identity matrices. As a consequence, Eq. (12) becomes

$$[\mathbf{G}^{-1}(j\omega) + \omega^2 m_{fr}(j\omega) \mathbf{I}] \mathbf{x}(j\omega) = \mathbf{G}_H^{-1}(j\omega) \mathbf{x}(j\omega) = \mathbf{f}(j\omega) - \mathbf{f}^{act}(j\omega) \quad (17)$$

where $\mathbf{G}_H(j\omega)$ is a $n \times n$ matrix containing the FRFs of the occupied structure. Obviously, this is an approximated approach, since the passive contribution of the people who occupy the structure is spared over the structure and not locally applied at the specific pedestrian position, as the AGRFs are.

The second approach was used, since it allowed to have a fixed $\mathbf{G}_H(j\omega)$ matrix in time (i.e. Time Invariant FRFs of the occupied structure), leading to easier and faster simulations of the coupled Human-Structure system to deal with. Furthermore, when the number of people on the structure increases (i.e. high pedestrian density situations), the accuracy of the approach was expected to increase as well, since its approximation (i.e. spread passive contributions) should better describe the HSI situation.

Chapter 2

Modeling of HSI

2.1 Pedestrian Interaction

As it was introduced in Section 1.2.2, a distinction between the active and passive contribution of a walking pedestrian was made in the previous contribution [2] and here it is done as well. Such distinction is possible thanks to superimposition principle, which is allowed by the linear hypothesis. Of course, the human body is far to be a linear dynamic system. More in general, its behavior change as a function of the undertaken activity. Indeed, different studies have demonstrated the dependency of human-induced forces on many factors. One of the most dominant, which was at the centre of different researches [43–45], is the gait speed. For instance, Galbraith et al. [43] measured the vertical force for speeds ranging from slow walking to running. Whereas, Keller et al. [46] collected over 1100 vertical Ground Reaction Force time histories for walking, slow jogging and running over a wide range of speeds. The results indicated that the maximum vertical GRF increases linearly with gait speed up to about 3.5 m/s. At higher walking speeds the maximum vertical forces were found constant, at approximately 2.5 times the body weight. Moreover, gait style appeared to be an important factor in the determination of the amplitude of the force peaks, as reported by other authors too [47,48].

Studies to account for the structural flexibility in the lateral direction were also conducted (e.g. Pizzimenti et al. [49] and Ronnquist [50]). These indicated that a negligible interaction takes place between pedestrians and structure in case of small amplitudes of vibrations. While large amplitudes of vibrations appeared when the harmonic multiples of the pacing rate approached the lateral vibration frequencies, leading to higher horizontal walking forces. A particular phenomenon that occurs when people change their gait to adapt to excessive vibration of the structure is known as Human–Structure synchronization [51] or lock-in effect [5], which involves strongly non-linear interactions.

Conversely to the lateral flexibility of the structures, when the vertical stiffness is so small to allow significant levels of the vibration amplitudes, the walking is obstructed and not synchronized. Indeed, changes in walking were observed when perceptible amplitudes of vibrations were present (Zivanovic et al.[52]), instead of a synchronization of the footfall as in the lateral case. The same happens during an earthquake, as limit case of course, when the amplitudes of the vibrations are so high to preclude walking. However, more in general, experimental studies on the vertical walking forces induced on flexible structures are not so common. In one of them, McMahan et al. [53] investigated the effect of surface stiffness on the running mechanism. A decrease in the surface stiffness resulted in a decrease of the vertical GRF. Alternatively, Ohlsson [54] compared the

spectra of vertical walking forces measured on a rigid surface and measured on a flexible timber floor. The force amplitude spectra were found to significantly reduce around the natural frequency of the structure.

Conversely, in the current studied case, the vertical displacements were not so relevant to obstacle or alter the walking. Negligible lateral vibration components were involved and so, no synchronization of the pedestrian rates could take place. Therefore, the source of the main non-linear Human-Structure Interaction was discarded (i.e. lock-in phenomenon due to lateral vibrations).

For what concern the lively behavior of the structure considered, due to its low damping, non-linear responses were engaged in the experimental section, since also the presence of few crossing pedestrians was enough to lead the structure in non-linearity. However, the variations in terms of natural frequencies were of the order of tenths of Hertz. Therefore, the magnitude of the non-linear behavior of the structure was considered acceptable.

The non-linearity of the human body instead was mitigated by considering the body in distinct configurations. This allowed to simplify the human body as a sequence of linear systems, and to describe each of them as the sum of two effects, an active and passive one. This permitted to have an easier dissertation of the human body.

Summing up, the presence of pedestrians is accounted in the present work by means of:

- I. An *active* contribution (f^{act} / Active Ground Reaction Force (AGRF)), which accounts for the active component of the walking dynamics exerted on an infinitely rigid ground. It is applied on the structure only, at the pedestrian contact point.
- II. A *passive* contribution (f^{PGR} / Passive Ground Reaction Force (PGRF)), which accounts for the interaction between the human body dynamics and the structure dynamics. It is introduced through the apparent mass, which represents the body response behavior, in a specific walking position, at the vibration of the structure.

It is noteworthy that the ground movement is considered in the passive contribution only, where the acceleration of the ground acts as input for the apparent mass. Whereas, the active contribution was evaluated on a nondeformable surface (as it is usually assumed in the modelling [26,30]). In such a way, it is possible to split the two effects.

2.1.1 Pedestrian Description

Once it is decided how to consider the interactions that occur when a walking pedestrian is considered, the next step is the definition of a mathematical description of such contributions. Among the possible ways in which this matter can be addressed, three potential methods are advanced in the following. At first, the use of an equivalent mechanical system is prompted, followed by a general black box schematization. Finally, a mathematical approach which would allow the direct use of the experimental measured passive contribution of a pedestrian, based on the convolution technique, was proposed. It is to be pointed out that in all the methods, the active contribution is considered as a time dependent force vector applied to the structure together the passive one. The passive part instead (i.e. the apparent mass) is the one that will be differently modeled with the next methods. It is also worth mentioning that the ways in which the active and passive contributions of pedestrians are schematized don't affect the ability of advanced Models of this thesis to account for the HSI, since their effect is in any case considered.

Mechanical system

There are different ways in which the apparent mass of a subject can be mathematically described, as was shown in the introduction (Section 1.1). Simple masses [15,31], Single Degrees Of Freedom (SDOF) systems [7,13,30,31,33,38], 2DOF systems [32–34,36,38] and even control

feedback loops [38] were utilised. Among them, given the simplicity brought by the number of DOFs involved, along with its good representation of the experimental data (as sustained by Matsumoto and Griffin [33] and confirmed by experiments (Section 3.2)), a 2DOF system was considered as the suitable representation as mechanical system of the apparent mass.

A detailed description of the 2DOFs system implementation in the HSI will be discussed in Section 2.3.

black box

Another possible way in which the apparent mass can be treated is just using a model as general as you want, with any shape and number of variables (i.e. without any physical meaning). It is enough that such a model fits the Frequency Response Functions (FRFs) of the involved pedestrians (i.e. a tuned model for each pedestrian, then stored in $\mathbf{H}_{blackbox}$), so that to give back the responses of the pedestrians (\mathbf{f}^{PGR}) for the given input accelerations of the structure ($\ddot{\mathbf{x}}$).

$$\begin{cases} \mathbf{M}\ddot{\mathbf{x}} + \mathbf{R}\dot{\mathbf{x}} + \mathbf{K}\mathbf{x} = -\mathbf{f}^{act} - \mathbf{f}^{PGR} \\ \mathbf{f}^{PGR} = \mathbf{H}_{blackbox}\ddot{\mathbf{x}} \end{cases} \quad (18)$$

Where \mathbf{M} , \mathbf{R} and \mathbf{K} are the mass, damping and stiffness matrices of the empty structure. Eq.(18) shows the use of several *black boxes* contained in $\mathbf{H}_{blackbox}$ to represent the apparent masses of the person involved. $\mathbf{H}_{blackbox}$ takes the accelerations of the structure $\ddot{\mathbf{x}}$ and provides the PGRFs (i.e. \mathbf{f}^{PGR}). They are then applied to the dynamic equation of the structure (first equation of Eq.(18)) along with the AGRF (i.e. \mathbf{f}^{act}).

It is to be underlined that the black box approach, and also the mechanical system one, which are used account for the presence of the passive contribution of a pedestrian, are valid for a specific configuration of the body, namely for a time lapse. Therefore, their implementation, for a mathematical treatment of the passive contribution of a moving people, should be constantly updated. Since a continuous upgrade of the parameters of the model (mechanical system or black box) would be extremely heavy from a computational point of view (given the constant update of the parameters required) and meaningless from a physical point of view (since a significant change of apparent mass, and so of parameters of the model, takes place only with a significant change of the body configuration) a possible solution could be the one offered by a discretization of the walking act. It would be enough to slice the walking motion in the most significant postures assumed and identify their correspondent model parameters. A detailed description of the procedure will be illustrated in Section 2.3 for the use of 2DOF mechanical systems. The passages for the use of a black box approach are the same. In this way, a good representation of the change of the passive contribution of a pedestrian, to be used in the HSI modeling for the numerical simulations, should be allowed.

Conversely, the next approach that will be introduced works in time domain by means of a convolution approach. Therefore, a continuous evaluation of the passive pedestrian contribution is directly assessed, through the direct use of the experimental passive pedestrian curves. This highlights the advantage in the use of such a method.

Convolution

A different procedure to treat the HSI is the one by a convolution approach. This method allows the direct use of the measured apparent mass curves (passive pedestrian contributions), without any use of a model-fitting, as it is instead required for the use of a *mechanical system* or a *black box* representation, to obtain the parameters of the model.

Indeed, give this advantage, a convolution methodology was implemented in the previous work [2] to estimate the vibration level of an occupied structure. In [2], a distinction between the active

and passive contribution was made, as explained in Section 1.2.2, considering the active one by means of a time-variant force vector and the passive one by means of pedestrian apparent mass curve. As for the time-variant force vector, it was moved on the structure with the pedestrian position. Conversely, the passive contribution was spread over the entire structure (i.e. a fractional apparent mass curve at each node of the discretized structure was placed), as explained in Section 1.2.2 (Eq.(13) and Eq.(14)). In such a way, instead of moving the passive and active component of each pedestrian present on the structure, only the active component was moved with its own pedestrian on a modified structure. This last was built up in the frequency domain by combination of the Frequency Response Function (FRF) of the empty structure, Eq.(2), with the total apparent mass of the pedestrians who occupied the structure, Eq.(14) and Eq.(17). In this way, a direct use of the apparent mass curves was possible, without the request of any model interpolation. Therefore, a Time Invariant structure was obtained, leading to a great advantage from the computational point of view. Indeed, fixed FRFs of the occupied structure were obtained, Eq.(17). The next step required was the passage from the frequency domain to the time domain one, since convolution works in time domain. To do that, an Inverse Fourier Transform (IFT) of the FRFs was performed, leading to the knowledge of the fixed (i.e. always the same) Impulse Response Functions (IRFs) of the nodes in which the structure was discretized. Then, the convolution between the active components (moving-time variant force vectors) and the IRFs was enough to assess the dynamic response of the structure produced by the presence of crossing pedestrians.

The same procedure is here applied without the introduction of any approximations, i.e. with moving apparent masses of the subjects together with their active forces (AGRFs). Hence, an evaluation of the new IRFs is necessary every time that any subject changes his/her position (node of the structure) to properly perform the convolution with the updated IRFs. The consequent Linear Time Variant (LTV) system can be described by State Space (SS) formulation of the occupied-by pedestrian structure:

$$\begin{cases} \dot{\mathbf{x}}(t) = \mathbf{A}(t)\mathbf{x}(t) + \mathbf{B}(t)\mathbf{u}(t) \\ \mathbf{y}(t) = \mathbf{C}(t)\mathbf{x}(t) \end{cases} \quad (19)$$

where the matrix $\mathbf{A}(t)$, $\mathbf{B}(t)$ and $\mathbf{C}(t)$ represent the state space matrix, the input matrix and the observation matrix of the occupied structure evaluated at time t (i.e. in a specific pedestrian configuration on the structure) respectively. The state vector $\mathbf{x}(t)$ contains the displacements and velocities of the nodes of the structure, while the vector $\mathbf{u}(t)$ contains the values of the AGRFs of the involved pedestrians assumed at time t . Instead, the vector $\mathbf{y}(t)$ contains the displacements of the nodes of the structure for a matrix $\mathbf{C}(t)$ properly set-up to extract only the displacement from the vector $\mathbf{x}(t)$. The solution of the of SS system is described by the following [55]:

$$\begin{cases} \mathbf{x}(t) = \boldsymbol{\varphi}(t, t_0)\mathbf{x}_0 + \int_{t_0}^t \boldsymbol{\varphi}(t, \tau)\mathbf{B}(\tau)\mathbf{u}(\tau)d\tau \\ \mathbf{y}(t) = \mathbf{C}(t)\boldsymbol{\varphi}(t, t_0)\mathbf{x}_0 + \int_{t_0}^t \boldsymbol{\Omega}(t, \tau)\mathbf{u}(\tau)d\tau \end{cases} \quad (20)$$

As the vector $\mathbf{y}(t)$ has size $n \times 1$, with n number of DOFs of the structure, and $\mathbf{u}(\tau)$ as well. The matrix $\boldsymbol{\Omega}(t, \tau)$ (i.e. $\mathbf{C}(t)\boldsymbol{\varphi}(t, \tau)\mathbf{B}(\tau)$) has size $n \times n$ ($\mathbf{C}(t)$ has size $n \times 2n$, $\boldsymbol{\varphi}(t, \tau)$ $2n \times 2n$ and $\mathbf{B}(\tau)$ $2n \times n$). Indeed, $\boldsymbol{\Omega}$ contains the above mentioned IRFs, which are evaluated by performing the IFT of the FRFs of the occupied structure (see from Eq.(2) to Eq.(10)) that contain the measured apparent mass curves (see Eq.(4), Eq.(5) and Eq.(6)). They are $n \times n$ IRFs (n co-located and $n \times n - n$ non-co-located), for impulses applied at time τ and observed at time t . While $\boldsymbol{\varphi}(t, t_0)$, which is equal to $e^{\int_{t_0}^t \mathbf{A}(\xi)d\xi}$, it is used to evaluate the free response reached from the state \mathbf{x} at time t , due to the initial condition \mathbf{x}_0 present at time t_0 . In order to obtain a constant $\boldsymbol{\varphi}(t, t_0)$ matrix (i.e.

$\boldsymbol{\varphi}(t, t_0) = e^{\mathbf{A}(t-t_0)}$) it is possible to split the overall time interval $[t_0, t]$ in subintervals obtained by cutting the time-line each time that a person moves, leading to a constant set of state space matrices \mathbf{A} , \mathbf{B} , \mathbf{C} for each sub-time interval/configuration of pedestrians assumed on the structure. Conversely, in [2], the interruption of the integration time was not required, since a Time Invariant occupied structure was used, as aforementioned, and a single global time integration was enough. Indeed, starting from null initial conditions the second equation of Eq. (20) becomes:

$$\mathbf{y}(t) = \int_{t_0}^t \boldsymbol{\Omega}(t, \tau) \mathbf{u}(\tau) d\tau \quad (21)$$

which is the convolution expression. Therefore, in the previous work, the knowledge on the IRFs (i.e. $\boldsymbol{\Omega}(t, \tau)$) was enough to compute the displacements of the structure $\mathbf{y}(t)$ and from them the vibration level through double time derivation of themselves. Now instead, even if the same null initial conditions are imposed, the free response term (i.e. $\mathbf{C}(t)\boldsymbol{\varphi}(t, t_0)\mathbf{x}_0$) is present, as null initial conditions ensure its deletion only for the first sub-time interval, but not for the following ones. Indeed, due to the integration time interval subdivision, every time that the integration is restarted, the value of the state reached at the end of the previous integration sub-time interval must be accounted as initial state \mathbf{x}_0 for the following sub-time interval. Hence, the knowledge of the free response matrix $\boldsymbol{\varphi}(t, t_0)$ appears now required.

It is to notice that, even if the expression of the matrix $\boldsymbol{\Omega}(t, \tau)$ of the known IRFs contains the free response matrix $\boldsymbol{\varphi}(t, t_0)$

$$\boldsymbol{\Omega}(t, \tau) = \mathbf{C}\boldsymbol{\varphi}(t, \tau)\mathbf{B}, \quad (22)$$

a $\boldsymbol{\varphi}(t, \tau)$ extraction by mean of matrix \mathbf{C} and \mathbf{B} inversion is not allowed, since their non-square sizes ($\mathbf{C}(t)$ has size $n \times 2n$ and $\mathbf{B}(\tau)$ $2n \times n$, with n the number of DOFs of the structure). The only possible way to evaluate $\boldsymbol{\varphi}(t, \tau)$ is through eigenvalues and eigenvectors evaluation. Indeed, the matrix $\boldsymbol{\varphi}(t, \tau)$ is function of the State Space matrix \mathbf{A} , Eq.(23). For a sub-time interval, i.e. for constant SS matrices:

$$\boldsymbol{\varphi}(t, \tau) = e^{\int_{\tau}^t \mathbf{A}(\xi) d\xi} = e^{\mathbf{A}(t-\tau)} \quad (23)$$

and the SS matrix \mathbf{A} can be expressed as the eigenvalue matrix thanks the eigenvector one [56]:

$$\mathbf{A} = \boldsymbol{\Phi}\boldsymbol{\lambda}_c\boldsymbol{\Phi}^{-1} \quad (24)$$

where $\boldsymbol{\Phi}$ is the matrix containing per column the eigenvectors of the SS matrix \mathbf{A} , and $\boldsymbol{\lambda}_c$ is the diagonal matrix containing its eigenvalues. Therefore, the free response matrix can be obtained from the modal parameters of the occupied structure: $\boldsymbol{\varphi} = f(\boldsymbol{\lambda}_c, \boldsymbol{\Phi})$. However, this is true for a sub-time interval, in which the occupied structure doesn't change configuration. As soon as a pedestrian changes position on the structure, the sub-time interval changes, the occupied structure configuration changes and with it its eigenvalues and eigenvectors, and so $\boldsymbol{\varphi}$. Hence, a modal extraction of the modal parameters (eigenvalues and eigenvectors) would be required any time that a pedestrian moves. Such computational burden definitely eclipses the advantage to directly use the experimental apparent mass curves for the modelization of the HSI and the consequent estimation of the vibration levels.

Our Case

Summing up, of the possible presented methods to account for the human body presence on the structure, the mechanical system made up by 2DOF is the one selected to be used in the HSI presented Models. The convolution approach is discarded for the reason just listed above, that is the continuous request of the modal information assessment (i.e. modal extraction). Instead, a 2DOF

mechanical system formulation is preferred to a black box one as it allows to maintain a physical description of the body mechanics, along with a quite good accuracy in the apparent mass representation, as will be shown in Section 3.2.4.

2.2 Background of the Models

As was introduced in Section 1.2.1 and Section 1.2.2, a previous contribution to the Human-Structure Interaction modelization was already present [2]. Such a Model was based on an average approach to deal with the pedestrian presence. Moreover, the contribution of the human body was split in an active and a passive contribution. The active one was applied to the structure coherently with the person position in time and space. Instead, the passive one of each subject was gathered in a huge global apparent mass that was then spread over the entire structure. This has led to a considerable simplification of the problem, as the new structure (empty structure plus the spread passive contributions) was a Time Invariant system. The physical justification behind such procedure was that, under the hypothesis of a large number of pedestrians crossing the structure (i.e. high pedestrian density), the effect of the application of moving passive contributions would be the same one of spreading the overall passive contributions, since all the available space on the structure would be occupied in a similar way. This was confirmed, as reported in the paper [2], as the experimental vibration level checked fell inside the range estimated by the Model. While, a great overestimation of the vibration level was obtained by using the model of the unoccupied structure to perform the estimation. This has shown the ability of people to damp the structure they occupy, in addition to their excitation ability (thought the AGRFs).

In the following the main core of this thesis is presented. The aim is to investigate the improvement that can be obtained in the estimation of the vibration level undertaken by a structure when subjected to the interaction with walking pedestrians, by increasing the complexity of HSI modelization. The starting point is the modelization proposed by the previous work just recalled [2]. For the sake of clarity, it will be from now on called Model 0. As just introduced, it utilizes an average approach which is more valid as the pedestrian density and the time interval increase. Going to augment the accuracy of the HSI modelization, by means of the Models proposed by this thesis (they will be shown starting from the next Section), two aspects want to be investigated:

- (i) what happens when the more accurate Models are used for the estimation of the vibration levels in high pedestrian density situations and long-time interval scenarios (i.e. Model 0 applicability conditions), with respect to the estimations made by Model 0;
- (ii) in the same way, what happens when the more accurate Models are used for the estimation of the vibration levels in conditions of few people crossing the structure (low pedestrian density) and short times considered (i.e. the ones just required to cross the structure). Always with respect to Model 0.

As Model 0 was thought to deal with the scenario depicted by in the first point, a more detailed description of the phenomenon it is expected to only confirm the results produced by Model 0. This would underline the uselessness of further increase the complexity of the HSI model for this type of pedestrian scenario. As for the second point, it is worth to remember that, while the active contribution (AGRF) excites the structure, the passive one, by means of the Passive Ground Reaction Force (PGRF), is able to damp the structure, as aforementioned. Hence, Model 0 spread the available damping effect over the structure. When this is done in case of few people, the resulting damping spread by Model 0 per unit area of structure drastically decreases. This leads to a decrease of the added local damping effect. While a higher value of local damping would be theoretically added in case that the passive contributions of pedestrians would be treated as the active ones (i.e. locally considered and not spread), that are moved in time and space coherently

with the single pedestrian position. Therefore, a more detailed description of the HSI should properly describe the dynamic behavior of the structure, and so its vibration levels, in case of few crossing pedestrians, with respect to the average approach (Model 0).

The conjecture about the time mentioned in point (i) and (ii) is only to distinguish between the case in which the time it is enough to allow the filling of the structure, thus a steady state dense condition can be established, and when the time it is not enough to have such a condition. More in general, the introduction of a local description of the passive contribution of the pedestrians allow to account for a series of effects that can take place in reality (e.g. the synchronization among pedestrians).

To check point (i) and (ii), three Models are proposed in this thesis. In the first one, Model 1, the introduction of moving with pedestrian apparent masses (passive contributions) will be presented. Therefore, both active and the passive effect of the single pedestrian will be locally considered. Then, in the second one, Model 2, the effect of the overlap between two consecutive footsteps, which normally occurs during the walking, will be analysed and introduced. Finally, in Model 3 will be treated the variation of apparent mass inside the single footstep, in order to reproduce the variation of the body posture within the single footstep. It is noted that, for the way in which Model 1, 2 and 3 are defined, they are supposed to be valid also for normal pedestrian densities. Indeed, the position of the PGRF and AGRF of each subject is correctly applied in time and space. Therefore, pedestrians modeled through these Models are expected to be more sensible to the local vibrations of the structure (i.e. the ones in correspondence of their positions). To verify such matter, different crowd scenarios have been numerically simulated with all the four Models. Not only, Model 1, 2 and 3 have been compared one by one with Model 0 to test point (i) and (ii). An experimental campaign on a real structure was performed too, in order to validate the numerical results. Of course, the virtual structure used in the numerical simulations was the same one used in the experimental campaign.

2.3 Model 1

With Model 1, a proper description of the PGRF of each subject (apparent mass) is introduced. While the AGRF is still modeled as it was done in Model 0, by means of a time variant force vector that is moved together with the pedestrian position, the PGRF is no more spread over the entire structure. Indeed, as introduced in Section 2.1.1, the passive contribution of each subject is mathematically described through a 2DOF mechanical system. Thanks to it, once the mechanical parameters of the system are identified (i.e. when the subject apparent mass curve is fit by the 2DOF model), a description of the passive interaction is obtained. It can be then easily moved with the pedestrian position along the structure.

An application of Model 1 is first presented for the case of one pedestrian who occupies a structure. For the sake of clarity, the structure will be synthesized as an equivalent 1DOF system at first. Then, the extension of the approach to multi-DOFs structures, occupied by m pedestrians, will be presented.

2.3.1 Single Pedestrian–1DOF Structure

A simple introduction to the application of Model 1 is presented in this Section. Beneath, the dynamic description of the mechanical system depicted in Fig. 3 (a 2DOF pedestrian on a 1DOF structure) is reported.

$$\begin{cases} m_s \ddot{x}_s + r_s \dot{x}_s + k_s x_s = -f^{act} + r_{p1}(\dot{x}_{p1} - \dot{x}_s) + k_{p1}(x_{p1} - x_s) \\ \begin{bmatrix} m_{p2} & 0 \\ 0 & m_{p1} \end{bmatrix} \begin{bmatrix} \ddot{x}_{p2} \\ \ddot{x}_{p1} \end{bmatrix} + \begin{bmatrix} r_{p2} & -r_{p2} \\ -r_{p2} & r_{p2} \end{bmatrix} \begin{bmatrix} \dot{x}_{p2} \\ \dot{x}_{p1} \end{bmatrix} + \begin{bmatrix} k_{p2} & -k_{p2} \\ -k_{p2} & k_{p2} \end{bmatrix} \begin{bmatrix} x_{p2} \\ x_{p1} \end{bmatrix} = \begin{bmatrix} 0 \\ -r_{p1}(\dot{x}_{p1} - \dot{x}_s) - k_{p1}(x_{p1} - x_s) \end{bmatrix} \end{cases} \quad (25)$$

Here, subscript s refers to the *structure* and p to the *pedestrian*. Moreover, x_s is the degree of freedom describing the motion of the structure, which is defined starting for the static equilibrium position of the empty structure. Instead, the x_p are the two degrees of freedom that describe the motion of the mechanical schematization of the passive contribution of the considered pedestrian. They are defined starting from the static equilibrium position of the 2DOF system reached when it is placed on the structure, with this last undeformed from the pedestrian static weight (i.e. empty structure configuration). This definition of the zeros will be better explained in Section 3.2.1, where a complete dissertation on the apparent mass is present. Basically, it is due to the fact that the apparent mass curves, and so the 2DOFs, were measured with the static weight filtered out, since the devices used to measure them were based on piezoelectric material. The static weight was instead measured/considered with the active component. Hence, it is present in f^{act} (AGRF). In this way, a correct representation of the pedestrian effects is possible, avoiding that the same term is considered more than once.

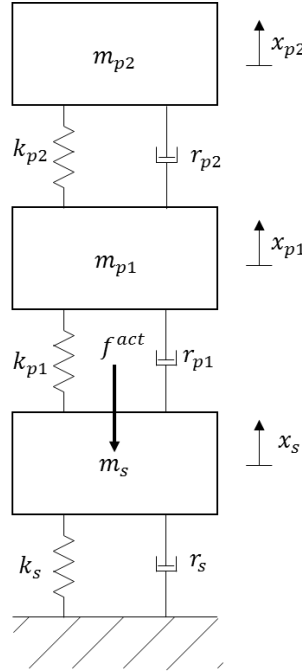


Fig. 3: Schematization of 1 pedestrian on a 1DOF structure.

From the right-hand side of the first and second equation of Eq.(25), which represent the structure and the body dynamic equation respectively, it is possible to see the passive coupling, given by the first spring-damper pair, that interacts with the structure and first mass of the 2DOF system.

Since the considered structure (at 1DOF) allows only two states: with and without the pedestrian on it, the simulation with Model 1 of such HSI situation would have three main phases:

- 1) unoccupied structure;
- 2) the pedestrian is crossing the structure;
- 3) the pedestrian has crossed the structure and now the structure is empty.

For each of the these three phases a description of the simulation of the HSI made with Model 1 is below reported:

- 1) The HSI model consists of 1DOF only, the structure one. Less than initial condition different from zero, the structure remains in its empty position (i.e. $x_s = 0$). Otherwise, free decay of the structure would be present starting from the imposed initial condition.
- 2) The HSI model becomes a 3DOF system, since the presence of the crossing pedestrian is felt. This is the configuration assumed at the instant zero of the crossing pedestrian phase: 3DOF with all the DOFs equal to zero value and no active force applied. As soon as the time rises, the active force time history of the crossing subject, which is applied to the structure only (i.e. on m_s), starts to assume non-null values. As a consequence, the 3DOF system starts to vibrate, and so the structure and the active and passive contribution start to interact. It is clear that the second phase lasts until the active force time history doesn't end. Therefore, the time length of the second phase is equal to the length of the active force time history. This makes sense, since the length of the active force time history represent the amount of time that the pedestrian foot stays in contact with the ground/structure.
- 3) Since now the pedestrian has left the structure, the HSI model comes back to 1DOF system representing the empty structure only, without any active force applied to it. Conversely to the first phase (1), even if the structure is unoccupied as well, an initial condition for the state describing the structure x_s is now present. Indeed, an initial condition equal to the structure state assumed at the last instant of phase two (2) must be imposed in order to properly describe the free decay of the structure.

This is the way in which Model 1 treats the HSI. Of course, this was the easiest possible example, since one pedestrian was present and only one position of the structure was available to be crossed/occupied. However, a more complex scenario, involving the presence of multi-pedestrians and a multi-DOF structure with available different positions that can be occupied by the crossing pedestrians, is not so much different from the just illustrated case. The greatest complexity concerns always the correct splitting of the integration time of the HSI dynamic equations (Eq.(25) for 1 pedestrian-1DOF structure case). Indeed, as it was mentioned in Section 2.1.1 (*Convolution*) to explain how the Linear Time Varian HSI system could be reduced to a series of Linear Time Invariant HSI systems, in Model 1 it is made the same thing. Since the occupied structure, which is given by the empty one plus the passive pedestrian contributions, is the same (LTI) for the time required for the application of the single active force time history, as it was shown in the second phase (2), it is enough to split the integration time every time that a pedestrian ends his/her active force history. Indeed, the end of the AGRF time history indicates that the pedestrian has to move to the next position of the structure. In this way, a series of LTI systems can be obtained, leading to an easier global system to be handled with respect to a LTV one. Therefore, any time that a person requires to change his/her position on the structure: (i) the integration of the dynamic equations of the HSI is stopped, (ii) the person is moved, (iii) the new LTI system given by the structure plus the passive contributions of the pedestrians is computed (which is the same of the previous LTI system less than the pedestrian just moved),(iv) an initial state for the structure and for the passive 2DOF system is imposed equal to the one assumed at the moment at which the integration was stopped, and then (v) the integration is restarted. Also for the moved pedestrian is provided the same initial condition that he/she had before to move, since null initial conditions after the 2DOF movement would be unphysical, since an instantaneous change of the body position represented by null initial conditions cannot happen. Instead, a natural continuance of the body motion, given by an initial state equal to the one just left, is physically correct.

Of course, as result of the overall integration stage, what is known is the displacement state vector, which contains the displacement time histories of the structure. Since the aim is the assessment of the vibration levels, and so the acceleration time histories, a double time derivation of the displacement state vector is required to obtain the acceleration time histories of the consider structure.

Summing up, any scenario can be simulated: people who start to cross the structure at different time instants, people who leave the structure, phases of free-decay due to the lack of pedestrians on the structure and then their reintroduction. Even the selection of the starting position of each subject is allowed, things that would be completely unphysical in case of a non-boundary position selection, as the appearance of a person in the middle of the structure would be unrealistic. However, such program feature could be used to simulate scenarios that involve the structure already occupied at time zero, as it was.

In the next Section, the just mentioned extension to a more general and realistic case of HSI is introduced, along with its most comprehensive mathematical description. This final version takes the name of Model 1.

2.3.2 Multi Pedestrians-Multi DOF Structure

Now that a preliminary introduction of how a pedestrian and a 1DOF structure are considered and made interact it is clear, its extension to a multi-degrees of freedom structure crossed by multi-pedestrians is illustrated.

In order to account for the presence of m walking pedestrians on a n -degrees of freedom structure, state vectors are first of all defined. The structure one, \mathbf{x}_s , contains the displacements of the nodes in which the structure is discretized. As for the pedestrians, their state vector is defined as follow

$$\mathbf{x}_p = [x_{p2,1}, x_{p1,1}, \dots, x_{p2,m}, x_{p1,m}]^T \quad (26)$$

that is a pair of state coordinates per person, since a 2DOF system is used to model the passive contribution of each person. As the approach here reported has to deal with a whatever number n of DOF of the structure and a whatever number m of walking pedestrians, a series of auxiliary matrices are utilized to make interact the different sizes of the matrices and vectors involved. The first is the position matrix \mathbf{W} (size $n \times m$), which allows to account for the interface between the m pedestrians and the n nodes of the structure:

$$\mathbf{W} = [\mathbf{w}_1, \dots, \mathbf{w}_m] \quad (27)$$

It contains m position vectors \mathbf{w}_k , with $k \in [1, m]$, one for each pedestrian present on the structure. \mathbf{w}_k is defined as

$$\mathbf{w}_k = [0, \dots, 1, \dots, 0]^T \quad (28)$$

with 1 placed at the position that corresponds to the node of the structure that is occupied by the considered k -th pedestrian. Hence, \mathbf{w}_k has size $n \times 1$. The second matrix is \mathbf{W}_{p1} , which allows to interact with the first DOF of the 2DOF systems, instead of with the full pedestrian state vector \mathbf{x}_s .

$$\mathbf{W}_{p1} = \begin{bmatrix} 0 & 1 & 0 & 0 & \dots & 0 & 0 \\ 0 & 0 & 0 & 1 & \dots & 0 & 0 \\ & & \vdots & & \ddots & & \vdots \\ 0 & 0 & 0 & 0 & \dots & 0 & 1 \end{bmatrix} \quad (29)$$

Its size is $m \times 2m$, since the size of the pedestrian state vector \mathbf{x}_s are $2m \times 1$ and m are the number of pedestrians that are present on the structure. Given its definition, a Boolean value equal to 1 is placed at each even column, changing row every time. For the sake of clarity, the definition of \mathbf{W}_{p1} in case of 3 pedestrians is reported in following, Fig. 4.

$$\begin{bmatrix} x_{p1,1} \\ x_{p1,2} \\ x_{p1,3} \end{bmatrix} = \begin{bmatrix} 0 & 1 & 0 & 0 & 0 & 0 \\ 0 & 0 & 0 & 1 & 0 & 0 \\ 0 & 0 & 0 & 0 & 0 & 1 \end{bmatrix} \begin{bmatrix} x_{p2,1} \\ x_{p1,1} \\ x_{p2,2} \\ x_{p1,2} \\ x_{p2,3} \\ x_{p1,3} \end{bmatrix} = \mathbf{W}_{p1} \mathbf{x}_p$$

Fig. 4: Application of \mathbf{W}_{p1} in case of 3 pedestrians.

Now that the necessary matrices and vectors are defined, the dynamic equations of the Human-Structure Interaction system can be written. A compact matrix notation is utilized, reporting at first the structure set of dynamic equations and then the pedestrian ones.

$$\begin{cases} \mathbf{M}_s \ddot{\mathbf{x}}_s + \mathbf{R}_s \dot{\mathbf{x}}_s + \mathbf{K}_s \mathbf{x}_s = -\mathbf{W} \mathbf{f}^{act} + \mathbf{W} \{ \mathbf{R}_{gr} (\mathbf{W}_{p1} \dot{\mathbf{x}}_p - \mathbf{W}^T \dot{\mathbf{x}}_s) + \mathbf{K}_{gr} (\mathbf{W}_{p1} \mathbf{x}_p - \mathbf{W}^T \mathbf{x}_s) \} \\ \mathbf{M}_p \ddot{\mathbf{x}}_p + \mathbf{R}_p \dot{\mathbf{x}}_p + \mathbf{K}_p \mathbf{x}_p = -\mathbf{W}_{p1}^T \{ \mathbf{R}_{gr} (\mathbf{W}_{p1} \dot{\mathbf{x}}_p - \mathbf{W}^T \dot{\mathbf{x}}_s) + \mathbf{K}_{gr} (\mathbf{W}_{p1} \mathbf{x}_p - \mathbf{W}^T \mathbf{x}_s) \} \end{cases} \quad (30)$$

The vector \mathbf{f}^{act} is the vector that contains the AGRFs of the pedestrians (e.g. Fig. 5 reports a single active force time histories and Fig. 6 two subsequent active force time histories). More in detail, as the AGRFs are force vector time histories, \mathbf{f}^{act} contains the instantaneous values assumed by the AGRF of each pedestrian. While \mathbf{R}_{gr} and \mathbf{K}_{gr} are the matrices that contain the part of the pedestrian passive system (2DOF) which allows the interact with the occupied structure (i.e. r_{p1} and k_{p1}). To allow their match with the sizes of the other matrices of Eq.(30), they are defined as diagonal matrices:

$$\mathbf{R}_{gr} = \begin{bmatrix} r_{p1,1} & \cdots & 0 \\ \vdots & \ddots & \vdots \\ 0 & \cdots & r_{p1,m} \end{bmatrix} \quad \mathbf{K}_{gr} = \begin{bmatrix} k_{p1,1} & \cdots & 0 \\ \vdots & \ddots & \vdots \\ 0 & \cdots & k_{p1,m} \end{bmatrix} \quad (31)$$

All the other matrices (i.e. \mathbf{M}_s , \mathbf{R}_s , \mathbf{K}_s , \mathbf{M}_p , \mathbf{R}_p and \mathbf{K}_p) are the ones that contain the mass, damping, and stiffness parameters of the structure and of the upper part of the 2DOF systems (i.e. m_{p2} , m_{p1} , r_{p2} and k_{p2} of each pedestrian) respectively.

Modal Description of the Structure

As next step, a description of the structure by means of its modal coordinate is introduced, Eq. (32). There are two advantages taken by the change of the free coordinates used to describe the structure. The first lies in a less heavy computational burden. Indeed, by using a modal coordinate description, a decoupling of the dynamic equations of the structure is obtained. Second, the requirement of only the modal parameters of the empty structure (i.e. eigenvalues, eigenvectors and damping ratios) to be able to describe its dynamics, instead of the local mass, damping and stiffness values are required.

$$\mathbf{x}_s(t) = \sum_{i=1}^N \boldsymbol{\phi}_i q_i(t) = \boldsymbol{\Phi} \mathbf{q}(t) \quad (32)$$

In the change of coordinates, N stands for the number of accounted modes of the structure, $\boldsymbol{\Phi}$ is the matrix that contains the unit modal mass normalized eigenvectors of the structure per columns and \mathbf{q} is the column vector that contains the N modal coordinates. Substituting Eq.(32) in Eq.(30), the following new decoupled matrices can be obtained

$$\boldsymbol{\Phi}^T \mathbf{M}_s \boldsymbol{\Phi} = \tilde{\mathbf{M}}_s = \begin{bmatrix} m_1 & \cdots & 0 \\ \vdots & \ddots & \vdots \\ 0 & \cdots & m_N \end{bmatrix} = \begin{bmatrix} 1 & \cdots & 0 \\ \vdots & \ddots & \vdots \\ 0 & \cdots & 1 \end{bmatrix} = \mathbf{I}$$

$$\boldsymbol{\phi}^T \mathbf{R}_s \boldsymbol{\phi} = \tilde{\mathbf{R}}_s = \begin{bmatrix} r_1 & \cdots & 0 \\ \vdots & \ddots & \vdots \\ 0 & \cdots & r_N \end{bmatrix} \begin{bmatrix} m_1 & \cdots & 0 \\ \vdots & \ddots & \vdots \\ 0 & \cdots & m_N \end{bmatrix}^{-1} = \begin{bmatrix} r_1 & \cdots & 0 \\ \vdots & \ddots & \vdots \\ 0 & \cdots & r_N \end{bmatrix} \quad (33)$$

$$\boldsymbol{\phi}^T \mathbf{K}_s \boldsymbol{\phi} = \tilde{\mathbf{K}}_s = \begin{bmatrix} k_1 & \cdots & 0 \\ \vdots & \ddots & \vdots \\ 0 & \cdots & k_N \end{bmatrix} \begin{bmatrix} m_1 & \cdots & 0 \\ \vdots & \ddots & \vdots \\ 0 & \cdots & m_N \end{bmatrix}^{-1} = \begin{bmatrix} \omega_{0,1}^2 & \cdots & 0 \\ \vdots & \ddots & \vdots \\ 0 & \cdots & \omega_{0,N}^2 \end{bmatrix} = \boldsymbol{\lambda}$$

where m_i, r_i and k_i are the unit modal mass, damping and stiffness of the i -th mode of the empty structure (given the use of unit modal mass normalized eigenvectors). Moreover, this last, the modal stiffness, is equal to the squared natural frequency of the i -th mode. Summing up, the matrix $\tilde{\mathbf{M}}_s$ is equal to the identity matrix \mathbf{I} , $\tilde{\mathbf{K}}_s$ to the diagonal squared natural frequency matrix $\boldsymbol{\lambda}$, and the diagonal matrix $\tilde{\mathbf{R}}_s$ contain the modal damping values of the modes.

After the substitution of Eq.(33), Eq.(30) becomes

$$\begin{cases} \ddot{\mathbf{q}}_s + \tilde{\mathbf{R}}_s \dot{\mathbf{q}}_s + \boldsymbol{\lambda} \mathbf{q}_s = -\boldsymbol{\phi}^T \mathbf{W} \mathbf{f}^{act} + \boldsymbol{\phi}^T \mathbf{W} \{ \mathbf{R}_{gr} (\mathbf{W}_{p1} \dot{\mathbf{x}}_p - \mathbf{W}^T \boldsymbol{\phi} \dot{\mathbf{q}}_s) + \mathbf{K}_{gr} (\mathbf{W}_{p1} \mathbf{x}_p - \mathbf{W}^T \boldsymbol{\phi} \mathbf{q}_s) \} \\ \mathbf{M}_p \ddot{\mathbf{x}}_p + \mathbf{R}_p \dot{\mathbf{x}}_p + \mathbf{K}_p \mathbf{x}_p = -\mathbf{W}_{p1}^T \{ \mathbf{R}_{gr} (\mathbf{W}_{p1} \dot{\mathbf{x}}_p - \mathbf{W}^T \boldsymbol{\phi} \dot{\mathbf{q}}_s) + \mathbf{K}_{gr} (\mathbf{W}_{p1} \mathbf{x}_p - \mathbf{W}^T \boldsymbol{\phi} \mathbf{q}_s) \} \end{cases} \quad (34)$$

Developing the first set of equations (the ones of the structure) of Eq. (34)

$$\begin{aligned} \ddot{\mathbf{q}}_s + [\tilde{\mathbf{R}}_s + \boldsymbol{\phi}^T \mathbf{W} \mathbf{R}_{gr} \mathbf{W}^T \boldsymbol{\phi}] \dot{\mathbf{q}}_s + [\boldsymbol{\lambda} + \boldsymbol{\phi}^T \mathbf{W} \mathbf{K}_{gr} \mathbf{W}^T \boldsymbol{\phi}] \mathbf{q}_s = \\ = -\boldsymbol{\phi}^T \mathbf{W} \mathbf{f}^{act} + \boldsymbol{\phi}^T \mathbf{W} \{ \mathbf{R}_{gr} \mathbf{W}_{p1} \dot{\mathbf{x}}_p + \mathbf{K}_{gr} \mathbf{W}_{p1} \mathbf{x}_p \} \end{aligned} \quad (35)$$

and the second set of equations (the ones of the pedestrians) of Eq. (34)

$$\begin{aligned} \mathbf{M}_p \ddot{\mathbf{x}}_p + [\mathbf{R}_p + \mathbf{W}_{p1}^T \mathbf{R}_{gr} \mathbf{W}_{p1}] \dot{\mathbf{x}}_p + [\mathbf{K}_p + \mathbf{W}_{p1}^T \mathbf{K}_{gr} \mathbf{W}_{p1}] \mathbf{x}_p = \\ = +\mathbf{W}_{p1}^T \{ \mathbf{R}_{gr} \mathbf{W}^T \boldsymbol{\phi} \dot{\mathbf{q}}_s + \mathbf{K}_{gr} \mathbf{W}^T \boldsymbol{\phi} \mathbf{q}_s \} \end{aligned} \quad (36)$$

and putting them back together:

$$\begin{cases} \ddot{\mathbf{q}}_s + [\tilde{\mathbf{R}}_s + \boldsymbol{\phi}^T \mathbf{W} \mathbf{R}_{gr} \mathbf{W}^T \boldsymbol{\phi}] \dot{\mathbf{q}}_s + [\boldsymbol{\lambda} + \boldsymbol{\phi}^T \mathbf{W} \mathbf{K}_{gr} \mathbf{W}^T \boldsymbol{\phi}] \mathbf{q}_s = \\ \quad = -\boldsymbol{\phi}^T \mathbf{W} \mathbf{f}^{act} + \boldsymbol{\phi}^T \mathbf{W} \{ \mathbf{R}_{gr} \mathbf{W}_{p1} \dot{\mathbf{x}}_p + \mathbf{K}_{gr} \mathbf{W}_{p1} \mathbf{x}_p \} \\ \mathbf{M}_p \ddot{\mathbf{x}}_p + [\mathbf{R}_p + \mathbf{W}_{p1}^T \mathbf{R}_{gr} \mathbf{W}_{p1}] \dot{\mathbf{x}}_p + [\mathbf{K}_p + \mathbf{W}_{p1}^T \mathbf{K}_{gr} \mathbf{W}_{p1}] \mathbf{x}_p = \\ \quad = +\mathbf{W}_{p1}^T \{ \mathbf{R}_{gr} \mathbf{W}^T \boldsymbol{\phi} \dot{\mathbf{q}}_s + \mathbf{K}_{gr} \mathbf{W}^T \boldsymbol{\phi} \mathbf{q}_s \} \end{cases} \quad (37)$$

$$\begin{cases} \ddot{\mathbf{q}}_s + \hat{\mathbf{R}}_s \dot{\mathbf{q}}_s + \hat{\mathbf{K}}_s \mathbf{q}_s = -\boldsymbol{\phi}^T \mathbf{W} \mathbf{f}^{act} + \boldsymbol{\phi}^T \mathbf{W} \{ \mathbf{R}_{gr} \mathbf{W}_{p1} \dot{\mathbf{x}}_p + \mathbf{K}_{gr} \mathbf{W}_{p1} \mathbf{x}_p \} \\ \mathbf{M}_p \ddot{\mathbf{x}}_p + \hat{\mathbf{R}}_p \dot{\mathbf{x}}_p + \hat{\mathbf{K}}_p \mathbf{x}_p = \mathbf{W}_{p1}^T \{ \mathbf{R}_{gr} \mathbf{W}^T \boldsymbol{\phi} \dot{\mathbf{q}}_s + \mathbf{K}_{gr} \mathbf{W}^T \boldsymbol{\phi} \mathbf{q}_s \} \end{cases}$$

Below, the matrix expressions of the last passage of Eq.(37) are reported:

$$\begin{aligned} \hat{\mathbf{R}}_s &= \tilde{\mathbf{R}}_s + \boldsymbol{\phi}^T \mathbf{W} \mathbf{R}_{gr} \mathbf{W}^T \boldsymbol{\phi} \\ \hat{\mathbf{K}}_s &= \boldsymbol{\lambda} + \boldsymbol{\phi}^T \mathbf{W} \mathbf{K}_{gr} \mathbf{W}^T \boldsymbol{\phi} \\ \hat{\mathbf{R}}_p &= \mathbf{R}_p + \mathbf{W}_{p1}^T \mathbf{R}_{gr} \mathbf{W}_{p1} \\ \hat{\mathbf{K}}_p &= \mathbf{K}_p + \mathbf{W}_{p1}^T \mathbf{K}_{gr} \mathbf{W}_{p1} \end{aligned} \quad (38)$$

State Space Formulation

In the following a *State Space* description of the system of equations (Eq.(37)) is reported [56]. Such an approach allows the reduction of the differential order from two to one, making enough a single integration to solve the time state description. To do that, two auxiliary identities was utilized, second and fourth row respectively:

$$\begin{cases} \ddot{\mathbf{q}}_s = -\widehat{\mathbf{R}}_s \dot{\mathbf{q}}_s - \widehat{\mathbf{K}}_s \mathbf{q}_s - \boldsymbol{\Phi}^T \mathbf{W} \mathbf{f}^{act} + \boldsymbol{\Phi}^T \mathbf{W} \{ \mathbf{R}_{gr} \mathbf{W}_{p1} \dot{\mathbf{x}}_p + \mathbf{K}_{gr} \mathbf{W}_{p1} \mathbf{x}_p \} \\ \dot{\mathbf{q}}_s = \dot{\mathbf{q}}_s \\ \ddot{\mathbf{x}}_p = -\mathbf{M}_p^{-1} \widehat{\mathbf{R}}_p \dot{\mathbf{x}}_p - \mathbf{M}_p^{-1} \widehat{\mathbf{K}}_p \mathbf{x}_p + \mathbf{M}_p^{-1} \mathbf{W}_{p1}^T \{ \mathbf{R}_{gr} \mathbf{W}^T \boldsymbol{\Phi} \dot{\mathbf{q}}_s + \mathbf{K}_{gr} \mathbf{W}^T \boldsymbol{\Phi} \mathbf{q}_s \} \\ \dot{\mathbf{x}}_p = \dot{\mathbf{x}}_p \end{cases} \quad (39)$$

Such system can be rewritten in matrix form as

$$\begin{bmatrix} \ddot{\mathbf{q}}_s \\ \dot{\mathbf{q}}_s \\ \ddot{\mathbf{x}}_p \\ \dot{\mathbf{x}}_p \end{bmatrix} = \begin{bmatrix} -\widehat{\mathbf{R}}_s & -\widehat{\mathbf{K}}_s & \mathbf{0} & \mathbf{0} \\ \mathbf{I} & \mathbf{0} & \mathbf{0} & \mathbf{0} \\ \mathbf{0} & \mathbf{0} & -\mathbf{M}_p^{-1} \widehat{\mathbf{R}}_p & -\mathbf{M}_p^{-1} \widehat{\mathbf{K}}_p \\ \mathbf{0} & \mathbf{0} & \mathbf{I} & \mathbf{0} \end{bmatrix} \begin{bmatrix} \dot{\mathbf{q}}_s \\ \mathbf{q}_s \\ \dot{\mathbf{x}}_p \\ \mathbf{x}_p \end{bmatrix} + \begin{bmatrix} \mathbf{0} & \mathbf{0} & \boldsymbol{\Phi}^T \mathbf{W} \mathbf{R}_{gr} \mathbf{W}_{p1} & \boldsymbol{\Phi}^T \mathbf{W} \mathbf{K}_{gr} \mathbf{W}_{p1} \\ \mathbf{0} & \mathbf{0} & \mathbf{0} & \mathbf{0} \\ \mathbf{M}_p^{-1} \mathbf{W}_{p1}^T \mathbf{R}_{gr} \mathbf{W}^T \boldsymbol{\Phi} & \mathbf{M}_p^{-1} \mathbf{W}_{p1}^T \mathbf{K}_{gr} \mathbf{W}^T \boldsymbol{\Phi} & \mathbf{0} & \mathbf{0} \\ \mathbf{0} & \mathbf{0} & \mathbf{0} & \mathbf{0} \end{bmatrix} \begin{bmatrix} \dot{\mathbf{q}}_s \\ \mathbf{q}_s \\ \dot{\mathbf{x}}_p \\ \mathbf{x}_p \end{bmatrix} + \begin{bmatrix} -\boldsymbol{\Phi}^T \mathbf{W} \\ \mathbf{0} \\ \mathbf{0} \\ \mathbf{0} \end{bmatrix} \mathbf{f}^{act}$$

As can be noticed, the first and the second term of the right-hand side have the same state vector $[\dot{\mathbf{q}}_s, \mathbf{q}_s, \dot{\mathbf{x}}_p, \mathbf{x}_p]^T$. Therefore, they can be collected in a unique term/matrix:

$$\begin{bmatrix} \ddot{\mathbf{q}}_s \\ \dot{\mathbf{q}}_s \\ \ddot{\mathbf{x}}_p \\ \dot{\mathbf{x}}_p \end{bmatrix} = \begin{bmatrix} -\widehat{\mathbf{R}}_s & -\widehat{\mathbf{K}}_s & \boldsymbol{\Phi}^T \mathbf{W} \mathbf{R}_{gr} \mathbf{W}_{p1} & \boldsymbol{\Phi}^T \mathbf{W} \mathbf{K}_{gr} \mathbf{W}_{p1} \\ \mathbf{I} & \mathbf{0} & \mathbf{0} & \mathbf{0} \\ \mathbf{M}_p^{-1} \mathbf{W}_{p1}^T \mathbf{R}_{gr} \mathbf{W}^T \boldsymbol{\Phi} & \mathbf{M}_p^{-1} \mathbf{W}_{p1}^T \mathbf{K}_{gr} \mathbf{W}^T \boldsymbol{\Phi} & -\mathbf{M}_p^{-1} \widehat{\mathbf{R}}_p & -\mathbf{M}_p^{-1} \widehat{\mathbf{K}}_p \\ \mathbf{0} & \mathbf{0} & \mathbf{I} & \mathbf{0} \end{bmatrix} \begin{bmatrix} \dot{\mathbf{q}}_s \\ \mathbf{q}_s \\ \dot{\mathbf{x}}_p \\ \mathbf{x}_p \end{bmatrix} + \begin{bmatrix} -\boldsymbol{\Phi}^T \mathbf{W} \\ \mathbf{0} \\ \mathbf{0} \\ \mathbf{0} \end{bmatrix} \mathbf{f}^{act} \quad (40)$$

The sizes of the above matrices are below reported:

$$\begin{aligned} \ddot{\mathbf{q}}_s, \dot{\mathbf{q}}_s, \mathbf{q}_s: & (N \times 1) \\ \ddot{\mathbf{x}}_p, \dot{\mathbf{x}}_p, \mathbf{x}_p: & (2m \times 1) \\ \boldsymbol{\Phi}: & (n \times N) \\ \widehat{\mathbf{R}}_s, \widehat{\mathbf{K}}_s: & (N \times N) \\ \mathbf{M}_p, \widehat{\mathbf{R}}_p, \widehat{\mathbf{K}}_p: & (2m \times 2m) \\ \mathbf{R}_{gr}, \mathbf{K}_{gr}: & (m \times m) \\ \mathbf{W}: & (n \times m) \\ \mathbf{W}_{p1}: & (m \times 2m) \\ \mathbf{f}^{act}: & (m \times 1) \end{aligned} \quad (41)$$

$$\left. \begin{aligned} n: & \text{ number of the points in which the structure is discretized;} \\ m: & \text{ number of pedestians present on the structure;} \\ N: & \text{ number of considered modes.} \end{aligned} \right\}$$

As can be observed, in Eq.(40) are present different null and identity matrices, $\mathbf{0}$ and \mathbf{I} respectively. Their sizes change as a function of neighbouring matrices to match the spaces.

Eq. (40) can finally be written in State Space matrices form [56], Eq.(42), through the definition of the State Space vector: $\mathbf{z} = [\dot{\mathbf{q}}_s, \mathbf{q}_s, \dot{\mathbf{x}}_p, \mathbf{x}_p]^T$.

$$\dot{\mathbf{z}} = \mathbf{A} \mathbf{z} + \mathbf{B} \mathbf{u} \quad (42)$$

which is the *State Equation* of the coupled Human-Structure system. Here, \mathbf{u} is equal to \mathbf{f}^{act} , and the \mathbf{A} and \mathbf{B} matrices are below extendedly reported.

$$\mathbf{A} = \begin{bmatrix} -\hat{\mathbf{R}}_s & -\hat{\mathbf{K}}_s & \boldsymbol{\phi}^T \mathbf{W} \mathbf{R}_{gr} \mathbf{W}_{p1} & \boldsymbol{\phi}^T \mathbf{W} \mathbf{K}_{gr} \mathbf{W}_{p1} \\ \mathbf{I} & \mathbf{0} & \mathbf{0} & \mathbf{0} \\ \mathbf{M}_p^{-1} \mathbf{W}_{p1}^T \mathbf{R}_{gr} \mathbf{W}^T \boldsymbol{\phi} & \mathbf{M}_p^{-1} \mathbf{W}_{p1}^T \mathbf{K}_{gr} \mathbf{W}^T \boldsymbol{\phi} & -\mathbf{M}_p^{-1} \hat{\mathbf{R}}_p & -\mathbf{M}_p^{-1} \hat{\mathbf{K}}_p \\ \mathbf{0} & \mathbf{0} & \mathbf{I} & \mathbf{0} \end{bmatrix}$$

$$\mathbf{B} = \begin{bmatrix} -\boldsymbol{\phi}^T \mathbf{W} \\ \mathbf{0} \\ \mathbf{0} \\ \mathbf{0} \end{bmatrix}$$

In order to obtain the State Space vector \mathbf{z} , the integration of *State Equation* must be performed. It is noted that the State Space matrices \mathbf{A} and \mathbf{B} of Eq.(42) are constant for a given configuration of pedestrians on the structure. Taking advantage from that, as it was explained at the end of the Section 2.3.1, is possible to split the integration time every time that a pedestrian moves. In such a way, a set of constant State Space matrices \mathbf{A} and \mathbf{B} can be obtained for any configuration assumed by the pedestrians on the structure (i.e. a series of LTI systems instead of a LTV system). Therefore, by means of a start and stop integration technique, such that in any integration time interval the *State Equation* results a LTI system, applying every time as initial State Space vector \mathbf{z}_0 , that is the State Space state \mathbf{z} reached at the end of the previous integration time interval, the integration of the *State Equation* can be performed.

Once that the integration of the of the *State Equation* has bene performed, and so the State Space vector \mathbf{z} is known, the extraction of the required information remains to be executed. It is noted that when it is said that the State Space vector \mathbf{z} is known, that means that the time history of each of its element is known for the whole simulation/integration time (which is made by all the integration time intervals). Therefore, henceforth, when it is spoken about vectors, such as \mathbf{z} , \mathbf{x}_s and \mathbf{q}_s , they are meant as their time histories along the whole integration time.

Coming back to the extraction, in case that the structure displacement state vector \mathbf{x}_s would be the desired output information, as it is, the *Observation Equation* of the State Space HSI system would be

$$\mathbf{x}_s = \mathbf{Cz} = \begin{bmatrix} \mathbf{0} & \boldsymbol{\phi} & \mathbf{0} & \mathbf{0} \end{bmatrix} \begin{bmatrix} \dot{\mathbf{q}}_s \\ \mathbf{q}_s \\ \dot{\mathbf{x}}_p \\ \mathbf{x}_p \end{bmatrix} \quad (43)$$

The sizes of the State Space matrices are in the following reported:

$$\begin{aligned} \dot{\mathbf{z}}, \mathbf{z}: & ((2N + 4m) \times 1) \\ \mathbf{A}: & ((2N + 4m) \times (2N + 4m)) \\ \mathbf{B}: & ((2N + 4m) \times m) \\ \mathbf{f}^{act}: & (m \times 1) \\ \mathbf{C}: & (n \times (2N + 4m)) \end{aligned} \quad (44)$$

It is to be pointed out that, once the State Space vector \mathbf{z} is obtained by integration of the *State Equation* (Eq. (42)), the modal coordinates of the structure \mathbf{q}_s are known too, as they are contained in \mathbf{z} . Moreover, from their knowledge it is possible to come back to the physical coordinates of the structure \mathbf{x}_s by means of the eigenvector matrix $\boldsymbol{\phi}$, Eq.(32) (from this comes the definition of the State Space matrix \mathbf{C} of Eq.(43)). However, the points of the structure at which the displacements are known (i.e. the elements of the state vector of the structure \mathbf{x}_s) are function of the points of the structure in which the mode shapes of the structure are known. Therefore, it is theoretically possible to use two eigenvector matrices:

- one in the *State Equation* (Eq.(42)): Φ
- and one in the *Observation Equation* (Eq.(45)): $\tilde{\Phi}$

$$\mathbf{x}_s = \mathbf{Cz} = [\mathbf{0} \quad \tilde{\Phi} \quad \mathbf{0} \quad \mathbf{0}] \begin{bmatrix} \mathbf{q}_s \\ \mathbf{q}_s \\ \dot{\mathbf{x}}_p \\ \mathbf{x}_p \end{bmatrix} \quad (45)$$

This can be desired as the eigenvector matrix Φ utilized in the *State Equation* must be necessarily the one containing the mode shapes of the structure evaluated at the points that can be assumed by the pedestrians during the simulation (see Section 3.3.4 for more details). Instead, the eigenvector matrix $\tilde{\Phi}$ utilized in the *Observation Equation* can be different, since the modal coordinates \mathbf{q}_s are known. Indeed, the information about the weight that each mode has in the global response of the structure, for every time instance, is present in them, regardless the points taken to describe the mode shapes. Therefore, mode shapes of the structure evaluated at different points, for example, at the ones in which the response of the structure is desired, can be used.

Now that the displacement time histories of the structure are known (i.e. \mathbf{x}_s), the final step is to perform a double time derivation of them, in order to obtain the acceleration time histories of the structure (i.e. $\ddot{\mathbf{x}}_s$) for the simulated HSI scenario. This passage was required, since the final aim of the simulation is the estimation of the acceleration levels reached.

In the following two Sections are introduced concerning the AGRFs (\mathbf{f}^{act}) and the PGRFs (2DOF systems representing the apparent masses) which are used in Model 1.

2.3.3 Apparent Mass

Conversely to Model 0, in which it was performed the spreading of the overall pedestrian apparent masses [2], in Model 1 the passive contribution of each person is individually modeled through his/her apparent mass and properly applied in time and space.

Since the apparent mass changes with the position assumed during walking, an average approach is utilized in Model 1. Indeed, instead of continuously change the apparent mass (passive contribution/PGRF) of a pedestrian during the single footstep, a mean apparent mass representing the positions assumed during the single footstep is implemented. Moreover, a visual motion study was performed to identify the most significant positions assumed during the single footstep, and for each of them, the corresponding apparent mass was identified. Finally, an averaging of these last was performed, obtaining the one that is utilized in Model 1.

However, since the structure which was consider for the experimental studies was a staircase, further considerations on the apparent mass were necessary. Indeed, the apparent mass strongly depends on the position assumed by the human body, and the positions assumed by the body during the ascent and the descent of a staircase are different. For this reason, the aforementioned mean apparent mass identification was done for both the crossing direction of the staircase: ascent and descent.

Not only, always by visual motion analysis, it was seen that for the ascending stroke the way in which the steps are crossed can significantly change, not only among different people but also with the same subject. Moreover, the main difference is due what part of the foot enters in contact with the steps. Two cases was observed. In the first one, the crossing of the step was performed with the tip of the foot only. Instead, in the second one, the heel of the foot entered in contact with the step too. No significant variations were observed for the descent. To mitigate the matter, the apparent mass curves for the ascending positions were measured for both the configurations: the “heel” one and the “tiptoe” one.

As the apparent mass contribution was synthesized and made interacting with the Model through a 2DOF mechanical system, a final fitting stage of the measured apparent mass curves, by means of the 2DOF systems, was performed.

A more detailed description of the procedures followed for the identification of the passive contribution will be illustrated in Section 3.2, as well as for the active contribution in Section 3.3, which will be shortly introduced in the next Section.

2.3.4 Active Force

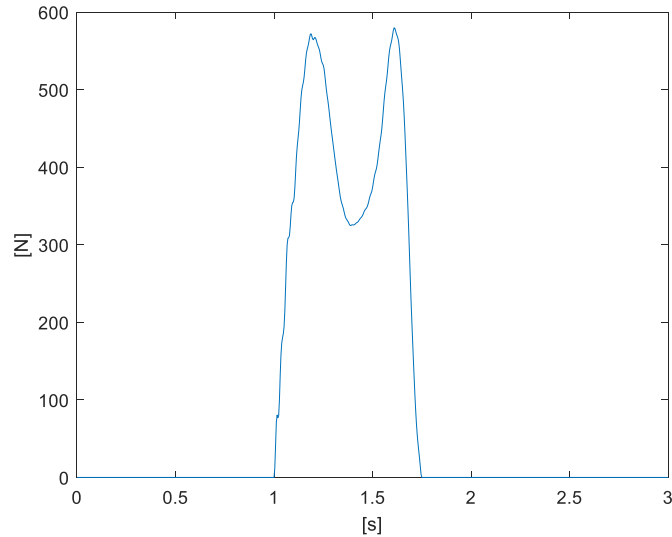


Fig. 5: Active force exerted by a pedestrian during the ascent of a staircase.

For what concerns the active contributions exerted by pedestrians (\mathbf{f}^{act}) during walking, one active force time history $f^{act}(t)$ (Fig. 5) is applied on each step crossed by a pedestrian. Therefore, the time required to each person to cross a step depends on the length of the active force time histories and, since a set of them was experimentally acquired for each person, it change every time.

As was introduced in the previous Section for the apparent mass, since the considered structure is a staircase, the human body behavior changes if an ascending stroke or a descending one is considered. For this reason, during the experimental stage, the active force time histories were recorded for both the crossing directions and coherently applied during the simulations. Not only, given the intrinsic natural variability of the human behavior (intra-subject variability), 10 active force time histories per subject were recorded for each direction, distinguishing also between the left and the right foot. A total number of 40 time histories per subject were obtained (10 acquisitions \times 2 feet \times 2 directions).

At the so built up active force database of each people was then added additional active force time histories coming from an already existing database. This was done for two main reasons. First, because of the low number of subjects involved (5 in this thesis). Hence, as the pre-existing database had been built up with a greater subject variability, with such an addition, a greater inter-subject variability (variability among subjects) was possible here too. Second, because of the intra-subject variability (variability of the same subject). Indeed, also if 40 time histories were acquired per person, they were acquired in a short time interval, just the one required for their acquisition. However, it is clear that two active force profiles of the same person measured at short time distance are more similar with respect to two measured at different times of the day. For example, two measured at 3 min of distance and two measured one in morning and one in the afternoon. This is due to a tiredness factor.

Summing up, the extra time histories were added to the database of active forces of each subject to both increase the intra and the inter subject variability. It is to be pointed out that the low number of subjects involved (5 people) was due to the time required to the subjects to take part to all the experiments. Indeed, any subject took part to all of three experimental sections to evaluate the active forces, the apparent mass curves and the real staircase test campaign, with the second one performed at the campus of Lecco of Politecnico di Milano.

As the aim of the present work is to investigate the improvement in the estimation of the vibration levels as the complexity of the model used for the description of the HSI increases, the overlap time that occurs between two consecutive footsteps is considered in Model 2. In Model 1 instead, as its main innovation is the introduction of a moving passive contribution, the additional complexity concerning the overlap time of the footsteps was discarded, utilising a simple start and stop approach. That means that as soon as the foot of a pedestrian ends its active force time history over a step, the next active force time history is done stated on the next step of the staircase (Fig. 6), along with the translation of the apparent mass (2DOF system) from the previous step (node of the structure) to the new one. Of course, this is an approximation with respect to what it really happens. However, such an approximation it is not so strong, since the overlap time is of the order of 0.1 s for normal walking (as the analysed cases are) and because of the magnitude of the active force at its beginning and ending, where the overlap takes place, it is not so high in magnitude.

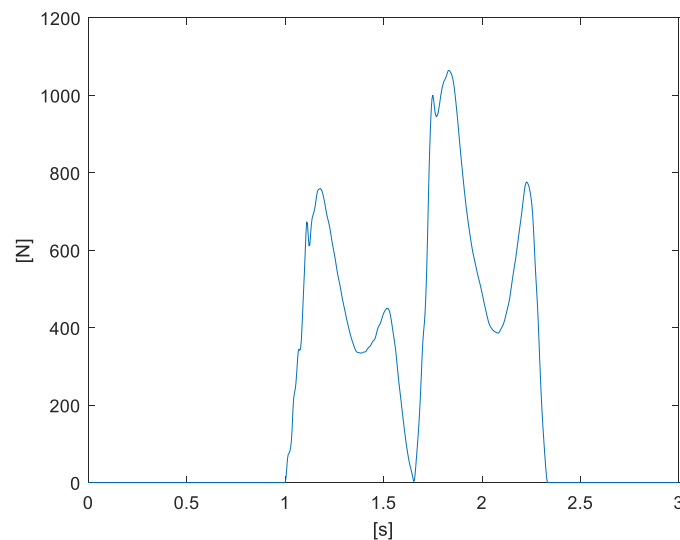


Fig. 6: Active forces exerted in Model 1 on two consecutive different steps by a pedestrian during the descent of a staircase.

2.4 Model 2

As the main improvement of Model 1 is the introduction of moving passive contributions by means of 2DOF systems that schematize the apparent mass of each subject, the further complexity accounted in Model 2, with respect to Model 1, is the introduction of the overlap time between two consecutive footsteps. Indeed, as was aforementioned, a time exists in which both the feet are in contact with the ground during the walking act, Fig. 7 and Fig. 8. Such time results function of the activity (walking, jogging and running), and it becomes always less as the speed increases, up to its negative value (separated steps) for running (e.g. [43]). However, in the analysed cases, at the subjects were asked to freely walk. As will be shown in the next Sections, the effect of the overlap time is accounted both from an active and from a passive point of view.



Fig. 7: Sequence of the ascent of a staircase to show the overlap of the two feet during the step transition.

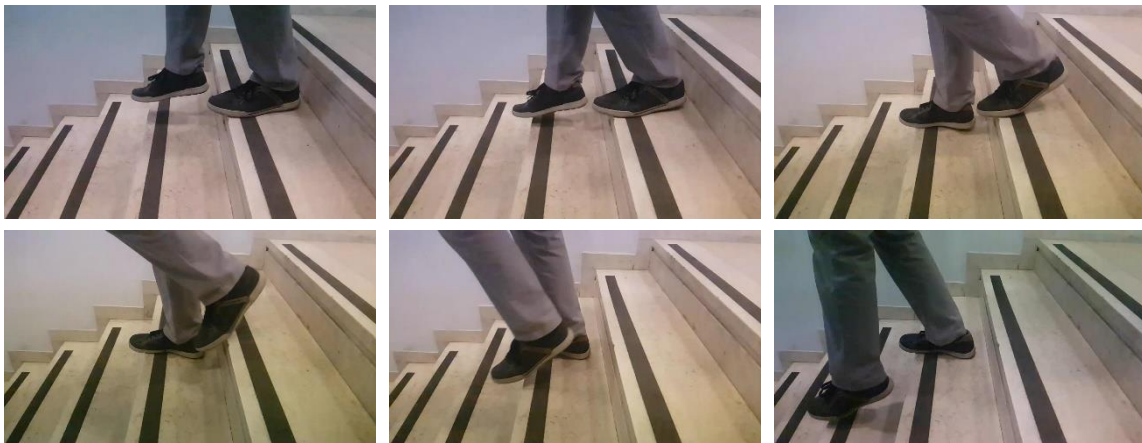


Fig. 8: Sequence of the descent of a staircase to show the overlap of the two feet during the step transition.

In the following, a Section concerning the selection of the overlap time is reported, then a dissertation about how the active and passive contributions (AGRFs and PGRFs respectively) are treated in Model 2 is shown.

2.4.1 Overlap Study

[ms]	ascent	descent
subject 1	134	88
	133	83
	121	104
subject 2	135	59
	127	89
	122	59
subject 3	124	75
	119	83
	115	81
mean	126	80

Table 1: Overlap time for the ascent and descent of a staircase of different subjects.

In order to quantify the time that the two feet spent together in contact with the ground/structure, a visual motion analysis was conducted. The optical device for the acquisition of the images was a slow-motion camera (resolution: 220-240 Frames Per Second). The tests were conducted for both the ascent and the descent of a staircase, leaving the subjects free to walk at his/her own speed. The analysis showed as average overlap time of 80 ms for the descent and of 126 ms for the ascent, Table 1.

Given the order of magnitude and the small difference between them (46 ms), an intermediate value of 100 ms was selected for both the ascending and the descending direction. Such an assumption was rebutted by preliminary simulations of a pedestrian who crosses the staircase one time and that continuously crosses the staircase in a closed loop for 5 min, imposing in turn 100 ms (the approximated intermediate value between the ones for the ascent and the descent) and 125 ms (the approximated value for the ascent). The results were evaluated in terms of the vibration levels reached by the staircase (i.e. $[\text{ms}^{-2}]$ RMS). They showed that using a mean overlap time of 100 ms leads to a difference of 3.9% and of 7% with respect to the case with 125 ms, for the one-stroke and for the 5 min loop simulation respectively. It is be put in evidence that, a greater overlap time means a greater amount of energy introduced into the structure, since the time interval in which two active forces excite the structure together increases. Therefore, the results obtained with an overlap time equal to 125 ms, for both ascent and descent of the staircase, overestimate the vibration levels, especially in the long simulation (pedestrian locked in a loop for 5 min). Indeed, in such a scenario, once that the simulation time is set, an higher number of steps are allowed with a high overlap time with respect to a lower one.

In conclusion, given the obtained results, the assumption made on the overlap time were consider acceptable and a value equal to 100 ms was imposed in Model 2 for both the crossing directions (ascent and descent).

2.4.2 Apparent Mass

Looking at the apparent mass, even it is influenced by the overlap time that occurs between two subsequent footsteps. Moreover, the mechanical parameters of the 2DOF system, which schematizes the passive pedestrian contribution, are left unchanged. What is changed in Model 2 is the interaction that the 2DOF system undertakes with the structure during such time interval. Remember that the apparent mass (2DOF system) takes the ground/structure acceleration as input and gives back the corresponding Passive Ground Reaction Force to be applied to the structure. Therefore, in the middle of a footstep, when only a foot is in contact with the structure and no overlap with the previous or the next footstep occurs, the interaction of the 2DOF system with the structure is the same of Model 1. During the overlap phase, instead, the thing changes. Indeed, since now the body is in contact with two steps, the 2DOF system is placed in contact with two steps of the staircase as well. Hence, the mechanical system now sees as input the accelerations of the old step and new step. However, given the linearity of the 2DOF system, the output PGRF would be the same given by the sum of two PGRFs obtained by putting a 2DOF system on each of the two steps of the staircase. Of course, this is different from what really happens. To mitigate such issue, the output PGRF of the so placed 2DOF system (in contact with both the new step and the old one) is halved. This allows to obtain an output PGRF proportional to the presence of only one pedestrian. The final thing to do is the repartition of the PGRF among the two steps, since both of them have participated to its creation. Thus, the PGRF is applied half on one step and half on the other one. This is equivalent to place half 2DOF system on the old step and half on the new one, which is exactly what happens in reality with the human body, when a person places one leg on a step and the other leg on the next step.

Thus, in this way is possible to account not only for the overlap of the active force time histories, but it is also possible to reproduce the transition of the apparent mass between two footsteps, without involving any change of apparent mass and so of the mechanical parameters of the 2DOF system. This last further complexity will be instead introduced in Model 3, where a change of apparent mass inside the same footstep will be used, allowing to account for the apparent mass footstep transition.

2.4.3 Active Force

For what concern the Active Ground Reaction Forces (AGRFs), the same active force database of Model 1 is used, which distinguishes between ascending and descending crossing direction, and between right and left foot of each subject (Section 2.3.4). The difference here, with respect to Model 1 is the introduction of the overlap time between two consecutive footsteps, which was set equal to 100 ms, as illustrated in Section 2.4.1. That means that once the active force time history of a pedestrian is at 100 ms from its end, the new active force time history of the next footstep on the next step starts, Fig. 9. In this way, it is possible to account for the overlap of the two footsteps from an active force point of view.

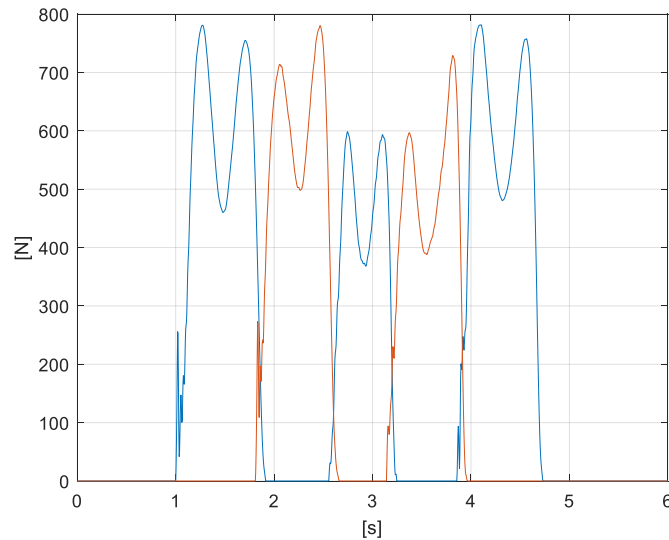


Fig. 9: Active force time histories of a pedestrian treated by Model 2, who goes upstairs five steps with an overlap time of 100ms, in blue the right foot, in red the left foot.

2.4.4 Mathematical Model

To introduce the shown variations of AGRF and PGRF in the equations of the Model, some adjustment was required with respect to the ones of Model 1. First of all, the matrix \mathbf{W} , Eq.(27). As explained in Section 2.3.2, it allows to account for the presence of each pedestrian on the staircase and of his/her specific position on it. In fact, at each pedestrian vector contained in \mathbf{W} (i.e. \mathbf{w}_k), is associated a Boolean value of 1 in correspondence of the pedestrian position, while the remaining part of the vector remains equal to zero, Eq.(28) (\mathbf{w}_k has size $n \times 1$, with n the number of DOF of the structure). In Model 2 instead, a value of 0.5 is assigned in \mathbf{w}_k at the corresponding step/node position of the structure, when a pedestrian is at the end of the previous step and at the beginning of the new one. This is the transition phase, with both the feet in contact with the structure, Eq.(46). To distinguish between the auxiliary matrix (and its pedestrian vectors contained in it) of Model 1 and Model 2, a tilde is placed on the Model 2 ones (i.e. Model 1: \mathbf{W} made by \mathbf{w}_k / Model 2: $\tilde{\mathbf{W}}$ made by $\tilde{\mathbf{w}}_k$). Nevertheless, the usual Boolean unit value is set when the pedestrian is in the middle of a footstep (i.e. on one leg only) leading to have $\tilde{\mathbf{w}}_k$ equal to \mathbf{w}_k (Eq.(28)).

$$\tilde{\mathbf{w}}_k = [0 \quad \dots \quad 0 \quad 0.5 \quad 0.5 \quad 0 \quad \dots \quad 0]^T \quad (46)$$

Another change concerns the application of the active force time histories. In fact, during the overlap time of a person, two active forces are applied to the structure by him/her (see the overlaps between the blue and red curves in Fig. 9). To deal with this issue, the active force vector \mathbf{f}^{act} size is doubled, passing from $(m \times 1)$ to $(2m \times 1)$, leading to the active force vector named $\tilde{\mathbf{f}}^{act}$. In this way, the application of two force time histories per person is ensured (i.e. the blue ones and the red ones of Fig. 9). Of course, both the slots of a person result occupied only during the overlap time of the footsteps (e.g. at 1.9 s of the Fig. 9; one slot occupied by the instantaneous blue curve line value and the other slot by the instantaneous red curve line value). A unique non-empty slot remains instead when no overlap it is present and the pedestrian is on one step only. Now that the active force vector matter is settled, a consequent adjustment of the matrix which allows its interaction with the size of the other matrices in the dynamic equations is required. In Model 1 this matrix was \mathbf{W} , Eq.(27). However, such a matrix is present in different points of the dynamic equations (Eq.(30) or Eq.(40)) to match the dimensions of the other matrices, since it is an auxiliary matrix (note that in Model 2 the dynamic equations are the same of Model 1 but they have $\tilde{\mathbf{W}}$ instead of \mathbf{W} , as explained above). Therefore, an ad hoc matrix \mathbf{W}_f is introduced for \mathbf{f}^{act} only. In it, a pair of columns is associated to a pair of slots of the active force vector. Moreover, one of the two columns assumes a unit Boolean value at the proper position only when the corresponding slot of the active force vector is non-empty.

Essentially the matrix \mathbf{W}_f has double columns with respect to $\tilde{\mathbf{W}}$, and it works with Boolean numbers only, while $\tilde{\mathbf{W}}$ utilizes also 0.5 in the overlap instants. An example is reported for clarity in case of a staircase made by three steps is considered (therefore the matrices $\tilde{\mathbf{W}}$ and \mathbf{W}_f have three rows) with a person placed once on the second step (Fig. 10) and once in transition phase between the second and third step (Fig. 11), while another person is always present on the first step without overlap (i.e. always 2 people present on the structure, so $\tilde{\mathbf{W}}$ and \mathbf{W}_f have 2 and 2×2 columns respectively).

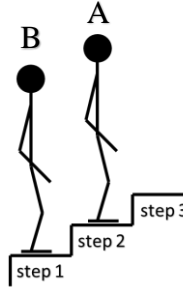
$$\tilde{\mathbf{W}} = \begin{array}{c} \begin{array}{cc} \text{A} & \text{B} \\ \begin{bmatrix} 0 \\ 1 \\ 0 \end{bmatrix} & \begin{bmatrix} 1 \\ 0 \\ 0 \end{bmatrix} \\ \text{A} & \text{B} \end{array} \\ \mathbf{W}_f = \begin{array}{cc} \begin{bmatrix} 0 & 0 \\ 1 & 0 \\ 0 & 0 \end{bmatrix} & \begin{bmatrix} 0 & 1 \\ 0 & 0 \\ 0 & 0 \end{bmatrix} \end{array}$$


Fig. 10: Matrices \mathbf{W} and \mathbf{W}_f for a pedestrian on the first step and one on the second step of a three-steps staircase.

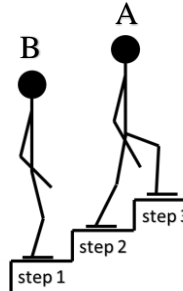
$$\tilde{\mathbf{W}} = \begin{array}{c} \begin{array}{cc} \text{A} & \text{B} \\ \begin{bmatrix} 0 \\ 0.5 \\ 0.5 \end{bmatrix} & \begin{bmatrix} 1 \\ 0 \\ 0 \end{bmatrix} \\ \text{A} & \text{B} \end{array} \\ \mathbf{W}_f = \begin{array}{cc} \begin{bmatrix} 0 & 0 \\ 1 & 0 \\ 0 & 1 \end{bmatrix} & \begin{bmatrix} 0 & 1 \\ 0 & 0 \\ 0 & 0 \end{bmatrix} \end{array}$$


Fig. 11 : Matrices \mathbf{W} and \mathbf{W}_f for a pedestrian on the first step and one in transition between the second and third step of a three-steps staircase.

Given the adjustments performed, the *State Equation* becomes:

$$\begin{bmatrix} \ddot{\mathbf{q}}_s \\ \dot{\mathbf{q}}_s \\ \ddot{\mathbf{x}}_p \\ \dot{\mathbf{x}}_p \end{bmatrix} = \begin{bmatrix} -\hat{\mathbf{R}}_s & -\hat{\mathbf{R}}_s & \boldsymbol{\phi}^T \tilde{\mathbf{W}} \mathbf{R}_{gr} \mathbf{W}_{p1} & \boldsymbol{\phi}^T \tilde{\mathbf{W}} \mathbf{K}_{gr} \mathbf{W}_{p1} \\ \mathbf{I} & \mathbf{0} & \mathbf{0} & \mathbf{0} \\ \mathbf{M}_p^{-1} \mathbf{W}_{p1}^T \mathbf{R}_{gr} \tilde{\mathbf{W}}^T \boldsymbol{\phi} & \mathbf{M}_p^{-1} \mathbf{W}_{p1}^T \mathbf{K}_{gr} \tilde{\mathbf{W}}^T \boldsymbol{\phi} & -\mathbf{M}_p^{-1} \hat{\mathbf{R}}_p & -\mathbf{M}_p^{-1} \hat{\mathbf{K}}_p \\ \mathbf{0} & \mathbf{0} & \mathbf{I} & \mathbf{0} \end{bmatrix} \begin{bmatrix} \dot{\mathbf{q}}_s \\ \mathbf{q}_s \\ \dot{\mathbf{x}}_p \\ \mathbf{x}_p \end{bmatrix} + \begin{bmatrix} -\boldsymbol{\phi}^T \mathbf{W}_f \\ \mathbf{0} \\ \mathbf{0} \\ \mathbf{0} \end{bmatrix} \tilde{\mathbf{f}}^{act} \quad (47)$$

2.5 Model 3

Model 3 is the last one advanced by the present thesis. Summarizing, Model 1 introduces the handling of the passive pedestrian contributions, so that both the active and the passive components can be moved coherently with pedestrians along the structure. From it, a further complexity, given by the consideration of the overlap of the footsteps during the walking of a pedestrian, is implemented in Model 2. Now, in order to evaluate the effect of each single added complexity, in the modelization of the HSI phenomenon, on the estimation of the vibration level, the next improvement in the HSI modeling is applied starting from Model 1, instead of Model 2. Indeed, Model 3 is exactly the same of Model 1, less than the way in which the apparent mass is treated. In Model 1, in order to have a fixed apparent mass during the footstep, and so LTI system (given by the structure plus the occupants) for the time of the footstep itself, an average apparent mass of the positions assumed during the single footstep for each pedestrian is used. In Model 3 such an averaging is not performed. As introduced in Model 1, a visual motion analysis of the walking act was executed in order to identify the most significant positions, and so their apparent masses, which were averaged to obtain the one representative of the entire footstep. Now, the apparent mass of each identified position is utilized.

More in details, to properly select the positions which schematize the walking of a person, a slow-motion images analysis was used. Since the structure selected for the validation of the models was a staircase, the motion analysis was executed for people who cross a staircase as well. Furthermore, since the positions assumed during an ascending crossing are different from the ones assumed during a descending crossing, positions were identified for both the crossing directions.

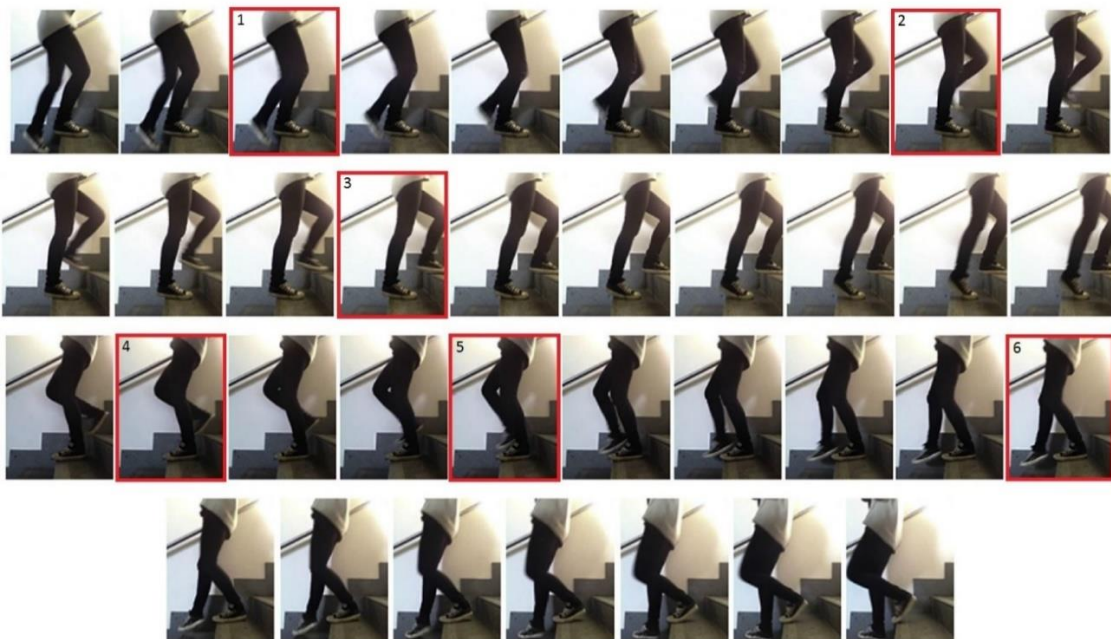


Fig. 12: Sequence of steps during the ascending and descending crossing of a staircase.

As can be observed from Fig. 12, three positions were considered significant to properly describe both the ascent (positions 1, 2 and 3) and the descent (positions 4, 5 and 6) of the staircase. It is to be pointed out that these are the positions whose apparent masses were averaged to obtain the two mean ones (one for the ascent and one for the descent) utilized in Model 1. Indeed, for each of these positions the corresponding apparent mass curve was experimentally measured (Section 3.2). Not only, as already mentioned, since it was observed that in the ascending crossing not always the heel of the foot enters in contact with the step of the staircase, the apparent masses of the ascending positions were measured for both the configurations: with the heel in contact with the ground (“heel” configuration) and with the subject on the tip of the foot (“tiptoe” configuration). Not only, even if the human body is symmetric, there are natural differences among the left and right side of it, both from a physical and from a dynamic point of view. For this reason, all the positions were measured for both feet of the subjects. Finally, a total number of 18 apparent masses were available per subject: 3 positions for the descent, 3 positions for the ascent with the heel, 3 positions for the ascent on tiptoe and each of them with the left and right foot.

Even if there are a lot of positions to deal with, there are only three of them, from a modeling point of view, since three positions were chosen. To account for them, in Model 3, the integration time of the single footstep is split in three sub intervals of integration. In this way, the change of apparent mass (by means of the mechanical parameters of the 2DOF system), inside the same footstep, is allowed, maintaining a LTI system inside the integration interval. Moreover, since the selected positions are assumed almost equally spaced in time (Fig. 12), an equal subdivision of the integration time interval of the single step was chosen (i.e. $1/3$).

Looking at the Active Ground Reaction Forces, they are applied and handled by Model 3 exactly as they are in Model 1. That means that as soon as a force time history of a footstep ends, the new force time history starts with the next footstep on the next step of the staircase, Fig. 6.

Summing up, in order to maintain a LTI system as objective of the integration, the integration time it is not only stopped and restated at each footstep ending and beginning with the proper initial conditions (i.e. the state of the system reached at the end of the previous integration interval) as it is done in Model 1, but the duration of each of the three position phases assumed in the single footstep is considered too.

Consider that: (i) a footstep lasts less than a second and (ii) that it is split in three; (iii) each footstep is different from the others (of the same person and of the other people) since its length is a consequence of the measured active force time history extracted randomly from the database; (iv) different people are present on the structure at the same time and they move all together. As a consequence, to simulate also few seconds of HIS, a lot of integration time intervals are required, since they can become very small.

Chapter 3

Inputs to the Models:

Experiments & Discussion

In this Chapter, the experiments conducted and the procedures followed for the collection of the necessary information that have been used in the numerical simulation stage are illustrated, i.e. databases containing pedestrian properties and the occupied structure characteristics. Moreover, the databases concern the active and passive contributions exerted by pedestrians when they occupy a structure, the Active Ground Reactive Forces (AGRFs) and the Passive Ground Reaction Forces (PGRFs) respectively. Even if in literature a lot of models were present with their own calibrated parameters to represent human body schematizations, the reason for which it was chosen the creation of self-made databases was the reliability of the physical data, since they would have been utilized in the proposed models for the numerical simulations. In this way, the goodness of the data was ensured, been the set-up of the tests and the data acquisition completely known. As for the structure characterization, it was a due step to have a modal description of the structure. Such an analysis was already performed by previous contributions [1,2] but it was here repeated to check that the dynamic structure characteristics were unchanged.

Therefore, in the following are dealt at first the acquisition of the active force components; then the measurement of the passive contribution exerted by the human body is treated (apparent mass); finally, the characterization of the structure, which is utilized for the experiments aimed to validate the proposed numerical Models, is faced.

3.1 Active Force Experiments

Usually, the force exerted by pedestrians at the ground is most of the times modeled though a Fourier series, both in literature (e.g. [15,18,23]) and by regulations (e.g. [4,16,25,27]). Indeed, they report the Dynamic Load Factors (DLFs) for the Fourier series as a function of the pedestrian activity (walking, jogging or running) and weight, in such a way a perfect periodic exciting profile in time is obtained. However, in this way it is neglected the intra-subject variability [57,58], since no change in two consecutive steps is contemplated. Not only, the Fourier series description of the walking force implicitly joins the contributions of the two feet, since it describes the overall active force time history, Fig. 13.

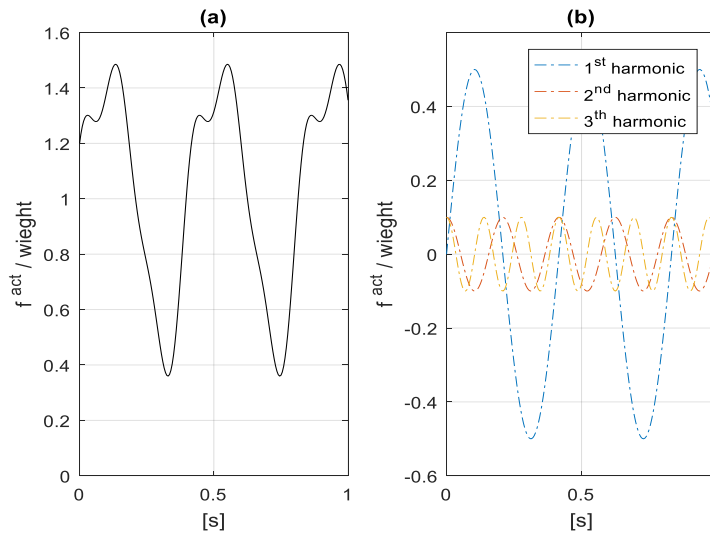


Fig. 13: Vertical active force (a) advised by regulation [51] computed as the summation of the first three harmonics (b) obtained by the Dynamic Load Factors (DLFs) and phase angles indicated for normal walking.

This condition was unacceptable for the present work, as the main objective of the experiments was a staircase. Indeed, a Fourier series approach would have prevented the possibility to apply to every step crossed from a pedestrian only one force time history exerted by the single foot, since it describes the overall time history (i.e. left and right foot time histories together). Of course, such problem would have been faced even if a footboard (so no steps of stair involved) would be considered as structure. However, in that contest (i.e. flat surface), the contribution of the two feet can be acceptably approximated to a unique force time history properly applied along the pedestrian path. This is what is usually done when the Fourier series description is adopted, and it is considered acceptable since the position of the sequence of footsteps of a person is reasonably approximated by a straight sequence of footsteps. To mitigate the matter, it was preferred to directly measure the exerted forces. To do that, a dedicated set-up was utilized.

Furthermore, given the great variability of the active force released by just a single walking pedestrian, it was chosen to add to the collected active forces of each involved subject a set of active forces coming from a previous active force database, which was utilized in the previous work [2]. In such a way, possible intra-subject variabilities didn't catch in the sequence of the here recorded active force time histories were theoretically artificially accounted for, leading to an increase of the robustness of the Models.

3.1.1 Experimental Set-up

In order to collect the active forces released by pedestrians during walking, a suited set-up was implemented. Since the experiments dealt with a staircase as occupied structure, the main arrangement of the experimental set-up was made by two wooden steps and on the first of them it was placed a force plate. The overall apparatus was then located at the end of a real stair case, Fig. 14. This configuration was chosen to allow to the tested subject to pass over the force plate as if it was a normal continuance of the real staircase. For the same reason, the second wooden step was posed after the one with the force plate.

The force plate was made by a thick steel palate connected to the ground through four load cells (HBM model Z6FD1, sensitivity: $981\text{N} \cong 2.00 \text{ mV/V}$, full-bridge). They were fed and conditioned (standard conditioning for strain gauge bridge) by a conditioning unit (HBM model Scout 5). The processed signals were then collected by personal computer via a National Instruments acquisition board (model NI 9239).

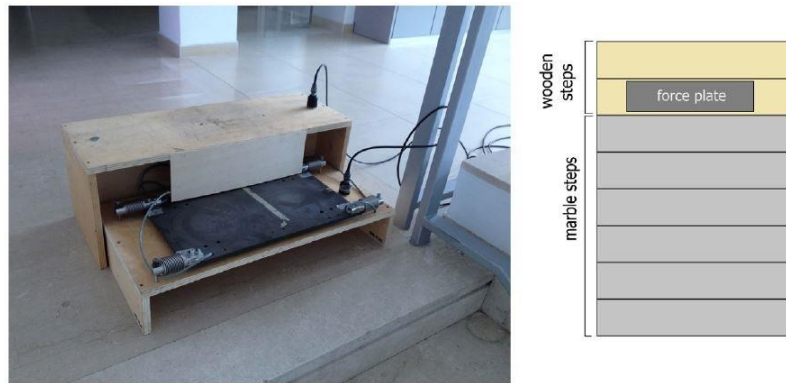


Fig. 14: Experimental set-up to measure the active force.

It is worth to recall that the active and passive contribution splitting of a pedestrian was theoretically allowed by the different interaction with the ground that occurs in both of them (Section 1.2.2). In fact, an infinitely rigid ground is assumed in the active interaction, while a deformable surface is considered in the passive interaction. For this reason, the force plate was designed such that the vibration of the plate itself was negligible for many tents of Hz, working in quasi-static condition. Indeed, the first mode of the plate was around 60 Hz., while the multiple harmonics of the active force profile barely reaches 10 Hz. However, a low pass-eighth order filter, with a cut off frequency of 25 Hz, was utilized to post-process the active force time histories recorded.

3.1.2 Tests

The tests were performed on the set-up described in the previous Section, and it involved 5 subject, 4 males and 1 female. The limited number of people was due to a lack of availability of volunteers, as the subjects had to take part to all three experimental sessions (active force acquisition, apparent mass measurement and staircase test campaign). However, as previously introduced, to all the subjects was added an additional set of active forces coming from a previous existing database. In this way, not only it was possible to artificially increase the intra subject variability, but also the inter one was really augmented. As for the measurement of the exact intra subject variability, it was asked to each person to cross the stair ten times. Moreover, a distinction between the left and right foot was also made to maximize the possible intra-variability of the single pedestrian. Not only, since the behavior of the human body changes if considered in an ascending or descending crossing of the staircase (as well as it was mentioned in Section 2.2.3 for the passive contribution), it was asked to the pedestrians to walk in both the directions too. A database with 200 active force time histories was obtained in the end (5 subjects, ascending and descending direction, two feet, 10 test per case), which was extended with the contribution of the already existing one (288 active force time histories).

3.1.3 Results

In this Section, the measured active forces of the subjects involved in the experiments are reported, which were collected as specified in the previous Section. As was mentioned, 5 people took part at the tests. Their weights are reported in Table 2.

subject	1	2	3	4	5
gender	male	male	female	male	male
weight [kg]	85	90	55	80	70

Table 2: List of subjects involved in the experiments.

It is to be recalled that one of the reason for which it was utilised a home-made database was the possibility to account for the intra and inter subject variability of the active profile with respect to its mathematical description, Fig. 13. About that, in Fig. 15 are reported all the tests undertaken by subject 1, split by direction and by foot, along with the corresponding average values for the four combinations (dashed red lines). As can be noticed, both the ascending and descending direction have two main lobes, which are more evident in the ascent. This phenomenon is due to the transition between the heel and the tip of the foot. Indeed, at the beginning of the footstep, a sudden increase of the force transmitted to the ground occurs, with a magnitude greater than the weight force, due to the addition of the dynamics of the body. Instead, in the middle of the footstep, such contribution decreases, to increase again, a little more than in the first part, in the final step instant. This last is due to force exerted to the ground necessary to reaccelerate the body to proceed with walking. Conversely, looking at the descent, the first lobe assumes a value greater than the second one and greater than the ones involved in the ascent (a direct comparison of the mean values of these last cases is shown in Fig. 16). Such trend can be explained by the fact that during the descent there is a phase in the middle of the step change in which the body is left to be accelerated by the gravity. As result, a much higher force would be exerted to stop the motion. Indeed, such a high contribution is not present for the ascent, when the gravitational field is constantly against, and so a softer transition between steps is allowed.

A comparison between the right and left foot is depicted in Fig. 17. As for the ascent, the mean behavior of the right and left foot is almost identical, while a small variation is present in the initial part for the descent. Nevertheless, such variability it is a natural aspect of the human walking activity, and it was accounted, since these curves are utilized in the simulation stage of the Models.

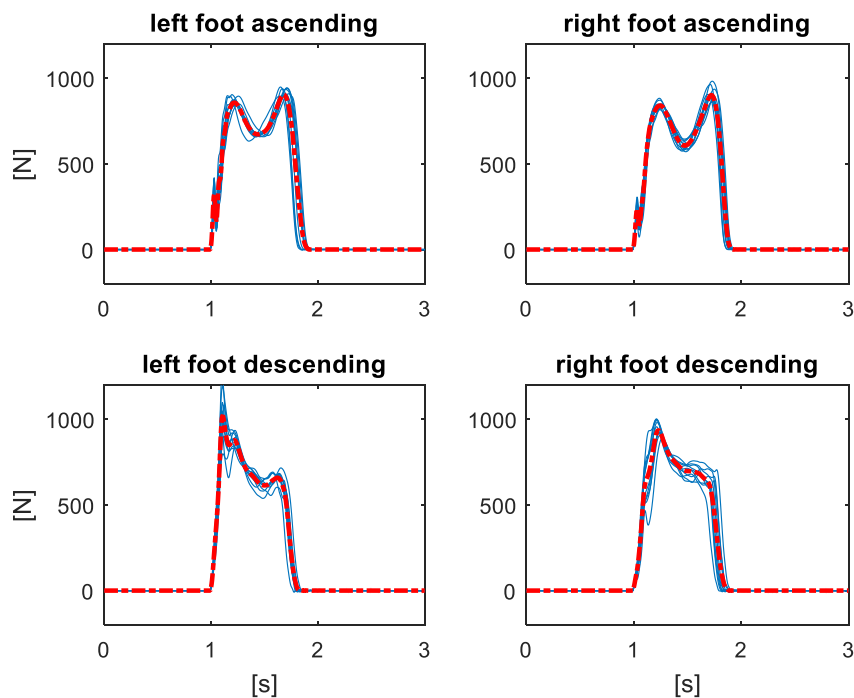


Fig. 15: Measured active forces (ten tests per foot and direction) of subject 1 with their mean values (red dashed line) evaluated with the starting points of the active force time histories aligned.

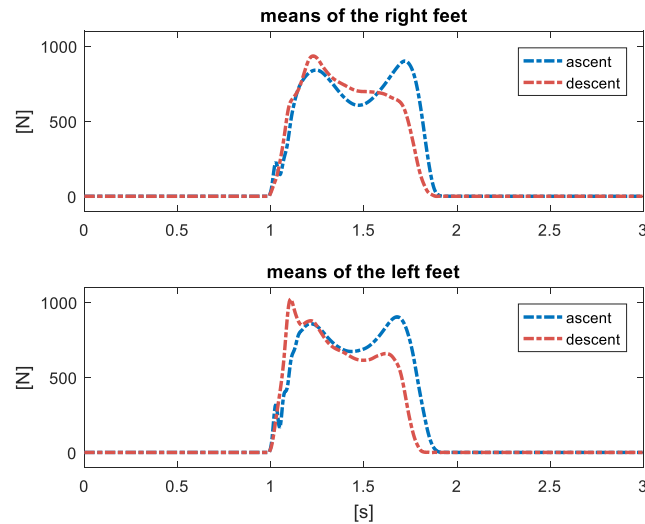


Fig. 16: Comparison of the average ascending and descending active forces per foot of subject 1.

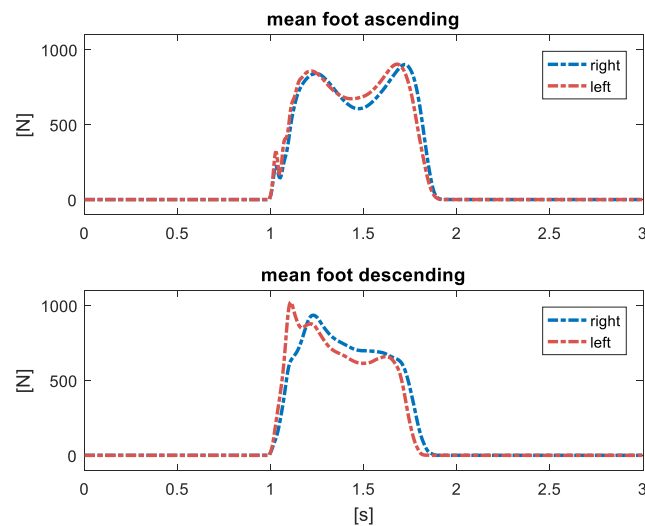


Fig. 17: Comparison of the average left and right foot in the ascending and descending direction of subject 1.

3.2 Passive Force Experiments

In the present work, the interaction with the body dynamics (passive contribution) was accounted through its apparent mass (Eq.(1)). The apparent mass depends on many factors: (a) the subject considered (inter-subject variability), (b) his posture, and (c) the amplitude of vibrations involved. Moreover:

- as for the inter-subject variability, the apparent mass depends on the characteristics of the person;
- the posture was found to have a high influence on the apparent mass;
- the vibration magnitude was found to have a smaller relevance, as also shown in [1] for the case of still people (i.e. only passive contribution present).

In the present dissertation, the passive contribution (see Section 1.2.1) of the human body was accounted through a 2DOF mechanical system, as assumed by Matsumoto et al. [32,33] and adopted

by others [34,36,38]. As was done for the active contribution, an experimental database for the passive components of pedestrians was created as well. Such a choice has been a consequence of the need of properly describe the variation of the human body properties, and so of its apparent mass, as the position along the single step, during walking, changes. Not only, a lack in literature concerning the modelization of pedestrians who cross stairs and the relative parameters was found.

For these reasons, a study of the body motion of pedestrians who cross staircase was conducted with the identification of the main positions assumed. Whereupon, a characterisation of these positions, by means of their apparent masses, was performed for each subject involved. Finally, in order to use these information in the HSI Models, a series of fitting by 2DOF models were performed, whose parameters were then easily incorporated in the HSI dynamical equations (Eq.(30) or Eq.(40)) to account for the passive presence of crossing occupants.

In the following, the above listed steps to incorporate the passive pedestrian contribution are detailed. At first, a mathematical treatment of the apparent mass to obtain its Transfer Function expression, that will be utilized in the fitting stage, is presented. Then, it follows a description of the set-up used for the apparent mass measurements and a description of the performed tests. Finally, the post-processing data analyses are illustrated, along with their interpolation by the apparent mass model and its parameters extraction.

3.2.1 2DOF Transfer Function

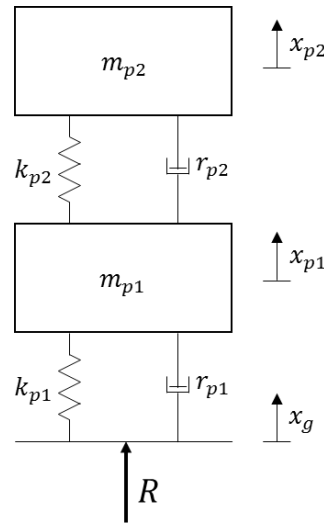


Fig. 18: 2DOF system schematization of the human body apparent mass.

The apparent mass $M_a(j\omega)$ is defined in the frequency domain as the ratio between the force released by a mechanical system when it is subjected to an input acceleration and the input acceleration itself, Eq.(1). In our case this ratio is between the force released on the structure and the acceleration of the structure itself. Bearing in mind that a 2DOF mechanical system was chosen to represent the $M_a(j\omega)$, Fig. 18, whose dynamic description is reported in the following, [56]:

$$\begin{cases} m_{p2}\ddot{x}_{p2} + r_{p2}\dot{x}_{p2} + k_{p2}x_{p2} = -m_2g + r_{p2}\dot{x}_{p1} + k_{p2}x_{p1} \\ m_{p1}\ddot{x}_{p1} + (r_{p1} + r_{p2})\dot{x}_{p1} + (k_{p1} + k_{p2})x_{p1} = -m_1g + r_{p2}\dot{x}_{p2} + k_{p2}x_{p2} + r_{p1}\dot{x}_g + k_{p1}x_g \\ 0 = R + r_{p1}(\dot{x}_{p1} - \dot{x}_g) + k_{p1}(x_{p1} - x_g) \end{cases} \quad (48)$$

where m_{p1} , m_{p2} , r_{p1} , r_{p2} , k_{p1} , k_{p2} are the mechanical parameters of the equivalent 2DOF system of the apparent mass. R represents the Passive Ground Reaction Force due to the 2DOF system (i.e. passive pedestrian contribution) and g is the acceleration of gravity. While x_{p1} , x_{p2} are the two

free coordinates of the 2DOF system and x_g is the free coordinate of the ground (i.e. the structure). It is possible to express the free coordinates starting from the static equilibrium position of the system (Eq.(49)), which can be obtained putting the system in static conditions (i.e. $[\ddot{x}_{p2}, \ddot{x}_{p1}, \dot{x}_{p2}, \dot{x}_{p1}, \dot{x}_g]^T = \underline{0}$). Furthermore, the ground static position was set equal to zero (i.e. $x_g = 0$). An overbar was introduced into the equations to underline that the static configuration was dealt.

$$\begin{cases} k_{p2}\bar{x}_{p2} = -m_{p2}g + k_{p2}\bar{x}_{p1} \\ (k_{p1} + k_{p2})\bar{x}_{p1} = -m_{p1}g + k_{p2}\bar{x}_{p2} + k_{p1}\bar{x}_g \\ 0 = R + k_{p1}(\bar{x}_{p1} - \bar{x}_g) \\ \bar{x}_g = 0 \end{cases} \quad (49)$$

$$\begin{cases} \bar{x}_{p1} = -(m_{p1} + m_{p2})g/k_{p1} \\ \bar{x}_{p2} = \bar{x}_{p1} - m_{p2}g/k_{p2} = -(m_{p1} + m_{p2})g/k_{p1} - m_{p2}g/k_{p2} \\ R = (m_{p1} + m_{p2})g \\ \bar{x}_g = 0 \end{cases}$$

Rewriting the dynamic equations of the system starting from the static equilibrium position just identified in Eq. (49) (i.e. setting the zeros of x_{p1} , x_{p2} and x_g equal to \bar{x}_{p1} , \bar{x}_{p2} and \bar{x}_g respectively), the system of equations is now free from the gravitational terms:

$$\begin{cases} m_{p2}\ddot{x}_{p2} + r_{p2}\dot{x}_{p2} + k_{p2}x_{p2} = r_{p2}\dot{x}_{p1} + k_{p2}x_{p1} \\ m_{p1}\ddot{x}_{p1} + (r_{p1} + r_{p2})\dot{x}_{p1} + (k_{p1} + k_{p2})x_{p1} = r_{p2}\dot{x}_{p2} + k_{p2}x_{p2} + r_{p1}\dot{x}_g + k_{p1}x_g \\ 0 = R + r_{p1}(\dot{x}_{p1} - \dot{x}_g) + k_{p1}(x_{p1} - x_g) \end{cases} \quad (50)$$

Now a shift to the frequency domain will be executed, since the apparent mass is defined per frequency: $M_a(j\omega)$, Eq.(1). To do that, the Fourier Transform \mathfrak{F} of the involved quantities is executed:

$$\begin{aligned} \mathfrak{F}(x_{p2}(t)) &= X_{p2}e^{j\omega t} \\ \mathfrak{F}(\dot{x}_{p2}(t)) &= j\omega X_{p2}e^{j\omega t} \\ \mathfrak{F}(\ddot{x}_{p2}(t)) &= -\omega^2 X_{p2}e^{j\omega t} \\ \mathfrak{F}(x_{p1}(t)) &= X_{p1}e^{j\omega t} \\ \mathfrak{F}(\dot{x}_{p1}(t)) &= j\omega X_{p1}e^{j\omega t} \\ \mathfrak{F}(\ddot{x}_{p1}(t)) &= -\omega^2 X_{p1}e^{j\omega t} \\ \mathfrak{F}(x_g(t)) &= X_g e^{j\omega t} \\ \mathfrak{F}(\dot{x}_g(t)) &= j\omega X_g e^{j\omega t} \\ \mathfrak{F}(R(t)) &= R_0 e^{j\omega t} \end{aligned} \quad (51)$$

Where the right-hand sides of Eq. (51) represent the left-hand side arguments in the frequency domain, with X_{p2} , X_{p1} , X_g and R_0 that are complex vectors and $e^{j\omega t}$ is the Euler's formula for the representation of the unit module vector rotating at the angular velocity ω in the complex plane. Therefore, by means of the Fourier Transform, Eq.(50) becomes Eq.(52), cancelling out the exponential terms $e^{j\omega t}$, since they are common to all the equation addenda.

$$\begin{cases} (-\omega^2 m_{p2} + j\omega r_{p2} + k_{p2})X_{p2} = (j\omega r_{p2} + k_{p2})X_{p1} \\ (-\omega^2 m_{p1} + j\omega(r_{p1} + r_{p2}) + (k_{p1} + k_{p2}))X_{p1} = (j\omega r_{p2} + k_{p2})X_{p2} + (j\omega r_{p1} + k_{p1})X_g \\ 0 = R_0 + (j\omega r_{p1} + k_{p1})(X_{p1} - X_g) \end{cases} \quad (52)$$

From equation (I) of Eq.(52) it is possible to express X_{p2} as a function of X_{p1} :

$$X_{p2} = \frac{(j\omega r_{p2} + k_{p2})}{(-\omega^2 m_{p2} + j\omega r_{p2} + k_{p2})} X_{p1}$$

which once replaced in equation (II) of Eq.(52) erases X_{p2}

$$\begin{aligned} & (-\omega^2 m_{p1} + j\omega(r_{p1} + r_{p2}) + (k_{p1} + k_{p2}))X_{p1} = \\ & = (j\omega r_{p2} + k_{p2}) \left\{ \frac{(j\omega r_{p2} + k_{p2})}{(-\omega^2 m_{p2} + j\omega r_{p2} + k_{p2})} X_{p1} \right\} + (j\omega r_{p1} + k_{p1})X_g \end{aligned}$$

$$\left\{ (-\omega^2 m_{p1} + j\omega(r_{p1} + r_{p2}) + (k_{p1} + k_{p2})) - \frac{(j\omega r_{p2} + k_{p2})^2}{(-\omega^2 m_{p2} + j\omega r_{p2} + k_{p2})} \right\} X_{p1} = (j\omega r_{p1} + k_{p1})X_g$$

writing X_{p1} as a function of X_g

$$X_{p1} = \frac{(j\omega r_{p1} + k_{p1})}{(-\omega^2 m_{p1} + j\omega(r_{p1} + r_{p2}) + (k_{p1} + k_{p2})) - \frac{(j\omega r_{p2} + k_{p2})^2}{(-\omega^2 m_{p2} + j\omega r_{p2} + k_{p2})}} X_g$$

and replacing it in equation (III) of Eq.(52) erases X_{p1}

$$R_0 = (j\omega r_{p1} + k_{p1})(X_g - X_{p1})$$

$$R_0 = (j\omega r_{p1} + k_{p1}) \left\{ 1 - \frac{(j\omega r_{p1} + k_{p1})}{(-\omega^2 m_{p1} + j\omega(r_{p1} + r_{p2}) + (k_{p1} + k_{p2})) - \frac{(j\omega r_{p2} + k_{p2})^2}{(-\omega^2 m_{p2} + j\omega r_{p2} + k_{p2})}} \right\} X_g$$

re-arranging the terms

$$\frac{R_0}{X_g} = \frac{-\omega^2 (j\omega r_{p1} + k_{p1}) (m_{p1} (-\omega^2 m_{p2} + j\omega r_{p2} + k_{p2}) + m_{p2} (j\omega r_{p2} + k_{p2}))}{(-\omega^2 m_{p1} + j\omega(r_{p1} + r_{p2}) + (k_{p1} + k_{p2})) (-\omega^2 m_{p2} + j\omega r_{p2} + k_{p2}) - (j\omega r_{p2} + k_{p2})^2} \quad (53)$$

Finally, it is enough to divide for $-\omega^2$ in order to pass from *dynamic stiffness (force / displacement)*, Eq.(53), to *apparent mass (force / acceleration)*, Eq.(54).

$$\frac{R_0}{-\omega^2 X_g} = \frac{(j\omega r_{p1} + k_{p1}) (m_{p1} (-\omega^2 m_{p2} + j\omega r_{p2} + k_{p2}) + m_{p2} (j\omega r_{p2} + k_{p2}))}{(-\omega^2 m_{p1} + j\omega(r_{p1} + r_{p2}) + (k_{p1} + k_{p2})) (-\omega^2 m_{p2} + j\omega r_{p2} + k_{p2}) - (j\omega r_{p2} + k_{p2})^2}$$

$$\frac{R_0}{-\omega^2 X_g} = M_a(j\omega) \quad (54)$$

It is worth to notice that the extended expression of the previous equation allows to link the mechanical parameters of the chosen 2DOF system with the apparent mass. Indeed, such expression was used to fit the experimental $M_a(j\omega)$ curves collected during the experimental campaign, as it will be illustrated in Section 3.2.4.

It is also to be pointed out that the apparent masses were defined with respect to their static equilibrium positions, Eq.(49), as it was introduced in Section 2.2.1. This was done since the load cells used to acquire the forces released by pedestrians (PGRFs) during the apparent mass experiments were made of piezoelectric material. Thus, the static component of the measured forces was automatically filtered out. The other reason was because the effect of the static weight of the subjects was already measured in the f^{act} tests (AGRFs), since load cells (Section 3.1.1), able to measure the static components, were used. Indeed, to mitigate the matter and to not double the subject weights, the 2DOF systems, representing the apparent masses of pedestrians, were applied already in equilibrium on the undeformed structure, i.e. the staircase in its unoccupied static equilibrium position. In such a way, the structure was left in its unoccupied static equilibrium position even if the 2DOF systems (i.e. the passive contribution of pedestrians) were present on it. The deformation of the structure due to the static weight of pedestrians (even if of negligible magnitude with respect to the vibration state induced) was obtained once the AGRFs were applied to the structure, as it really happens.

3.2.2 Experimental Set-Up

The experiments to collect the apparent masses of the subjects involved were carried out at the campus of Lecco of Politecnico di Milano. Since the aim were the measured apparent masses, it was required to impose the ground vibration and measure the response force released at the ground (PGRF). To do that, an electro-dynamic shaker was used (Fig. 19) to generate a ground-like vibration, imposing a random-white noise profile: vibration amplitude set to $0.25 \text{ ms}^{-2}\text{RMS}$ in a frequency range of 3.5-20 Hz. Such a frequency range was chosen as the first two significant modes of the considered structure (staircase) were both between 7 and 10 Hz (see Section 3.3.4). Moreover, from literature [32,33] and from previous works [1,2] it was evident that any frequency dynamics of the human body apparent mass already ended at 20 Hz. Instead, the lower bound was selected as the reliability of the piezoelectric load cells drastically decreases as frequencies lower than 3.5 Hz are measured. Not only, at lower frequencies the displacement of the electrodynamic shaker to which the people would have been exposed would have been so high to prevent a standing position without holding on to some handrail. Indeed, keeping a constant acceleration level, the lower is the frequency, the higher the displacement has to be. Finally, the magnitude of the displacements reached at frequencies lower than 3.5 Hz would be so high to be unrealistic with respect to the ones engaged by civil structures, at less of earthquakes.

As for the vibration amplitude, it was set equal to 0.25 ms^{-2} RMS since from previous publication [1] it was found that the selection of the amplitude of the ground vibration doesn't significantly affect the measured apparent mass curves and 0.25 ms^{-2} was among the tested amplitudes. Moreover, an increase of the vibration amplitude RMS would have been produce an unsustainable vibration level, as for the case of low frequencies at fixed acceleration level just above mentioned.

The vibration induced by the electrodynamic shaker was measured and fed back by accelerometer (B&K, model 4508B, sensitivity: 10.22 mV/ms^{-2}), while the response force released by the tested subject (PGRF) was acquired by a force plate built-up by three piezoelectric load cells (PCB, model 212, sensitivity: 4047 pC/kN), Fig. 20.



Fig. 19: Electro-Dynamic Shaker, model V875 LDS.

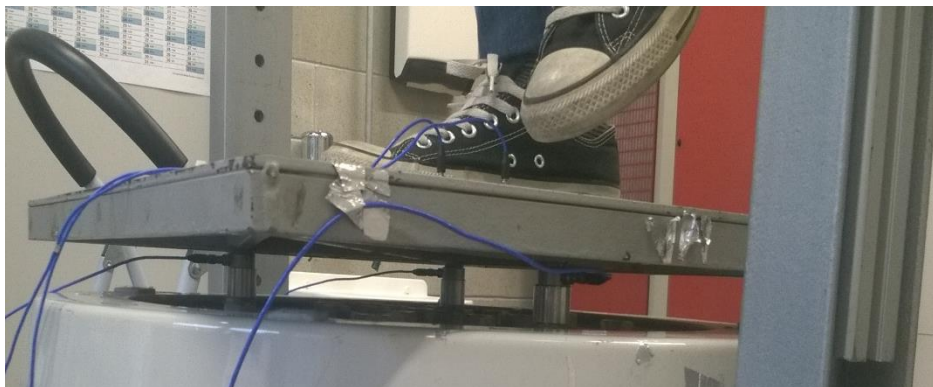


Fig. 20: Three load cell placed under the plate to form a force plate and the two accelerometers placed on it.

3.2.3 Tests

The experiments were carried out to measure the apparent mass of the people that would have been involved in the experimental campaign performed on the real structure (a staircase), and to use them in the proposed Models for the estimation of the vibration levels of the structure itself. Therefore, it was required to capture the apparent mass of each subject. The apparent mass of a person continuously change during the walking act, due to the change of the body configuration, and so of its biomechanical characteristics. Of course, it was not possible to acquire a continuous change of M_a , since the procedure to measure a single position of it (Section 3.2.2) required 2 min. For this reason, the more significant positions assumed during the walking were selected. More in detail, as the experiments involved a staircase structure, an additional variability was present, since the body configuration of a person ascending or descending a staircase are different. The selection of the positions was based on a visual motion analysis. The tests were conducted for ascending and descending crossing of the staircase, leaving the subjects free to walk at their own speed. As reported in Fig. 12, 6 positions were selected as the most significant (red squares), three for the

ascent (positions 1, 2 and 3) and three for the descent (positions 4, 5 and 6). Of course, since the walking act involves alternatively the right and left foot, each position was tested for both the feet of a subject.

Not only, after other visual motion analyses it was observed that a same person can change the way in which he/she approach the ascent of a stair, while negligible variations were noticed for the descent. Indeed, a subject can go upstairs leaning on the tip of his/her feet or by involving his/her heel as well. For this reason, it was chosen to perform the apparent mass tests for both the configurations of the ascent: with the heel and on tiptoe.

Summing up, the experiments involved 5 subjects and for each of them 9 positions of apparent masses were measured (3 descending positions per foot, 3 ascending positions with heel per foot and 3 ascending positions on tiptoe per foot). As an example, the three-ascending positions with the heel and right foot of subject 1 are reported: in Fig. 21 the first position, in Fig. 22 the second one and in Fig. 23 the third one. Instead, the three-descending positions with the right foot of subject 5 are reported: in Fig. 24 the first position, in Fig. 25 the second one and in Fig. 26 the third one. As can be noticed by Fig. 27, two supports were placed on the two sides of the shaker as sustain for the tested subject, given the amount of time spent in uncomfortable standing positions. It is worth to be mentioned that at the subjects were conceded to lean laterally only on them, in order to limit the influence on the vertical Ground Reaction Force exerted, since it was the aim of the test.

For what concerned the time length of each position tested, since the measurements were based on noise vibration of the platform, the higher the time of exposure to such a vibration would have been, the longer the final time history would have been. This leads to the possibility of a greater signal averaging, and so to a cleaner M_a curve in the frequency domain, given by the higher number of sub-time histories available. The length of the sub-time histories is a consequence of the frequency resolution imposed (0.5 Hz). Conversely, a long time would have been unsustainable by the people, especially for the 6 position on tiptoe. A time length equal to 2 min per position was finally set as a compromise, leading to an overall time of 38 min of one leg standing posture per subject over the shaker.



Fig. 21: Subject 1, first ascending position, heel contact, right foot.



Fig. 22: Subject 1, second ascending position, heel contact, right foot.



Fig. 23: Subject 1, third ascending position, heel contact, right foot.



Fig. 24: Subject 5, first descending position, right foot.



Fig. 25: Subject 5, second descending position, right foot.



Fig. 26: Subject 5, third descending position, right foot.



Fig. 27: Subject 1, second ascending position, heel contact, right foot.

3.2.4 Apparent Mass Curves

Data Processing

From the experimental stage the gathered information to assess the apparent mass were the time histories of acceleration at which the subjects were exposed to and the time histories of the response forces exerted to the ground (PGRFs) in response to such accelerations. Consider $a(t)$ the single acceleration time history which generated the single passive force time history $f(t)$. First thing, the two time histories were split in a sequence of sub-time histories of 2 sec length: $a_k(t)$ and $f_k(t)$ (with k the number of the sub-time history considered among the N ones), such that a frequency resolution equal to 0.5 Hz was obtained. Then, the Fast Fourier Transform (FFT) of the subset of input and output windowed signals was performed. The window applied was a Hanning window, as it is usually used. The cut signals in the frequency domain are: $a_k(f)$ and $f_k(f)$. For each of the sub-history k , the following Power and Cross Spectrum were evaluated:

$$G_{xy}(ndf) = \frac{1}{N} \sum_{k=1}^N \frac{X_k^*(ndf)Y_k(ndf)}{2} \quad (55)$$

$$G_{xx}(ndf) = \frac{1}{N} \sum_{k=1}^N \frac{X_k^*(ndf)X_k(ndf)}{2} \quad (56)$$

where df is the spectrum resolution (0.5 Hz), n is the counter to obtain the allowed discrete frequency f of the spectrum, given by the frequency resolution df , and $X_k(ndf)$ and $Y_k(ndf)$ stand for $a_k(f)$ and $f_k(f)$ respectively. The power * stands for the complex conjugate term.

Even if the apparent mass is defined as Eq.1, and so

$$H(f) = \frac{Y(f)}{X(f)} \quad (57)$$

such a definition of Transfer Function would account for an ideal input-output Transfer Function (TF). However, given a sequence of issues: (i) linearity of the considered system (the human body is not a linear system); (ii) problems due to bias of the signals like noise on the measurements; problems due to the signals elaboration such as (iv) sampling and (v) windowing, leading to aliasing and leakage respectively; the apparent mass TF would not be properly evaluated. To discard or reduce these problems, estimators can be used. One estimator of $H(f)$ is $H_1(f)$, which is defined as

$$H_1(f) = \frac{G_{xy}(f)}{G_{xx}(f)} \quad (58)$$

The choice was fallen on $H_1(f)$, since it works with the Cross-Spectrum $G_{xy}(f)$ at numerator. This was required since the response of the human body (i.e. PGRF/ $f(t)$) was generated by a non-linear system, as the body for its nature is. However, thanks to $G_{xy}(f)$ at numerator, the output signal $f(t)$ (i.e. $y(t)$), even if it was the result of a non-linear system, it would have been filtered out by means of complex averaging with the input spectrum of $a(t)$, (i.e. $X(f)$), leading to a kind of linearization of the body response. In this way, the best possible estimation of the apparent mass M_a was obtained.

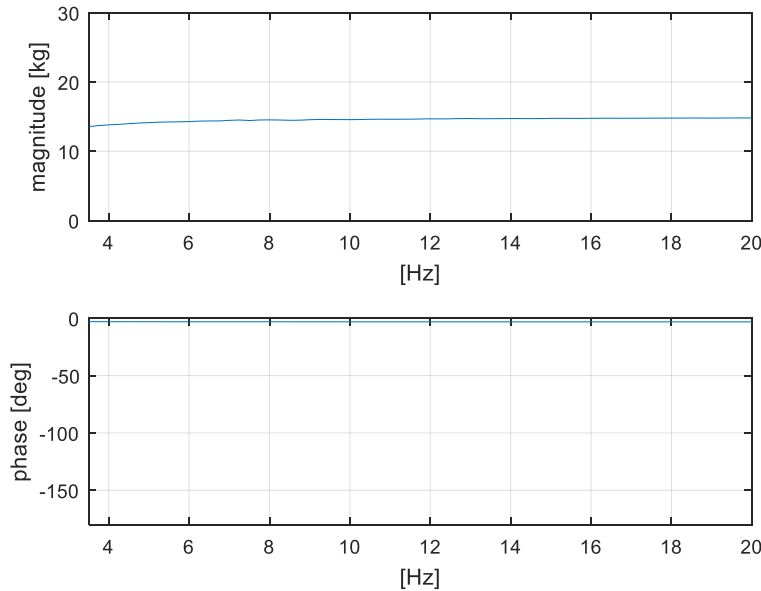


Fig. 28: Apparent mass of the empty force plate placed on the electrodynamic shaker.

Since the electrodynamic shaker was equipped with a plate, in order to allow the placement of the tested subject on it and to build up the force plate to acquire the Passive Ground Reaction Force (Fig. 19, Fig. 20), the contribution of this component had to be compensated from the measured apparent masses. To do that, an initial measurement session with no subject was performed to identify the plate contribution only. The apparent mass of the plate, which should theoretically have been a TF with module equal to the mass of the plate and null phase at any frequency, was experimentally identified and its trend confirmed (Fig. 28). More in detail, as it is depicted by the scheme in Fig. 29, the input control system supplied the input acceleration $a(t)$ (a vibration white noise profile: 0.25 ms^{-2} RMS at the accelerometer position, i.e. on the top of the plate) which excited both the person and the plate. As result, an extra contribution, given by the acceleration of the mass of the plate $f^{plate}(t) = m_{plate}a(t)$, was measured by the three piezoelectric load cells too, Eq.(59) and Eq.(60).

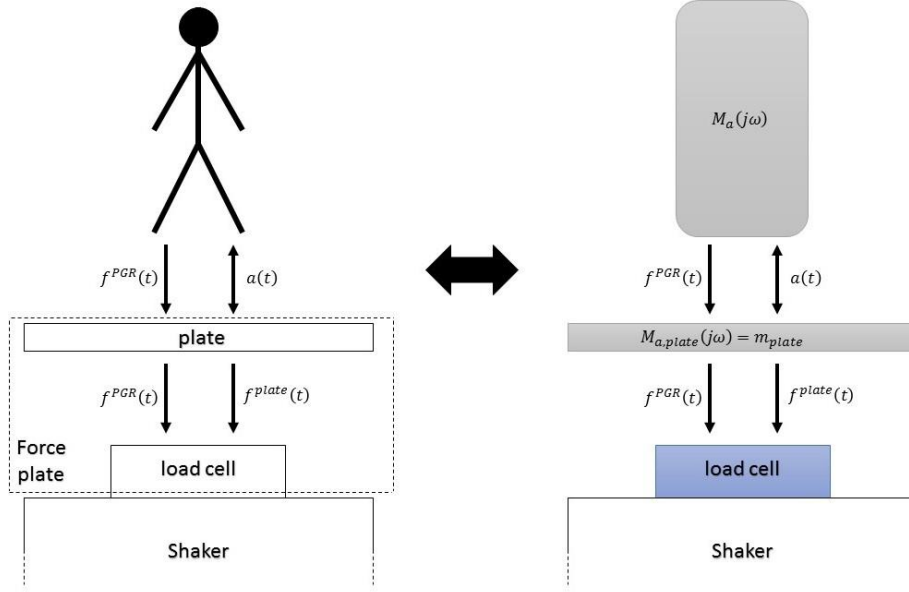


Fig. 29: Modeling of the apparent mass measurement set-up.

$$\begin{aligned} f(f) &= f^{PGR}(f) + f^{plate}(f) = M_a(f)a(f) + M_{a,plate}(f)a(f) \\ &= [M_a(f) + M_{a,plate}(f)]a(f) \end{aligned} \quad (59)$$

$$\frac{f(f)}{a(f)} = M_a(f) + M_{a,plate}(f) \quad (60)$$

$$M_a(f) = H_1(f) - M_{a,plate}(f) \quad (61)$$

Therefore, after the identification of each body apparent mass with the estimator H_1 , it was enough to compensate the TF of the plate (Fig. 28), which was a TF with magnitude equal to the mass of the plate, as reported by Eq.(61).

Fitting

At this point, being the experimental apparent mass curves known (Eq.(61)), as well as their mathematical expression for a 2DOF system schematization (Eq.(54)), a fitting of them remains to be performed. The aim was the assessment of the 2DOF mechanical parameters ($m_{p1}, m_{p2}, r_{p1}, r_{p2}, k_{p1}, k_{p2}$) of the apparent mass for each configuration and for each subject, in order to use them in the simulation stage to reproduce the passive effects of pedestrians. The fitting was executed by means of minimization (Eq.(62)) of the square error difference between the magnitude of the 2DOF model and of the experimental curve, for each position and subject in the considered frequency range, i.e. 3.5-20 Hz (Section 3.2.2). For the minimization was used an algorithm based on the *Interior-Point* method.

$$\min \left(\sum_{f=3.5\text{Hz}}^{20\text{Hz}} |\text{model}(f) - M_a(f)|^2 \right) \quad (62)$$

As an example, in the following, all the apparent masses of subject 3 with the corresponding fitted 2DOF model curves are reported (Fig. 30, Fig. 31 and Fig. 32). As can be observed, the equivalent mechanical system selected to represent the apparent mass (2DOF) well fits the experimental curves. Especially, it fits around the first two modes of the structure (1st mode at 7.81 Hz and 2nd

mode at 8.87 Hz), which are the ones used for the modal description of the structure in the simulation stage. These results confirm the fidelity of the 2DOF system to represent the human body passive contribution.

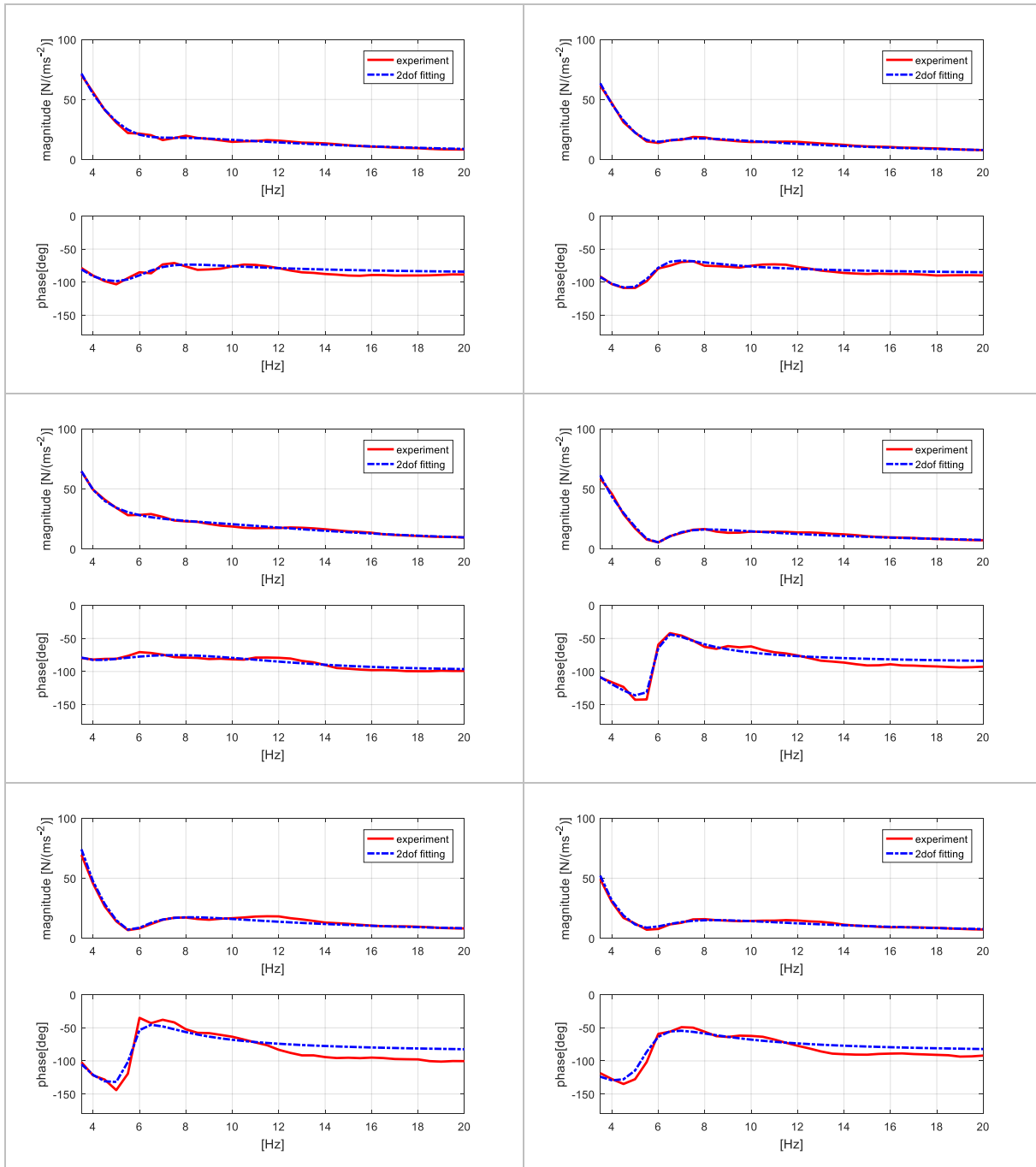


Fig. 30: Subject 3 apparent masses; ascending direction with heel; left column for the left foot and right column for the right foot; the three positions (positions 1, 2 and 3 of Fig. 12) are reported per row with descending order.

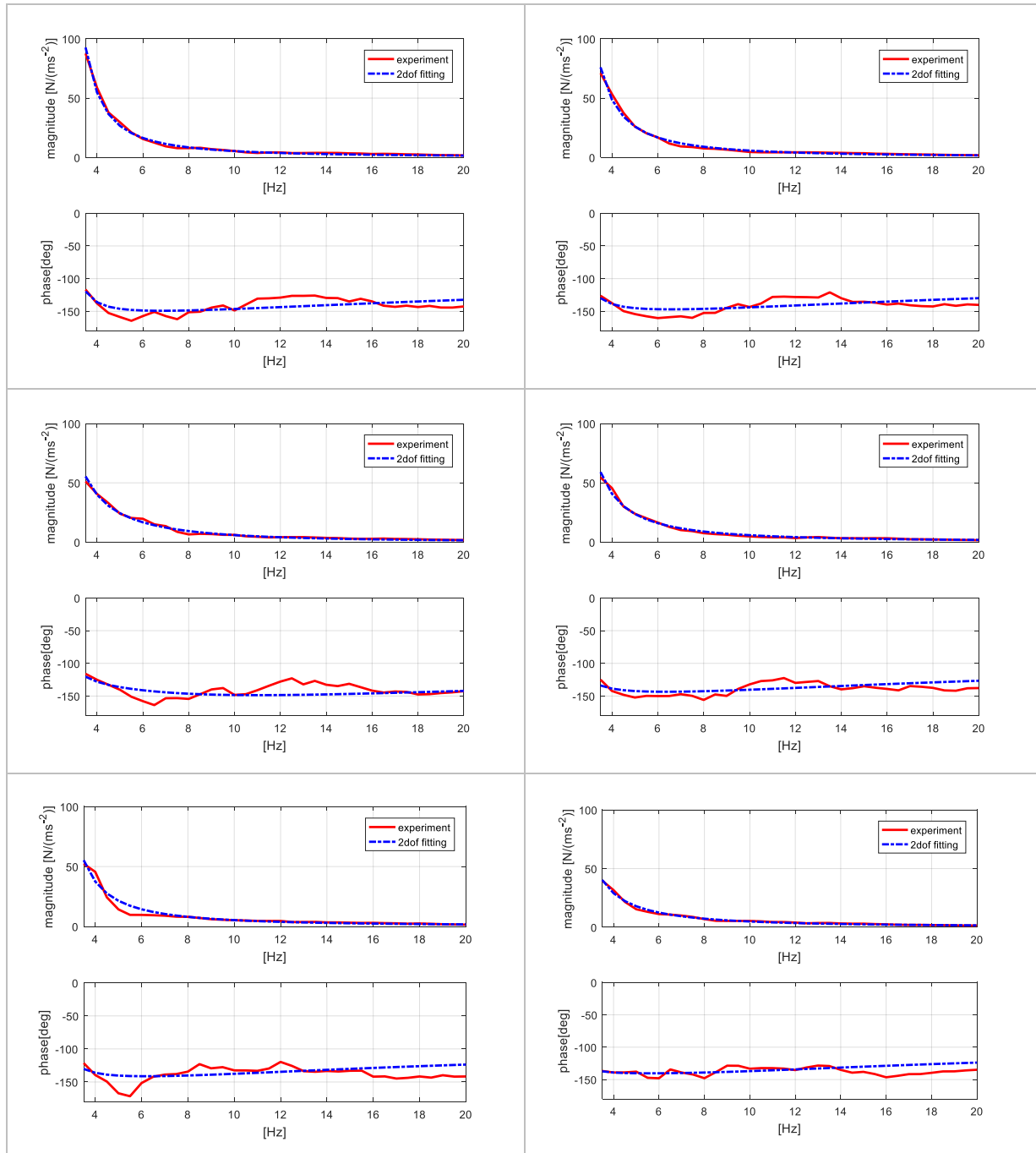


Fig. 31: Subject 3 apparent masses; ascending direction on tiptoe; left column for the left foot and right column for the right foot; the three positions (positions 1, 2 and 3 of Fig. 12) are reported per row with descending order.

Looking at Fig. 30 and Fig. 31, a comparison between the heel and the tiptoe positions is possible. Apart for a slightly faster decreasing trend of the magnitude for the curves of the tiptoe configurations, the main differences among them can be observed from the phases. Indeed, for the heel configurations, the phases become stable around 90° . While, for the tiptoe configurations, the phases tend to assume values higher than 90° , around 150° . That highlights the higher damping capability of the heel configurations with respect to the tiptoe ones.

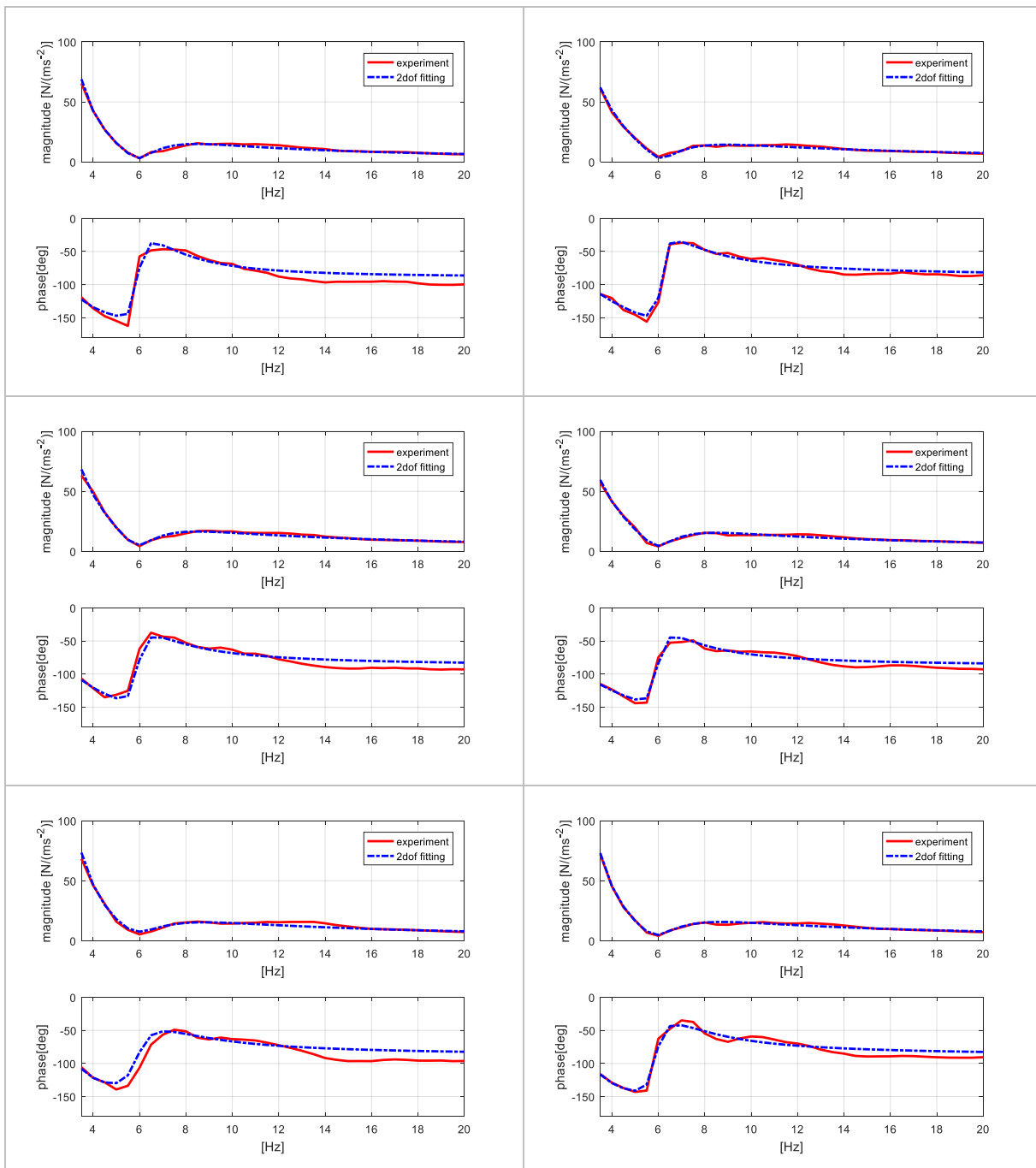


Fig. 32: Subject 3 apparent masses; descending direction; left column for the left foot and right column for the right foot; the three positions (positions 4, 5 and 6 of Fig. 12) are reported per row with descending order.

Intra and Inter Subject Variability

The experiments were performed with different subjects to take into account the inter subject variability. Nevertheless, each subject was tested for enough time (2 min per position) to have a reliable frequency trend and for both of his/her feet (Fig. 30, Fig. 31 and Fig. 32). By means of these two expedients, the intra subject variability was got too. For example, the greatest difference for subject 3 was observed between the right and left foot of the second ascending position with the foot completely in contact (heel configuration) (Fig. 30 for the apparent mass curves and Fig. 12

for the photo of the position). The intra subject variability, i.e. the 18 apparent mass curves per subject, were used in Model 3(Section 2.5), after their fitting by the 2DOF model. Indeed, it was made up to consider the change of apparent mass due to the body configurations assumed inside the same step, distinguishing between ascent and descent, and between ascent with the heel and on tiptoe. These last two matter are considered in the first two Models too.

Working the Model 1 and 2 with a unique apparent mass per step, distinguishing always between direction (ascent/descent) and style (heel/tiptoe) as just mentioned, it was required to pass from 18 apparent masses per subject to 3 apparent masses per subject (descent, ascent with heel and ascent on tiptoe). Therefore, a vector-per frequency averaging was executed on each sub set of 6 apparent masses of the 18, to obtain the 3 per subject required ones. It is to be pointed out that the three averaging were executed on the fitted apparent mass curves, that were the 2DOF model ones. The last step was the refitting of these 3 mean curves per subject with the 2DOF model to obtain their six mechanical parameters ($m_{p1}, m_{p2}, r_{p1}, r_{p2}, k_{p1}, k_{p2}$). For clarity are reported the mean curves of subject 3 for the 3 averages (Fig. 33, Fig. 34 and Fig. 35). As can be observed from pictures, the refitting by means of 2DOF model perfectly fitted.

As the proposed three Models were compared with the simpler approach proposed by Model 0 (Section 1.2), this last requires an equivalent spread apparent mass $m_{fr}(f)$ (Eq.(14)). It is obtained by dividing the total apparent mass (obtained as the mean apparent mass of the people who occupied the structure $M_{eq}(f)$ (Eq.(13)) multiplied by the number of people m) by the number of possible positions on the structure (i.e. equal to the number of DOFs of the structure: n -DOF). Since some numerical simulations were conducted with a random extraction of the subjects to be applied on the structure (Section 4.1), a fitting of their spread overall apparent mass $m_{fr}(f)$, to obtain its equivalent 2DOF model to be apply to each node of the structure n , was necessary at the beginning of each simulation. This because of the lack of knowledge of the involved subjects before of the beginning of the numerical simulation. Therefore, as soon as the pedestrians on the structure are randomly extracted, and so their apparent masses become known, the spread overall apparent mass $m_{fr}(f)$ is calculated and then fitted by 2DOF model (e.g. Fig. 36).

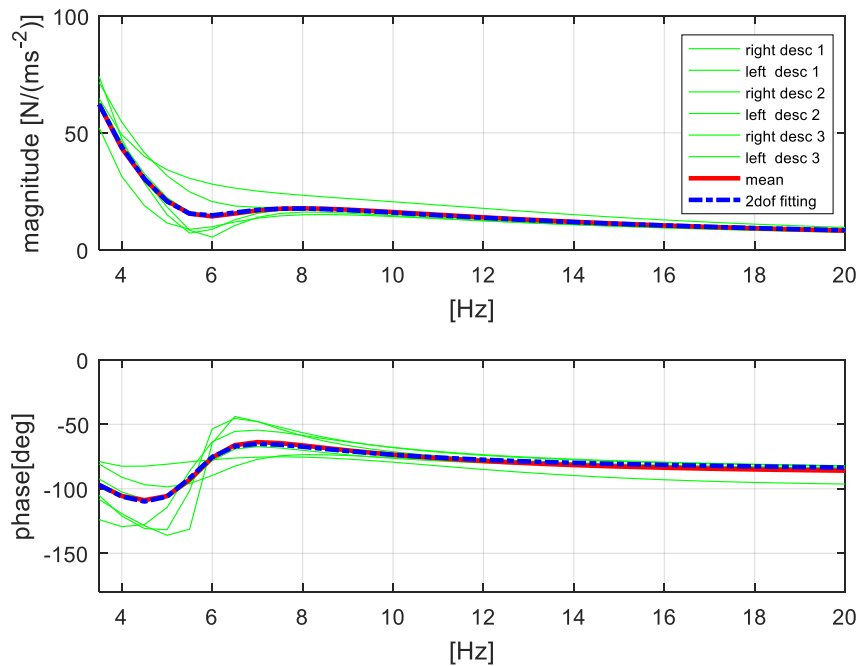


Fig. 33: Subject 3, mean of the six apparent masses of the ascent with the heel contribution.

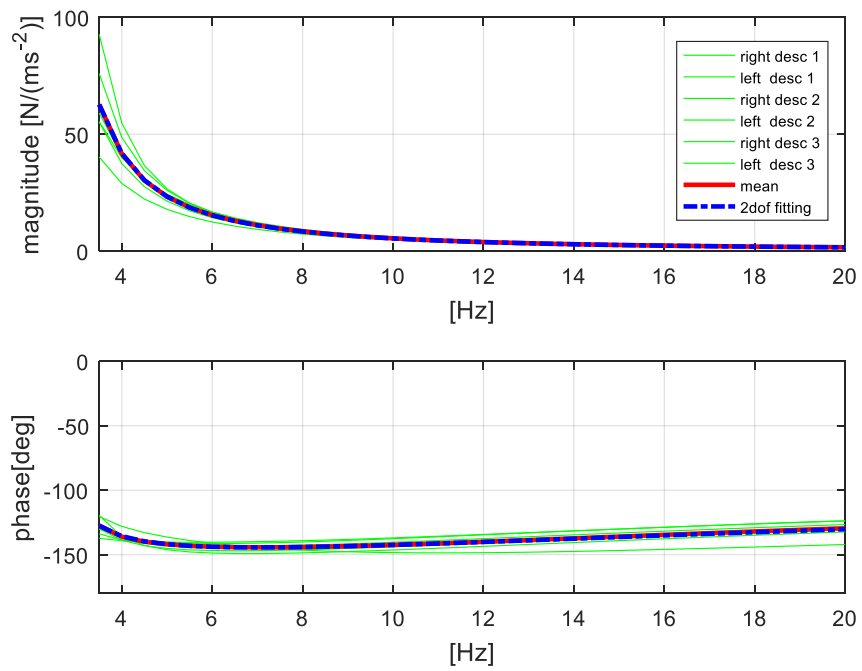


Fig. 34: Subject 3, mean of the six apparent masses of the ascent on tiptoe.

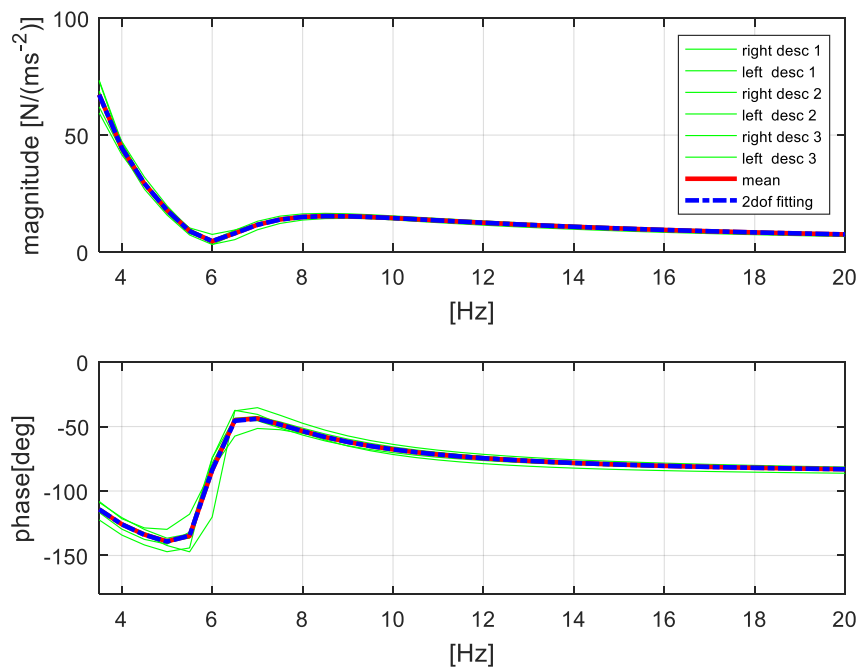


Fig. 35: Subject 3, mean of the six apparent masses of the descent.

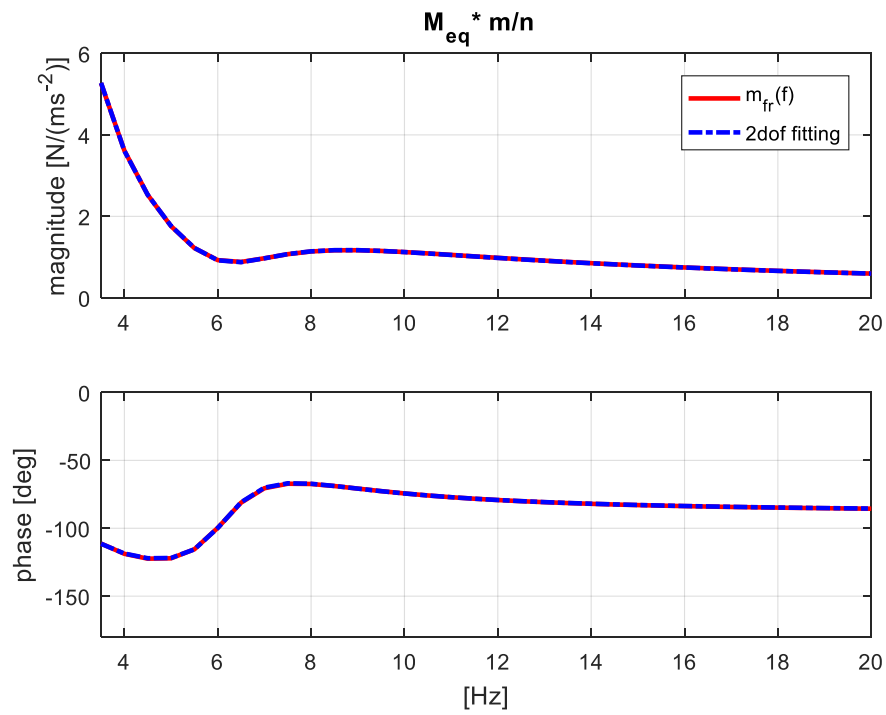


Fig. 36: Fitting of the spread/fractional apparent mass $m_{fr}(f)$ by 2DOF system for five different pedestrians ($m = 5$) on a structure of n nodes (i.e. $n/2$ steps).

3.3 Structural Modal Analysis

3.3.1 Description of the Structure

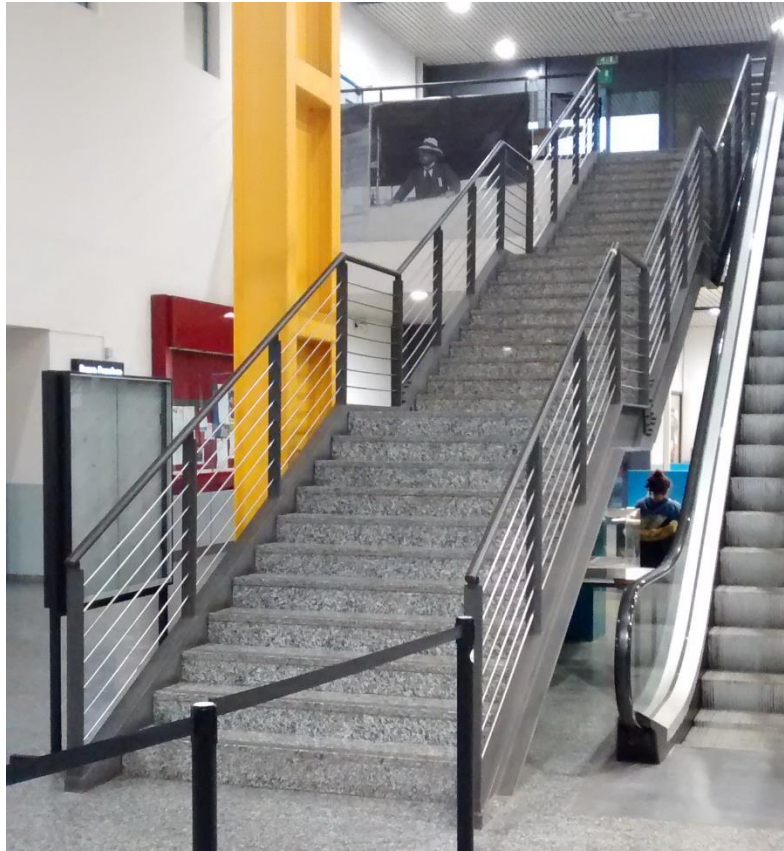


Fig. 37: Main staircase of building B12, north Milan campus of Politecnico di Milano, which connects the ground and the first floor of the building.

In order to figure out the key points and their importance for a correct HSI modeling in different possible scenarios, distinct characteristics of walking pedestrians were separately accounted in each Model. Therefore, one of the main aspect of this work was the assessment of the proposed Models. Hence, the response a of real structure subjected to the effect of moving pedestrians was required. To this purpose, the main staircase of building B12 placed at Politecnico di Milano campus of Bovisa in Milan that connects the ground floor with the first one was chosen (Fig. 37). Such a structure was suited for our analysis, since it is characterised by a lively low frequency dynamic behavior given by its geometry and material composition, which is particularly indicated to be excited by pedestrian effects. The staircase has a slender profile with a steel core and a step coverage made of marble. There are three flights of stairs. The first of ten steps, the second of nine steps and the third again of ten steps. These three are spaced by two landings. It is to be reported that for structural reasons, a support beam made of steel too was placed under the first landing after the opening of the stair, since its response to crossing pedestrian was excessively high, leading to serviceability problems for the users. The geometry of the structure is reported below in Table 3.

length [m]	width [m]	height [m]	step width [cm]	step height [cm]
12,03	1,8	5,22	31	16

Table 3: Staircase size.

For the simulation stage the proposed Models, to work, require structure information in the form of modal characteristics (i.e. natural frequencies, damping ratios and mode shapes) along with a structure discretization. These aspects are treated in the following Sections: at first, the equivalent discretization of the staircase; then, a description of the experimental stage conducted to gather the structure information; finally, a presentation of the post-processing analysis of such data for their final use.

3.3.2 Discretization of the structure

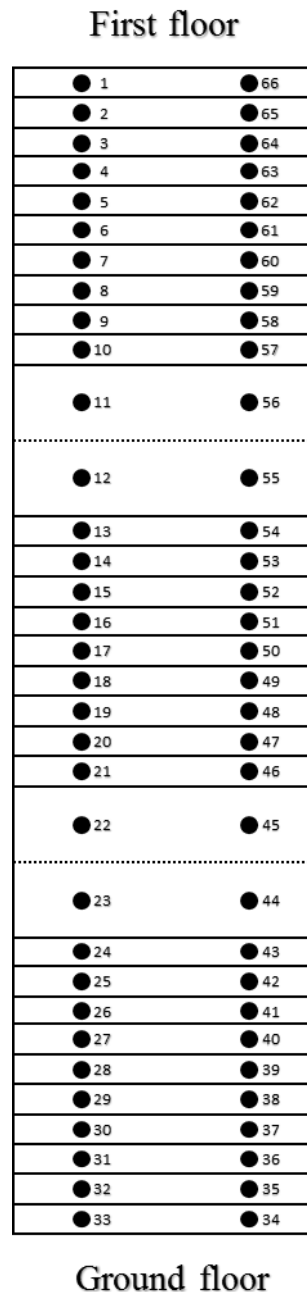


Fig. 38: Discretisation of the analysed structure.

The built-up Models need of a structure description to simulate the HSI. They see the staircase through its modal representation. Moreover, the points of the structure at which the mode shapes of the staircase itself are considered are obtained by a discretization of the structure in nodes. Such

nodes are the ones on which the pedestrians are applied during the numerical crossing of the staircase. The staircase was split in two sides, assuming the left one for the descent and the right one for the ascent of crossing pedestrians. This was done both for simplicity and because free pedestrians usually walk keeping the right side of the way. Each step was then synthesized by a node per side, i.e. one node on the left and one node on the right of the single step. The position of the nodes was chosen in agreement with the distance assumed by pedestrian from the handrail during the crossing, which was observed in the experimental campaign. Since the pedestrians walked on the instrumented stairs, they were forced to cross the stairs between two virtual paths made by the pattern of the accelerometer positions. Therefore, even if it was asked to not walk at the center of each half side of the staircase, since it doesn't normally happen, but at a distance closer to the handrail, as it is usually done, after few cycle the subjects unconsciously started to walk at the center of each half side, between the central accelerometers and the lateral ones. Hence, the staircase was discretized by mean of nodes placed in the middle of each half side (i.e. 45 cm from the handrails; width of the staircase: 180 cm), as depicted in Fig. 38.

Concerning the two landings, even if their length was equivalent to the length of five side by side steps, they were discretized by two nodes per half side, Fig. 38. Such a choice was based on the observation of the experimental campaign as well. Indeed, it was observed that once a pedestrian reached a landing, instead of placing the next foot at the usually distance used to cross a step, he/she placed the foot at a higher distance, since he/she had more space available in front of himself/herself. Not only, before to engage the next flight of stairs, the pedestrian placed the other foot just once more on the landing and then reengaged the steps of the new flight of stairs.

3.3.3 Structure Analysis

To have a modal description of the analysed structure, an experimental stage was performed. The equipment utilized for the measurements comprehended:

- an electrodynamic shaker to excite the structure (LDS, model V406);
- 10 PCB accelerometers model 393B31, sensitivity: 1.02 V/ms^{-2} ;
- 15 PCB accelerometers model 393B12, sensitivity: $1019.4 \text{ mV/ms}^{-2}$;
- a PCB accelerometer model 393A03, sensitivity: 102 mV/ms^{-2} ;

They were applied to the structure as depicted in Fig. 39. The 10 accelerometers model 393B31 were applied at the accelerometer positions 1, 2, 3, 4, 19, 21, 22, 23, 24 and 25 respectively. While accelerometers model 393B12 were placed at the accelerometer positions 5, 6, 7, 8, 9, 10, 11, 12, 13, 14, 15, 16, 17, 18 and 20. Such subdivision was thought as the less noise affected accelerometers (393B31) were placed in correspondence of the DOFs with the smallest eigenvector components, to measure the smallest contributions too. The electrodynamic shaker was placed close to position 2, such that a co-located configuration was obtained.

Such accelerometer pattern was chosen because from previous works [1,2] it had been observed that the first two modes of the structure, which are the ones that have been considered in the simulation stage here too, are bending and twisting. Therefore, with such an accelerometer mesh, both of them would have been properly measured.

For what concern the position of the electrodynamic shaker, it was selected as a trade-off between the capability to excite the structure (i.e. a position with non-null eigenvectors, thus far from the nodes of the modal shapes) and a not too high capability to excite the structure. This last caution was due to not lead the structure in a non-linear behavior, since its very low damped characteristic, which was already underlined by previous analyses.

As can be noticed by the presentation of the set-up, the accelerometers were not placed at the selected nodes in which was discretized the structure, i.e. the point in which pedestrians can walk both in practices and in the simulations. The choice was taken for practical reasons, since the place-



Fig. 39: Instrumented staircase (on the left) with electrodynamic shaker (small photo) and accelerometers; layout of the experimental set-up for the instrumented staircase (on the right).

ment of the accelerometers in correspondence of the positions where the subjects walk would have been an unsafe condition for the people themselves. Not only, the natural walking act would have been affected by the presence of the accelerometers. For this reason, it was preferred the accelerometer pattern illustrated in Fig. 39. However, that meant that the modal shapes of the staircase would have been known at points different from the required ones (accelerometers and nodes of the structure respectively). Hence, an interpolation of the mode shapes, based on the known points, was then performed to extend the shape of each mode over the whole staircase, as will be shown in the next Section (3.3.4).

To excite the staircase, a known mass was connected to the shaker. Once an acceleration profile was generated by the shaker, it was applied to such a mass producing the exciting force. On the mass was placed an accelerometer (PCB 393A03) to measure the effective input acceleration at which the mass was subjected. The total mass, given by the placed mass plus the one of the

accelerometer and the one associated to the moving part of the shaker, was equal to 3.1 kg. The acceleration profile provided by the shaker was a random one, characterized by the Power Spectrum Density profile depicted in Fig. 40. As can be observed, the frequency range of interest in which was introduced the energy of the input signal was from 2 to 20 Hz. At the beginning was used a white noise profile (i.e. a flat one) to excite in the specified frequency range. However, this was not used, since the impossibility of the electrodynamic shaker to significantly excite at 2 Hz with such a profile. Instead, a double integration of it was used, obtaining the acceleration PSD profile depicted in Fig. 40, which allowed a proper excitation with the shaker even at 2 Hz. The structure was exposed to such excitation profile for 1h, in order to allow a relevant statistic exposure.

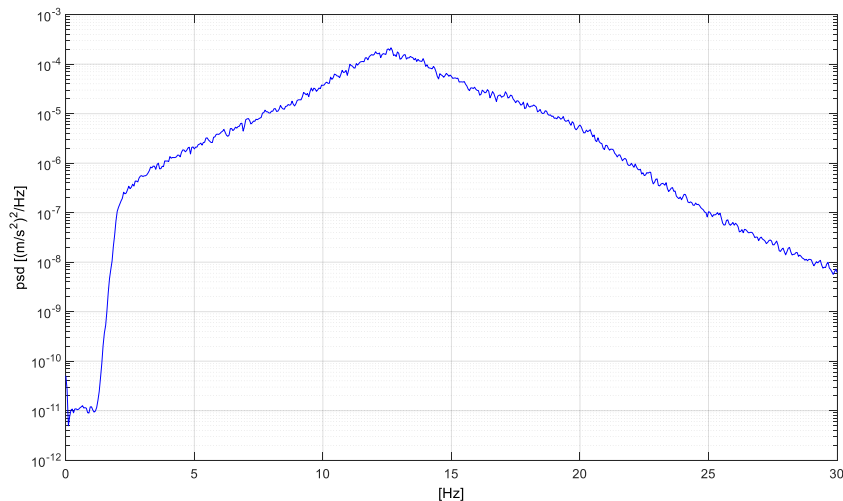


Fig. 40: Acceleration profile provided to the electrodynamic shaker, excitation range: 2-20 Hz.

3.3.4 Post-Processing

Summing up, from the experimental campaign for the modal structure characterization were acquired the exciting force profile (acceleration profile of the shaker times the moved total mass) and the 25 accelerations response time histories at the accelerometer positions, Fig. 39. These signals, after subdivision in sub-time history and averaging in the frequency domain, were utilised for the modal analysis of the structure. The modal parameters (i.e. natural frequencies, damping ratios and mode shapes) were identified by Experimental Modal Analysis (EMA) technique: Poly-Reference of the Least Square Complex Frequency Domain Estimation [59]. This technique was selected because of its accuracy in the modal parameter estimation with respect to other methods. The procedure is basically a multi-modal minimization of the experimental data, with the modal parameters as variables for the fitting. The natural frequencies and the damping ratios as output of the analysis are reposted in

Table 4. As the excitation produced by pedestrian walking barely reaches more than 10 Hz with its harmonic components and his/her passive damping effect drastically decreases for higher frequencies, the first two modes of the structure were considered only, as they were the only to be susceptible to such components (active and passive). The mode shapes of the first two modes are reposted in Fig. 41 at the known points, i.e. the accelerometer positions.

Mode	Natural frequency [Hz]	Damping ratio [%]
1	7.81	0.38
2	8.87	0.35

Table 4: Natural frequencies and damping of the analysed structure.

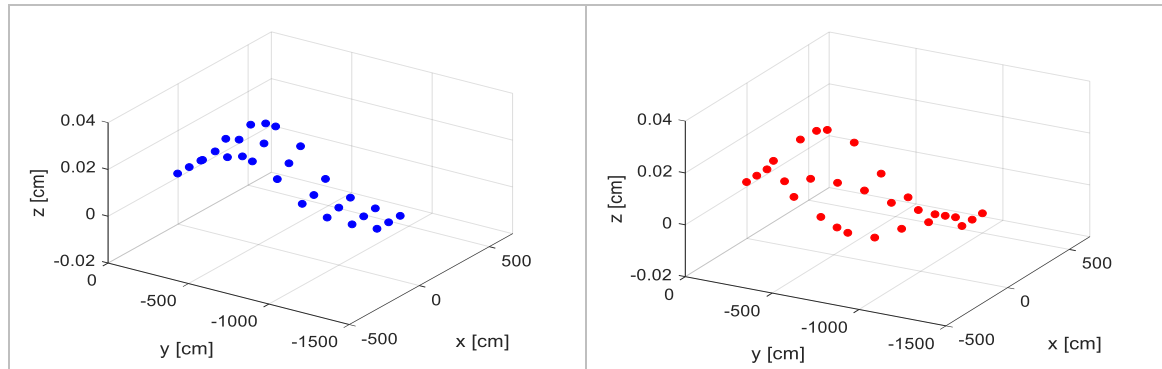


Fig. 41: First mode on the left, second mode on the right.

As was anticipated in the previous Section, an interpolation of the mode shapes to extend their shape to the nodes of the structure through which the pedestrians crossed the staircase was required for the numerical simulations. To do that, it was employed a biharmonic spline interpolation. However, other interpolation techniques were considered and tested (e.g. thin plate spline interpolation or a cubic spline interpolation), but not significant improvement were observed (in terms of SSE (Sum of Squares due to Error), R-square and RMSE (Root Mean Squared Error)). The interpolation of the first and second mode of staircase are reported in Fig. 42 and Fig. 43 respectively. While the extraction of the first and second modal coordinates at the nodes of the discretized structure are depicted in Fig. 44 and Fig. 45 respectively.

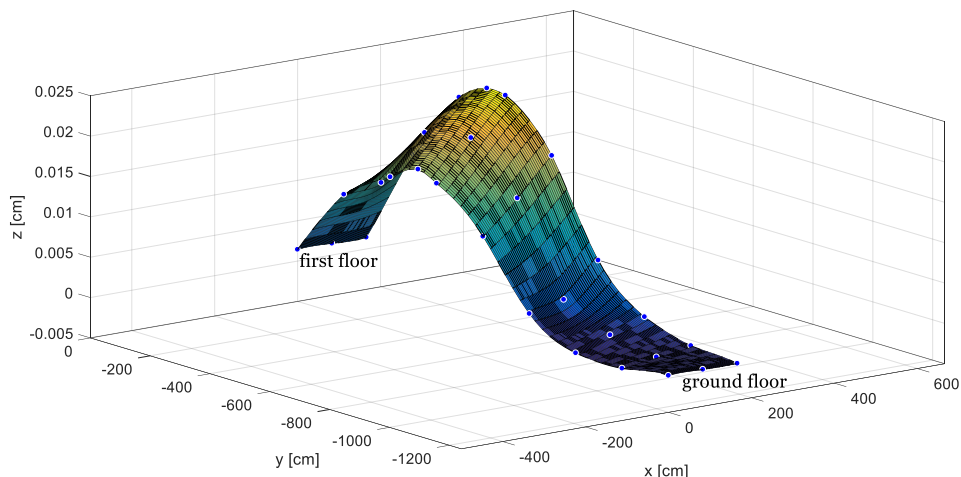


Fig. 42: Interpolation of the first mode starting from the accelerometer positions (blue dots).

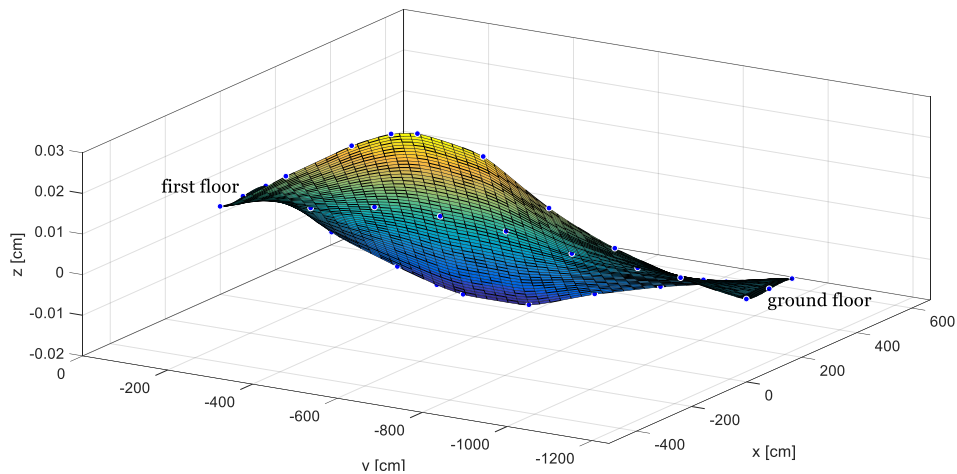


Fig. 43: Interpolation of the second mode starting from the accelerometer positions (blue dots).

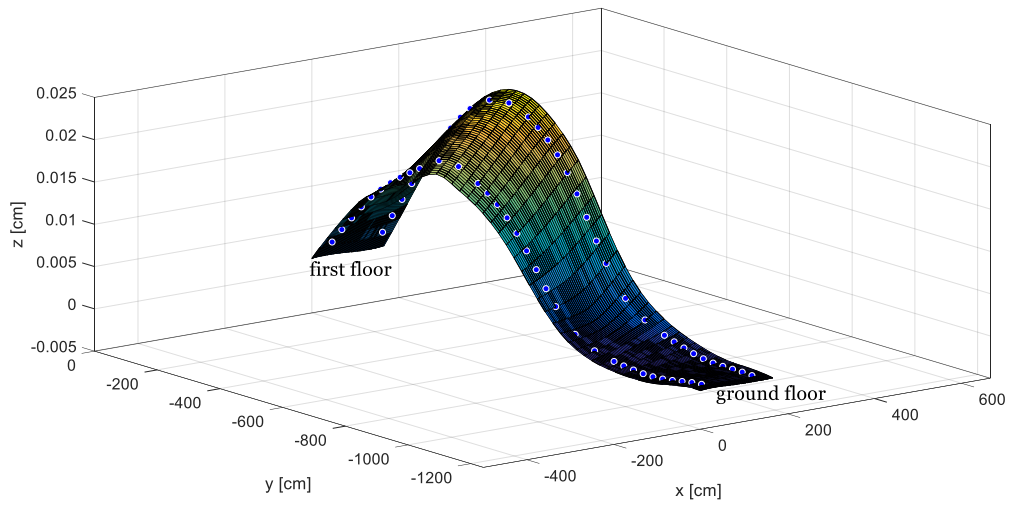


Fig. 44: Extraction of the first modal components in correspondence of the nodes of the discretized structure.

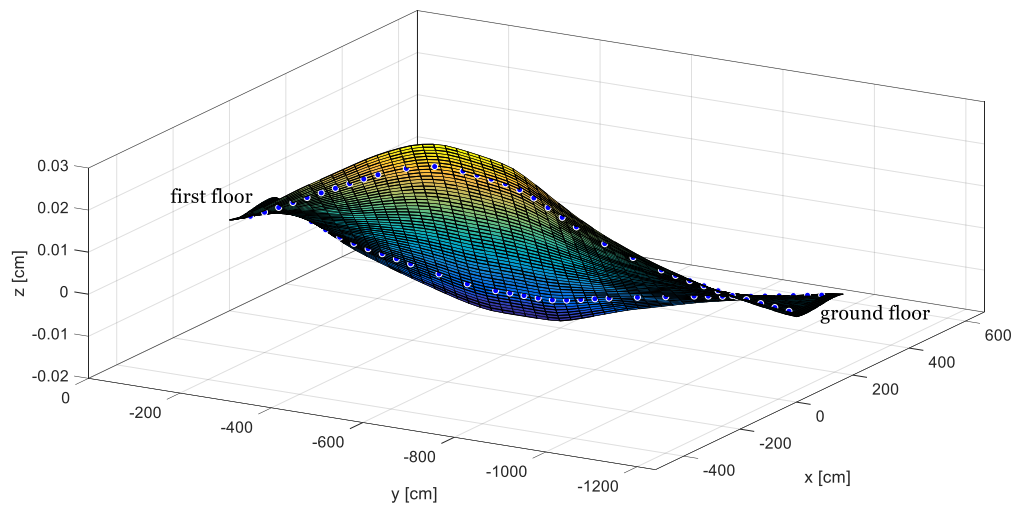


Fig. 45: Extraction of the second modal components in correspondence of the nodes of the discretized structure.

Chapter 4

Numerical Simulations & Experimental Campaign

In this Chapter, the fourth, the proposed Models (i.e. Model 1, 2 and 3) and the old one (Model 0) are numerically applied to simulate the response of a real reference structure, a staircase (the one showed in Section 3.3). The experimental campaign performed on the structure will be presented too. Since the different characteristics of the Models had to be tested, several pedestrian scenarios were thought and then reproduced both numerically and tested on the real structure. Of course, the main aspect to be checked was the reliability of the Models for the estimation of the vibration levels. However, as already introduced in Section 2.2, another important feature to assess was the strong difference between Models 1, 2 and 3 and the old one, Model 0, that is how the apparent mass of the subjects (PGRFs) is treated. Indeed, Model 0 was designed to deal with situations of high pedestrian density, and with long periods of observation (Section 1.2) [2]. The long-time intervals are required to ensure the filling of the structure by pedestrians, so that a steady state dense pedestrian condition can be assumed. Given the high density of people, Model 0 approximates the effect of the local pedestrian passive contributions (i.e. apparent masses/PGRFs) with a mean global one, obtained by spreading over the entire structure the global passive contribution exerted by all the pedestrians present on the structure itself. Since the main effect of the passive contribution is the addition of damping to the structure, the localized pedestrian damping effect is in such a way diluted over the entire structure. Of course, in the condition in which Model 0 is supposed to be used, this approximation is not so strong and different for what really happens. Indeed, in case of dense pedestrian conditions, pedestrians are present on the entire structure in an almost equally spaced way. Conversely, the main aspect accounted by the new Models, at first by Model 1 and then by Model 2 and 3 (since they start from the background of Model 1), is a moving passive contribution. In this way, not only the active part (AGRF) is properly describe in time and space coherently with the pedestrian position, but now also the passive one (PGRF) is. As a consequence, the first thing to investigate was the validity of the new Models for the estimation of the vibration levels, even in case of low number of pedestrians and short time intervals (i.e. just the ones required to cross the structure). Bearing in mind the applicability conditions of each Model, a series of tests were thought to validate such conjectures. The list of tests is reported in Table 5.

Test #	Type	# of persons	Involved	Initial positions					Subjects					Initial time [s]				
1	loop	5	fixed	1	10	22	46	63	2	1	3	5	4	0	0	0	0	0
2	loop	3	fixed	1	41	46			4	5	3			0	0	0		
3	loop	1	random	34					-					0				
4	run	5	fixed	1	1	1	34	34	1	2	4	3	5	9	9.9	10.8	0	0.9
5	run	5	random	1	1	1	34	34	-	-	-	-	-	9	9.9	10.8	0	0.9
6	run	3	fixed	1	1	34			5	3	4			7.2	8.1	0		
7	run	2	fixed	34	34				3	5				0	9			
8	run	2	fixed	1	1				3	5				0	9			
9	run	2	fixed	1	34				5	3				0	0			
10	run	1	random	34					-					0				
11	run	1	random	1					-					0				

Table 5: List of tests performed both numerically and experimentally with pedestrians of a staircase.

As can be observed, a main distinction was done between the long tests and the short ones: “loop” and “run” type respectively. In the loop tests, pedestrians walked for 5 min on the structure and the number of pedestrians on the staircase was kept constant. This was done by reintroducing pedestrians on the structure as soon as they ended the crossing of the staircase. Moreover, as was explained in Section 3.3.1, the structure was crossed by pedestrians keeping the right side for the ascending crossings and the left side for the descending crossings, both in the numerical simulations and in the real tests. Conversely, in the run type tests, pedestrians crossed the structure only one time and, once they ended the crossing, they left the structure. In these two macro categories are gathered all the tests performed: in the loop type fallen tests number 1, 2 and 3, in the run type fallen tests from the 4th to 11th.

In the column “Involved” is declared if the specific test involved specific pedestrians or not. More in detail, for the “fixed” cases, the subjects listed in the “Subject” column were used/performed the test. In case of “random” test, it means that a random extraction of a number of pedestrians equal to the number reposted in the “# of pedestrians” column was done for the numerical simulations. Conversely, for the tests performed on the real staircase that are classified with the label “random” (i.e. test number 3, 5, 10 and 11), they were repeated different times with different subjects involved (see Table 6 in Section 4.2 for details). It is noted that the configuration of the pedestrians in test number 5 is the same of test number 4. The only difference is that in test number 4 the subjects were always the same, while in test number 5 they changed/were randomly extracted.

Instead, In the “Initial position” column, the initial positions assumed by the subjects at the beginning of each test are indicated, taking as reference the discretization of the staircase reposted in Fig. 38 of Section 3.3. Beside to it, the list of subjects involved and the corresponding time at which the specific pedestrian assumed the initial position indicated in the dedicated column, are reported. For example, in test 7, subject 3 and 5 go upstairs (step 34 is the first of the ascending crossing, Fig. 38) with subject 5 who starts 9 s after subject 3 and both of them leave the structure at the end of the crossing. The initial times were evaluated considering that the average length of an active force time history was 0.9 s. Since this last was the factor that imposes the permanence of the pedestrian on each step, it was enough to select the distance in terms of number of steps and multiply it by 0.9 s to obtain the distance in time.

In the following are presented: at first a Section concerning the numerical simulations of the aforementioned scheduled tests, then a Section about the experiments conducted on the real staircase.

4.1 Numerical Simulations

The numerical simulations of the scheduled tests (Table 5) with the proposed Models were implemented and performed in a Matlab ambient (MathWorks Matlab 2016 b).

4.1.1 Input Data

The necessary information required by the program, in which all the Models were implemented, to execute the numerical simulations of HSI problem, are of three types:

- A database containing the active force time histories of each subject collected in the experimental stage (Section 3.1).
- A database containing the 2DOF model parameters to reproduce the apparent masses of each subject in each position considered. A distinction was done between the database for Model 1 and 2 and the one for Model 3. Indeed, the first contains the mean apparent mass curves of the most significant position assumed during the single step, while the second contains the apparent mass curves of the most significant position assumed during the single step. It is noted that the apparent mass curves were acquired and fitted by the 2DOF models for both the cases of foot completely in contact with the step (“heel” configuration) and for pedestrians walking on the tip of the foot (“tiptoe” configuration). Therefore, two databases for Model 1 and 2 and two databases for Model 3 were available. For details see Section 3.2.
- The modal parameters of the structure for its description in modal coordinates (Section 2.3.2 and 3.3). They include: the natural frequencies, the damping ratios and the mode shapes of the accounted modes, that were the first two.

4.1.2 Working Principle

All the Models (i.e. Model 0, 1, 2 and 3) were developed one by one (Model 0 was reproduced too). Then, since the same simulation had to be run with all of them, they were joined in a unique program with a common initial interface. Therefore, before to start a simulation, a series common settings, shared with all the Models, had to be/have to be set:

- Number of simulations.
- Time length of the single simulation. If walking pedestrians are again present on the structure when the time length of the simulation exhausts, they are stopped and the simulation is concluded. Conversely, if all the pedestrians have already left the structure, but the time length of the simulation is not finished, a free decay of the structure is reproduced for the remaining amount of time.
- Sampling frequency of the simulation. From it, the discretization of the time length of the simulation is evaluated. It was set equal to 256 Hz, since it is enough to properly describe the dynamic of the passive HSI (i.e. empty structure + 2DOF models) and the pedestrian active force time histories.
- A Boolean value for the loop condition. When it is set equal to 1, as soon as a pedestrian leaves the structure, he/she is reintroduced on the other side of the staircase with opposite direction. For example, if a person reaches the first floor, in the following instant he/she will be on the first step for the descending crossing, on the left side of the staircase. In this way, the number of pedestrians present on the structure is kept constant. Conversely, when it is set equal to 0, pedestrians cross the stairs only one time.
- The overlap time value. This time is used in Model 2, where the overlap between two consecutive footsteps is considered. Such value was left as an initial input parameter so that

different walking activity (walking, jogging or running) can be simulated. In this thesis the value was kept fixed and equal to 0.1 s, as exposed in Section 2.4.1.

- A Boolean value for the type of ascent style. Indeed, as was explained in Section 3.2.3, pedestrians can go upstairs with a complete contact of the feet with the steps of the staircase (“heel” configuration) or lean on the tip of the feet (“tiptoe” configuration). Thus, a set value equal to 1 means a heel configuration, while 0 a tiptoe one.
- Number of modes N of the structure. Since the structure was treated though a modal description (Section 2.3.2), the information about the number of modes that are considered is required to properly size the matrices.
- Number of steps of the staircase.
- The table with the pedestrian information. It contains the initial position of each pedestrian, the time at which he/she have to be applied at his/her position, and the name of the pedestrian. This last entry is discarded in case of the Boolean value associated to the random extraction of the involved pedestrians is set equal to 1. In the following is shown an example of table, Fig. 46. In this case, all the 5 subjects start at time zero. T_s is defined as the invers of the Sampling frequency of the simulation. Whereby, by means of $\text{round}(time/T_s)*T_s$, with $time$ equal to the time at which the subject is introduced, it is possible to ensure that an integer multiple of the fundamental time interval T_s is always selected as initial instant.

```

%%% Pedestrian table:-----
info_pers_cell = {...
%   position      time      Name
      34          round( 0 /Ts)*Ts  'marcello';...
      22          round( 0 /Ts)*Ts  'francesco';...
      17          round( 0 /Ts)*Ts  'marta';...
      37          round( 0 /Ts)*Ts  'loris';...
      34          round( 0 /Ts)*Ts  'stefano'...
};

```

Fig. 46: Picture of the table that contains the information about the pedestrians involved in the simulation.

- A Boolean value associated to the random extraction of the involved pedestrians. When it is set equal to 1, the specific subject listed in the pedestrian information table is randomly assigned. Remember that at each subject is associated his/her own database of active force time histories and his/her own database with the 2DOF system mechanical parameters (Section 3.1 and 3.2 respectively). Conversely, when it is set equal to 0, the specific subject listed in the pedestrian information table is used.

These information are then passed to the main core of the program that is made by the 4 Models.

The first Model to be run is Model 1, which is followed by Model 0, then Model 2 and finally Model 3. That means that at first, Model 1 is run as many times as the Number of simulations was set in the initial interface, and then all the other programs in turn one by one. Since the same situations have to be reproduced by all the HSI Models, the specific subjects involved in each simulation, whether they are assigned or randomly extracted, have to be the same. For this reason, Model 1 saves at each simulation an information file containing the list of the subjects used. In this way, the other Models can apply at each simulation the same subjects of Model 1, and so the proper databases of active force time histories and of 2DOF model parameters (i.e. apparent mass curves).

In Section 2.3.1 and 2.3.2 was explained as Model 1, but mainly also the other Models, works. For the sake of clarity, the working principle is here reported too. First thing, it is to underline that all the simulations are conducted in the time domain. Therefore, an integration of the dynamic equations of the HSI system (Eq.(30) or Eq.(40), this last is expressed by a State Space formulation) is required. As the HSI system is a Time Variant system, since the pedestrians on the structure continuously change their positions, further considerations were done to make the system more

manageable. Basically, average apparent mass curves representative of the main apparent mass curves assumed during the single footstep (remember that the apparent mass depends on the position of the body and it changes during the single footstep) were utilized in Model 1 and 2. While in Model 3, 3 apparent mass curves concerning the most significant 3 positions assumed during the single footstep, were implemented. In this way, as long as a person has a specific apparent mass curve (i.e. for a footstep in Model 1 and 2, while for 1/3 of footstep in Model 3), the HIS system becomes a Time Invariant system. Therefore, the integration was stopped and restarted any time that a person moved, leading to the integration of a series of Linear Time Invariant systems.

The integration of each HSI LTI system was performed by means of a Matlab ODE solver. The ODE solvers are solvers to solve Ordinary Differential Equations. Even if ode45 is the most versatile integrator and the first prompted by MathWorks among the ones of the Matlab ODE packet, the second most suggested was tested too, that is ode23. It was tested with the version for both the non-stiff problems (ode23) and for the stiff problems (ode23s), since ode45 is only for non-stiff problems. Where, with stiff problem is meant an Ordinary Differential Equation that forces the numeric method of the solver to assume an unnecessary small size of the discretization step with respect to the one sufficient to describe the trend of the exact solution, [60]. Because of no significant changes were observed among the solutions evaluated with the different solvers, ode45 was deployed as numerical integrator for all the Models. Since the numerical method of the ODE solver needs to freely evaluate the ODE system within the integration time interval imposed to it, a re-sampling of the active force time histories was necessary at every integration time interval.

After the integration, which provides the solution of the HSI system in terms of displacements of the structure, a double time derivation of the integration output is required, since the final aim is the estimation of the vibration levels, which come from the accelerations of the structure. Indeed, from the integration stage, the displacement time histories of the nodes of the structure are evaluated (e.g. Fig. 47). Passing through a double time derivative, the corresponding acceleration levels can be assessed (e.g. Fig. 48).

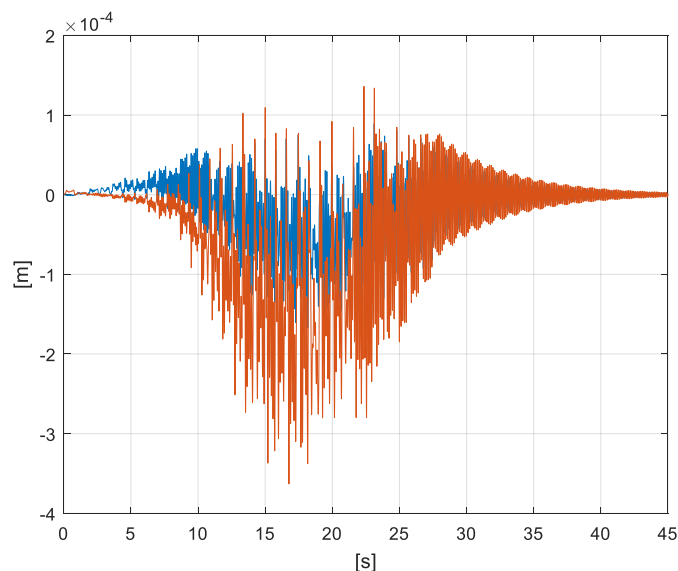


Fig. 47: Displacement responses of the structure in correspondence of the positions occupied in the experimental campaign by accelerometers 8 (blue curve) and 9 (red curve) (accelerometer positions Fig. 39), which is subjected to a pedestrian who goes upstairs and then leaves the structure (final free decay present).

In Fig. 47 and Fig. 48 is depicted the response of the numerical simulation in correspondence of the positions assumed by accelerometer 8 and 9 during the experimental campaign (blue and red curve respectively). Indeed, the points in which the structure was discretized (i.e. the positions that the pedestrians can assume in the numerical simulations, Fig. 38) are different from the ones at

which the response of the numerical structure was observed/extracted. This was allowed by the use of two different sets of eigenvectors, as explained in Section 2.3.2 and 3.3.4. Eigenvectors, evaluated at the points in which the structure was discretized, were used in the simulation stage. Eigenvectors, evaluated in correspondence of the positions that accelerometer 8 and 9 had during the tests on the real structure, were used in the observation of the numerical results stage. These last (i.e. the points at which the numerical accelerations are read) were selected equal to the positions of the accelerometer 8 and 9 for two reasons: to have a direct comparison of the results (numerical vs experimental) and because these two points are the ones in which the modal shapes of the first and second mode of the structure assume their highest modal displacements. Moreover, two points instead of one, to have an information for both the sides of the staircase.

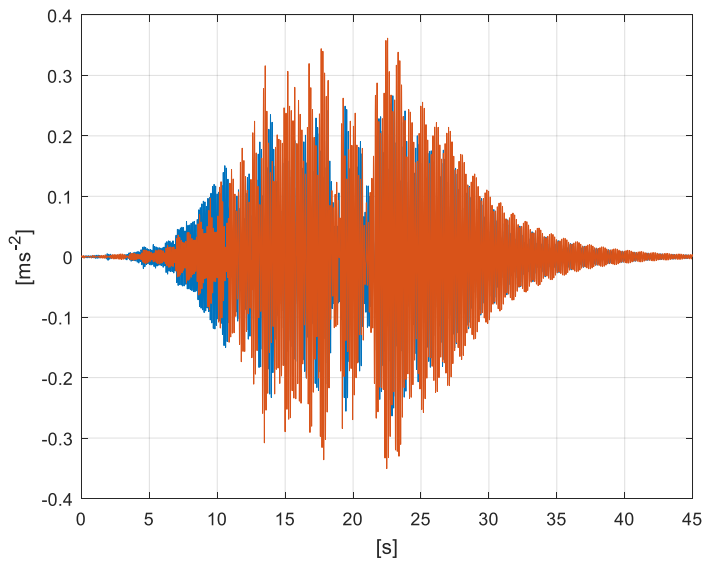


Fig. 48: Acceleration responses of the structure in correspondence of the positions occupied in the experimental campaign by accelerometers 8 (blue curve) and 9 (red curve) (accelerometers positions Fig. 39), which is subjected to a pedestrian who goes upstairs and then leaves the structure (final free decay present).

4.1.3 Number of Simulations & Computational Effort

The number of simulations, for which every pedestrian configuration was run, was set equal to 100. Such number was considered sufficiently high to have a reliable distribution of the estimated vibration levels, both in cases of tests with selected pedestrians or of tests with pedestrians randomly extracted. Indeed, for the tests in which the pedestrians are selected, at every simulation a different sequence of active force histories for each pedestrian is extracted, since the AGRF extraction is always a random process. Therefore, performing 100 simulations, robust results with respect to the intra-subject variability (i.e. the variability of the same subject) were assumed. While, in case of tests with a random extraction of the pedestrians involved at each simulation, the robustness of the results with respect of the inter-subject variability (i.e. variability among different subjects) was assumed for 100 simulations too.

It is to highlight that each scenario of Table 5 was simulated for both pedestrians walking with the feet completely in contact with the steps (“heel” configuration) and for pedestrians walking on the tip of the feet (“tiptoe” configuration). Indeed, two different sets of 2DOF mechanical parameters were obtained for each subject during the preliminary experiments (Section 3.2), and collected in two different databases to account for the passive contributions.

As for the computational effort led by the program, of course it changes with the type of simulation considered, mainly between the long tests (pedestrian in loop for 5 min) and the short ones (pedestrians leave the structure at the end of the crossing), and it depends from the hardware

employed. As an example, the case of a computer equipped with a processor type Intel Core i7 6500U 2.50 GHz (up to 3.3 GHz), a RAM of 12GB and an internal memory type SSD is reported. In case of a person who crosses the staircase one time:

- Model 0 plus Model 1: 3.29 s.
- Model 2: 1.61 s.
- Model 3: 1.41 s.

Note that the time required by Model 1 is given together with Model 0. That is due to how Model 0 runs, that is always consecutive to Model 1, leading to a split of the two times not possible.

In case of a person who walks in loop on the staircase for five minutes:

- Model 0 plus Model 1: 3.29.
- Model 2: 15.99 s.
- Model 3: 14.98 s.

As for heaviest case among the simulated ones, 5 pedestrians who walk for five minutes in loop:

- Model 0 plus Model 1: 64.45s.
- Model 2: 44.88 s.
- Model 3: 68.85 s.

Of course, all the times are referred to a single simulation of the stated case.

4.1.4 Simulations

The numerical simulations that were run with the program were the ones listed in Table 5. Each of them was run 100 times, in order to have enough simulations to have a reliable distribution of the estimated vibration levels, as just introduced in the previous Section. For each simulation, the initial settings of the program were set (Section 4.1.2) coherently with the type of test to be run, Table 5. Thus: if pedestrians are in a loop condition or they are not, the initial positions, the initial times, the specific subjects, etc. Finally, as was explained in Section 4.1.2, the outcome of each simulation are the acceleration time histories in correspondence of the positions of accelerometer 8 and 9. As the scheduled tests in Table 5 are 11, 1100 acceleration time histories, for both the accelerometer positions (8 and 9) and both the walking styles (heel/tiptoe), were obtained at the end of the numerical simulations.

4.1.5 Post-Processing

As result of the numerical simulation stage, a huge number of acceleration time histories were available. In order to analyse the response of the structure in each tested pedestrian configuration and in order to condensate the large amount of information available, a post-processing session was made followed the simulation one. More in detail, two quantities were used for such purpose: the global RMS value and the moving RMS one.

Global RMS

As the main information of a signal is the power associated to the signal itself, the Root Mean Square value (RMS) of the signal is strictly correlated to the power of the signal as well. Indeed, the RMS value represents the amplitude that a constant signal has to have in order to have a power equivalent to the one of the consider signal over the same time interval. The advantage, with respect to the power value, is that the RMS keeps the same unit of measure of the evaluated signal. Its definition follows:

$$\text{RMS} = \sqrt{\frac{1}{T} \int_0^T a^2(t) dt} \quad (63)$$

where T is the time length of the acceleration time history $a(t)$. As can be noted, its unit of measure is the same of the acceleration time history one, that is ms^{-2} . Not only, the RMS value can be evaluated also through the mean value μ (Eq.(64)) and the standard deviation σ (Eq.(65)) of the signal, as reported by Eq.(66).

$$\mu = \frac{1}{T} \int_0^T a(t) dt \quad (64)$$

$$\sigma = \sqrt{\frac{1}{T} \int_0^T (a(t) - \mu)^2 dt} \quad (65)$$

$$\text{RMS} = \sqrt{\mu^2 + \sigma^2} \quad (66)$$

Therefore, as first index of the vibration level of the structure, the global RMS value of each of the 100 acceleration time histories was evaluated. Of course, this was done for both the points at which the numerical accelerations were observed (that are equivalent to the positions in which accelerometers 8 and 9 were placed during the experimental campaign) and for each of the 11 tested situations listed in Table 5. Hence, for each HSI configuration tested, 100 RMS acceleration values were available.

Such RMS values were evaluated on the whole time length of each acceleration time history. More in detail, they were assessed on the entire time length of the loop tests (i.e. the first three tests of Table 5), since the time of this type of tests was a setting parameter (i.e. 5 min). As for the run tests (i.e. tests from test number 4 to test number 11 of Table 5), in which the pedestrians cross the structure only one time, a free decay of the structure was present, both in the numerical simulations and in the experimental tests. For this reason, in both the experimental and numerical tests, a trigger value was set for the free decays, under which, the acceleration time histories were cut. The threshold value was set in agreement with the steady state values of the free decays observed in the experimental tests (i.e. 0.025 ms^{-2}), which were given by the noise threshold of the signals.

It is to be pointed out that, before to compute the RMS values, the acceleration time histories were filtered by a Low Pass Filter (LPF). This was done since the same procedure was performed for the experimental acceleration time histories. The experimental data were Low Pass Filtered to discard the frequency components of the signals at frequencies higher than the ones of the first two modes of the structure. Only these two modes were kept into account, and used in the modal description of the structure in the Models, since they were found to be the only ones sensible to the excitation of the pedestrians. Hence, the filter was applied to discard the contributions of the modes at higher frequencies. The same filter was applied to the numerical simulation outcomes, even if they were obtained considering only the first two modes, in order to have the same distortion of the signals that is intrinsically produced by the application of a filter. In addition, the numerical acceleration signals only, were also Band Pass Filtered: once around the first mode (7.81 Hz) and once around the second mode (8.87 Hz). In this way, the contribution of each mode to the vibration level was separately evaluated too. Summing up, the three filters were applied:

- Low Pass Filter: Butterworth filter, 8th order, cut-off frequency: 12 Hz.
- Band Pass Filter: Butterworth filter, 12th order, cut-off frequencies: 6 – 8.3 Hz.
- Band Pass Filter: Butterworth filter, 12th order, cut-off frequencies: 8.3 - 11 Hz.

The next steps which follow were performed for all of three type of filtered signals.

As an example, it is reported one acceleration time history (the one in correspondence of accelerometer 8) of test number 10 of Table 5 (a random extracted pedestrian goes upstairs and then leaves the structure). In Fig. 49 are depicted in red the LPF signal and in blues the original one, while in Fig. 50 the RMS value of the LPF acceleration signal in purple. As can be seen by Fig. 49, the filtering introduces a slight delay in the filtered signal. This is right and it doesn't change the results, since the RMS value doesn't change, given its definitions Eq.(18).

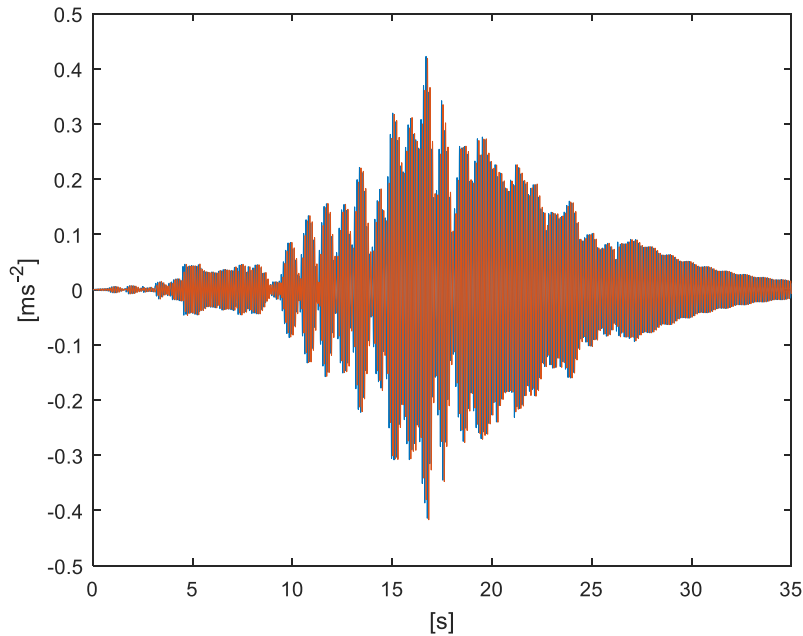


Fig. 49: Acceleration time histories extracted in correspondence of the position of accelerometer 8 for a pedestrian who goes upstairs obtained with Model 1. In blue the original time history, in red the LPF one at 12 Hz with an 8th Order Butterworth filter.

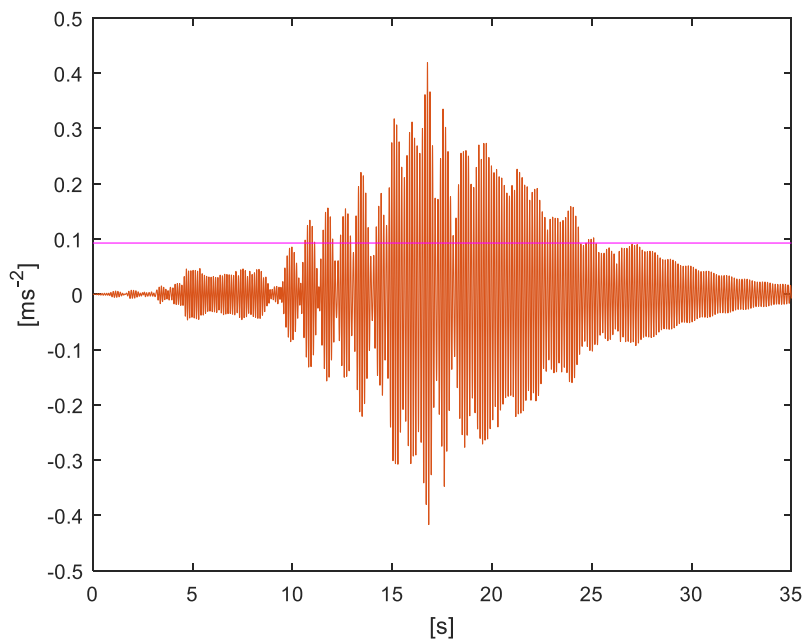


Fig. 50: LP filtered acceleration time history (in red) in correspondence of the position of accelerometer 8 for a pedestrian who goes upstairs obtained with Model 1. Its equivalent RMS value in purple.

Now, in order to combine the 100 RMS acceleration values (e.g. the purple line of Fig. 50), without losing any information about the powers of the signals involved, the mean value and the standard deviation were evaluated for the squared RMS acceleration values, Eq.(67) and Eq. (68) respectively.

$$\bar{\mu} = \frac{1}{N} \sum_{i=1}^N \text{RMS}_i^2 \quad (67)$$

$$\bar{\sigma} = \sqrt{\frac{1}{N-1} \sum_{i=1}^N (\text{RMS}_i^2 - \bar{\mu})^2} \quad (68)$$

With N equal to 100. This was done to leave the information of the powers unchanged during the combination of the 100 values, since the power is proportional to the square of the signal amplitude, and so of the RMS value. Since the final aim is not a precise value of the expected vibration level, but a range of the most probable vibration levels that could be observed for the specific HSI scenario tested, a probability density function, to describe the result of the 100 simulations, was used. The description of such distribution was provided as for a Normal one, that is through the mean value (Eq.(70)) and the limit values for the confidence interval selected. A confidence interval at 95 % (i.e. 2×Standard Deviation) (Eq.(69) and Eq.(71)) was chosen.

$$\triangleleft = \sqrt{\bar{\mu} - 2\bar{\sigma}} \quad (69)$$

$$\square = \sqrt{\bar{\mu}} \quad (70)$$

$$\triangleright = \sqrt{\bar{\mu} + 2\bar{\sigma}} \quad (71)$$

Where the symbols \triangleleft \square \triangleright represent the lower limit at the confidence interval at 95 % of the RMS acceleration value, the mean value of RMS acceleration level and the higher limit at the confidence interval at 95 % of the RMS acceleration value respectively. As an example, the probability distributions obtained with every Model for the case 10 of Table 5 are reported in Fig. 51 (a random extracted pedestrian goes upstairs and then leaves the structure).

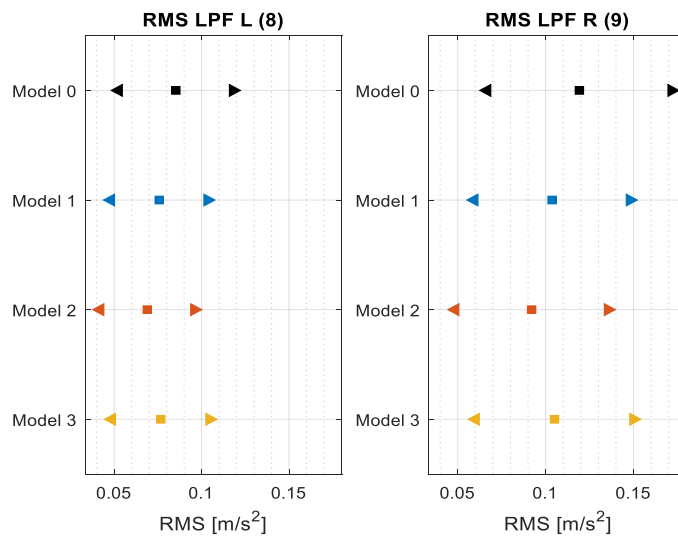


Fig. 51: Estimation of the vibration RMS levels undertaken by the staircase when a pedestrian goes upstairs and then live the structure. Heel contact footstep. With \square that represents the mean RMS acceleration value and \triangleleft \triangleright that represent the RMS acceleration values for a confidence interval at 95 %. On the left, the values observed in correspondence of the position of accelerometer 8. On the right, the values observed in correspondence of the position of accelerometer 9. All the signals are filtered by a Low Pass Filter at 12 Hz.

The formulation used has allowed to obtain a probability distribution for the estimation of the global vibration level undertaken by the structure, leaving unchanged the power of the single acceleration signals used for the distribution assessment.

One of the main aspect to be checked of the new Models, was the difference in the estimation of the vibration levels brought by the modelization of the apparent masses of the pedestrians as moving passive contributions, with respect to a spread one, as Model 0 does (Section 2.2). To assess this matter, a direct comparison with Model 0 was done for every Models. Moreover, for each of the 100 simulations, the equivalent RMS acceleration value of the Models (coming from Eq.(18) or Eq.(66)) was normalized for the one assumed by the Model 0:

$$\text{RMS}_{\text{ratio},i,j} = \left(\frac{\text{RMS}_{\text{Model } i}}{\text{RMS}_{\text{Model } 0}} \right)_j \quad i = 1, 2, 3 \quad j = 1, \dots, 100 \quad (72)$$

Then, the 100 RMS acceleration ratios of each Model were processed with Eq.(67), Eq.(68), Eq.(69), Eq.(70) and Eq.(71) as well. In addition, the maximum (Δ) and the minimum (∇) ratio values among the 100 ratios were taken for each Model. As an example, in Fig. 52 the ratios of the Models with Model 0 for the case showed before in Fig. 51 (i.e. a random extracted pedestrian who goes upstairs and then leaves the structure, case 10 of Table 5) are reported.

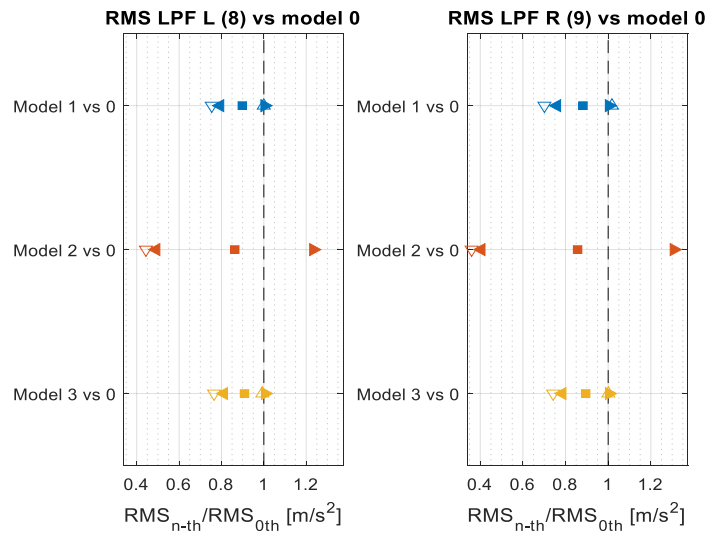


Fig. 52: Distributions of the RMS acceleration values of each Model normalized by Model 0, for the case of a pedestrian who goes upstairs and then live the structure. Heel contact footstep. With \square that represents the mean RMS acceleration ratio value, $\triangleleft \triangleright$ that represent the RMS acceleration ratio values for a confidence interval at 95 % and $\Delta \nabla$ that represent the maximum and minimum ratio value observed respectively. On the left, the values observed in correspondence of the position of accelerometer 8. On the right, the values observed in correspondence of the position of accelerometer 9.

The estimated vibration level distributions, which were shown in Fig. 51 and Fig. 52 (for the case of an pedestrian who goes upstairs) by means of the mean value (\square) and the confidence interval at 95 % ($\triangleleft \triangleright$), were then fully depicted through histograms. As an example, the case of a pedestrian who goes downstairs, in Fig. 53.

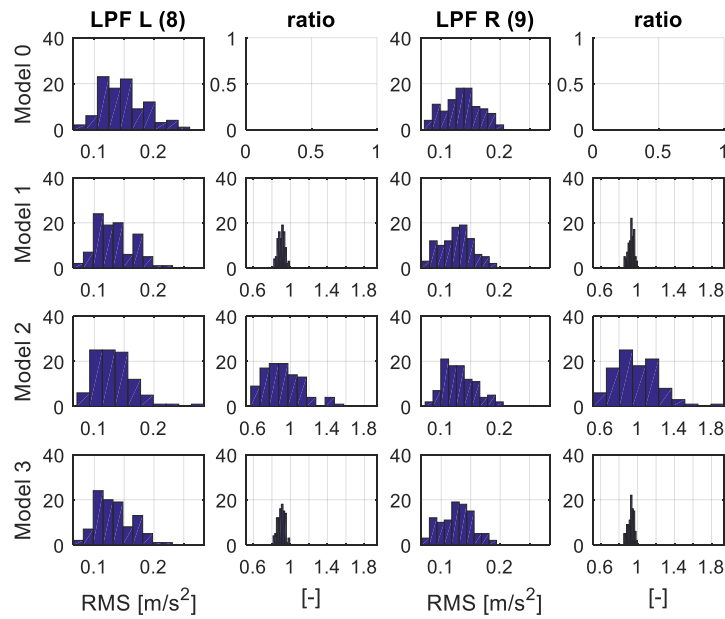


Fig. 53: Histograms related to the global RMS acceleration values of 100 simulations, for a person who goes downstairs. Estimation of the 4 Models on the left; ratio (simulation by simulation) of each Model with Model 0 on the right.

Moving RMS

Another important parameter used to analyse the data is the moving RMS. Its definition doesn't change, it is the same of the one reported in Eq.(18) or Eq.(66). What changes is the time interval of the signal on which the RMS is evaluated. Indeed, the RMS value is function of the time interval of the signal on which it is evaluated. Therefore, going to evaluate the RMS over a smaller time interval (3 s) for all the time length of a signal, will allow to observe the dynamics of the trend of the power as a function of time, since the RMS value is strictly correlated to the power. In this way, an observation of the differences among the Models from an almost instantaneous point of view (every 3 s) was also possible. As an example, the case of one pedestrian who go upstairs and then leaves the structure (10th case of Table 5) is reported in Fig. 54 (just 1 moving RMS acceleration time history evaluated every 3 s). It is to be recalled that, also for the moving RMSs, the accelerations time histories were filtered, as explained in the previous Section.

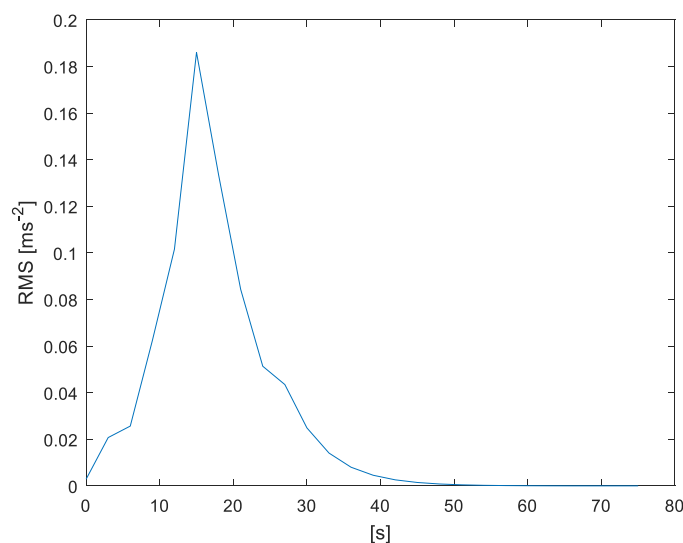


Fig. 54: Moving RMS acceleration time history evaluated every 3 s for a pedestrian who goes upstairs, obtained with Model 1, in correspondence of the position of accelerometer 8.

The so obtained 100 moving RMS acceleration time histories per scenarios of Table 5 and for both the points at which the accelerations were extracted from the simulations (i.e. in correspondence of the positions of the accelerometer 8 and 9 of the experimental section) were processed likewise the global RMS values (previous Section). The difference is that not only a unique global RMS acceleration value is available for each of the 100 acceleration time histories, but a sequence of moving RMS evaluated every 3 s (e.g. Fig. 54). For the sake of clarity, the actual situation, with the next passages, is depicted in Fig. 55.

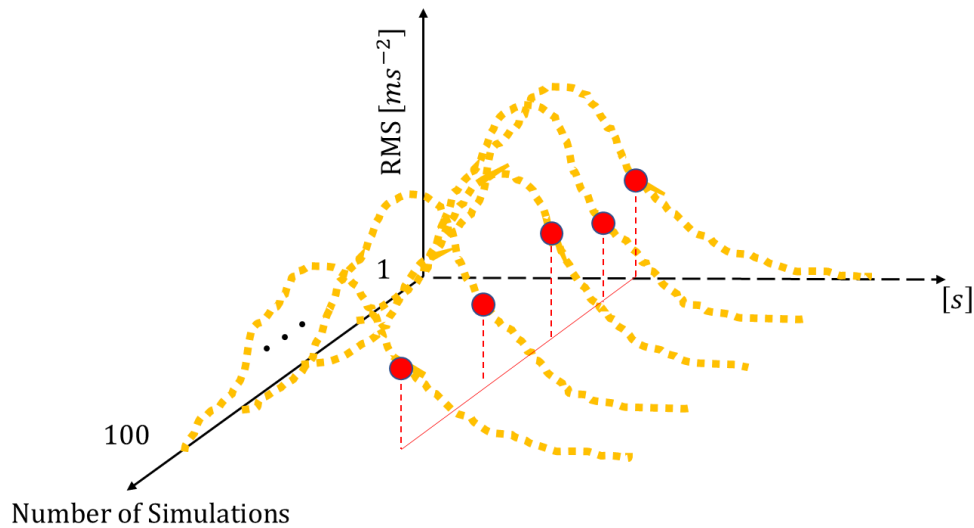


Fig. 55: Representation of the set of 100 moving RMS acceleration curves for the case of a pedestrian who goes upstairs and then leaves the structure (i.e. bell shape of the moving RMS curves). Every yellow dot of a curve represents a RMS acceleration value evaluated on a time window of 3 s. The red line represents the consideration of a specific 3 s time interval, and so of a specific set of 100 RMS acceleration values coming from all the curves (red dots).

In Fig. 55, the yellow lines represent the moving RMS acceleration curves. Indeed, since they are evaluated every 3 s (as can be observed by the time axis, where every segment represents a time interval of 3 s), they are made up by a sequence of RMS evaluations spaced of 3 s (the yellow dots of a single curve). The next point is their processing. For every time interval of 3 s, is available a RMS from each of the 100 moving RMS curves. Therefore, at first, a time interval of 3 s is selected (the red line in Fig. 55) and with it the corresponding RMS value of each moving RMS curve (the 100 red dots of Fig. 55). Then, at this set of 100 RMSs, Eq.(67), Eq.(68), Eq.(69), Eq.(70) and Eq.(71) are applied. Doing so, for every 3 s time interval available, the curves depicted in Fig. 56 are obtained (one for each Model) (the example case is always the 10th test of Table 5, that is the one of a pedestrian who goes upstairs). It is noted that, with respect to the global RMS acceleration case, where \square was used to represent the mean RMS acceleration value and $\langle \triangleright$ the RMS acceleration values for a confidence interval at 95 %, here they are substituted by a continuous line for the mean values and by two dashed lines to show the confidence interval at 95 %, as shown by Fig. 56.

It is to be pointed out that, also if the discussion about the results will be performed in the next Chapter, from Fig. 56 is possible to observe a physical sense in the outcome of the simulated case, also without any experimental data. Indeed, a like bell shape of the moving RMS acceleration curves is present for the simulated case: a person who goes upstairs, with a numerical observation point placed in correspondence of accelerometer 8 (Fig. 39). Such shape is coherent with the pedestrian path and the measurement point located at a point with high modal components. Indeed, this last is placed in correspondence of the range of points with the maximum modal components of the accounted modes of structure. Therefore, since that location of the staircase is the most susceptible one to the excitation of the walking pedestrians, it is expected that the vibration levels,

at the measurement point, have to increase while the pedestrian is reaching that staircase zone and to decrease while the pedestrian is leaving it, measuring the maximum values when the pedestrian is closest to such point (i.e. around 18 s of Fig. 56).

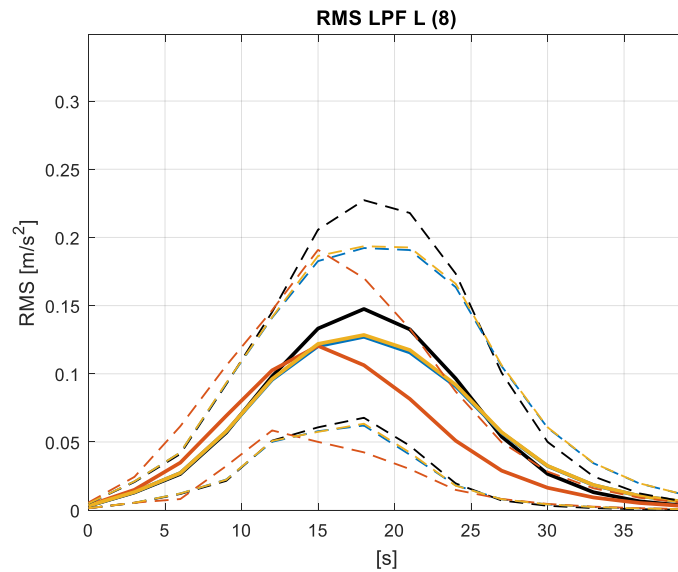


Fig. 56: Moving RMS acceleration curves (extracted in correspondence of the position of accelerometer 8) for the case 10 of Table 5 (one person goes upstairs), with the continuous lines equal to the mean value and the dashed lines equal to the confidence interval at 95 %. In the plot, the results of the simulation with Model 0 (in black), Model 1 (in blue), Model 2 (in red) and Model 3 (in yellow) are reported.

Going ahead, as was introduced in the previous Section, one of the aspect to be checked was the variation in the estimation of the vibration levels brought by the use of moving passive contributions of the pedestrians (i.e. apparent mass) with respect to a spread over the structure one, like Model 0 does. Therefore, also for the moving RMS acceleration case, a normalization with respect to Model 0 of the results obtained with Model 1, 2 and 3 was made. To do that, once a 3 s time interval is selected, a set of 100 RMS values is available from each of the 4 Models (red lines in Fig. 57). Then, each of these RMS values of Model 1, 2 and 3 is divided for the corresponding one of Model 0 (the red dots of Fig. 57 show a single ratio), applying in this way Eq.(72).

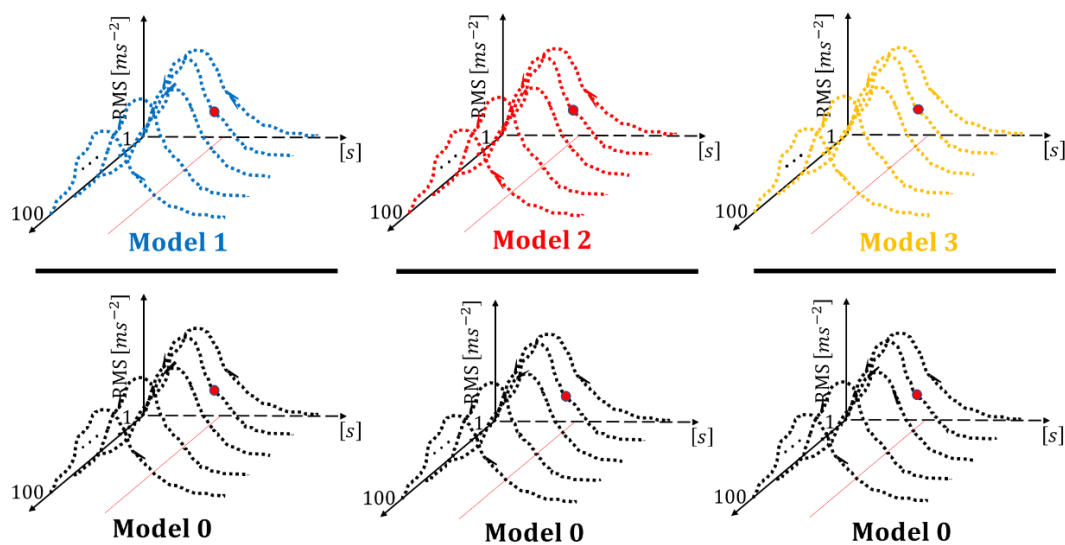


Fig. 57: Normalization by Model 0 procedure for a single RMS value of a moving RMS acceleration curve for Model 1, 2 and 3, in case of a pedestrian who goes upstairs (i.e. bell shape of the moving RMS acceleration curves).

As results, 100 RMS ratios are obtained for each 3 s time intervals (single segments of the dashed time axes of Fig. 57) and for Model 1, 2 and 3. At every set of 100 RMS acceleration ratios so evaluated, Eq.(67), Eq.(68), Eq.(69), Eq.(70) and Eq.(71) are applied. A unique set of curves (mean value (continuous line) and the confidence interval at 95 % (dashed lines)) per Model normalized with respect to Model 0 was obtained, Fig. 58 (case 10th of Table 5).

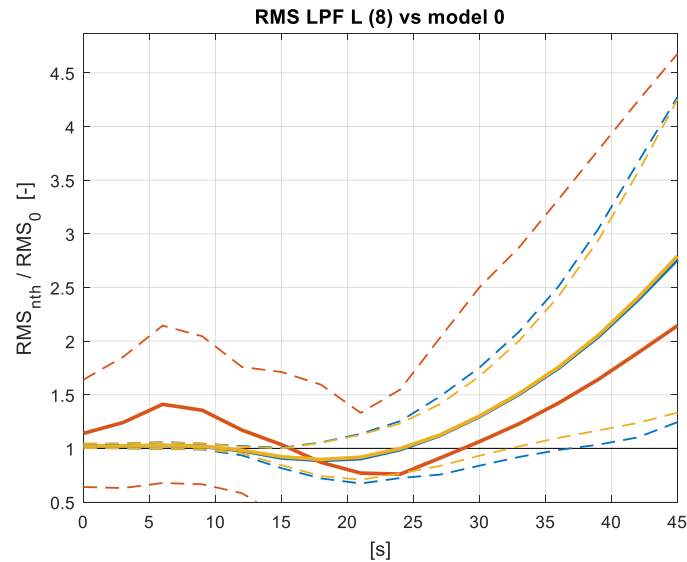


Fig. 58: Comparison of Model 1 (blue lines), Model 2 (red lines) and Model 3 (yellow lines) with Model 0 through normalization of them by Model 0 for the case of a pedestrian who goes upstairs (10th of Table 5). The continuous lines represent the mean values, the dashed lines the confident intervals at 95 %.

In order to highlight an issue, in the following are reported the equivalent plots of Fig. 56 and Fig. 58 for the case of a pedestrian walking in loop for 5 min over the staircase (third case of Table 5), Fig. 59 and Fig. 60 respectively.

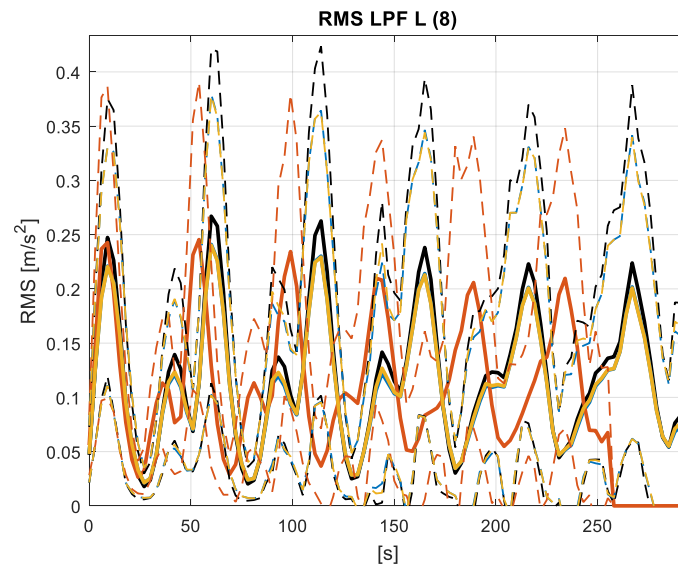


Fig. 59: Moving RMS acceleration curves for one person walking in loop over the staircase for 5 min; continuous line: mean value, dashed lines: confidence interval at 95 %; black line: Model 0, blue line: Model 1, red line: Model: 2, yellow line: Model 3. Low Pass Filtered signals; values of accelerations extracted in correspondence of the position of accelerometer 8 (i.e. left side of the staircase).

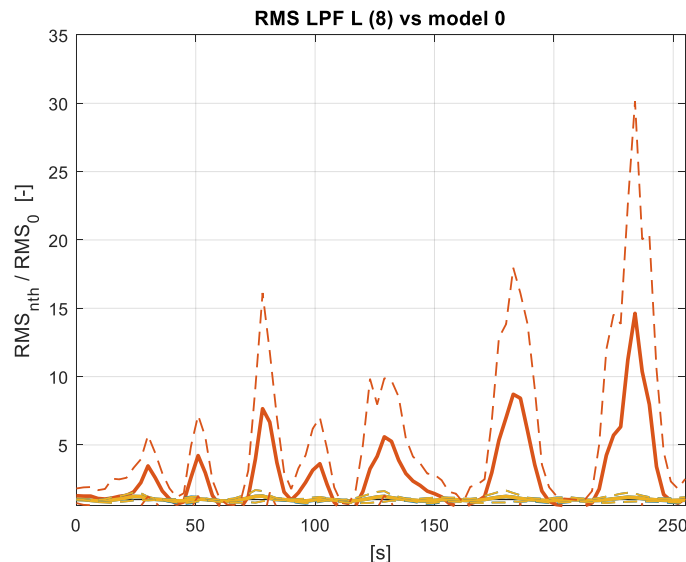


Fig. 60: Moving RMS acceleration curves, normalized by Model 0, for one person walking in loop over the staircase for 5 min; continuous line: mean value, dashed lines: confidence interval at 95 %; blue line: Model 1, red line: Model 2, yellow line: Model 3. Low Pass Filtered signals; values of accelerations extracted in correspondence of the position of accelerometer 8 (i.e. left side of the staircase).

As can be observed from Fig. 59, all the Models have the same moving RMS trend in time. However, Model 2, even if it has the same trend of the other Models, it is shorter than the others. Indeed, in Model 2 is considered the overlap between two consecutive footsteps, while in the other Models a new footstep is started only when the old one is ended. As a consequence, the same pedestrian requires less time in Model 2 to do the same number of footsteps with respect to the other Models. This shift means that, when a comparison between the RMS values of Model 2 and Model 0 is performed through their ratio, the ratio values will be far from 1 (1: the two Models produce the same results), since the two trends are out of phase, Fig. 60. Therefore, the normalization of Model 2 with respect to Model 0 is not worth. Not only, the normalization of Model 2 hides the normalization of Model 1 and 3, since they are in phase with Model 0 and so their ratio values are closer to the 1. For this reason, the normalized by Model 0 curve (mean + confidence interval at 95 %) of Model 2 was no more evaluated, leading to clearer plots, Fig. 61 (i.e. Fig. 60 without normalized Model 2).

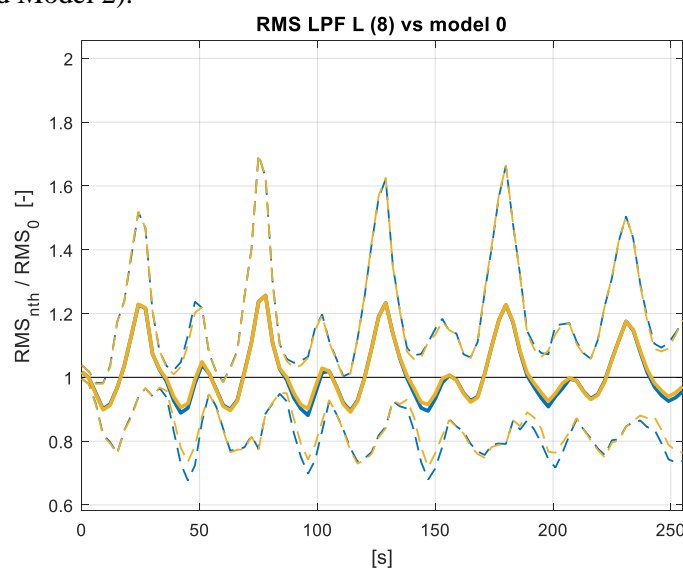


Fig. 61: Moving RMS acceleration curves, normalized by Model 0, for one person walking in loop over the staircase for 5 min; continuous line: mean value, dashed lines: confidence interval at 95 %; blue line: Model 1, yellow line: Model 3. Low Pass Filtered signals; values of accelerations extracted in correspondence of the position of accelerometer 8 (i.e. left side of the staircase).

Since for the evaluation of the vibration levels it is more interesting to look at the maximum value of the expected vibrations, the moving RMS acceleration curves were further processed. Indeed, their maximum value (in mean and confidence interval at 95 %) of the moving RMS acceleration curve of each Model was stored. Where with maximum is meant the upper limit of the confidence interval at the 95 %, as explained in

Fig. 62. The maximum stored values were then reported in a graph like the following right one:

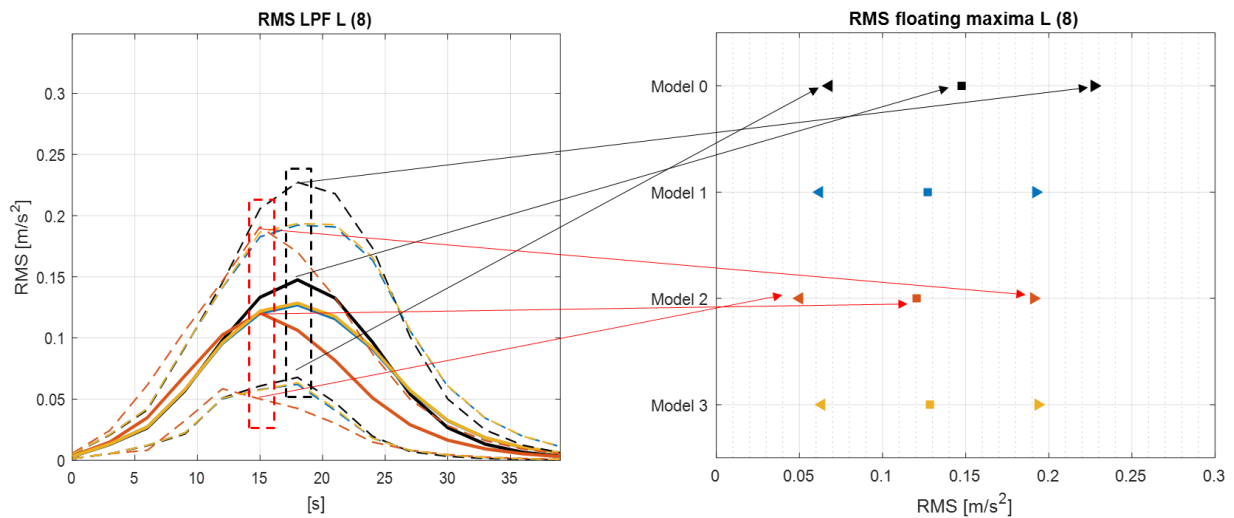


Fig. 62: Extraction of the maximum moving RMS acceleration values reached by each Model in case of a pedestrian who goes upstairs.

Summing up, at the end of the post processing stage, for each pedestrian case of Table 5, for both the “heel” and the “toe” database used (see Section 3.2) and for both the side of the staircase (in correspondence of the positions of the real accelerometer 8 and 9), the following type graphs were available:

- The Global RMS.
- The Model 0 normalized Global RMS.
- The histogram of the Global RMS.
- The histogram of the Model 0 normalized Global RMS.
- The Moving RMS.
- The Model 0 normalized Moving RMS.
- The Moving RMS maximum.

They depict the numerical estimation of the vibration level of every Models.

4.2 Experimental Campaign

In the experimental campaign, the pedestrian scenarios listed in Table 5 were tested on a real staircase (Fig. 37) with real people (Table 2). The instrumented structure was the same already discussed in Section 3.3.3 for the *Structure Analysis*, with the only difference that the electrodynamic shaker was removed by the staircase. The accelerometer pattern was the same one depicted in Fig. 39.

Coming back to the experiments, a more detailed list of the features of each tested scenario in the experimental campaign is reported in Table 6, always keeping Table 5 as the main reference.

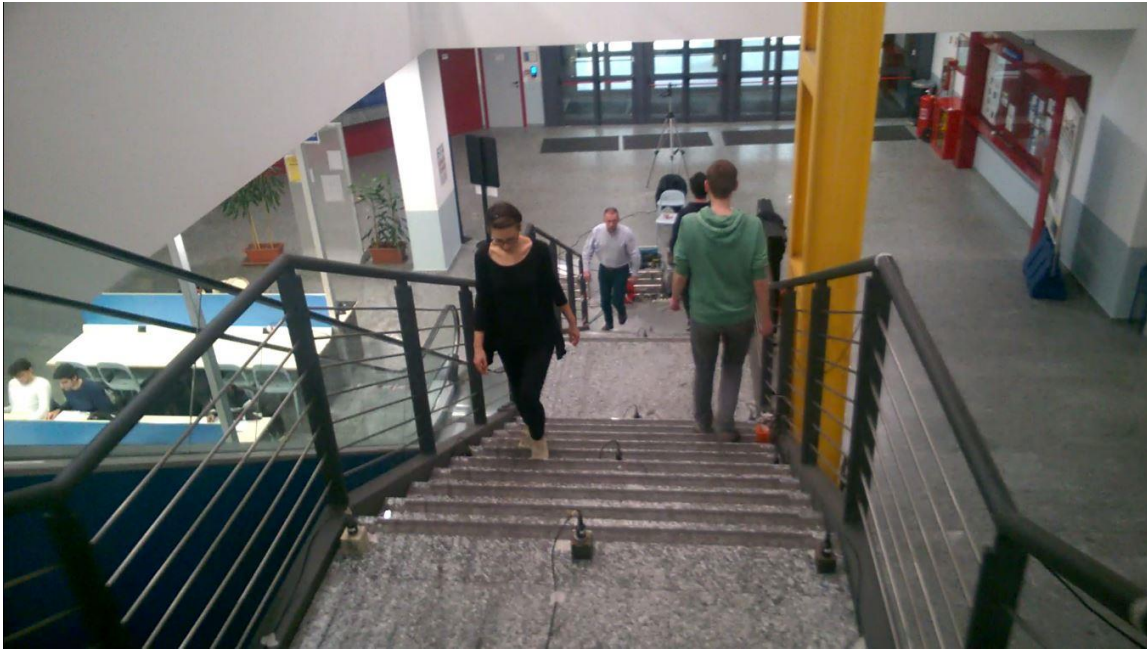


Fig. 63: Example of an experimental test on the real structure: 1st test of Table 6; 5 people walk for 25 min.

Test #	Type	# of persons	# of times	time	Initial positions					Subjects					Initial time [s]				
1	loop	5	1	25 min	1	10	22	46	63	2	1	3	5	4	0	0	0	0	0
2	loop	3	1 x group	5 min	1	41	46			4	5	3			0	0	0		
										1	5	4			0	0	0		
										2	3	4			0	0			
3	loop	1	1 x subject	5 min	34					1					0				
										2					0				
										3					0				
										4					0				
										5					0				
4	run	5	5 x group	required	1	1	1	34	34	1	2	4	3	5	9	9.9	10.8	0	0.9
5	run	5	1 x group	required	1	1	1	34	34	3	1	2	5	4	9	9.9	10.8	0	0.9
										3	1	4	5	2	9	9.9	10.8	0	0.9
										5	3	1	4	2	9	9.9	10.8	0	0.9
										5	4	2	1	3	9	9.9	10.8	0	0.9
4	5	3	2	1	9	9.9	10.8	0	0.9										
6	run	3	10 x group	required	1	1	34			5	3	4		7.2	8.1	0			
7	run	2	10 x group	required	34	34				3	5			0	9				
8	run	2	10 x group	required	1	1				3	5			0	9				
9	run	2	10 x group	required	1	34				5	3			0	0				
10	run	1	5 x subject	required	34					1					0				
										2					0				
										3					0				
										4					0				
										5					0				
11	run	1	5 x subject	required	1					1					0				
										2					0				
										3					0				
										4					0				
										5					0				

Table 6: Detailed list of tests performed with pedestrians on the real staircase.

The main difference with respect to Table 5 is a more detailed list of the tests that were classified with the label “random”, for what concerned the extraction of the subjects (i.e. test number 3, 5 10 and 11). Not only, here is also present a column that indicates the number of times for which the specific test was repeated. Another difference is the length of the first test: 25min. Indeed, a continuous long record was preferred during the experiments at a series of short experimental tests.

In post-processing phase, the acceleration time histories of the loop tests (i.e. test number 1, 2 and 3) were cut in shorter time histories of 2.30 min length. This passage was mandatory for test number 1, since a unique time history was acquired. Test number 2 and 3 instead, were further cut in order to increase the number of experimental observations. A final time length of 2.30 min was selected, since it was again long enough to represent the tested case, and because 2.30 min was half of 5 min (the length of test 2 and 3). In this way, 10 acceleration time histories were obtained for the test number 1 (25 min / 2.30 min), 6 for the second test (3 x 5 min / 2.30 min) and 10 for the third test (5 x 5 min / 2.30 min).

It is noted that when the term acceleration time history was used in the previous paragraph, that was referred to the set of 25 time histories coming from all the accelerometers placed along the staircase (Fig. 39). However, as was already mentioned in the previous Section, not all of them were used. Of course, the measurement of all the accelerometers was required for the identification of the modal parameters of the structure (Section 3.3). Here instead, the acceleration time histories coming from the accelerometers placed in correspondence of the points with the highest modal displacements of the structure were only considered, that are accelerometer 8 and 9 (Fig. 39). Accelerometer 8 was placed on the left side of the structure, while accelerometer 9 was placed on the right side of the structure. It is noted that in the numerical simulations, the acceleration time histories were extracted in correspondence of the points in which accelerometer 8 and 9 were applied on the real structure in the experimental campaign, in order to compare the numerical results with the experimental ones.

The acquired acceleration signals of the two specified accelerometers were then post-processed as was done for the acceleration time histories of the numerical simulations. Hence, they were passed in a Low Pass Filter (Butterworth filter, 8th order, cut-off frequency: 12 Hz) and then the global RMS and moving RMS (evaluated every 3 s) were computed. As an example, the case of a people who goes upstairs (test 10 of Table 5 and Table 6) is reported: the global RMS acceleration values in Fig. 64 and the moving RMS acceleration values in Fig. 65.

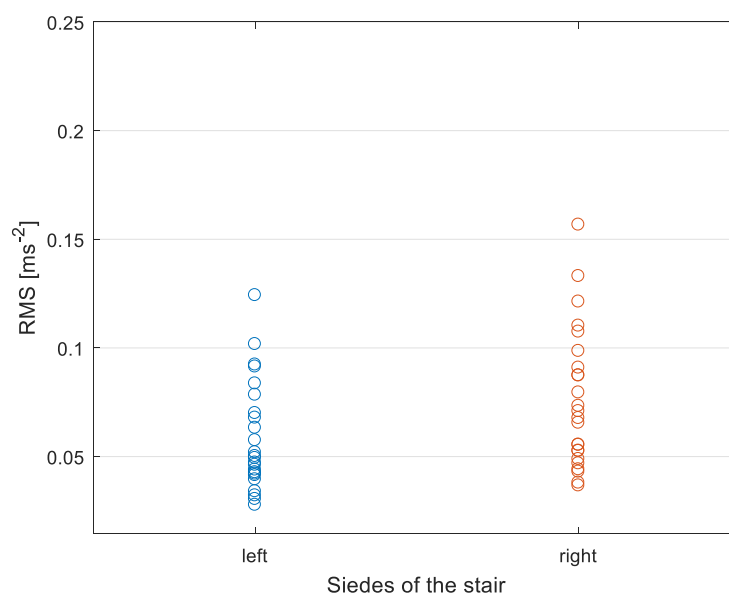


Fig. 64: Global RMS values of the accelerations measured by accelerometer 8 (left) and 9 (right). Case 10 of the experimental campaign (see Table 6): 25 experimental values per side (5 subject, 5 test per subject).

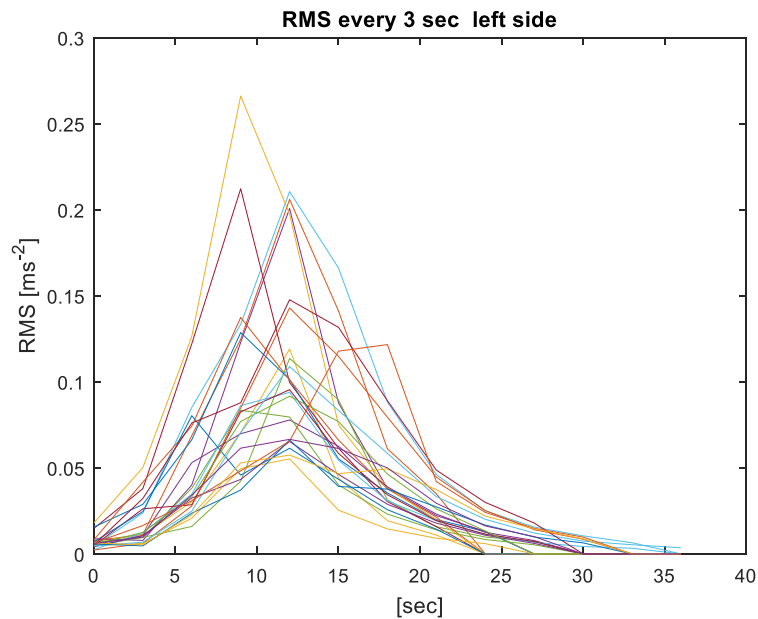


Fig. 65: Moving RMS curves evaluated every 3 s on the accelerations measured by accelerometer 8. Case 10 of the experimental campaign (see Table 6): 25 experimental curves (5 subject, 5 test per subject).

Not only, as was done for the numerical moving RMS values, also for the experimental ones the peak values of each moving RMS curves were stored and separated plotted:

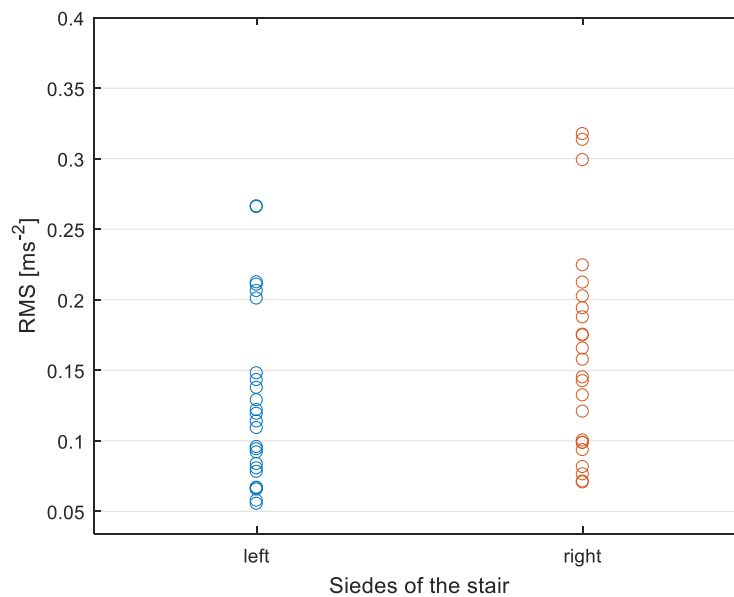


Fig. 66: Maximum values assumed by the moving RMS acceleration curves measured by accelerometer 8 (left) and 9 (right). Case 10 of the experimental campaign (see Table 6): 25 peaks per side (5 subject, 5 test per subject, 1 peak per test (due to the type of test: “run”)).

It is to be pointed out that the peak values of the moving RMS curves for the “loop” cases (i.e. test number 1, 2 and 3 of Table 5 and Table 6) were evaluated every 40 s. Indeed, in the loop tests, the moving RMS trends present a periodicity given by the loop condition. Such a periodicity is equal to the time required from a person to complete a round of the staircase. To determine the periodicity, the autocorrelations of the moving RMS curves were evaluated, obtaining as average value 40 s. As an example, in Fig. 67 and Fig. 68 are reported the autocorrelation curves for a moving RMS curve of a subject who walks for 5 min in loop (test number 3 of Table 6) and of 5

subjects who walk for 25 min in loop (test number 1 of Table 6) respectively. A plot of the maximum values assumed by the moving RMSs in test number 3 (a person walks in loop for 5 min) is reported in Fig. 69, as an example too.

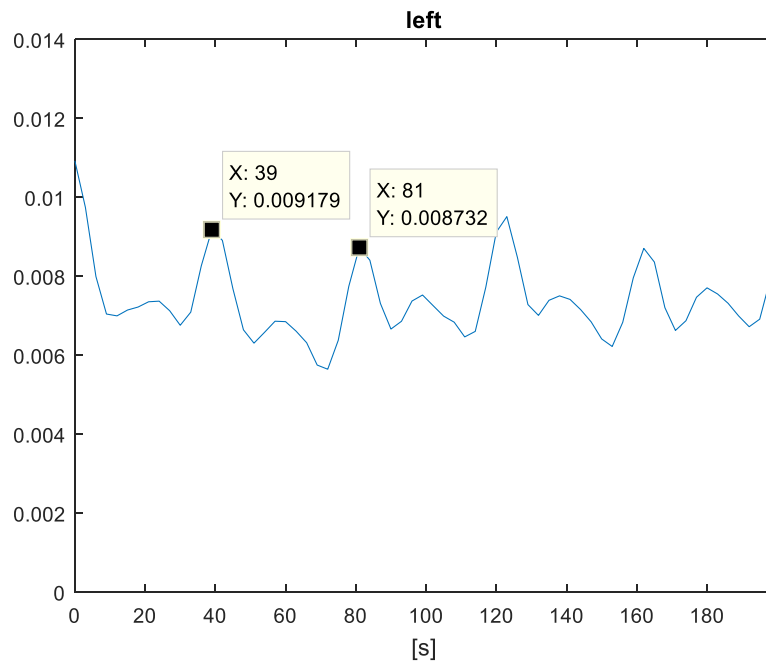


Fig. 67: Autocorrelation curve of an experimental moving RMS curve for a pedestrian who walks in loop for 5 min, evaluated on the left side of the staircase (accelerometer 8).

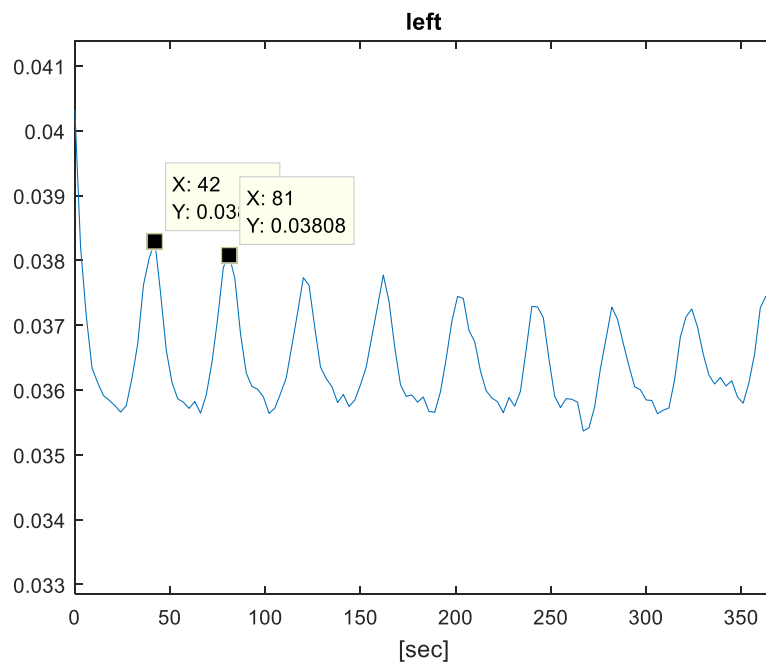


Fig. 68: Autocorrelation curve of an experimental moving RMS curve for 5 pedestrians who walk in loop for 25 min, evaluated on the left side of the staircase (accelerometer 8).

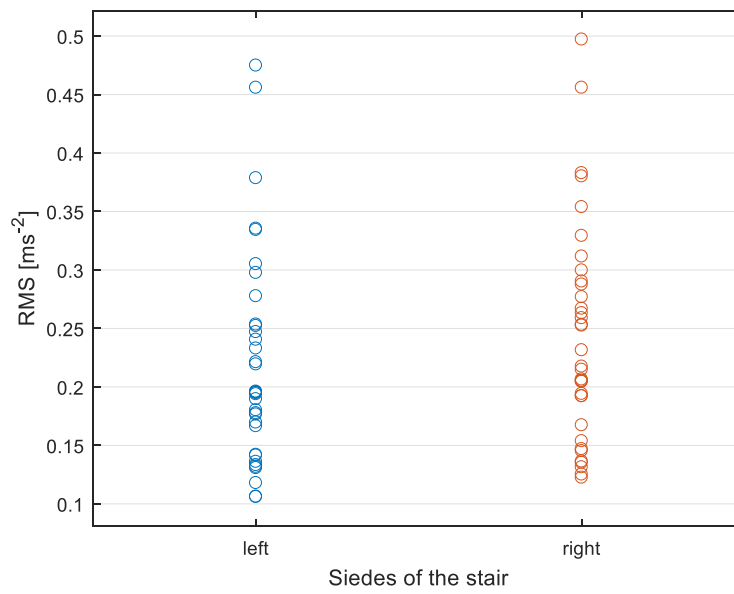


Fig. 69: Maximum values assumed by the moving RMS acceleration curves measured by accelerometer 8 (left) and 9 (right). Case 3 of the experimental campaign (see Table 6). 35 peaks per side, since 5 moving RMS curves of 5 min were available (5 subject, 1 test per subject) and the assessment of the peaks was made every 40 s.

Chapter 5

Results & Discussion

In this Chapter, all the results of the numerical simulations and of the experimental campaign on the real structure are reported, along with a discussion about them. More in detail, some of the results of the most significant HSI tested scenarios will be at first summarized in a series of tables (Table 7, Table 8, Table 9 and Table 10), in order to allow a sight of the way in which the considered structure dynamically behaves and to provide a comparison of the used Models. Then, the results of every tested case will be shown, through its own sequence of plots, like the ones illustrated in Chapter 4 (i.e. global RMSs and moving RMSs). They contain both the numerical and the experimental outcomes, to allow a faster comparison of them. It is to be recalled that, in the numerical simulations, both the case of pedestrians walking with complete contact of the feet with the steps of the stair (“heel” configuration) and the case of pedestrians walking on the tip of the feet (“tiptoe” configuration) for the ascending crossings were considered (seen Section 3.2 for details). Therefore, the results of the simulated HSI cases are reported for both the walking configurations. It is noted that all the results are reported for the accelerometers 8 and 9, for the experimental ones, and in correspondence of the positions of accelerometer 8 and 9, for the numerical ones. Such positions were selected as they are the ones in which the mode shapes of the structure have their greatest modal components per side: accelerometer 8 for the left and accelerometer 9 for the right one. See the end of Section 2.3.2 and Section 3.3 for details.

As explained in Chapter 4, all the signals were filtered before to be processed. The aforementioned graphs will be reported for the Low Pass Filtered (LPF) signals (cut-off frequency: 12 Hz). Summary tables, as the ones that will be presented at the beginning of the LPF results, will be reported for the numerical acceleration time histories filtered around the first and second mode of the structure (i.e. Band Pass Filtered signals): cut-off frequency range of 6-8.3 Hz for the first mode and 8.3-11 Hz for the second mode. That to evaluate the contribution of each mode to the global dynamic response of the structure. Finally, a Frequency Response Analysis of the occupied structure will be shown, for the occupied structure implemented with the different Models. In this way, an evaluation of how the Models consider the occupied structure, under a Frequency Response point of view, is also investigated.

For the sake of clarity, even if the table with the scheduled HSI scenarios tested (i.e. Table 5) have been already included in Chapter 4, it is here below reported too. The same holds for the scheme of the discretized staircase with on it the accelerometer positions, which is reported in Fig. 70. In it, the positions of accelerometer 8 and 9 are highlighted.

Test #	Type	# of persons	Involved	Initial positions	Subjects	Initial time [s]
1	loop	5	fixed	1 10 22 46 63	2 1 3 5 4	0 0 0 0 0
2	loop	3	fixed	1 41 46	4 5 3	0 0 0
3	loop	1	random	34	-	0
4	run	5	fixed	1 1 1 34 34	1 2 4 3 5	9 9.9 10.8 0 0.9
5	run	5	random	1 1 1 34 34	- - - - -	9 9.9 10.8 0 0.9
6	run	3	fixed	1 1 34	5 3 4	7.2 8.1 0
7	run	2	fixed	34 34	3 5	0 9
8	run	2	fixed	1 1	3 5	0 9
9	run	2	fixed	1 34	5 3	0 0
10	run	1	random	34	-	0
11	run	1	random	1	-	0

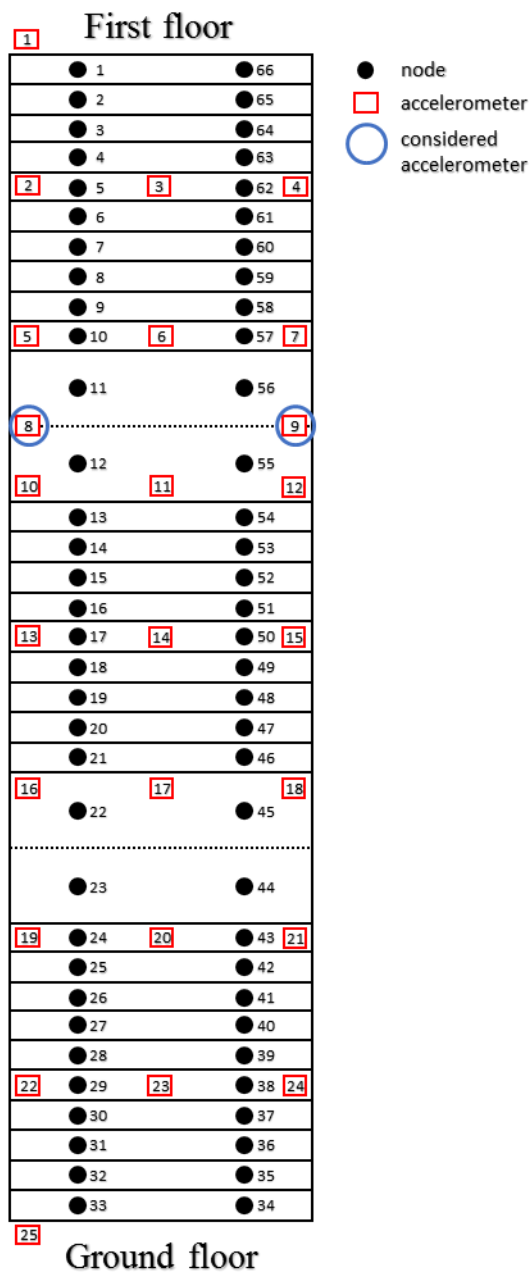


Fig. 70. Discretized structure, with highlighted the positions of the consider accelerometers for the evaluation of the results (blue circles).

5.1 Summary Tables

In this section, a series of tables are presented. Here, the results of some of the most significant tests are reported, in order to show the behavior of the structure and in order to compare the different Models. Since the estimation of the vibration levels performed by each Model was evaluated by means of mean RMS acceleration values and the RMS acceleration values for a confidence interval at 95 %, these same values are reported in the tables. Since the aim is a comparison of the Models in different situations, the results are reported for the simulations conducted with the heel database only. However, in the next Section, the whole results will be shown for both the types of databases implemented.

RMS [m/s ²]	1 person goes downstairs on the left side				1 person goes upstairs on the right side			
	Left side		Right side		Left side		Right side	
	μ	$\pm 2\sigma$	μ	$\pm 2\sigma$	μ	$\pm 2\sigma$	μ	$\pm 2\sigma$
model 0	0.153	0.065	0.139	0.051	0.085	0.033	0.119	0.052
model 1	0.137	0.055	0.129	0.046	0.076	0.028	0.104	0.044
model 2	0.137	0.061	0.133	0.049	0.069	0.027	0.092	0.043
model 3	0.137	0.055	0.129	0.046	0.077	0.028	0.105	0.045

Table 7: Estimations of the vibration levels by means of Global RMS acceleration values obtained with the four Models, expressed in terms of mean value and confidence interval at 95 % with respect to the mean value. Left column: test number 11 of Table 5, right column: test number 10 of Table 5. Acceleration values read in correspondence of accelerometer 9, heel tests.

From Table 7 it is possible to observe the results in terms of global RMS values of acceleration for the simulations for a pedestrian who go downstairs on the left side and for a one who goes upstairs on the right side (test number 10 and 11 of Table 5 respectively).

Looking at the behavior of the structure utilized for the experiments (staircase of Fig. 37) it is possible to observe how the dynamical response of the right side of the structure is greater than the left one for a person who goes upstairs, while the responses of the two sides are much more similar for a pedestrian who goes downstairs. Of course, these are the results of the numerical simulations, but they are conducted with the modal parameters of the structure, obtained by an Experimental Model Analysis conducted on purpose (Section 3.3). The great contribution of the right side in the response of the staircase is present both in case of the pedestrian that crosses the right side (ascending crossing) and in case of he/she that crosses the left side (descending crossing). This is confirmed also by the experimental tests (Fig. 71 and Fig. 72), where the global RMS values of the left side assume values more similar to the right side ones in case of descent of the pedestrian, while are lower for the ascent of the pedestrian.

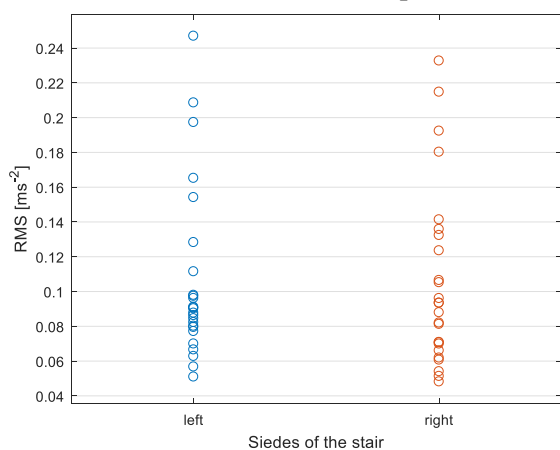


Fig. 71. Global RMS values of acceleration (left: accelerometer 8/ right: accelerometer 9) for the experimental test number 11.

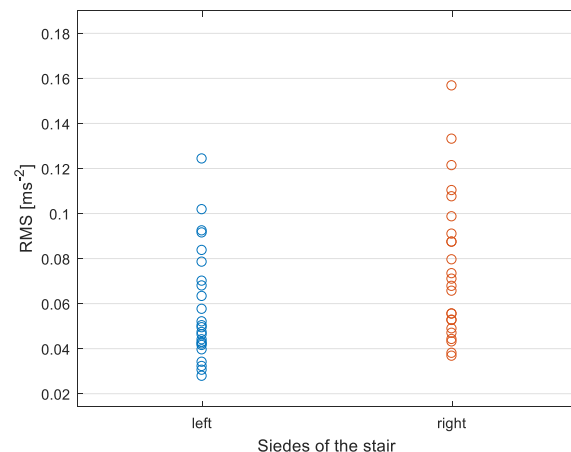


Fig. 72. Global RMS values of acceleration (left: accelerometer 8/ right: accelerometer 9) for the experimental test number 10.

Looking at the specific Model in Table 7, all the estimations of the vibration levels obtained with the new Models (i.e. 1, 2 and 3) are slightly lower than the ones obtained with Mode 0, both in terms of mean value and confidence interval (95 %).

RMS [m/s ²]			Left side		Right side	
			μ	$\pm 2\sigma$	μ	$\pm 2\sigma$
5 min	1 person	model 0	0.135	0.035	0.143	0.032
		model 1	0.125	0.032	0.133	0.031
		model 2	0.130	0.031	0.133	0.029
		model 3	0.125	0.032	0.134	0.031
	3 persons	model 0	0.205	0.037	0.213	0.037
		model 1	0.194	0.035	0.203	0.035
		model 2	0.201	0.031	0.202	0.031
		model 3	0.195	0.035	0.206	0.034
	5 persons	model 0	0.234	0.019	0.238	0.017
		model 1	0.230	0.018	0.234	0.017
		model 2	0.238	0.020	0.235	0.019
		model 3	0.232	0.018	0.239	0.018

Table 8: Estimations of the vibration levels by means of Global RMS acceleration values obtained with the four Models, expressed in terms of mean value and confidence interval at 95 % with respect to the mean value. The tests per rows are: third test of Table 5 in the first set of rows, second test of Table 5 in the second set of rows and first test of Table 5 in the third set of rows. Acceleration values read in correspondence of accelerometer 9, heel tests.

Hence, from Table 7 it is possible to observe the results for fast tests, since they required just the time to cross the structure. Conversely, in Table 8, the results of the long tests are reported (test number 1, 2 and 3 of Table 5), in which the people walk in loop on the staircase for 5 min. the results are always in terms of global RMS values of acceleration. As observed in the previous table (Table 7) the right side of the structure has an important contribution in the dynamic response of the staircase. The same is shown here by Table 8, even if the differences among the two sides are smoothed by the type of test (high number of pedestrians and long times). Fig. 73 is reported as experimental example (test number 1: 5 pedestrians walk in loop).

Looking at the specific Model, no significant variations are observed, both in terms of mean value and confidence interval.

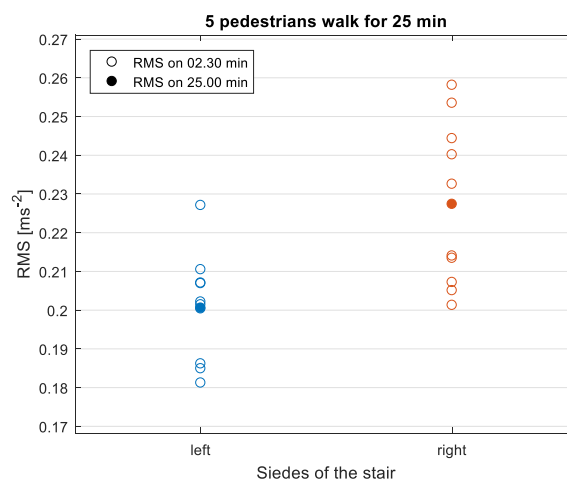


Fig. 73: Global RMS values of acceleration (left: accelerometer 8/ right: accelerometer 9) for the experimental test number 1.

RMS n-th / RMS 0		fast test (one stroke)		long test (5 min)	
		μ	$\pm 2\sigma$	μ	$\pm 2\sigma$
1 person	model 0	0,119	0,052	0,143	0,032
	model 1	0,092	0,043	0,133	0,029
	model 3	0,105	0,045	0,134	0,031
5 persons	model 0	0,213	0,064	0,238	0,017
	model 1	0,168	0,045	0,235	0,019
	model 3	0,174	0,047	0,239	0,018

Table 9: Estimations of the vibration levels by means of Global RMS acceleration values obtained with Model 0, 1 and 3, expressed in terms of mean value and confidence interval at 95 % with respect to the mean value. Acceleration values read in correspondence of accelerometer 9, heel tests. The tests reported are the following:

- 2nd quadrant (1 person/fast test): test number 10 of Table 5.
- 1st quadrant (1 person/long test): test number 3 of Table 5.
- 3rd quadrant (5 person/fast test): test number 5 of Table 5.
- 4th quadrant (5 person/long test): test number 1 of Table 5.

RMS n-th / RMS 0		fast test (one stroke)		long test (5 min)	
		μ	$\pm 2\sigma$	μ	$\pm 2\sigma$
1 person	model 1 / model 0	88.2%	12.3%	92.8%	4.4%
	model 3 / model 0	89.5%	11.0%	93.5%	4.2%
5 persons	model 1 / model 0	81.2%	10.7%	98.4%	2.9%
	model 3 / model 0	82.4%	10.6%	100.4%	3.1%

Table 10: Estimations of the vibration levels by means of Global RMS acceleration values obtained with Model 1 and 3 normalized by Model 0, expressed in terms of mean value and confidence interval at 95 % with respect to the mean value. Acceleration values read in correspondence of accelerometer 9, heel tests. The tests reported are the following:

- 2nd quadrant (1 person/fast test): test number 10 of Table 5.
- 1st quadrant (1 person/long test): test number 3 of Table 5.
- 3rd quadrant (5 person/fast test): test number 5 of Table 5.
- 4th quadrant (5 person/long test): test number 1 of Table 5.

Table 10 can be considered one of the most important outcomes of the current thesis. It reports the global RMS values of acceleration of Model 1 and 3 normalized by Model 0. Model 2 is not reported for the reason already explained in Section 4.1.5, that is its out of phase of the simulation time with respect to the one of Model 0 (and also Model 1 and 3). Therefore, with a point by point normalization, different instances of the simulation would be compared, leading to the meaningfulness of the values obtained by such normalization with Model 0. In Table 9, the absolute values of the normalized cases of Table 10 are reported for completeness. However, the table considered in the following discussion is Table 10. It is noted that the normalized values of Table 10 are not obtained by ratio of the absolute values of Table 9, but by a one by one ratio of each of the 100 simulations of the specific case, as explained in Chapter 4.

As can be noted, four completely different scenarios are reported in Table 10 (see the caption for details). Before of the discussion of the results, it is worth to be recalled how the different Models work. All of them treat the AGRFs of pedestrians locally. Conversely, the PGRFs (i.e. the passive pedestrian contributions) are managed in different ways: Model 1, 2 and 3 locally considered the PGRFs (like the AGRFs), while Model 0 spreads the overall passive pedestrian contributions over the entire structure (see Section 1.2 and 2.1 for details). It is noted that the main effect of PGRFs (i.e. the forces provided as response of the human body by the apparent mass curves, as responses of the vibration of the structure) is the addition of damping to the structure. Therefore, with the new Models the damping is locally introduced with the pedestrians (i.e. concentrated damping effects), while, with Model 0, it is distributed over the entire structure (i.e. so present everywhere but with a lower magnitude).

In the fourth quadrant of Table 10 (5 pedestrians/long test) are reproduced the applicability conditions of Model 0. Indeed, as was just explained, it is an approximated approach, which was built up [2] to deal with high number of spread people (i.e. dense pedestrian situations) and long times. The same situation of the fourth quadrant, since the 5 pedestrians were distributed over the entire structure before to start to walk. From the fourth quadrant is clear as the Models produce results close each other (mean values close to 100 %) with low differences among them (confidence intervals at 95 % close to 3 %). Such results confirm that, in the current scenario, Model 0 is a good approximation of the more detailed Models. This is due to the fact that the local addition of damping, brought by each of the moving pedestrian in the new Models, produces an effect which is similar to the one produced by the same amount of passive components spread over the structure. This works because the pedestrians were placed over the entire structure.

Instead, in the third quadrant (5 pedestrians/fast test), even if the number of pedestrian is the same of the fourth quadrant case, considerable variations are present among the estimated vibrations of the new Models and the ones of the old one (Model 0). Indeed, a global RMS acceleration value up to 18.8 % lower than Model 0 is obtained with Model 1 in the estimation of the mean vibration expected (Model 1/ Model 0: $\mu = 81.2\%$, Table 10). This with a confidence interval ($\pm 2\sigma$) of 10.7 %. Hence, a lower limit difference of 29.5 % (i.e. 18.8 % + 10.7 %), with respect to the estimation made by Model 0, is obtained. This change of the results, with respect to the fourth quadrant ones, is due to how the available pedestrians were applied to the structure. Indeed, three of them were done go downstairs, (starting the crossing at a distance of one step) and two of them were made go upstairs (always starting with a distance of 1 step) and the descending group was made start 9 s after the upstairs group (test number 5 of Table 5). With this time delay between the starting instants, the two groups of crossing pedestrians were made meet in correspondence of the second landing (nodes of the structure 11, 12, 13, 55 and 56, Fig. 70). In correspondence of the second landing, the modal coordinates of the first and second mode of structure (the one considered) have their higher components. This means that those are the points of the structure where the pedestrians have the highest effect, both in terms of excitation and damping. Therefore, at the instant of the meeting of the two groups, they are exciting the structure in the powerful possible way.

All the Models do this, since all of them place the AGRFs where the pedestrians are on the structure. What changes, is the passive contributions, the apparent mass curves. Indeed, as already introduced, Model 0 is the only one that spread the passive contributions, and so the damping effect. As a consequence, a less effective damping action is applied in correspondence of the highly excited points, leading to high vibration levels estimated. Conversely, the new Models concentrate the damping effects in the same points of the AGRFs. Therefore, of course they strongly excite the structure (as Model 0), but at the same time they are able to properly locally damp the structure, leading to much lower vibration levels estimated. It is to be pointed out that, even if Model 2 is not reported in Table 10 for the aforementioned reason, similar results to the ones of Model 1 and 3 were obtained with it, as will be shown in the next Section with the complete results reported.

In the second quadrant (1 pedestrian/fast test) instead, a single pedestrian who goes upstairs is considered. The results are almost the same, but with slightly lower differences with respect to the ones of Model 0. This is due to the fact that, even if what happens is the same just explained for the third quadrant, only one person is present on the structure. Therefore, the localized damping capability of the new Models result lower with respect to the previous case (five pedestrians who converge in the area of the structure with the higher modal components), leading to a decrease of differences with respect to Model 0. This issue will be better addressed in Section 5.1.5, where a Frequency Response analysis of the occupied structure, exactly with one pedestrian as example case, will be reported.

In the last quadrant of Table 10 (the first one: 1 pedestrian in loop on the staircase), mean results are obtained, between the ones of the second and fourth quadrant, with a great decrease of

variability ($\pm 2\sigma$ /confidence interval at 95 %). However, always an underestimation (around 7 %) of the vibration levels, with respect to Model 0, is present.

Summing up, a clear difference is so depicted by Table 10 in the adoption of the different Models in different scenarios. A great agreement is found between the new Models and Model 0 in case of a high number of people spread over the structure (i.e. the design condition of Model 0). While a lower estimation of the vibration levels is reported with the new Models in case of high number of pedestrians, but with no spread initial positions, and also for the case of low number of pedestrians (only 1, as limit case, in quadrant 2 and 1). In terms of global RMS value, differences up to 18.8 % in mean value and up to 29,5 % with a confidence interval at 95 % are obtained.

5.2 Whole Results

In this Section, the full set of results, for each tested scenario, is shown. The numerical outcomes are reported per simulation executed, with both the apparent mass databases: one for the configurations with the complete contact of the feet with the ground (“heel” configurations) and for the ones with only the tip of the feet in contact with the ground (“tiptoe” configurations), for the ascending crossing. They are split on the left side of the pages (the “heel” ones) and on the right side of the pages (the “tiptoe” ones). The results are divided per tested scenario, following the order of Table 5. As explained in Chapter 4, the label “fixed” or “selected” means that the pedestrians were chosen and always the same were used during the experimental test and the corresponding simulations. While, the label “random” means that a random selection of the involved pedestrians during the simulations, and a sequence of different pedestrians in the experimental tests (see Table 6 for details), was done.

Test number 1: 5 pedestrians (selected) walk in loop

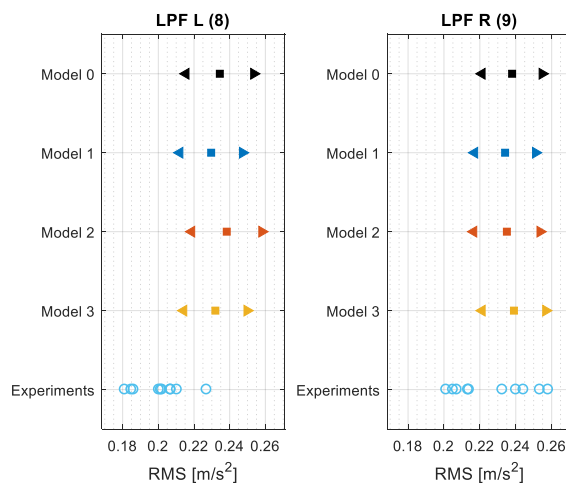


Fig. 74 Global RMS values of the acceleration; accelerometer 8 (left) and 9 (right); simulations made with the “heel” database; \square : mean value / $\triangleleft\triangle$: confidence interval at 95 %; test number 1.

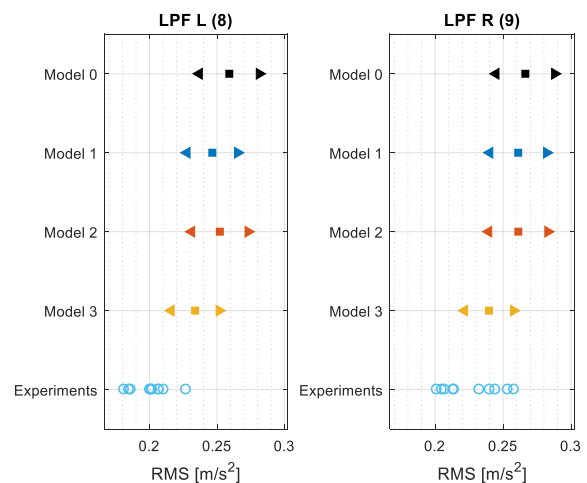


Fig. 75 Global RMS values of the acceleration; accelerometer 8 (left) and 9 (right); simulations made with the “tiptoe” database; \square : mean value / $\triangleleft\triangle$: confidence interval at 95 %; test number 1.

Fig. 74 and Fig. 75 represent the Global RMS values of acceleration, evaluated on both the side of the staircase (left side: L (accelerometer 8) /right side: R (accelerometer 9)). Fig. 74 shows the results obtained with the Models by using the heel database, while Fig. 75 the ones obtained with the tiptoe database. As for the experimental global RMS points, they are the same between the two figures (per side).

Since test number 1 involves un high number of people (5) spread over the structure, and lasts a lot (5min), the ideal applicability conditions of Model 0 occur. Indeed, the estimated vibration ranges by the Models of Fig. 74 are almost identical.

The tiptop configuration is characterized by apparent mass curves which provide a lower damping effect (Section 3.2.4). Indeed, the value of vibrations estimated by the Models with the use of the tiptoe database increase with respect to the ones with the heel one, and in different ways.

For what concern the experimental points (see Chapter 4 for details on how they are obtained), the ones of the right side of the structure are well estimated with the use of the heel database, while they are predicted by Model 3, and only the higher values are estimated by the other Models, for the tiptoe database. Instead, the experimental values of the left side are over estimated by the Models, with both the databases. It is to be pointed out that the maximum experimental values fall in the predicted vibration intervals, and that the Models overestimate and do not underestimate the vibrations of the structure, leading to a safer prediction with respect to an underestimating evaluation of the vibration levels.

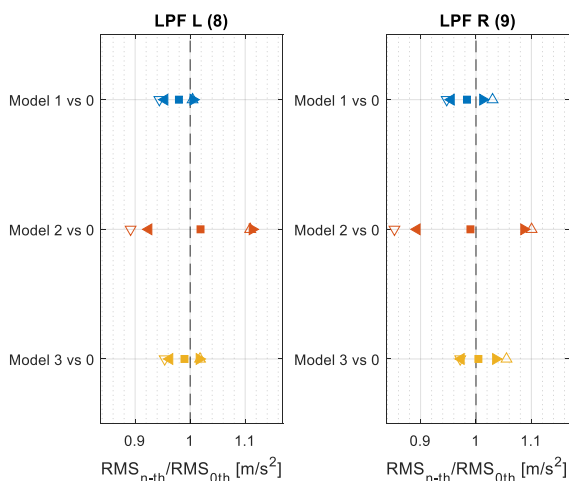


Fig. 76 Global RMS values of acceleration normalized by Model 0; accelerometer 8 (left) and 9 (right); simulations made with the “heel” database; \square : mean value / $\langle \triangleright \triangleleft$: confidence interval at 95 % / Δ : maximum ratio value / ∇ : minimum ratio value; test number 1.

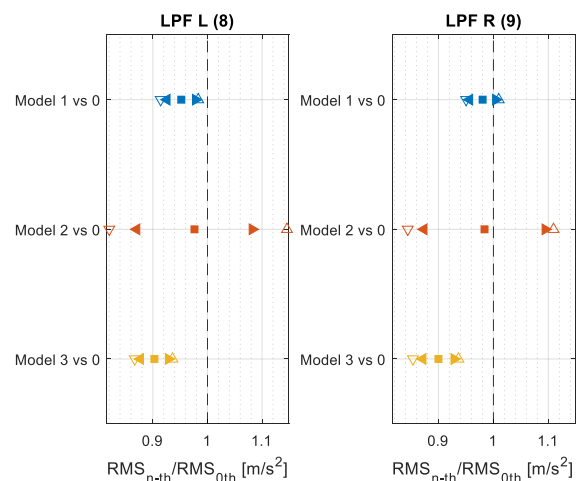


Fig. 77 Global RMS values of acceleration normalized by Model 0; accelerometer 8 (left) and 9 (right); simulations made with the “tiptoe” database; \square : mean value / $\langle \triangleright \triangleleft$: confidence interval at 95 % / Δ : maximum ratio value / ∇ : minimum ratio value; test number 1.

In Fig. 76 (heel database use) and Fig. 77 (tiptoe database use) are reported the normalized by Model 0 global RMS acceleration values of the Models, obtained with the procedure explained in Chapter 4. As was shown by the absolute values reported in Fig. 74 and Fig. 75, a high agreement is present for all the Models with Model 0 (variations less than 5 %), but Model 3 for the case of the tiptoe database use. The larger difference of Model 2 (variations of 10 %) with respect to Model 0, compared to the ones of Model 1 and 3, is due to the fact that Model 2 is out of phase with respect to all the other Models, as explained before and in details in Chapter 4. For these reason, even if these are global RMS values, the dispersions of the ratios of Model 2 are higher than the ones of the other two Models.

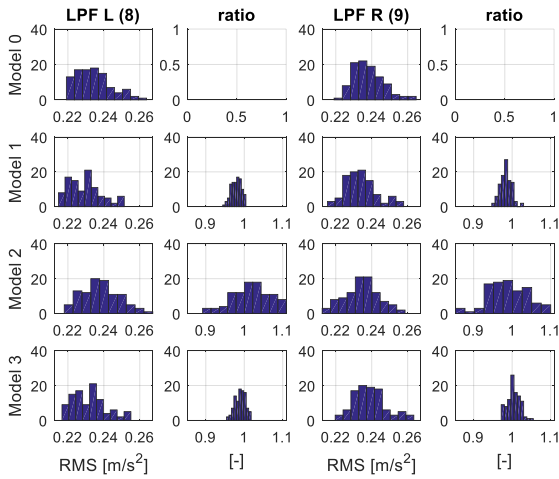


Fig. 78 Histograms of the Global RMS of acceleration and of the normalized by Model 0 ones; accelerometer 8 (left) and 9 (right); simulations made with the “heel” database; test number 1.

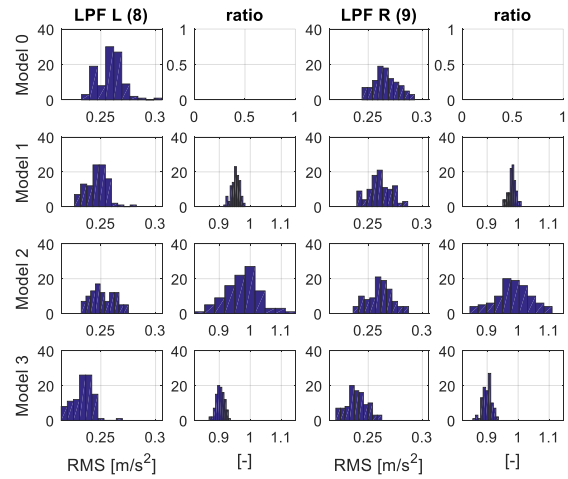


Fig. 79 Histograms of the Global RMS of acceleration and of the normalized by Model 0 ones; accelerometer 8 (left) and 9 (right); simulations made with the “tiptoe” database; test number 1.

In Fig. 78 and Fig. 79 are depicted the histograms of the 4 plots just showed: Fig. 78 for the heel configuration of the ascending crossing, while Fig. 79 for the tiptoe configuration of the ascending crossing. The firsts and the thirds columns shows the absolute values of the two side of the staircase, while the second and the fourth columns show the values normalized by the Model 0 ones. The considerations about Fig. 78 and Fig. 79 are the same done for Fig. 74, Fig. 75, Fig. 76 and Fig. 77.

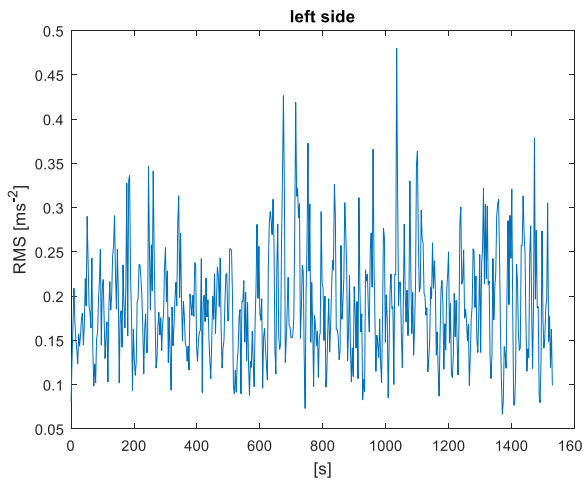


Fig. 80 Moving RMS of acceleration evaluated every 3 s; experimental data - accelerometer 8, test number 1.

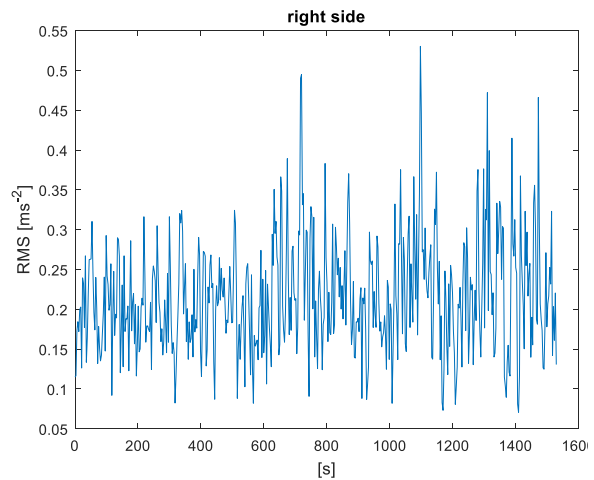


Fig. 81 Moving RMS of acceleration evaluated every 3 s; experimental data - accelerometer 9, test number 1.

Above (Fig. 80 and Fig. 81) are reported the experimental moving RMS values of acceleration, evaluated every 3 s. Fig. 80 shows the values for accelerometer 8 (left side of the staircase), while Fig. 81 shows the values for accelerometer 9 (right side of the staircase). Since the experimental test lasted 25 min (i.e. 1500 s), and only in post processing 10 sub-time histories of 2.30 min were obtained, the moving RMS was evaluated directly on the whole acceleration time history (for both the sides/accelerometers). While the sub-time histories were used only for the global experimental RMS (blue circles in Fig. 74 and Fig. 75), as was fully explained in Chapter 4.

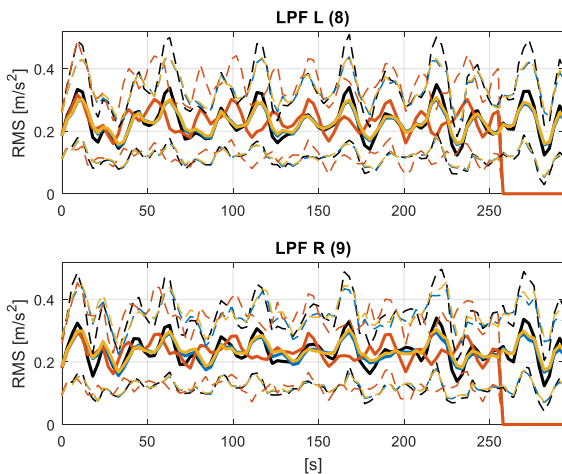


Fig. 82 Moving RMS of acceleration evaluated every 3 s; accelerometer 8 (up) and 9 (down); simulations made with the “heel” database; continuous line: mean value / dashed lines: confidence interval at 95 %; black curve: Model 0, blue curve: Model 1, red curve: Model 2, yellow curve: Model 3; test number 1.

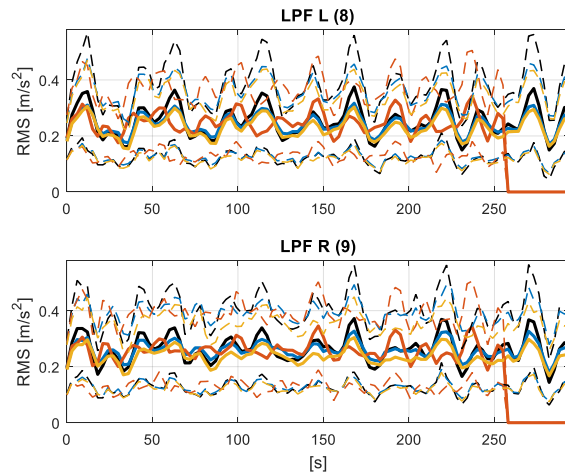


Fig. 83 Moving RMS of acceleration evaluated every 3 s; accelerometer 8 (up) and 9 (down); simulations made with the “tiptoe” database; continuous line: mean value / dashed lines: confidence interval at 95 %; black curve: Model 0, blue curve: Model 1, red curve: Model 2, yellow curve: Model 3; test number 1.

Fig. 82 and Fig. 83 show the moving RMS acceleration curves obtained with both the heel and tiptoe database, respectively. The upper graphs are for the left side of the structure, while the downer ones for the right side. In all the four plots can be observed how Model 2 (red curves) ends before the other Models. Indeed, since the pedestrians in it require lower time to cross the same number of steps, due to the consideration of the overlap between subsequent footsteps, it was stopped when the pedestrians reached the same number of steps crossed by the pedestrians in the other Models.

The main reason for which was decided to evaluate the RMS of the accelerations also every 3 s (moving RMS), and not only on the global signals (global RMS), is depicted in the plots. Because in this way it is possible to observe the evolution of the RMS value estimated by each Model, and so it is possible to compare them along the evolution of the simulation, and not only globally, as it is done with the global RMS values.

Indeed, from Fig. 82 and Fig. 83, the periodic trends of the RMS values, due to the loop condition of the pedestrians, can be observed, which underline the correctness of the simulated situation. Moreover, mainly two RMS lobes can be seen that are continuously repeated, with one higher than the other. They are due to the passage of some pedestrians in correspondence of accelerometer 8 (small lobes) and in correspondence of the accelerometer 9 (high lobes). Indeed, at the positions of these two accelerometers, the modal coordinates of the first two modes of the structure assume their highest values, with the right side (i.e. accelerometer 9) with higher values. Of course, the pedestrians were spread over the entire structure, but not perfectly equally spaced initial positions were assumed (see table 1). Therefore, the passage of a slightly closer number on pedestrians in loop have produced the depicted RMS trends in Fig. 82 and Fig. 83.

Looking at the trends, a higher value of Model 0 (black line) can also be noted at the peaks of the lobes. That indicate a lower damping action with respect to the other Models, when the less spread sequence of pedestrians (as just explained above) cross the positions close to accelerometer 8 and 9. The opposite behavior is observed in proximity of the grooves, that occurs when the less spread sequence of pedestrians is far from accelerometer 8 and 9 (i.e. far from area of the structure with the highest modal components). There Model 0 shows a higher damping with respect to the other Models. This issue will be further examined in Section 5.1.5. These exchanges of damping behaviours among the Models, between the peaks of the lobes and the bottoms of the grooves, are the reasons for which the global RMSs provide almost the same estimated values for all the Models.

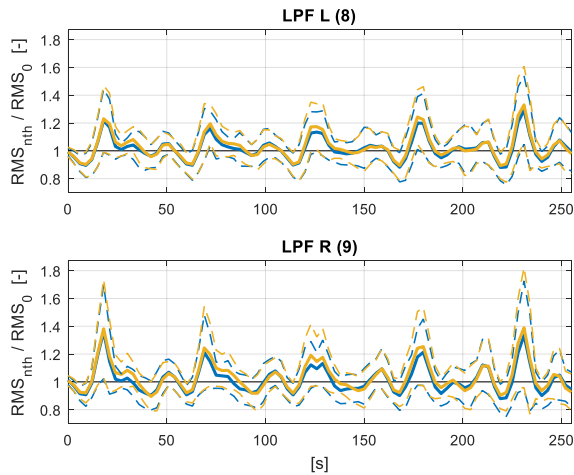


Fig. 84 Moving RMS of acceleration evaluated every 3 s normalized by Model 0; accelerometer 8 (up) and 9 (down); simulations made with the “heel” database; continuous line: mean value / dashed lines: confidence interval at 95 %; black curve: Model 0, blue curve: Model 1, yellow curve: Model 3; test number 1.

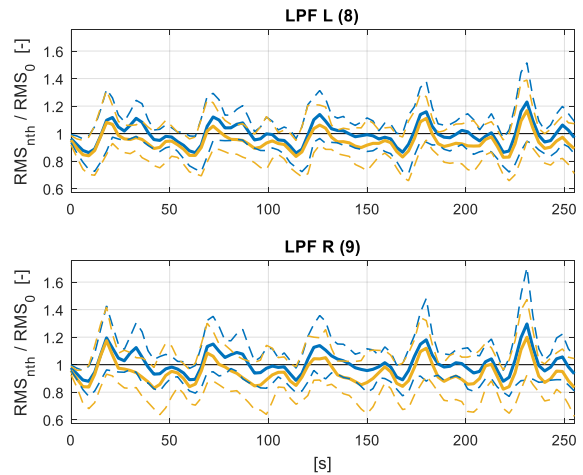


Fig. 85 Moving RMS of acceleration evaluated every 3 s normalized by Model 0; accelerometer 8 (up) and 9 (down); simulations made with the “tiptoe” database; continuous line: mean value / dashed lines: confidence interval at 95 %; black curve: Model 0, blue curve: Model 1, yellow curve: Model 3; test number 1.

The positions of the peaks of the lobes and the bottoms of the grooves can be clearly observed by Fig. 84 and Fig. 85, which depict the normalization by Model 0 moving RMS curves (for all the passages see Chapter 4). Model 2 (the missing red line) is omitted for the aforementioned reason. The positions of the lobes coincide with the instants in which the Models assume values lower than 1, while the positions of the grooves are shown by the overestimations of the vibration levels predicted by Model 0. Therefore, at the peaks of the lobes, where the vibration levels are higher, an instantaneous difference up to 20 % (i.e. a value of 0.8 in the plots) can be observe with Model 1 and 3 with respect to Model 0, for a confidence interval at 95 %, for the heel database (i.e. Fig. 84). While up to 30 % with the tiptoe database (i.e. Fig. 85).

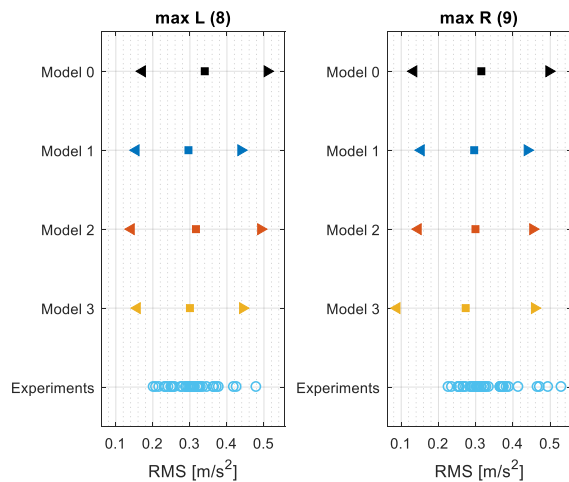


Fig. 86 Maximum Moving RMS values of acceleration evaluated by each Model; maximum of the experimental moving RMS evaluated every 40 s; accelerometer 8 (up) and 9 (down); simulations made with the “heel” database; \square : mean value / $\langle \rangle$: confidence interval at 95 %; test number 1.

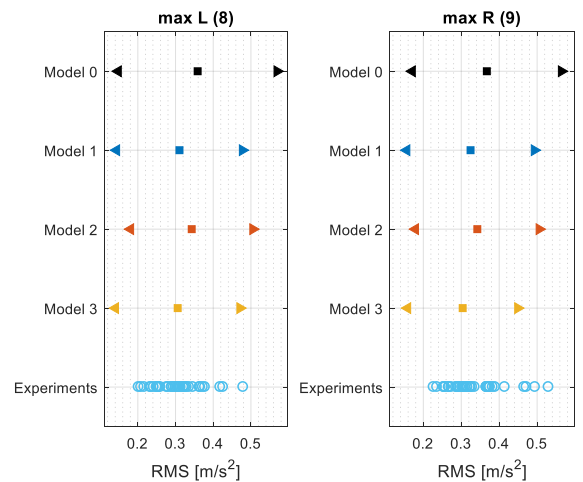


Fig. 87 Maximum Moving RMS values of acceleration evaluated by each Model; maximum of the experimental moving RMS evaluated every 40 s; accelerometer 8 (up) and 9 (down); simulations made with the “heel” database; \square : mean value / $\langle \rangle$: confidence interval at 95 %; test number 1.

The maximum values of the moving RMS curves per Model are here reported for the two databases: in Fig. 86 the heel one and in Fig. 87 the tiptoe one. The experimental peaks values of the experimental moving RMS curves (Fig. 80 and Fig. 81) were extracted every 40 s, since such

time was identified as the period of the moving RMS trend (for details see Chapter 4). All the experimental peak points fall in the estimations made by the Models. There are only one or two cases that fall in the Model 0 intervals only. However, it is to be recalled that the intervals are confidence intervals at 95 %, so not all the possible cases are covered by the showed ranges. Then, unavoidable random effects (e.g. a subject who walks too close to an accelerometer and hits it) could take place during the simulations.

Summarizing, the plots of Fig. 86 and Fig. 87 are considered as another important outcome of the current thesis, since they clearly show as the Models are able to predict the peaks of RMS of acceleration for the tested pedestrian scenario and for the considered structure. This is an important information, since it is the one considered at the design stage of new structure, for the assessment of the serviceability of the structure itself.

Since the results of the other tested pedestrian situations, scheduled in Table 5, are reported with the same graphs just explained and with the same sequence, in the following, a direct discussion of the results will be performed. See Chapter 4 for any doubt on the plots.

Test number 2: 3 pedestrians (selected) walk in loop

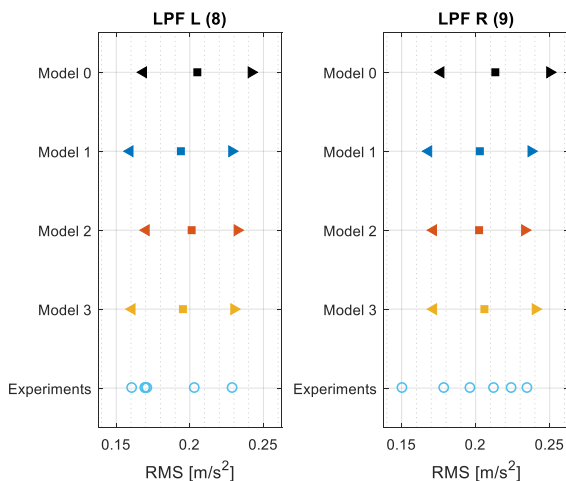


Fig. 88 Global RMS values of the acceleration; accelerometer 8 (left) and 9 (right); simulations made with the “heel” database; \square : mean value $\langle \Delta \rangle$: confidence interval at 95 %; test number 2.

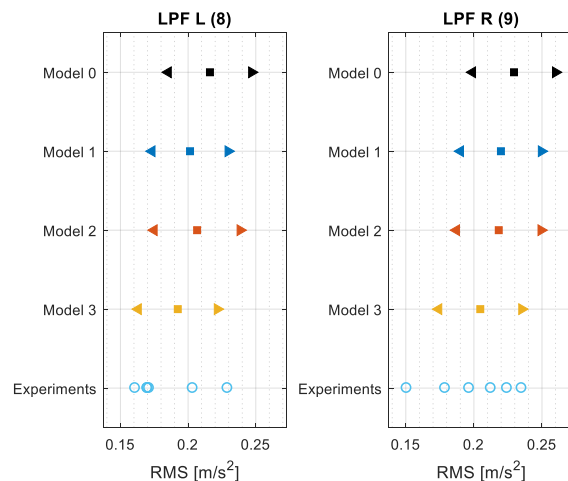


Fig. 89 Global RMS values of the acceleration; accelerometer 8 (left) and 9 (right); simulations made with the “tiptoe” database; \square : mean value $\langle \Delta \rangle$: confidence interval at 95 %; test number 2.

In this tested scenario (number 2 of Table 5) a greater agreement is present in Fig. 88 and Fig. 89 between the Models and the experimental data, in terms of global RMS values. Instead, in the previous case (test number 1 of Table 5), an overestimation of the experimental global RMS values were present for the left side of the structure (Fig. 74 and Fig. 75). Here, the RMS intervals estimated with the tiptoe database are also in this case higher with respect to the ones obtained with the heel database, confirming the lower damping action introduced by the tiptoe apparent masses. In this tested situation (three pedestrians walking in loop on the staircase) a higher difference is observed between the new Models and Model 0. Such a difference is reported also by the normalized by Model zero curves (Fig. 90 and Fig. 91). The highest ones reach 85 % (15 % of difference) with the lower limits of the ranges (e.g. Model 2 and Model 3 for the tiptoe case).

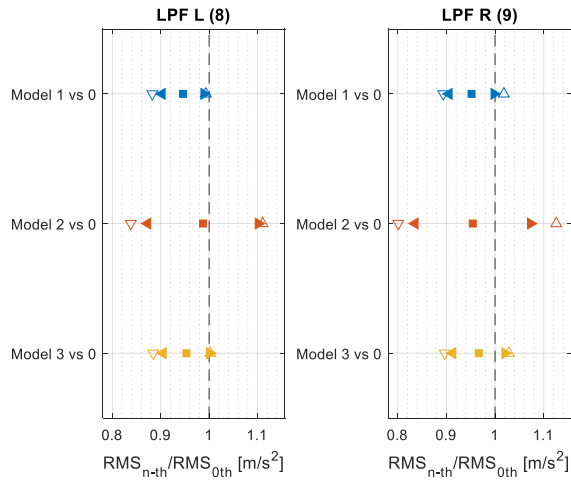


Fig. 90 Global RMS values of acceleration normalized by Model 0; accelerometer 8 (left) and 9 (right); simulations made with the “heel” database; \square : mean value / \diamond : confidence interval at 95 % / Δ : maximum ratio value / ∇ : minimum ratio value; test number 2.

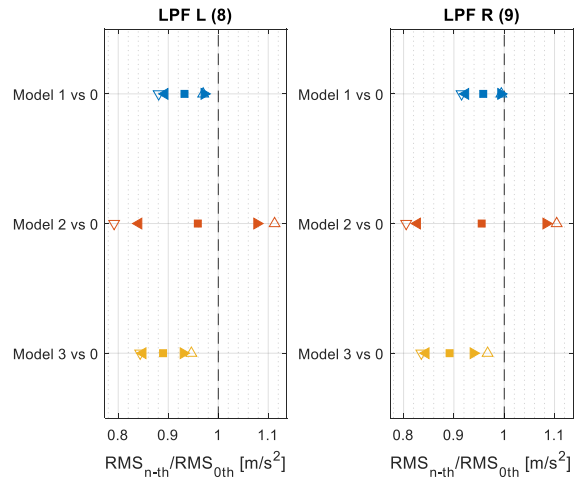


Fig. 91 Global RMS values of acceleration normalized by Model 0; accelerometer 8 (left) and 9 (right); simulations made with the “tiptoe” database; \square : mean value / \diamond : confidence interval at 95 % / Δ : maximum ratio value / ∇ : minimum ratio value; test number 2.

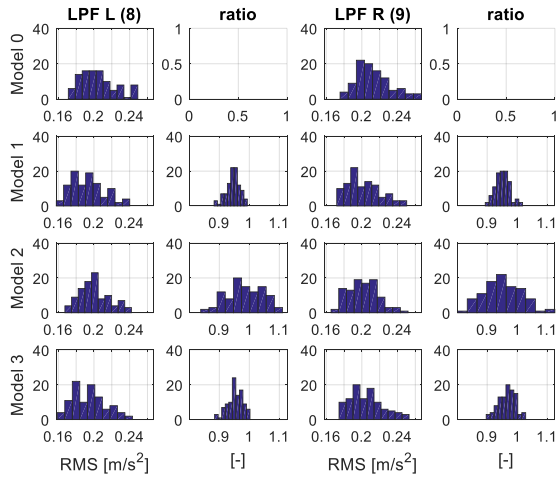


Fig. 92 Histograms of the Global RMS of acceleration and of the normalized by Model 0 ones; accelerometer 8 (left) and 9 (right); simulations made with the “heel” database; test number 2.

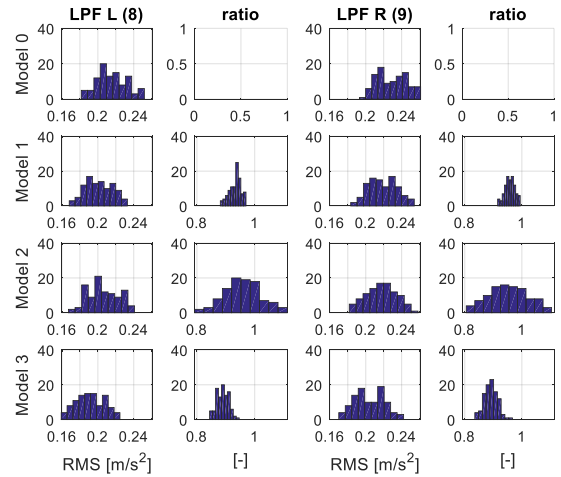


Fig. 93 Histograms of the Global RMS of acceleration and of the normalized by Model 0 ones; accelerometer 8 (left) and 9 (right); simulations made with the “tiptoe” database; test number 2.

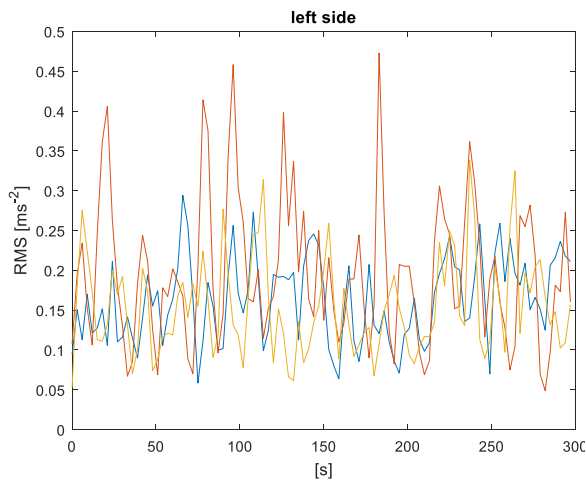


Fig. 94 Moving RMS of acceleration evaluated every 3 s; experimental data - accelerometer 8, test number 2.

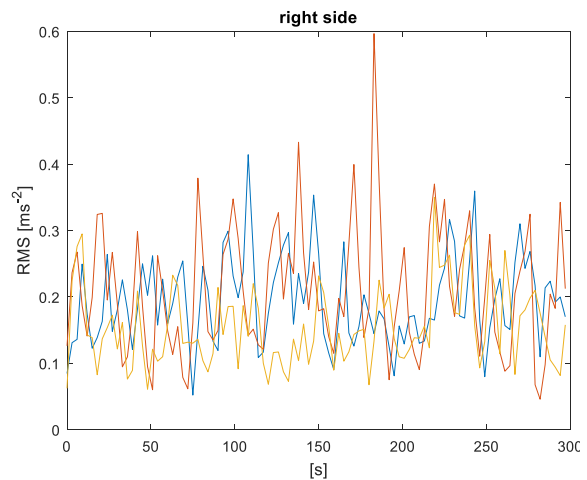


Fig. 95 Moving RMS of acceleration evaluated every 3 s; experimental data - accelerometer 9, test number 2.

In Fig. 94 and Fig. 95 are represented the experimental moving RMS curves. As reported by Table 6, three sets of three pedestrians were involved in the experiments (indeed three curves are present per plot), each of them walking for 5 min (i.e. 300 s).

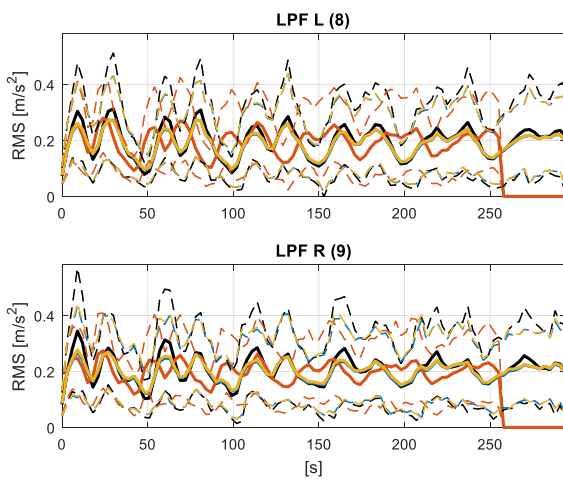


Fig. 96 Moving RMS of acceleration evaluated every 3 s; accelerometer 8 (up) and 9 (down); simulations made with the “heel” database; continuous line: mean value / dashed lines: confidence interval at 95 %; black curve: Model 0, blue curve: Model 1, red curve: Model 2, yellow curve: Model 3; test number 2.

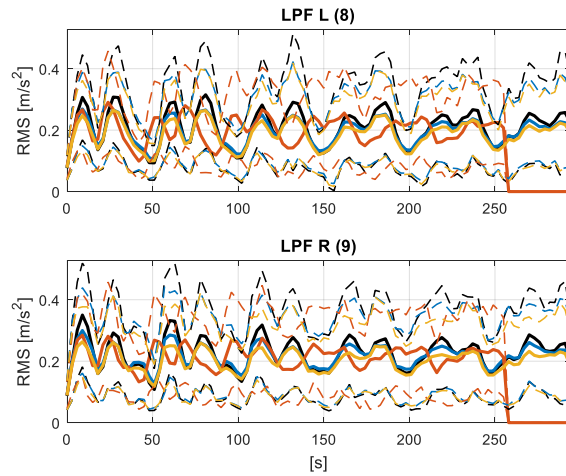


Fig. 97 Moving RMS of acceleration evaluated every 3 s; accelerometer 8 (up) and 9 (down); simulations made with the “tiptoe” database; continuous line: mean value / dashed lines: confidence interval at 95 %; black curve: Model 0, blue curve: Model 1, red curve: Model 2, yellow curve: Model 3; test number 2.

As anticipated by the global RMS curves (Fig. 88 and Fig. 89), Model 0 estimates a vibration range slightly higher with respect to the other Models. Indeed, higher RMS values are predicted at the peaks of lobes by Model 0 in Fig. 96 Fig. 97 (as happened in the previous scenario: Fig. 82 and Fig. 83), while the RMS values at the grooves are similar among the Models (conversely with respect to before: Fig. 82 and Fig. 83). This explains the trend of the global RMS values of Fig. 88 and Fig. 89., which show higher vibrations estimated by Model 0.

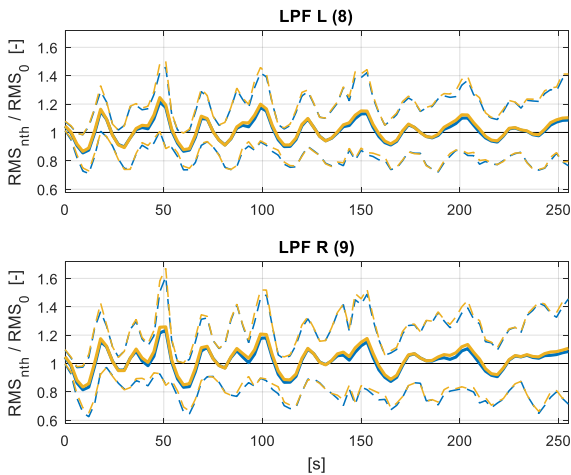


Fig. 98 Moving RMS of acceleration evaluated every 3 s normalized by Model 0; accelerometer 8 (up) and 9 (down); simulations made with the “heel” database; continuous line: mean value / dashed lines: confidence interval at 95 %; black curve: Model 0, blue curve: Model 1, yellow curve: Model 3; test number 2.

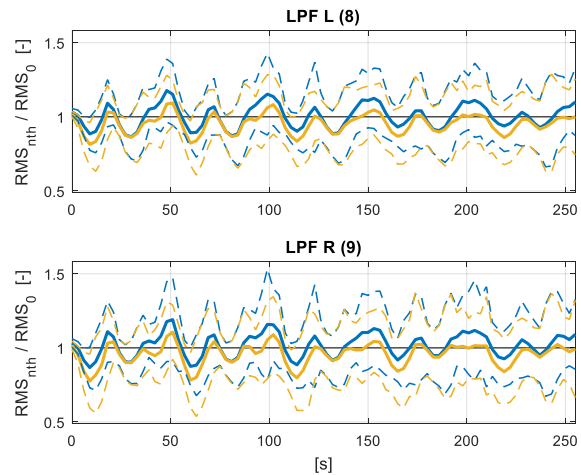


Fig. 99 Moving RMS of acceleration evaluated every 3 s normalized by Model 0; accelerometer 8 (up) and 9 (down); simulations made with the “tiptoe” database; continuous line: mean value / dashed lines: confidence interval at 95 %; black curve: Model 0, blue curve: Model 1, yellow curve: Model 3; test number 2.

The considerations made for the previous scenarios (test number 1) are still valid. Differences with values up to 40 % can be observe in Fig. 98 for the normalized curves.

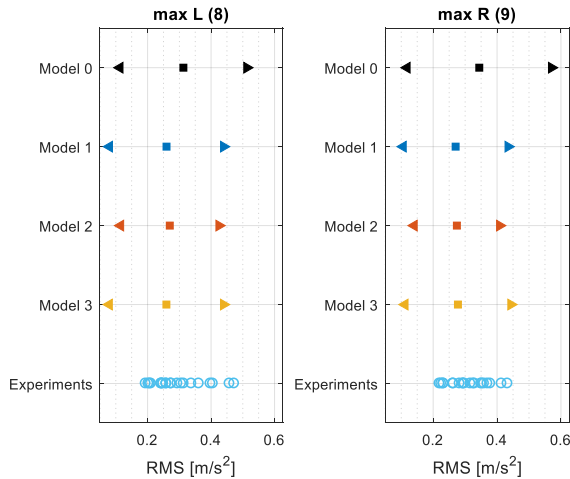


Fig. 100 Maximum Moving RMS values of acceleration evaluated by each Model; maximum of the experimental moving RMS evaluated every 40 s; accelerometer 8 (up) and 9 (down); simulations made with the “heel” database; \square : mean value $\langle \Delta \rangle$: confidence interval at 95 %; test number 2.

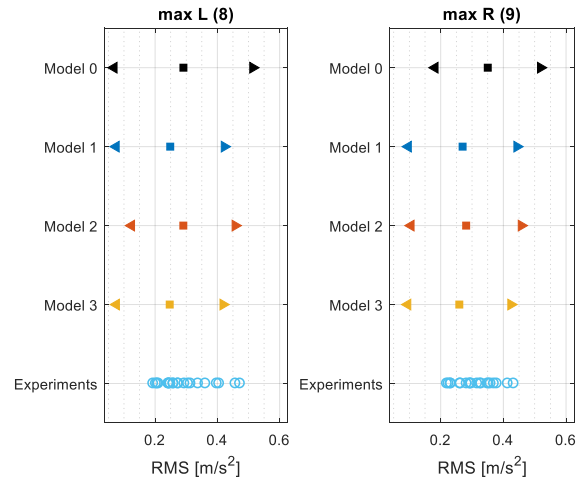


Fig. 101 Maximum Moving RMS values of acceleration evaluated by each Model; maximum of the experimental moving RMS evaluated every 40 s; accelerometer 8 (up) and 9 (down); simulations made with the “heel” database; \square : mean value $\langle \Delta \rangle$: confidence interval at 95 %; test number 2.

Also in this case, the peaks of the experimental moving RMS curves of acceleration (Fig. 94 and Fig. 95) are properly predicted by all the Models. Only two experimental observations result at the upper limits of the new Models. However, the main cloud of the experimental points fall almost in correspondence of the mean values predicted by the Models. Then, as mentioned before, the reported ranges are evaluated for confidence intervals at 95 %.

Test number 3: 1 pedestrian (random) walks in loop

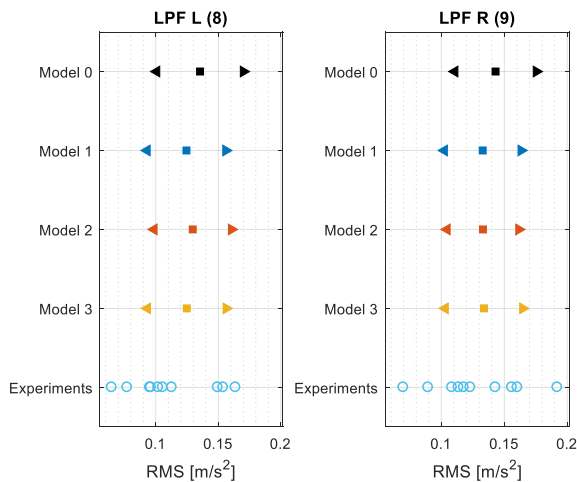


Fig. 102 Global RMS values of the acceleration; accelerometer 8 (left) and 9 (right); simulations made with the “heel” database; \square : mean value $\langle \Delta \rangle$: confidence interval at 95 %; test number 3.

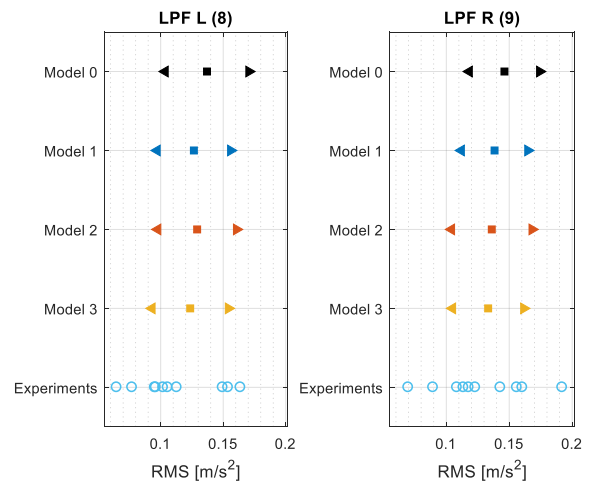


Fig. 103 Global RMS values of the acceleration; accelerometer 8 (left) and 9 (right); simulations made with the “tiptoe” database; \square : mean value $\langle \Delta \rangle$: confidence interval at 95 %; test number 3.

The experimental results obtained for the current scenario (third of Table 5) have a great dispersion with respect to the ranges estimated by the Models. However, the mean values of the experimental clouds fall in the predicted ranges, as well as the majority of the points. A higher number of experimental observations probably would have defined a clearer experimental trend. Nevertheless, this is a long-time simulation (i.e. 5min, both numerically and experimentally). Hence, a trade-off between the number of time for which every experimental test should have been

repeated and the total number of tests was required, since only one day was available for all the experimental campaign, including the build-up of the set up on the staircase and Experimental Modal Analysis of the structure.

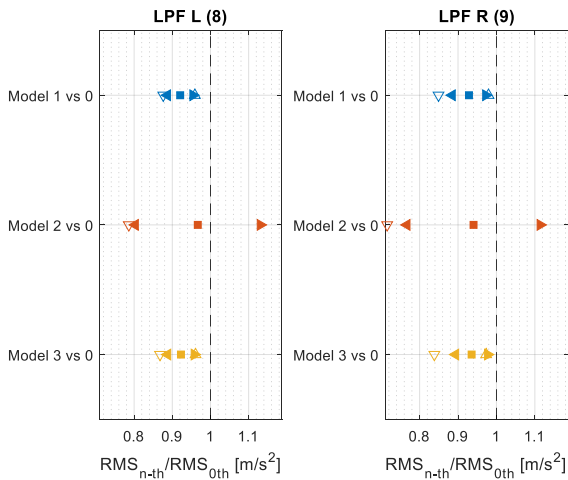


Fig. 104 Global RMS values of acceleration normalized by Model 0; accelerometer 8 (left) and 9 (right); simulations made with the “heel” database; \square : mean value / $\langle \triangleright \rangle$: confidence interval at 95 % / Δ : maximum ratio value / ∇ : minimum ratio value; test number 3.

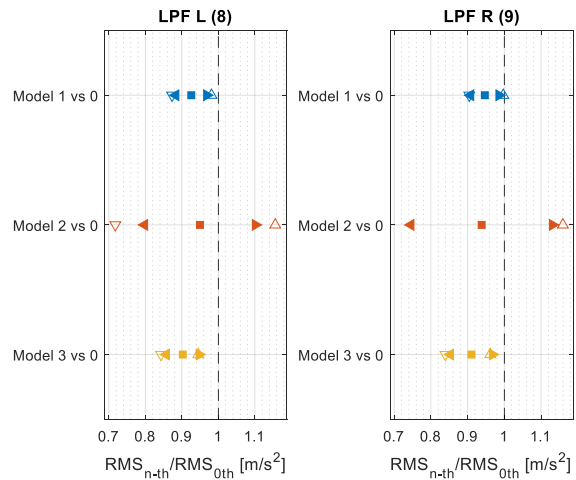


Fig. 105 Global RMS values of acceleration normalized by Model 0; accelerometer 8 (left) and 9 (right); simulations made with the “tiptoe” database; \square : mean value / $\langle \triangleright \rangle$: confidence interval at 95 % / Δ : maximum ratio value / ∇ : minimum ratio value; test number 3.

Even if the greater variability of Model 2 is always present, this time, a complete detachment of the estimated ranges of Model 1 and Model 3, with respect to the Model 0 ones, is present, leading to differences up to 15 % of the global RMS values. This can also be clearly seen by the ratio plots in the histogram Fig. 106 and Fig. 107.

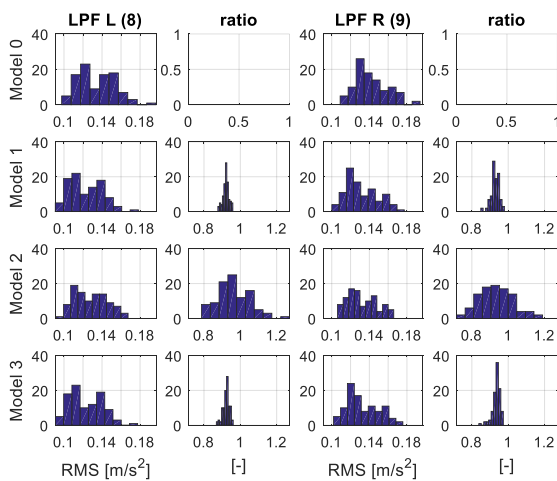


Fig. 106 Histograms of the Global RMS of acceleration and of the normalized by Model 0 ones; accelerometer 8 (left) and 9 (right); simulations made with the “heel” database; test number 3.

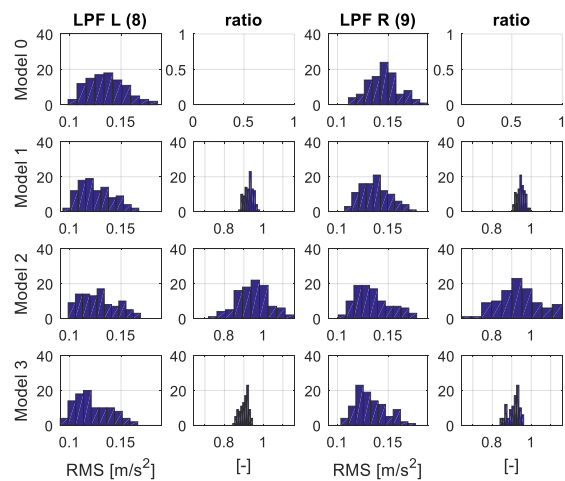


Fig. 107 Histograms of the Global RMS of acceleration and of the normalized by Model 0 ones; accelerometer 8 (left) and 9 (right); simulations made with the “tiptoe” database; test number 3.

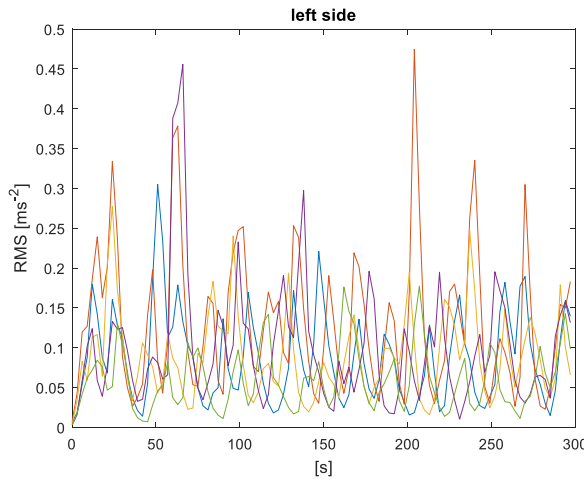


Fig. 108 Moving RMS of acceleration evaluated every 3 s; experimental data - accelerometer 8, test number 3.

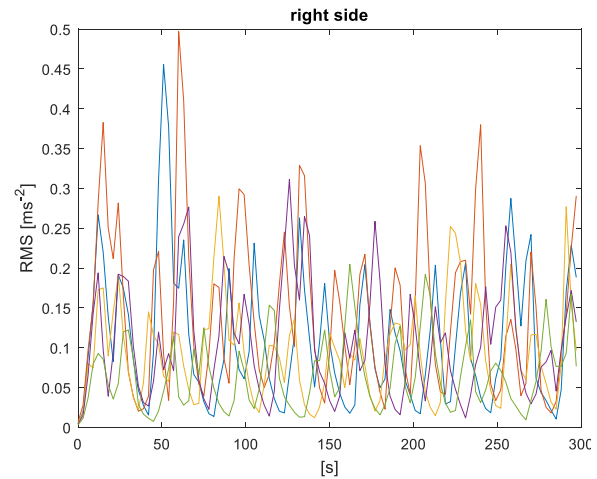


Fig. 109 Moving RMS of acceleration evaluated every 3 s; experimental data - accelerometer 9, test number 3.

Since every subject involved performed the test number 3 (i.e. 1 person walks in loop for five min) one time, five experimental moving RMS curves are present in Fig. 108 and Fig. 109. For the sake of clarity, the moving RMS curves of subject 1, in correspondence of accelerometer 8, is reported in Fig. 110. From it, it is possible to observe the periodicity of the trend, with a mean period equal to 40 s, as evaluated in Chapter 4. The single subject starts to walk from the ground floor. Increasing the time, the second landing (where accelerometer 8 is located and the mode shapes are higher) is reached in correspondence of the first peak. The first groove instead, corresponds to the achievement of the first floor. The level of RMS doesn't reach lower values since the subject, as soon as he/she reaches the first floor, he/she restarts the crossing in the descending direction. The second peak corresponds to the descending passage for the second landing. The achievement of the ground floor, and so the end of the first loop, corresponds to the second groove. Indeed, the second groove has lower RMS values since more time is required to the subject to return on the second landing, where the mode shapes have higher values. While lower time passes to go from the second landing to the first floor and from the first floor to the second landing (first groove case).

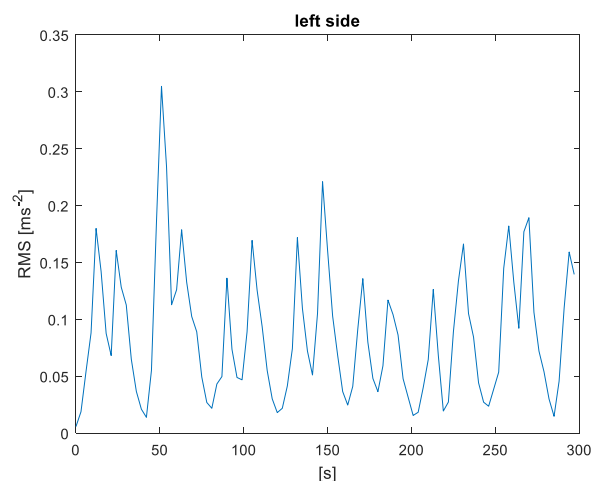


Fig. 110: Moving RMS of acceleration evaluated every 3 s; experimental data - accelerometer 8, test number 3, subject number 1.

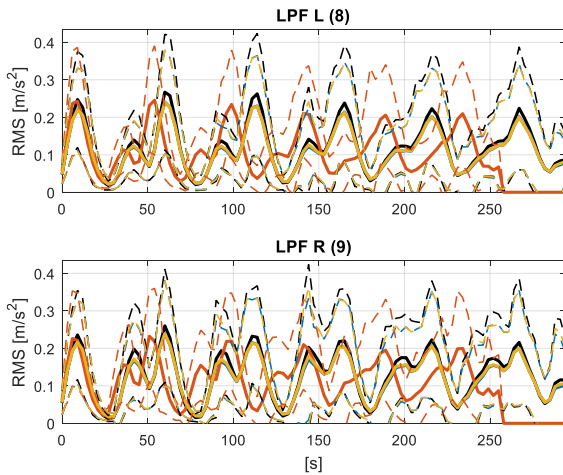


Fig. 111 Moving RMS of acceleration evaluated every 3 s; accelerometer 8 (up) and 9 (down); simulations made with the “heel” database; continuous line: mean value / dashed lines: confidence interval at 95 %; black curve: Model 0, blue curve: Model 1, red curve: Model 2, yellow curve: Model 3; test number 3.

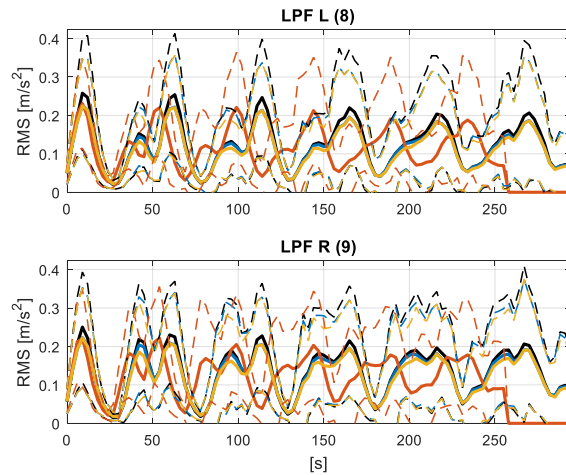


Fig. 112 Moving RMS of acceleration evaluated every 3 s; accelerometer 8 (up) and 9 (down); simulations made with the “tiptoe” database; continuous line: mean value / dashed lines: confidence interval at 95 %; black curve: Model 0, blue curve: Model 1, red curve: Model 2, yellow curve: Model 3; test number 3.

As reported for the previous two pedestrian tests, also here Model 0 produce higher peaks values, showing in this way a lower damping attitude in correspondence of the passage for the second landing.

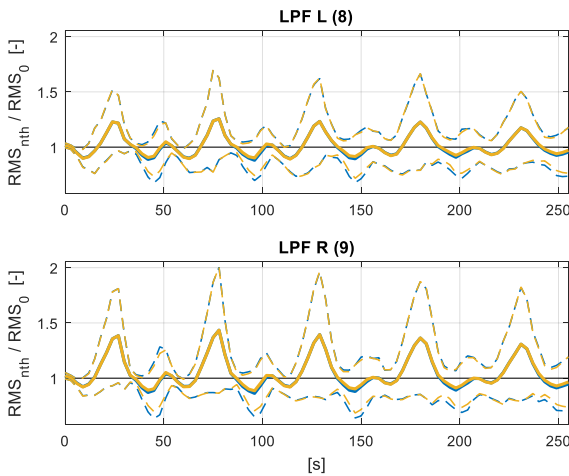


Fig. 113 Moving RMS of acceleration evaluated every 3 s normalized by Model 0; accelerometer 8 (up) and 9 (down); simulations made with the “heel” database; continuous line: mean value / dashed lines: confidence interval at 95 %; black curve: Model 0, blue curve: Model 1, yellow curve: Model 3; test number 3.

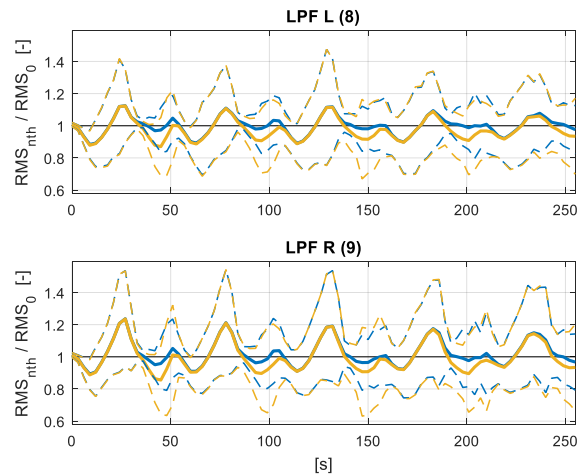


Fig. 114 Moving RMS of acceleration evaluated every 3 s normalized by Model 0; accelerometer 8 (up) and 9 (down); simulations made with the “tiptoe” database; continuous line: mean value / dashed lines: confidence interval at 95 %; black curve: Model 0, blue curve: Model 1, yellow curve: Model 3; test number 3.

In Fig. 113 and Fig. 114, very high variations are depicted with respect to Model 0. Variations up to the 35 % can be noted with the confidence intervals, while up to 10 % with the mean values.

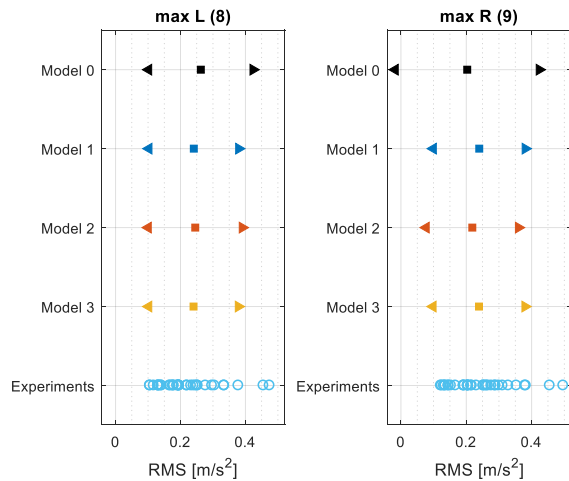


Fig. 115 Maximum Moving RMS values of acceleration evaluated by each Model; maximum of the experimental moving RMS evaluated every 40 s; accelerometer 8 (up) and 9 (down); simulations made with the “heel” database; \square : mean value $\langle \Delta \rangle$: confidence interval at 95 %; test number 3.

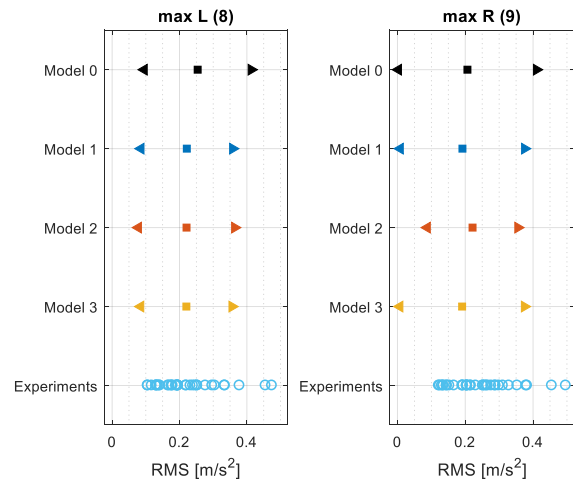


Fig. 116 Maximum Moving RMS values of acceleration evaluated by each Model; maximum of the experimental moving RMS evaluated every 40 s; accelerometer 8 (up) and 9 (down); simulations made with the “heel” database; \square : mean value $\langle \Delta \rangle$: confidence interval at 95 %; test number 3.

Also in this case, the experimental RMS peaks of acceleration are properly described by peak ranges predicted by the Models.

Test number 4: 5 pedestrians (selected) meet during the crossing

This pedestrian scenario is considered one of the most relevant, together with the following two (i.e. test number 5 and 6 of table 1). Indeed, in these tests, even if a high number of pedestrians is considered, they are made to meet on the structure, and are made to meet at the greatest modal component point of the structure (i.e. the second landing). This should strongly underline the differences between how Model 0 and the new Models work.

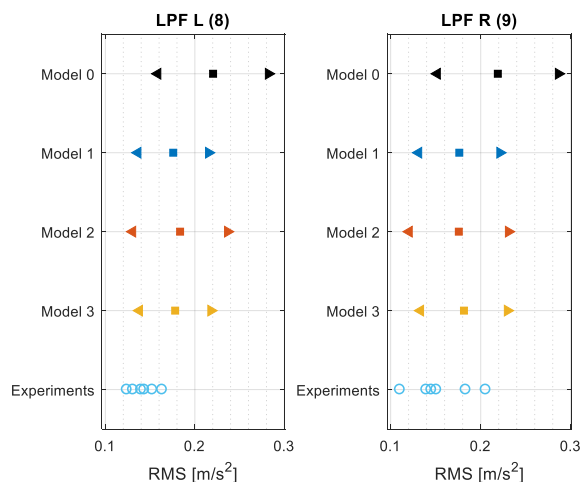


Fig. 117 Global RMS values of the acceleration; accelerometer 8 (left) and 9 (right); simulations made with the “heel” database; \square : mean value $\langle \Delta \rangle$: confidence interval at 95 %; test number 4.

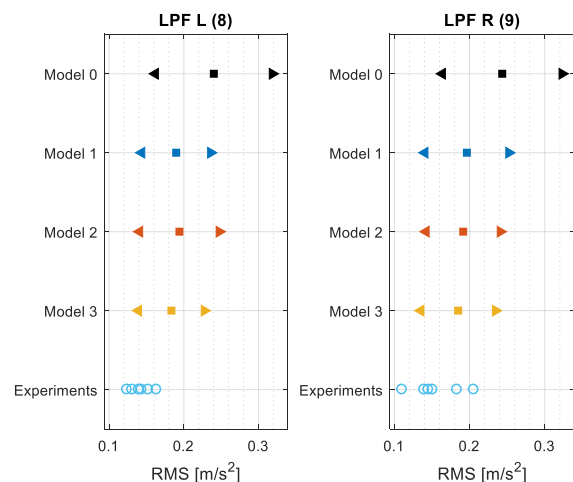


Fig. 118 Global RMS values of the acceleration; accelerometer 8 (left) and 9 (right); simulations made with the “tiptoe” database; \square : mean value $\langle \Delta \rangle$: confidence interval at 95 %; test number 4.

Indeed, high differences are shown by Fig. 117 and Fig. 118. That is due to the different way in which the passive contributions, and so the damping effects of the pedestrians, are managed by the new Models and Model 0, as already explained for the 3rd quadrant case of Table 10 (i.e. the next one treated). Summarizing, the point is that, even if all the Models manage the active forces in the

same way (i.e. locally with the pedestrians), Model 0 is the only one that do not do the same with the passive contributions (i.e. the damping capability of the pedestrians). Indeed, it gathers them and then it spread their sum over the entire structure. Therefore, Model 0 is unable to properly damp the extremely high vibrations induced by the confluence of all the subjects in correspondence of the most sensible point of the structure, the second landing. Conversely, all the other three Models, locally consider the passive contributions, and so, even if the active excitations are the same of Model 0, they are able to locally damp the high vibrations induced. Indeed, form Fig. 117 and Fig. 118 appears clear that Model 0 drastically overestimate the experimental values, while less overestimations are present for Model 1, 2 and 3. However, the overestimations ensure to take in consideration the most severe cases, and so to be in a safer condition.

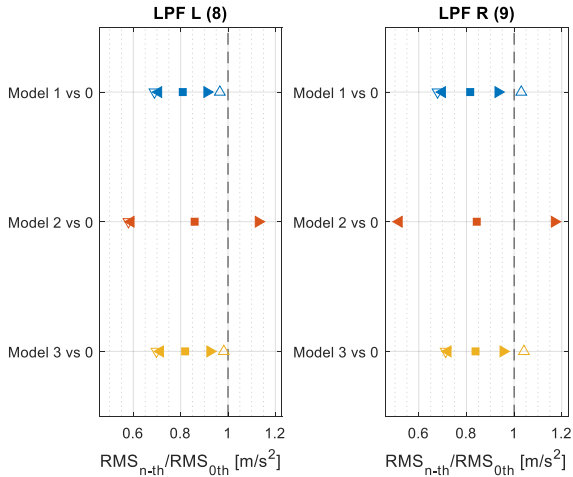


Fig. 119 Global RMS values of acceleration normalized by Model 0; accelerometer 8 (left) and 9 (right); simulations made with the “heel” database; \square : mean value / $\triangleleft \triangleright$: confidence interval at 95 % / Δ : maximum ratio value / ∇ : minimum ratio value; test number 4.

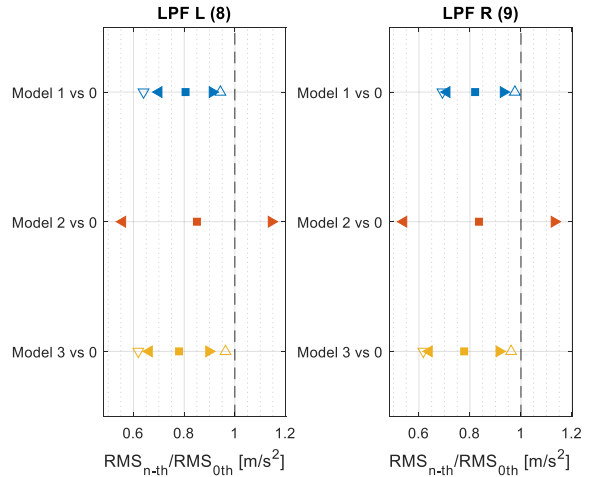


Fig. 120 Global RMS values of acceleration normalized by Model 0; accelerometer 8 (left) and 9 (right); simulations made with the “tiptoe” database; \square : mean value / $\triangleleft \triangleright$: confidence interval at 95 % / Δ : maximum ratio value / ∇ : minimum ratio value; test number 4.

The global RMS ratio plots confirm the significant difference among the Methods. Just with the mean values, a 20 % of differences with respect to Model 0 are obtained. Such an order of differences, until now, were only observed in the moving RMS curves, never with the global ones.

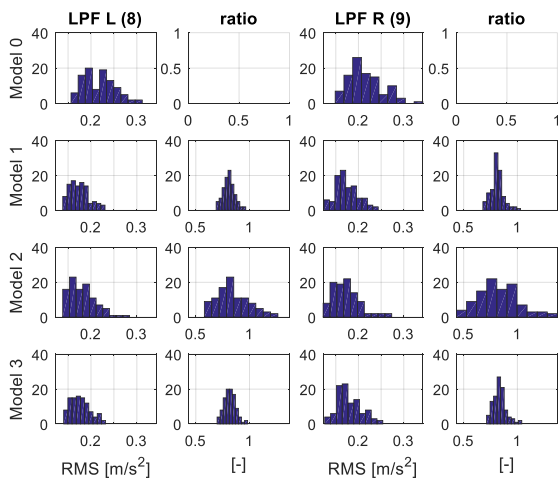


Fig. 121 Histograms of the Global RMS of acceleration and of the normalized by Model 0 ones; accelerometer 8 (left) and 9 (right); simulations made with the “heel” database; test number 4.

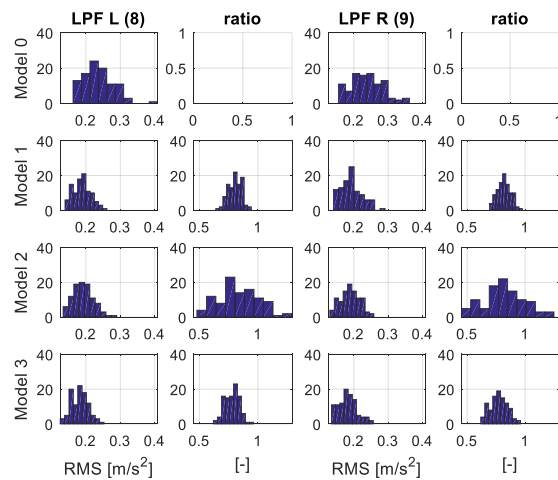


Fig. 122 Histograms of the Global RMS of acceleration and of the normalized by Model 0 ones; accelerometer 8 (left) and 9 (right); simulations made with the “tiptoe” database; test number 4.

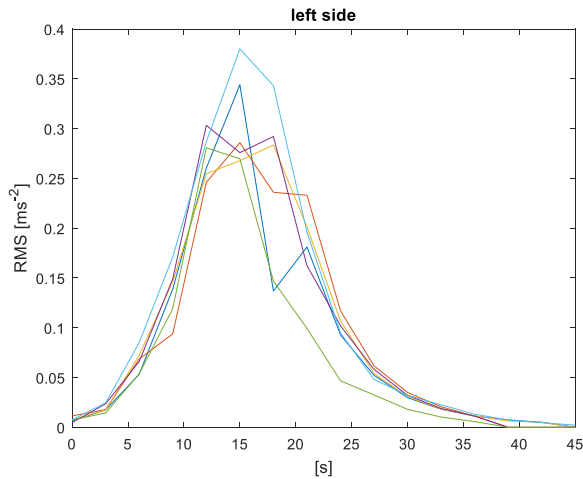


Fig. 123 Moving RMS of acceleration evaluated every 3 s; experimental data - accelerometer 8, test number 4.

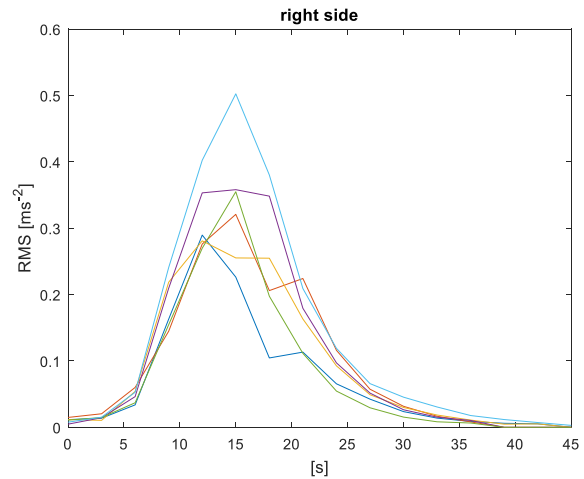


Fig. 124 Moving RMS of acceleration evaluated every 3 s; experimental data - accelerometer 9, test number 4.

The bell shapes of the experimental and numerical moving RMS curves (Fig. 123 and Fig. 124 experimental / Fig. 125 and Fig. 126 numerical) confirm the correctness of the numerical simulations. Indeed, the increase of the moving RMS values, up to the point in which the subjects reach the second landing (where accelerometer 8 and 9 are located and the modal components of the structure are higher), and their decrease, from the moment in which the second landing is left, result properly described.

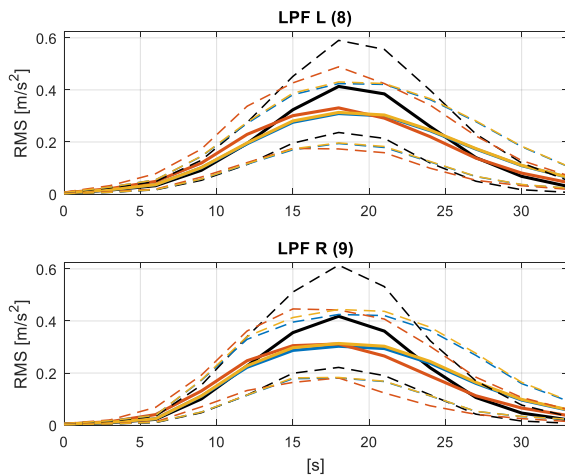


Fig. 125 Moving RMS of acceleration evaluated every 3 s; accelerometer 8 (up) and 9 (down); simulations made with the “heel” database; continuous line: mean value / dashed lines: confidence interval at 95 %; black curve: Model 0, blue curve: Model 1, red curve: Model 2, yellow curve: Model 3; test number 4.

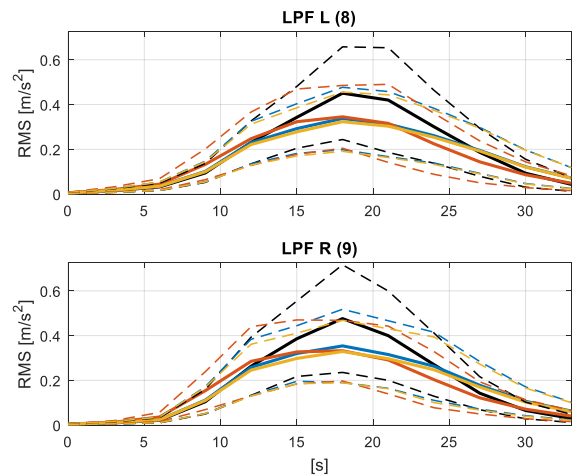


Fig. 126 Moving RMS of acceleration evaluated every 3 s; accelerometer 8 (up) and 9 (down); simulations made with the “tiptoe” database; continuous line: mean value / dashed lines: confidence interval at 95 %; black curve: Model 0, blue curve: Model 1, red curve: Model 2, yellow curve: Model 3; test number 4.

The discussion above introduced for Fig. 117 and Fig. 118, can be clearly observed here in Fig. 125 and Fig. 126. At 19 s, when all the Models place the active components of the pedestrians at the second landing, where the modal shapes assume their higher values, Model 1, 2 and 3 do the same with the passive components, ensuring a consistent damping action. Meanwhile, Model 0 continues to consider such components (the passive ones) as spread over the structure, leading to have a much lower addition of damping effect on the second landing, where the vibrations are higher, due to the modal coordinates and the concentrated forcing terms.

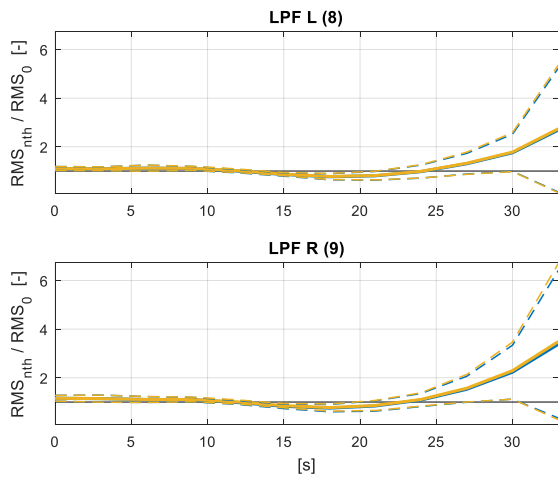


Fig. 127 Moving RMS of acceleration evaluated every 3 s normalized by Model 0; accelerometer 8 (up) and 9 (down); simulations made with the “heel” database; continuous line: mean value / dashed lines: confidence interval at 95 %; black curve: Model 0, blue curve: Model 1, yellow curve: Model 3; test number 4.

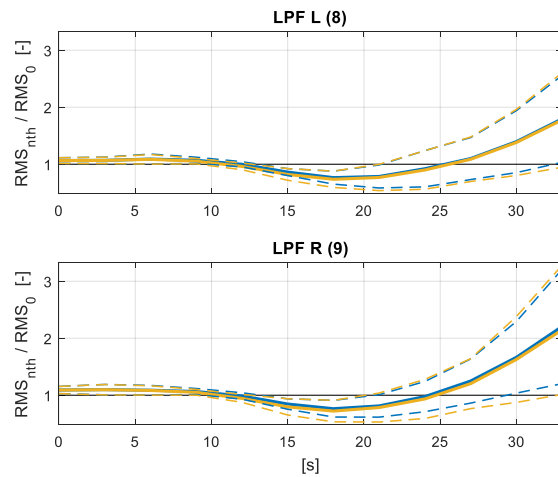


Fig. 128 Moving RMS of acceleration evaluated every 3 s normalized by Model 0; accelerometer 8 (up) and 9 (down); simulations made with the “tiptoe” database; continuous line: mean value / dashed lines: confidence interval at 95 %; black curve: Model 0, blue curve: Model 1, yellow curve: Model 3; test number 4.

The normalized by Model 0 moving RMS curves (Fig. 127 and Fig. 128) point out two important aspects. First, in correspondence of the maximum (around 19 s) the ratios strongly decrease. Second, starting from almost 25 s, the Models even strongly overestimate Model 0. Of course, they do it on lower absolute values of RMS (Fig. 117 and Fig. 118), but this is not the point. At 25s, the pedestrians end the crossing. That means that for Model 1, 2 and 3 no pedestrians are present on the structure, and so, a free decay of the excited structure, now empty, is numerically simulated for the rest of the time. Conversely, since Model 0 applied the pedestrian passive contributions as spread over the structure, it considers a particular structure in the simulations, which is made by the empty one plus the spread passive contributions. On this new structure, it applies the pedestrian active forces. That means that, even if the pedestrians have left the structure, Model 0 considers again their passive contributions, since they are part of the new structure. This, of course, leads to a more damped free decay behavior with respect to the one of the empty structure (as in Model 1, 2 and 3), leading to the trends depicted in Fig. 127 and Fig. 128.

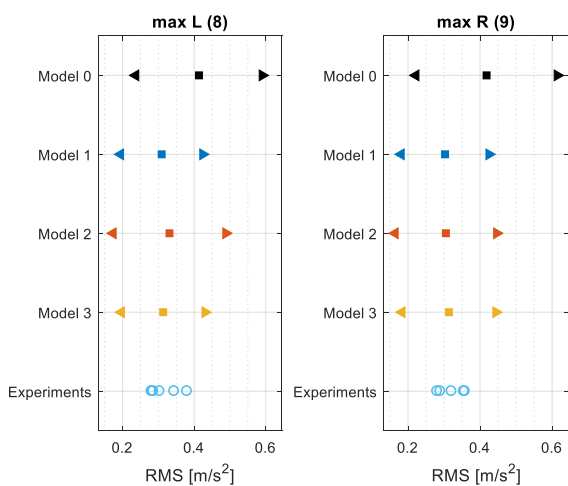


Fig. 129 Maximum Moving RMS values of acceleration evaluated by each Model; maximum of the experimental moving RMS; accelerometer 8 (up) and 9 (down); simulations made with the “heel” database; \square : mean value / $\langle \rangle$: confidence interval at 95 %; test number 4.

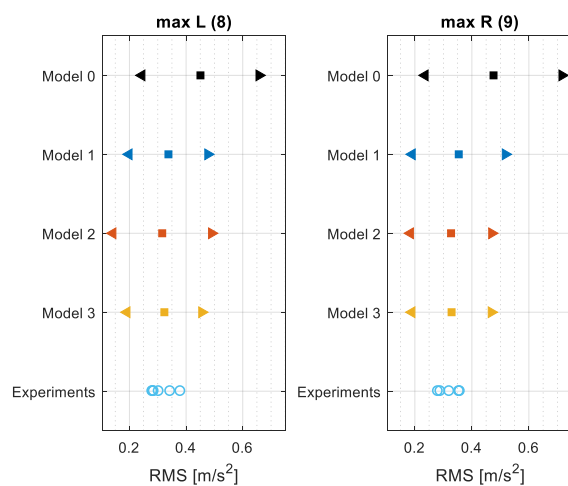


Fig. 130 Maximum Moving RMS values of acceleration evaluated by each Model; maximum of the experimental moving RMS; accelerometer 8 (up) and 9 (down); simulations made with the “heel” database; \square : mean value / $\langle \rangle$: confidence interval at 95 %; test number 4.

The peak analysis of the experimental moving RMS acceleration values shows a high agreement with the estimated ranges of the new Models (i.e. 1, 2 and 3), while the ones of Model 0 present a high overestimation, as for the global RMS ranges.

Since the remaining pedestrian situations are all of type “run” (see Table 5), which means that the pedestrians cross the structure only one time and then left it, the analysis of the following results are all similar to the one just made for the current pedestrian scenario.

Test number 5: 5 pedestrians (random) meet during the crossing

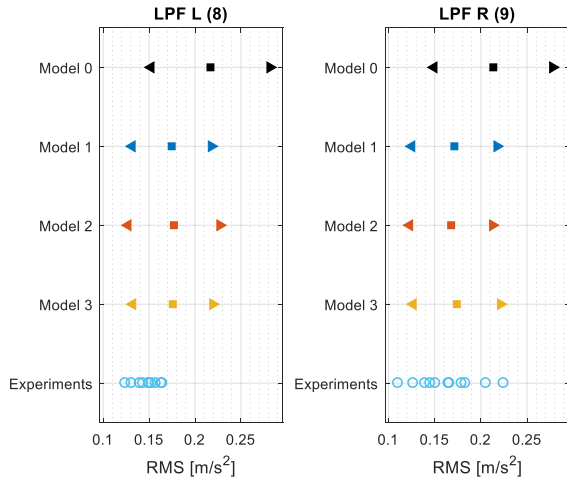


Fig. 131 Global RMS values of the acceleration; accelerometer 8 (left) and 9 (right); simulations made with the “heel” database; \square : mean value / $\langle \rangle$: confidence interval at 95 %; test number 5.

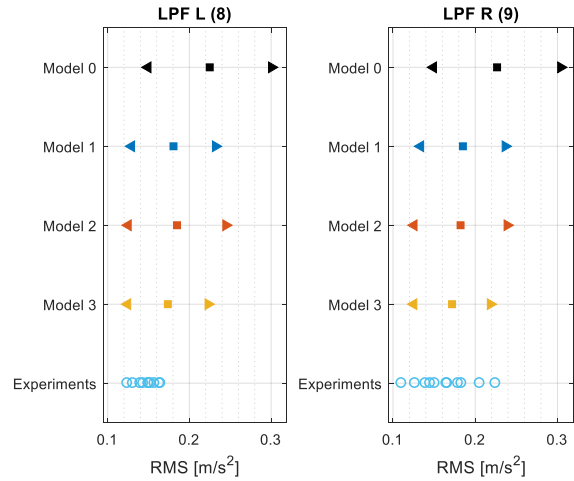


Fig. 132 Global RMS values of the acceleration; accelerometer 8 (left) and 9 (right); simulations made with the “tiptoe” database; \square : mean value / $\langle \rangle$: confidence interval at 95 %; test number 5.

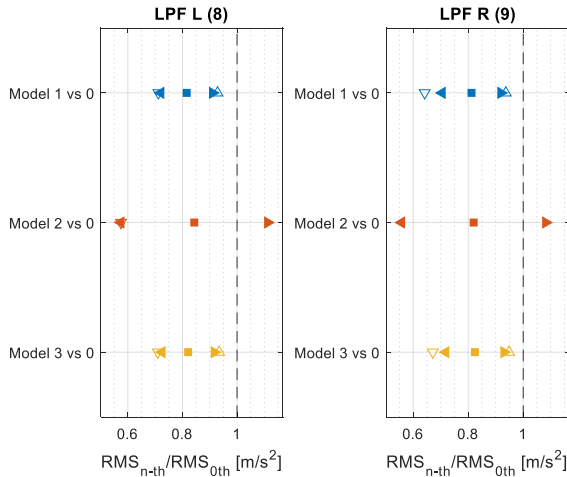


Fig. 133 Global RMS values of acceleration normalized by Model 0; accelerometer 8 (left) and 9 (right); simulations made with the “heel” database; \square : mean value / $\langle \rangle$: confidence interval at 95 % / Δ : maximum ratio value / ∇ : minimum ratio value; test number 5.

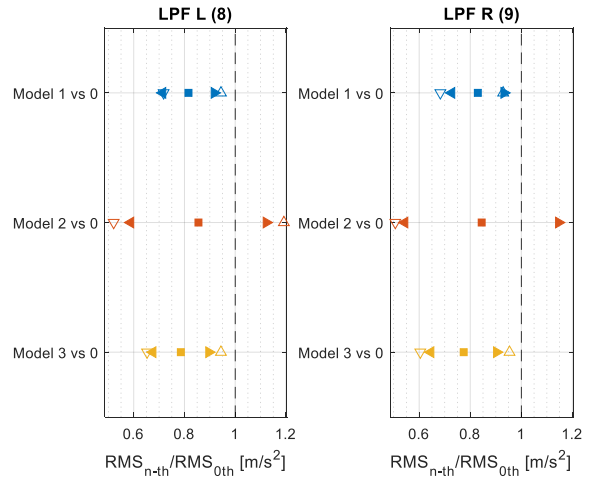


Fig. 134 Global RMS values of acceleration normalized by Model 0; accelerometer 8 (left) and 9 (right); simulations made with the “tiptoe” database; \square : mean value / $\langle \rangle$: confidence interval at 95 % / Δ : maximum ratio value / ∇ : minimum ratio value; test number 5.

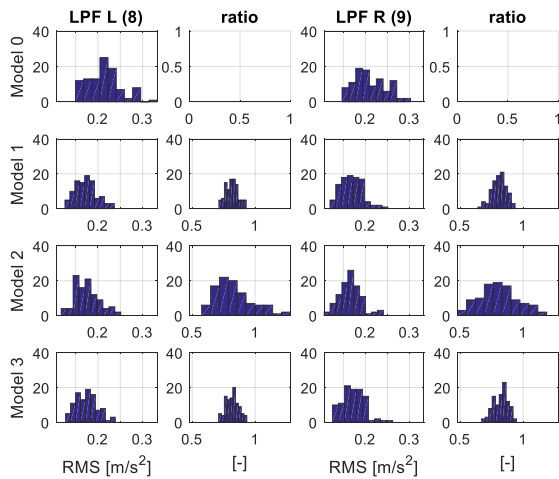


Fig. 135 Histograms of the Global RMS of acceleration and of the normalized by Model 0 ones; accelerometer 8 (left) and 9 (right); simulations made with the “heel” database; test number 5.

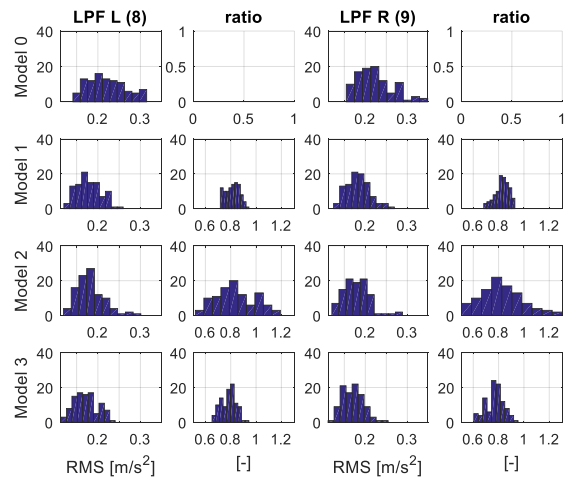


Fig. 136 Histograms of the Global RMS of acceleration and of the normalized by Model 0 ones; accelerometer 8 (left) and 9 (right); simulations made with the “tiptoe” database; test number 5.

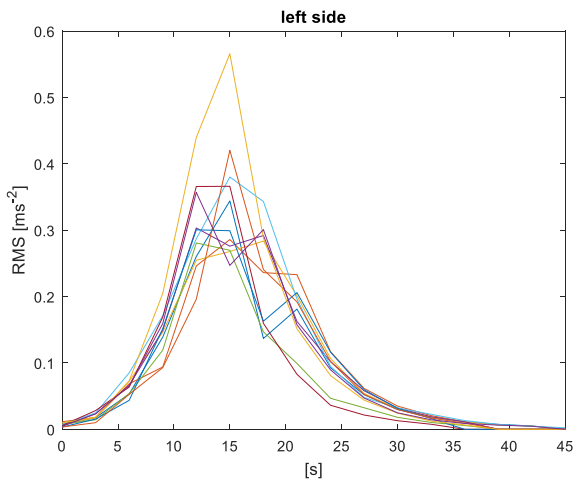


Fig. 137 Moving RMS of acceleration evaluated every 3 s; experimental data - accelerometer 8, test number 5.

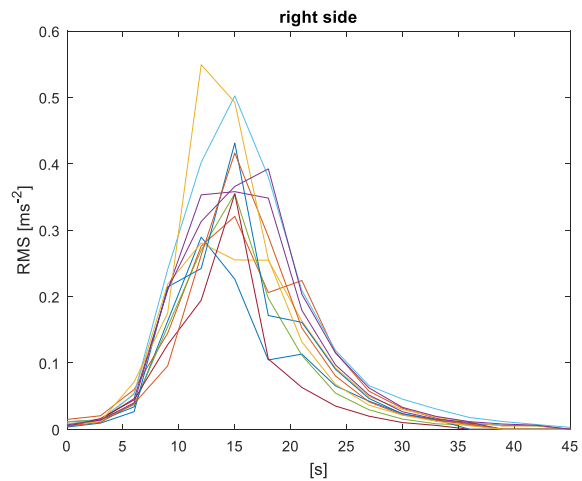


Fig. 138 Moving RMS of acceleration evaluated every 3 s; experimental data - accelerometer 9, test number 5.

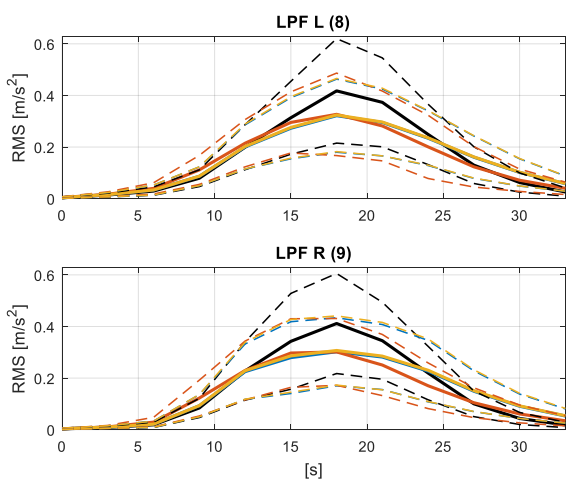


Fig. 139 Moving RMS of acceleration evaluated every 3 s; accelerometer 8 (up) and 9 (down); simulations made with the “heel” database; continuous line: mean value / dashed lines: confidence interval at 95 %; black curve: Model 0, blue curve: Model 1, red curve: Model 2, yellow curve: Model 3; test number 5.

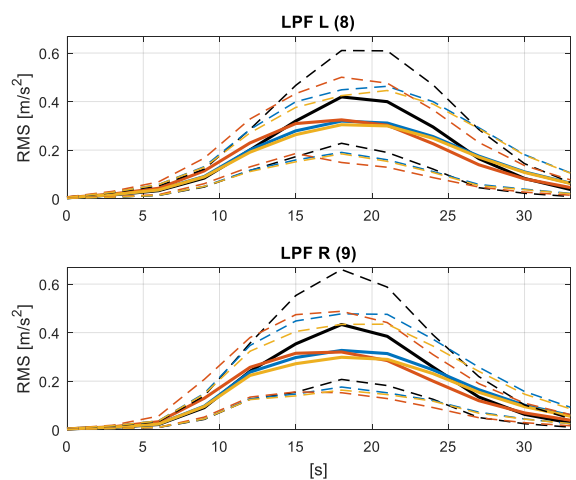


Fig. 140 Moving RMS of acceleration evaluated every 3 s; accelerometer 8 (up) and 9 (down); simulations made with the “tiptoe” database; continuous line: mean value / dashed lines: confidence interval at 95 %; black curve: Model 0, blue curve: Model 1, red curve: Model 2, yellow curve: Model 3; test number 5.

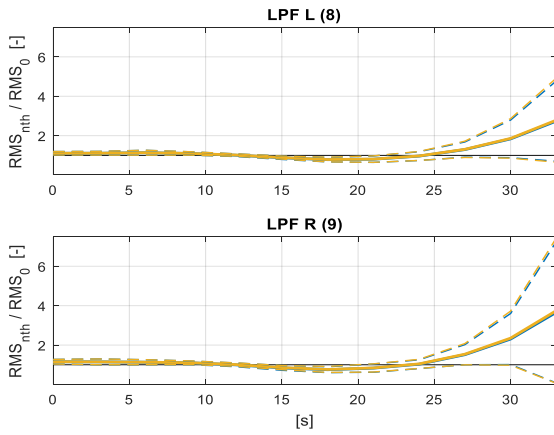


Fig. 141 Moving RMS of acceleration evaluated every 3 s normalized by Model 0; accelerometer 8 (up) and 9 (down); simulations made with the “heel” database; continuous line: mean value / dashed lines: confidence interval at 95 %; black curve: Model 0, blue curve: Model 1, yellow curve: Model 3; test number 5.

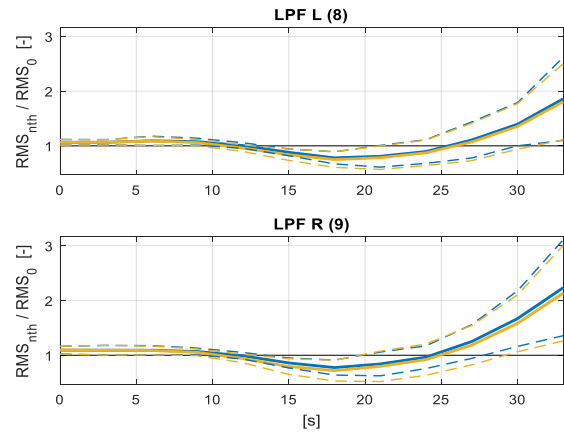


Fig. 142 Moving RMS of acceleration evaluated every 3 s normalized by Model 0; accelerometer 8 (up) and 9 (down); simulations made with the “tiptoe” database; continuous line: mean value / dashed lines: confidence interval at 95 %; black curve: Model 0, blue curve: Model 1, yellow curve: Model 3; test number 5.

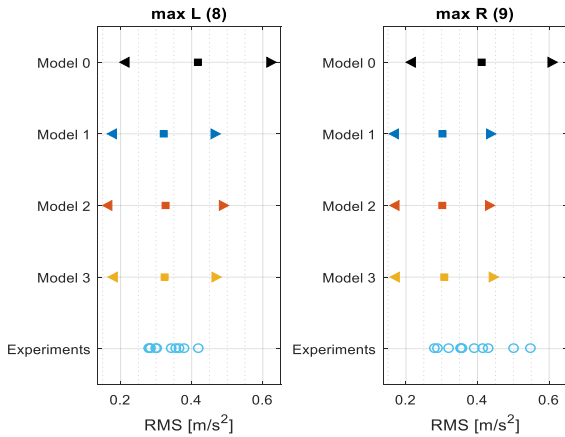


Fig. 143 Maximum Moving RMS values of acceleration evaluated by each Model; maximum of the experimental moving RMS; accelerometer 8 (up) and 9 (down); simulations made with the “heel” database; \square : mean value / $\triangleleft \triangleright$: confidence interval at 95 %; test number 5.

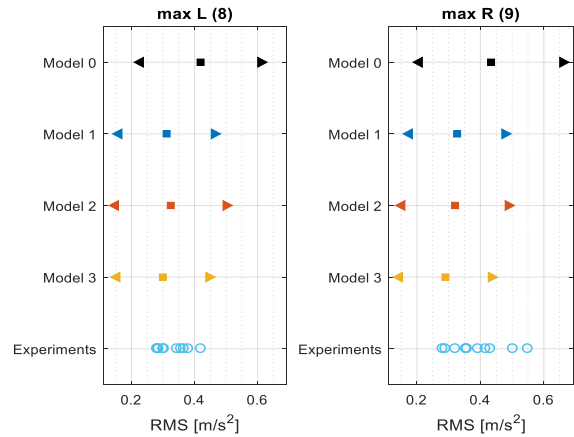


Fig. 144 Maximum Moving RMS values of acceleration evaluated by each Model; maximum of the experimental moving RMS; accelerometer 8 (up) and 9 (down); simulations made with the “heel” database; \square : mean value / $\triangleleft \triangleright$: confidence interval at 95 %; test number 5.

Test number 6: 3 pedestrians (selected) meet during the crossing

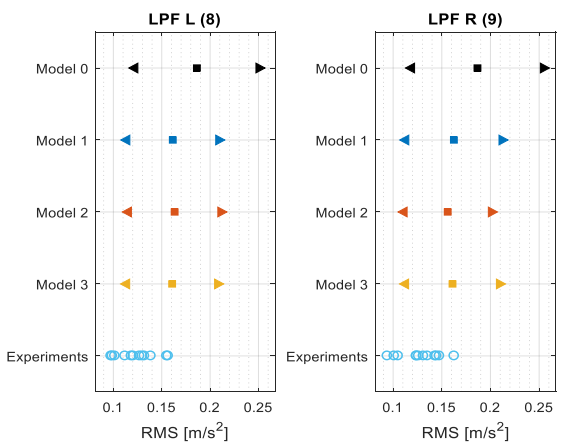


Fig. 145 Global RMS values of the acceleration; accelerometer 8 (left) and 9 (right); simulations made with the “heel” database; \square : mean value / $\triangleleft \triangleright$: confidence interval at 95 %; test number 6.

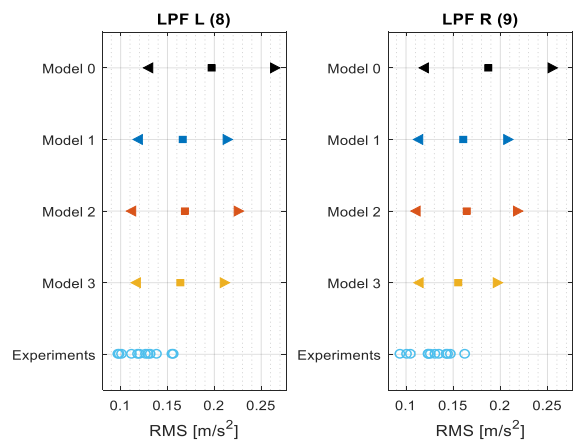


Fig. 146 Global RMS values of the acceleration; accelerometer 8 (left) and 9 (right); simulations made with the “tiptoe” database; \square : mean value / $\triangleleft \triangleright$: confidence interval at 95 %; test number 6.

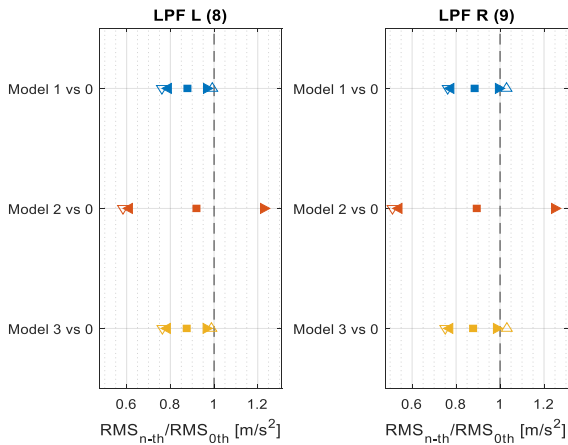


Fig. 147 Global RMS values of acceleration normalized by Model 0; accelerometer 8 (left) and 9 (right); simulations made with the “heel” database; \square : mean value / $\triangleleft \triangleright$: confidence interval at 95 % / Δ : maximum ratio value / ∇ : minimum ratio value; test number 6.

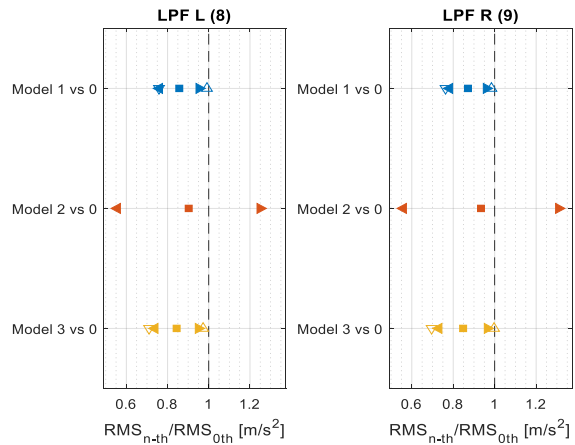


Fig. 148 Global RMS values of acceleration normalized by Model 0; accelerometer 8 (left) and 9 (right); simulations made with the “tiptoe” database; \square : mean value / $\triangleleft \triangleright$: confidence interval at 95 % / Δ : maximum ratio value / ∇ : minimum ratio value; test number 6.

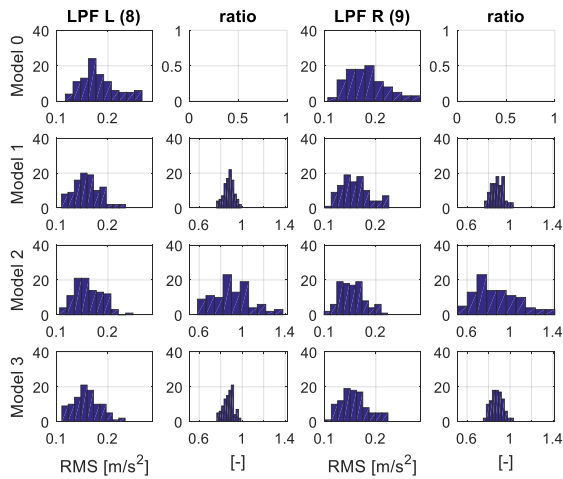


Fig. 149 Histograms of the Global RMS of acceleration and of the normalized by Model 0 ones; accelerometer 8 (left) and 9 (right); simulations made with the “heel” database; test number 6.

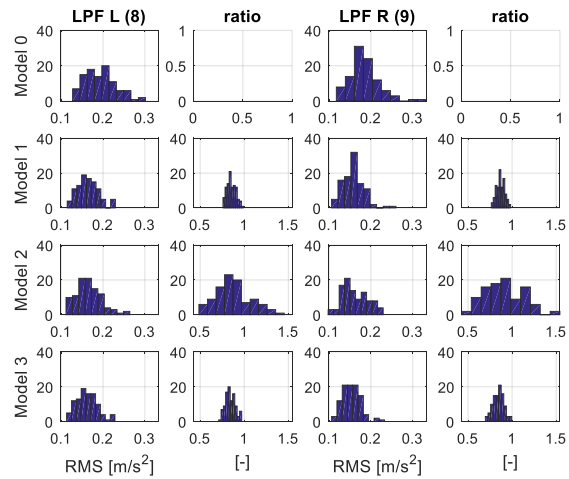


Fig. 150 Histograms of the Global RMS of acceleration and of the normalized by Model 0 ones; accelerometer 8 (left) and 9 (right); simulations made with the “tiptoe” database; test number 6.

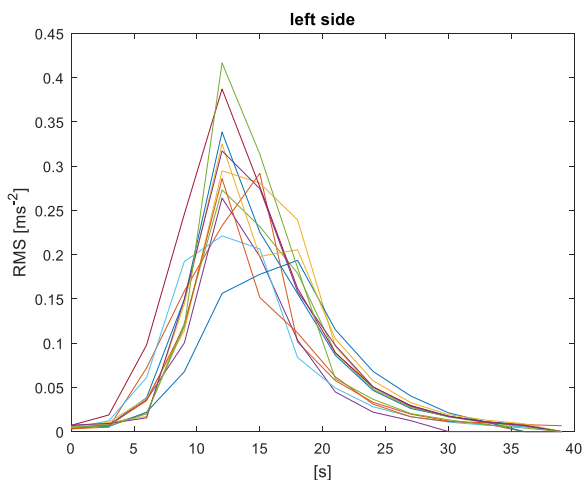


Fig. 151 Moving RMS of acceleration evaluated every 3 s; experimental data - accelerometer 8, test number 6.

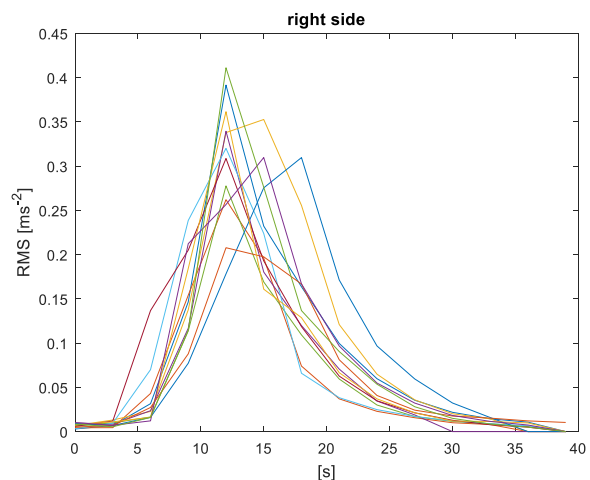


Fig. 152 Moving RMS of acceleration evaluated every 3 s; experimental data - accelerometer 9, test number 6.

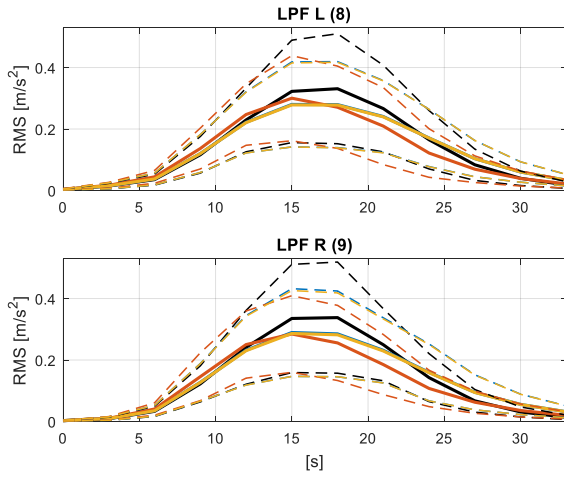


Fig. 153 Moving RMS of acceleration evaluated every 3 s; accelerometer 8 (up) and 9 (down); simulations made with the “heel” database; continuous line: mean value / dashed lines: confidence interval at 95 %; black curve: Model 0, blue curve: Model 1, red curve: Model 2, yellow curve: Model 3; test number 6.

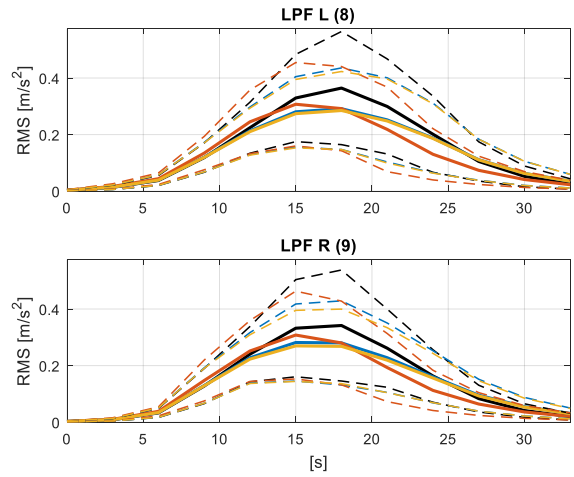


Fig. 154 Moving RMS of acceleration evaluated every 3 s; accelerometer 8 (up) and 9 (down); simulations made with the “tiptoe” database; continuous line: mean value / dashed lines: confidence interval at 95 %; black curve: Model 0, blue curve: Model 1, red curve: Model 2, yellow curve: Model 3; test number 6.

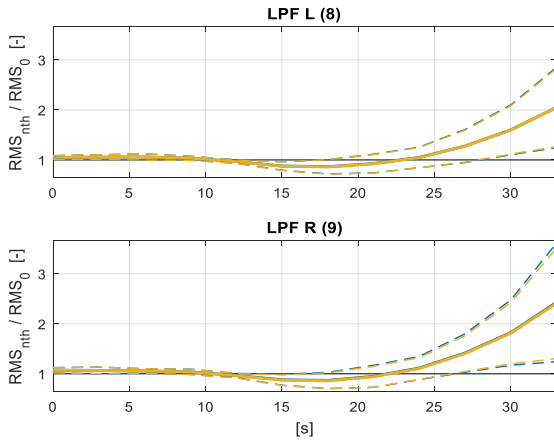


Fig. 155 Moving RMS of acceleration evaluated every 3 s normalized by Model 0; accelerometer 8 (up) and 9 (down); simulations made with the “heel” database; continuous line: mean value / dashed lines: confidence interval at 95 %; black curve: Model 0, blue curve: Model 1, yellow curve: Model 3; test number 6.

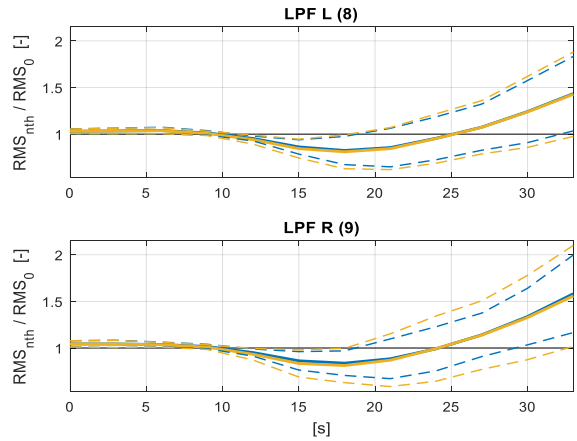


Fig. 156 Moving RMS of acceleration evaluated every 3 s normalized by Model 0; accelerometer 8 (up) and 9 (down); simulations made with the “tiptoe” database; continuous line: mean value / dashed lines: confidence interval at 95 %; black curve: Model 0, blue curve: Model 1, yellow curve: Model 3; test number 6.

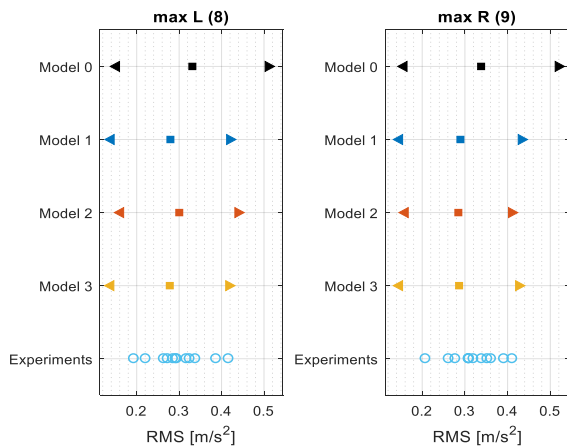


Fig. 157 Maximum Moving RMS values of acceleration evaluated by each Model; maximum of the experimental moving RMS; accelerometer 8 (up) and 9 (down); simulations made with the “heel” database; \square : mean value / $\triangleleft \triangleright$: confidence interval at 95 %; test number 6.

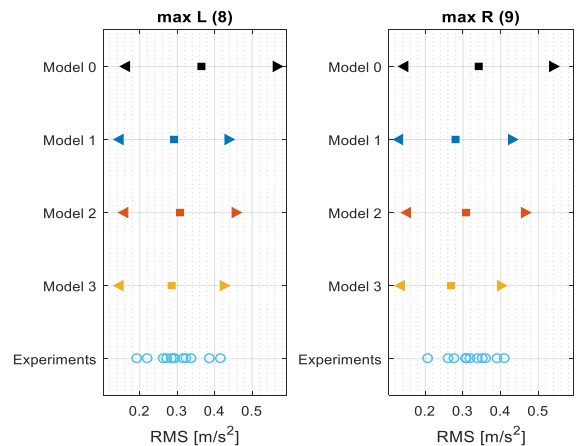


Fig. 158 Maximum Moving RMS values of acceleration evaluated by each Model; maximum of the experimental moving RMS; accelerometer 8 (up) and 9 (down); simulations made with the “heel” database; \square : mean value / $\triangleleft \triangleright$: confidence interval at 95 %; test number 6.

Test number 7: 2 pedestrians (selected) go upstairs

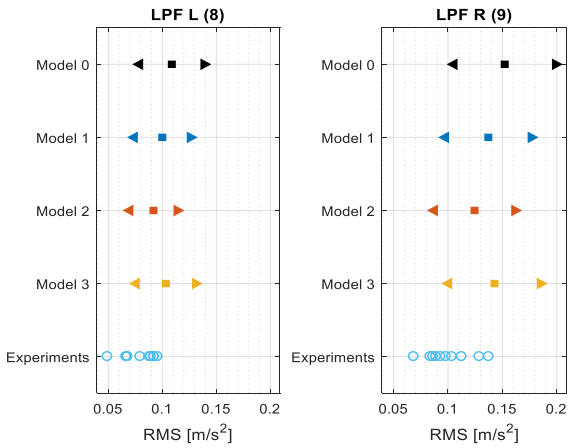


Fig. 159 Global RMS values of the acceleration; accelerometer 8 (left) and 9 (right); simulations made with the “heel” database; \square : mean value / $\triangleleft \triangleright$: confidence interval at 95 %; test number 7.

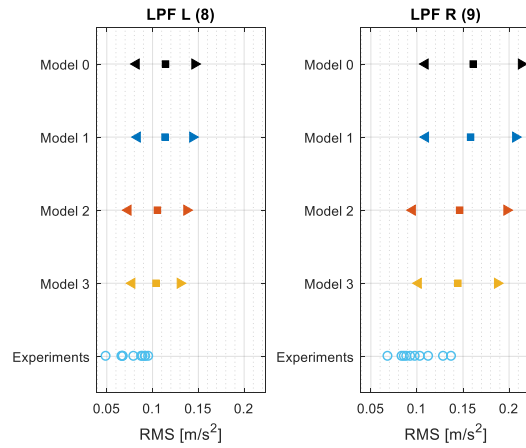


Fig. 160 Global RMS values of the acceleration; accelerometer 8 (left) and 9 (right); simulations made with the “tiptoe” database; \square : mean value / $\triangleleft \triangleright$: confidence interval at 95 %; test number 7.

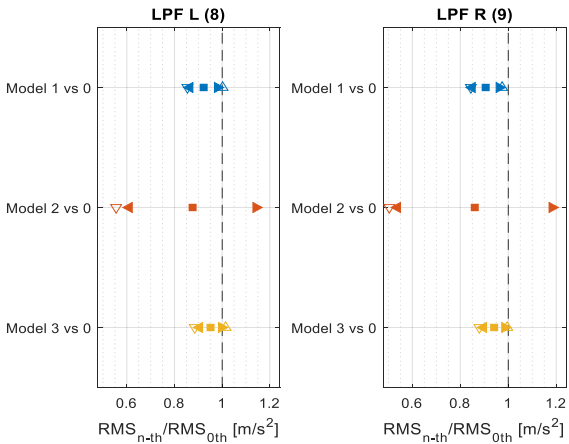


Fig. 161 Global RMS values of acceleration normalized by Model 0; accelerometer 8 (left) and 9 (right); simulations made with the “heel” database; \square : mean value / $\triangleleft \triangleright$: confidence interval at 95 % / \triangle : maximum ratio value / ∇ : minimum ratio value; test number 7.

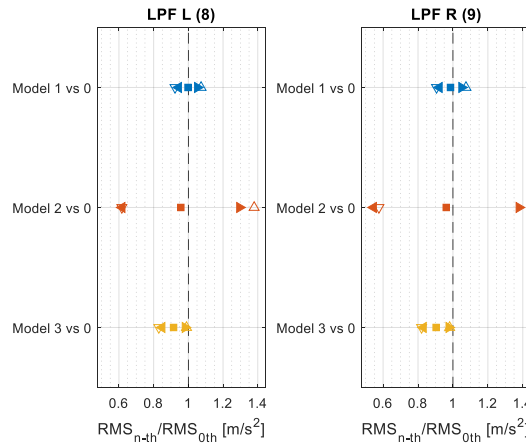


Fig. 162 Global RMS values of acceleration normalized by Model 0; accelerometer 8 (left) and 9 (right); simulations made with the “tiptoe” database; \square : mean value / $\triangleleft \triangleright$: confidence interval at 95 % / \triangle : maximum ratio value / ∇ : minimum ratio value; test number 7.

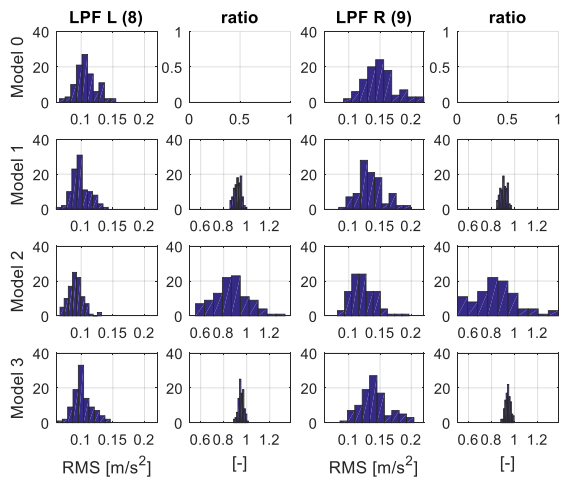


Fig. 163 Histograms of the Global RMS of acceleration and of the normalized by Model 0 ones; accelerometer 8 (left) and 9 (right); simulations made with the “heel” database; test number 7.

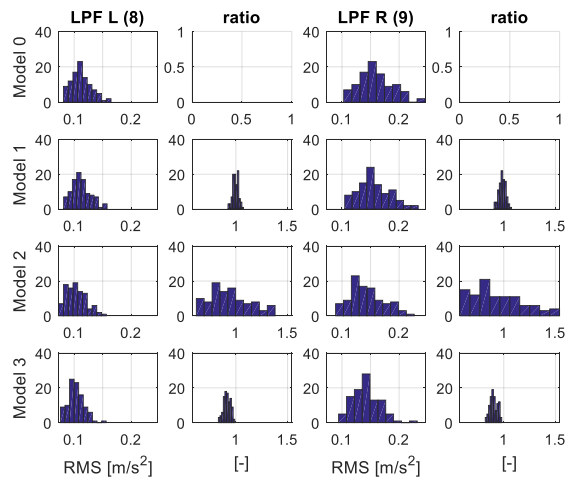


Fig. 164 Histograms of the Global RMS of acceleration and of the normalized by Model 0 ones; accelerometer 8 (left) and 9 (right); simulations made with the “tiptoe” database; test number 7.

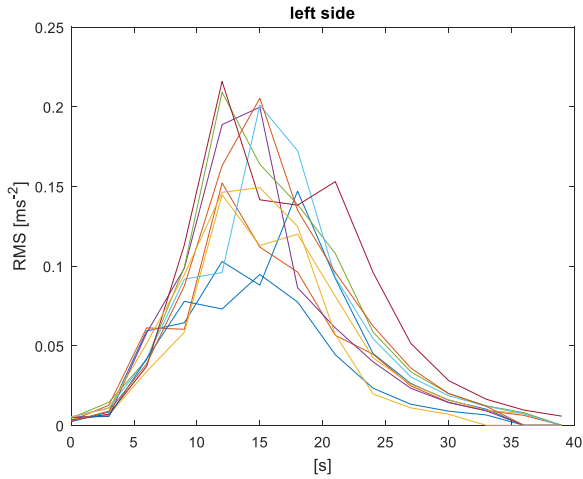


Fig. 165 Moving RMS of acceleration evaluated every 3 s; experimental data - accelerometer 8, test number 7.

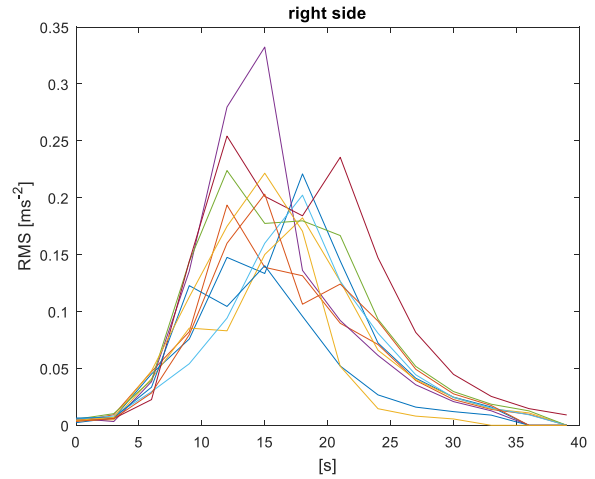


Fig. 166 Moving RMS of acceleration evaluated every 3 s; experimental data - accelerometer 9, test number 7.

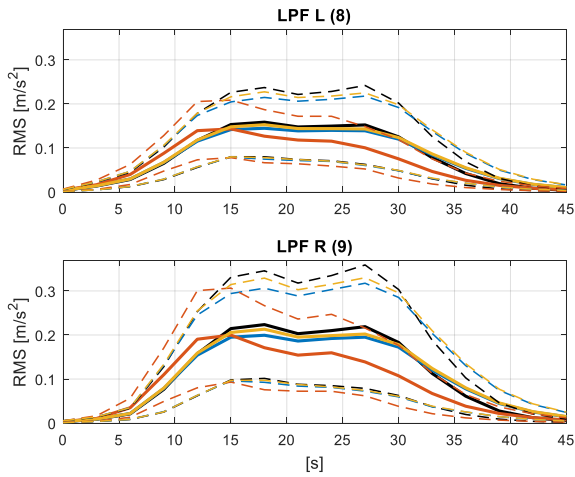


Fig. 167 Moving RMS of acceleration evaluated every 3 s; accelerometer 8 (up) and 9 (down); simulations made with the “heel” database; continuous line: mean value / dashed lines: confidence interval at 95 %; black curve: Model 0, blue curve: Model 1, red curve: Model 2, yellow curve: Model 3; test number 7.

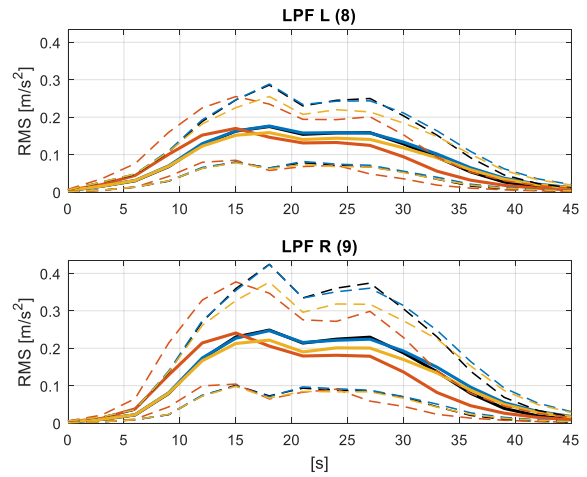


Fig. 168 Moving RMS of acceleration evaluated every 3 s; accelerometer 8 (up) and 9 (down); simulations made with the “tiptoe” database; continuous line: mean value / dashed lines: confidence interval at 95 %; black curve: Model 0, blue curve: Model 1, red curve: Model 2, yellow curve: Model 3; test number 7.

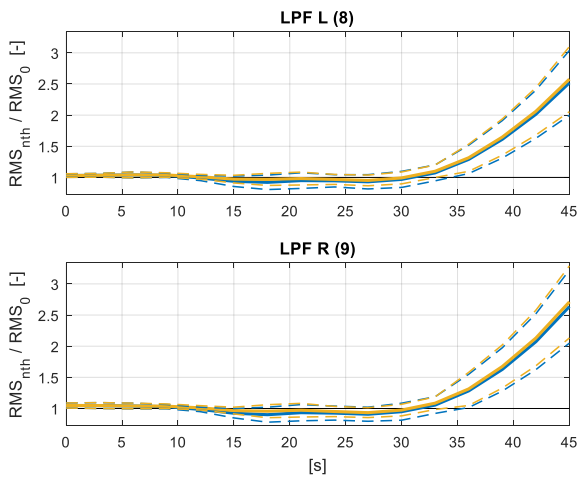


Fig. 169 Moving RMS of acceleration evaluated every 3 s normalized by Model 0; accelerometer 8 (up) and 9 (down); simulations made with the “heel” database; continuous line: mean value / dashed lines: confidence interval at 95 %; black curve: Model 0, blue curve: Model 1, yellow curve: Model 3; test number 7.

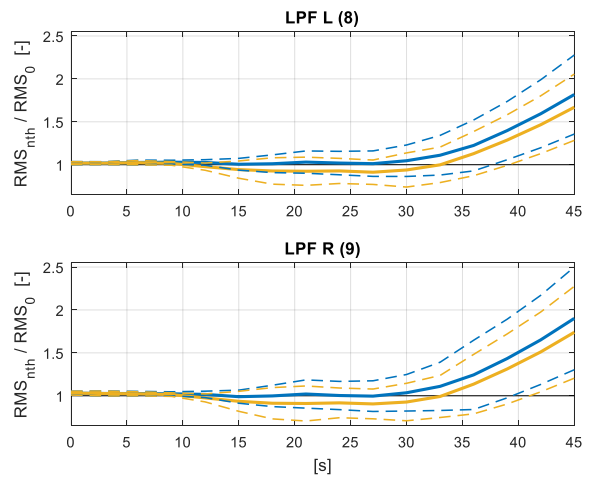


Fig. 170 Moving RMS of acceleration evaluated every 3 s normalized by Model 0; accelerometer 8 (up) and 9 (down); simulations made with the “tiptoe” database; continuous line: mean value / dashed lines: confidence interval at 95 %; black curve: Model 0, blue curve: Model 1, yellow curve: Model 3; test number 7.

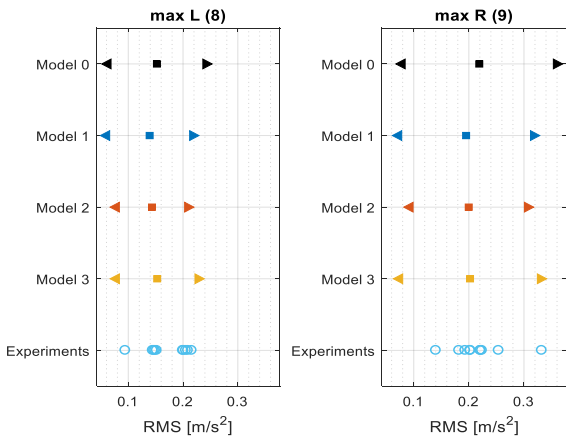


Fig. 171 Maximum Moving RMS values of acceleration evaluated by each Model; maximum of the experimental moving RMS; accelerometer 8 (up) and 9 (down); simulations made with the “heel” database; \square : mean value / $\triangleleft \triangleright$: confidence interval at 95 %; test number 7.

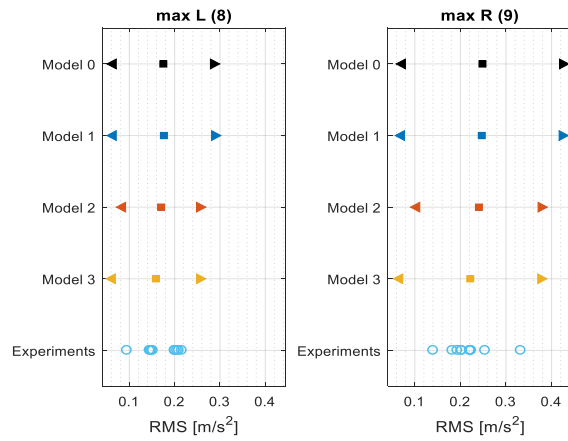


Fig. 172 Maximum Moving RMS values of acceleration evaluated by each Model; maximum of the experimental moving RMS; accelerometer 8 (up) and 9 (down); simulations made with the “heel” database; \square : mean value / $\triangleleft \triangleright$: confidence interval at 95 %; test number 7.

Test number 8: 2 pedestrians (selected) go downstairs

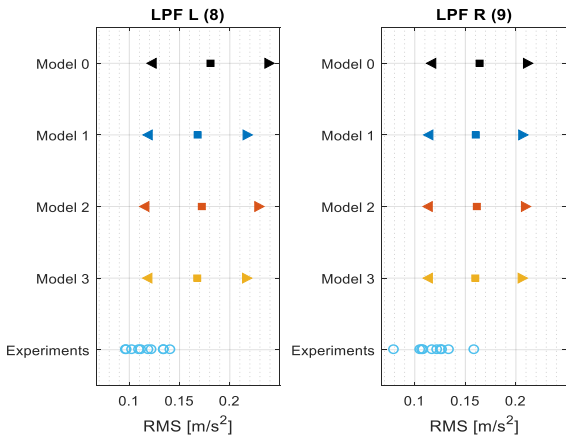


Fig. 173 Global RMS values of the acceleration; accelerometer 8 (left) and 9 (right); simulations made with the “heel” database; \square : mean value / $\triangleleft \triangleright$: confidence interval at 95 %; test number 8.

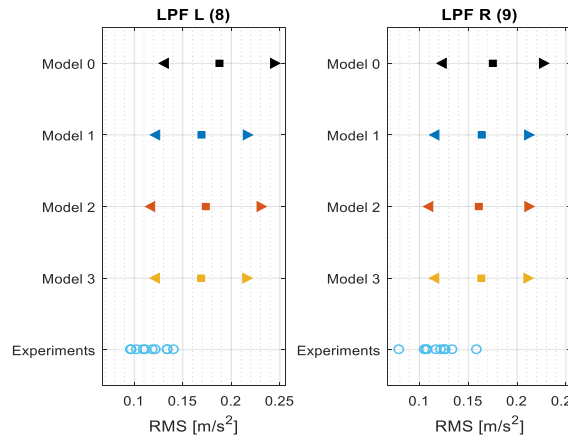


Fig. 174 Global RMS values of the acceleration; accelerometer 8 (left) and 9 (right); simulations made with the “tiptoe” database; \square : mean value / $\triangleleft \triangleright$: confidence interval at 95 %; test number 8.

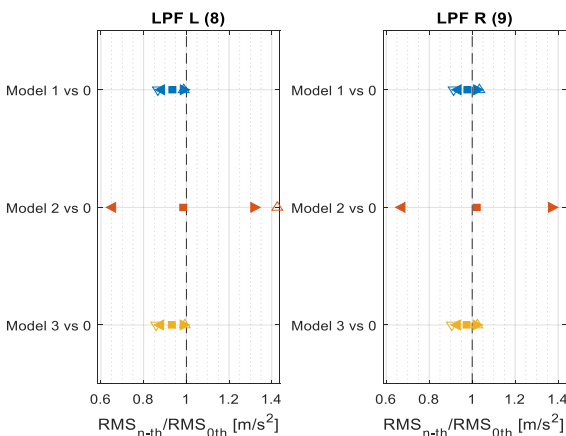


Fig. 175 Global RMS values of acceleration normalized by Model 0; accelerometer 8 (left) and 9 (right); simulations made with the “heel” database; \square : mean value / $\triangleleft \triangleright$: confidence interval at 95 % / \triangle : maximum ratio value / ∇ : minimum ratio value; test number 8.

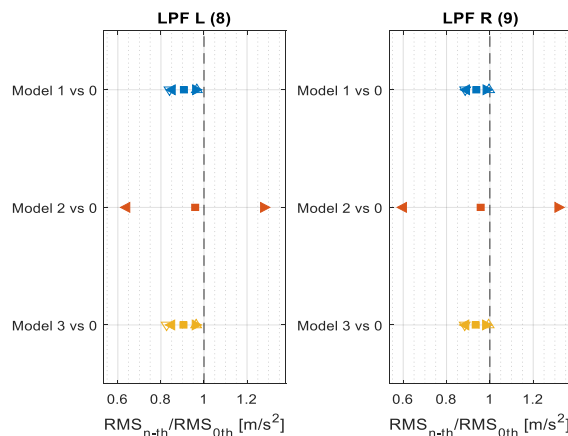


Fig. 176 Global RMS values of acceleration normalized by Model 0; accelerometer 8 (left) and 9 (right); simulations made with the “tiptoe” database; \square : mean value / $\triangleleft \triangleright$: confidence interval at 95 % / \triangle : maximum ratio value / ∇ : minimum ratio value; test number 8.

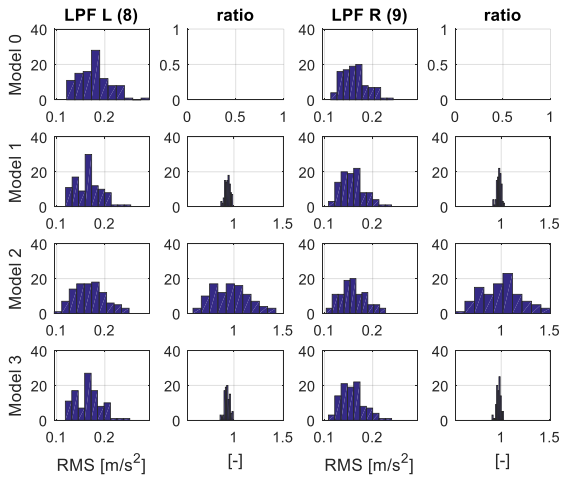


Fig. 177 Histograms of the Global RMS of acceleration and of the normalized by Model 0 ones; accelerometer 8 (left) and 9 (right); simulations made with the “heel” database; test number 8.

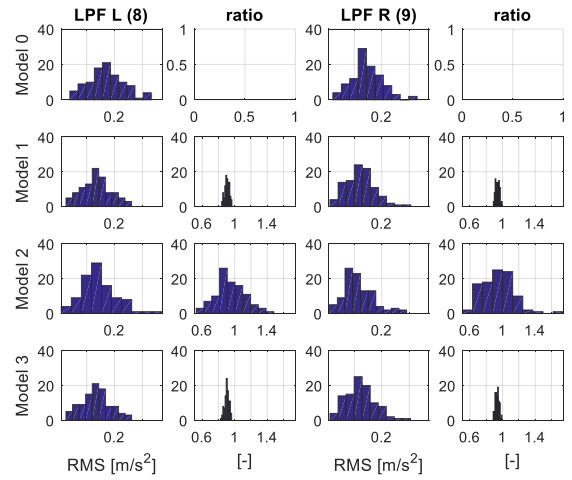


Fig. 178 Histograms of the Global RMS of acceleration and of the normalized by Model 0 ones; accelerometer 8 (left) and 9 (right); simulations made with the “tiptoe” database; test number 8.

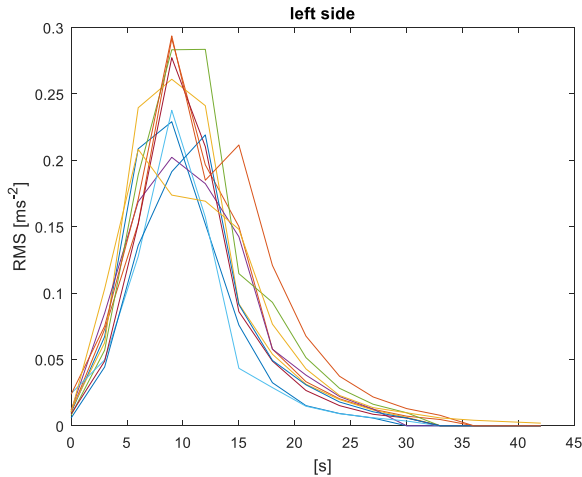


Fig. 179 Moving RMS of acceleration evaluated every 3 s; experimental data - accelerometer 8, test number 8.

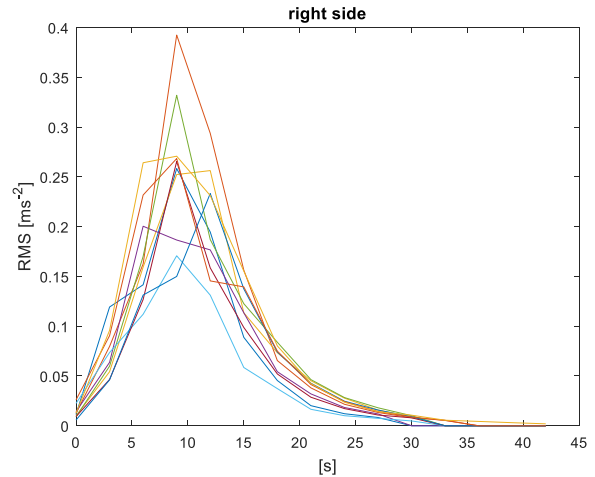


Fig. 180 Moving RMS of acceleration evaluated every 3 s; experimental data - accelerometer 9, test number 8.

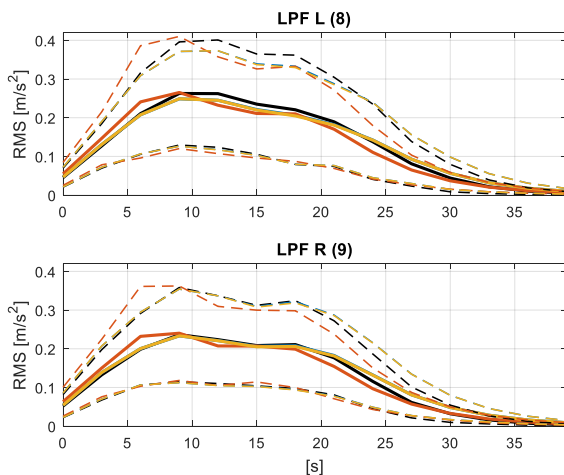


Fig. 181 Moving RMS of acceleration evaluated every 3 s; accelerometer 8 (up) and 9 (down); simulations made with the “heel” database; continuous line: mean value / dashed lines: confidence interval at 95 %; black curve: Model 0, blue curve: Model 1, red curve: Model 2, yellow curve: Model 3; test number 8.

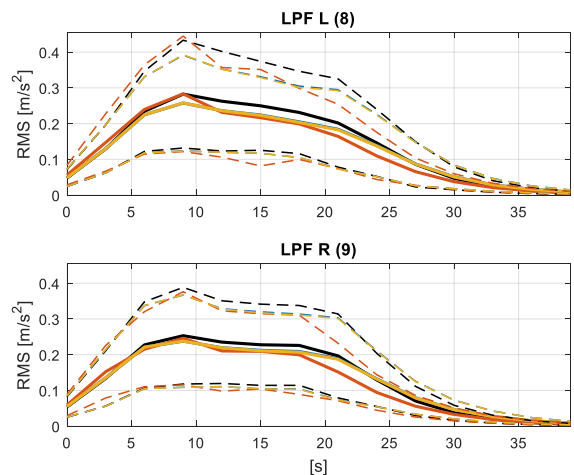


Fig. 182 Moving RMS of acceleration evaluated every 3 s; accelerometer 8 (up) and 9 (down); simulations made with the “tiptoe” database; continuous line: mean value / dashed lines: confidence interval at 95 %; black curve: Model 0, blue curve: Model 1, red curve: Model 2, yellow curve: Model 3; test number 8.

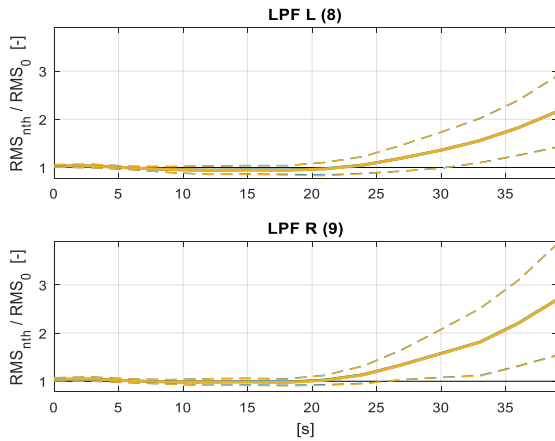


Fig. 183 Moving RMS of acceleration evaluated every 3 s normalized by Model 0; accelerometer 8 (up) and 9 (down); simulations made with the “heel” database; continuous line: mean value / dashed lines: confidence interval at 95 %; black curve: Model 0, blue curve: Model 1, yellow curve: Model 3; test number 8.

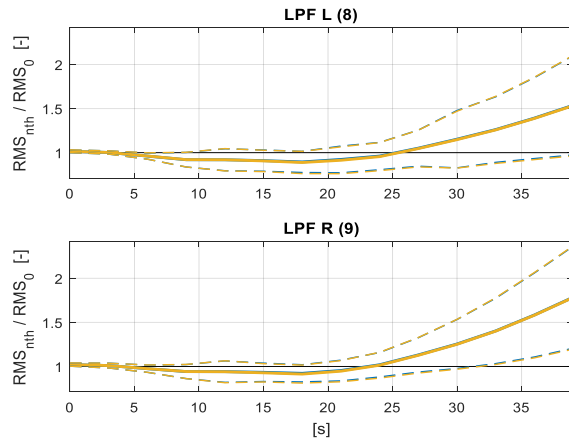


Fig. 184 Moving RMS of acceleration evaluated every 3 s normalized by Model 0; accelerometer 8 (up) and 9 (down); simulations made with the “tiptoe” database; continuous line: mean value / dashed lines: confidence interval at 95 %; black curve: Model 0, blue curve: Model 1, yellow curve: Model 3; test number 8.

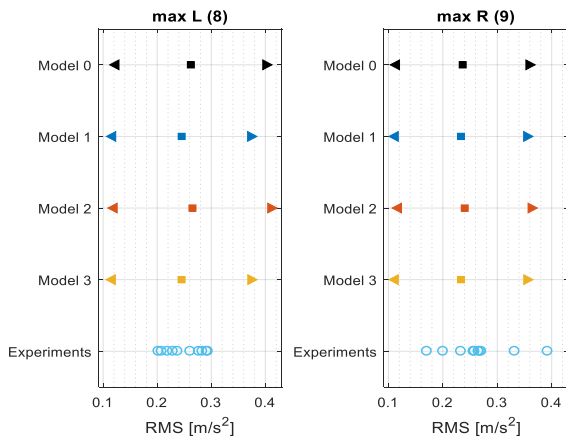


Fig. 185 Maximum Moving RMS values of acceleration evaluated by each Model; maximum of the experimental moving RMS; accelerometer 8 (up) and 9 (down); simulations made with the “heel” database; \square : mean value / $\langle \rangle$: confidence interval at 95 %; test number 8.

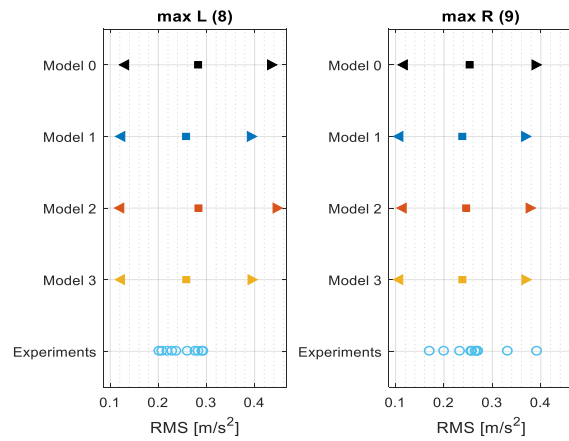


Fig. 186 Maximum Moving RMS values of acceleration evaluated by each Model; maximum of the experimental moving RMS; accelerometer 8 (up) and 9 (down); simulations made with the “tiptoe” database; \square : mean value / $\langle \rangle$: confidence interval at 95 %; test number 8.

Test number 9: 1 pedestrians go upstairs and 1 go downstairs (both selected)

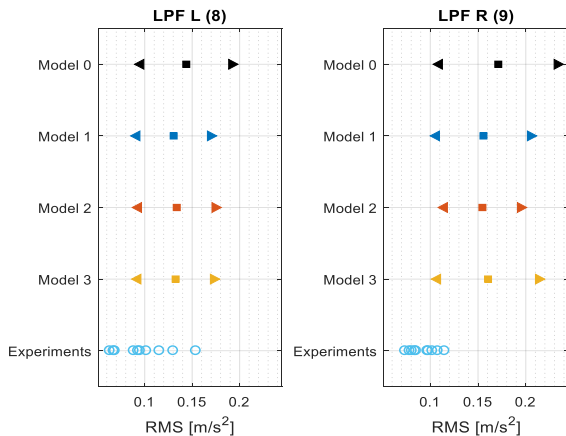


Fig. 187 Global RMS values of the acceleration; accelerometer 8 (left) and 9 (right); simulations made with the “heel” database; \square : mean value / $\langle \rangle$: confidence interval at 95 %; test number 9.

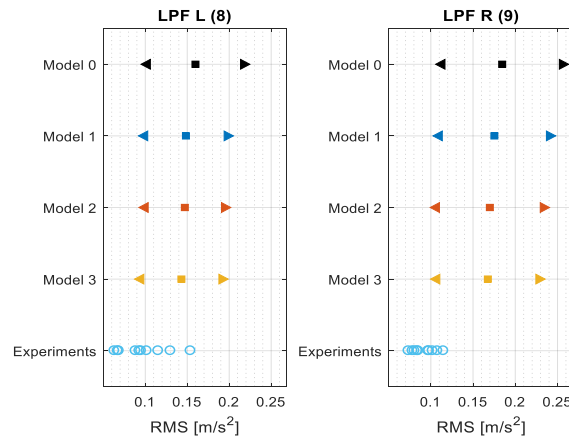


Fig. 188 Global RMS values of the acceleration; accelerometer 8 (left) and 9 (right); simulations made with the “tiptoe” database; \square : mean value / $\langle \rangle$: confidence interval at 95 %; test number 9.

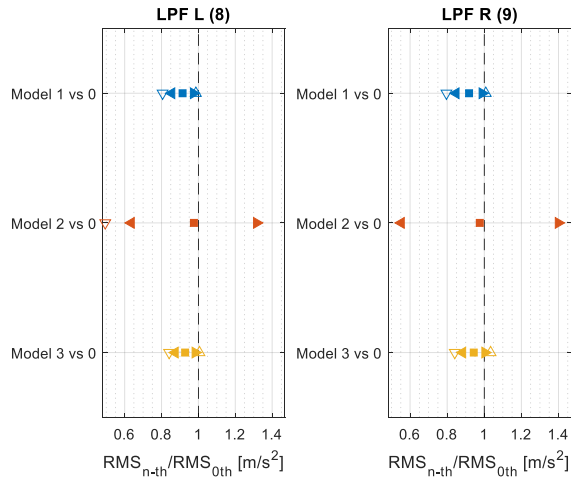


Fig. 189 Global RMS values of acceleration normalized by Model 0; accelerometer 8 (left) and 9 (right); simulations made with the “heel” database; \square : mean value / $\triangleleft \triangleright$: confidence interval at 95 % / \triangle : maximum ratio value / ∇ : minimum ratio value; test number 9.

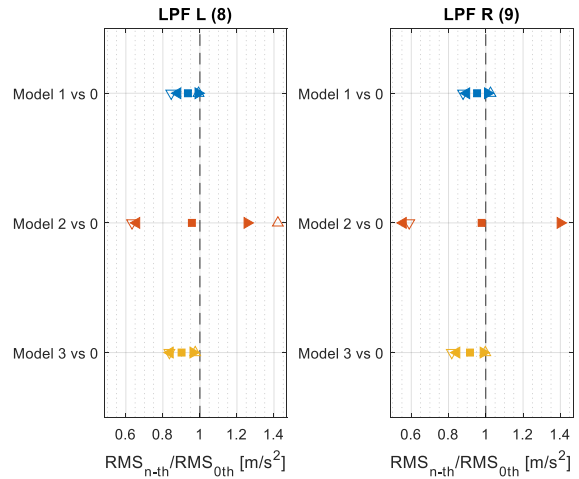


Fig. 190 Global RMS values of acceleration normalized by Model 0; accelerometer 8 (left) and 9 (right); simulations made with the “tiptoe” database; \square : mean value / $\triangleleft \triangleright$: confidence interval at 95 % / \triangle : maximum ratio value / ∇ : minimum ratio value; test number 9.

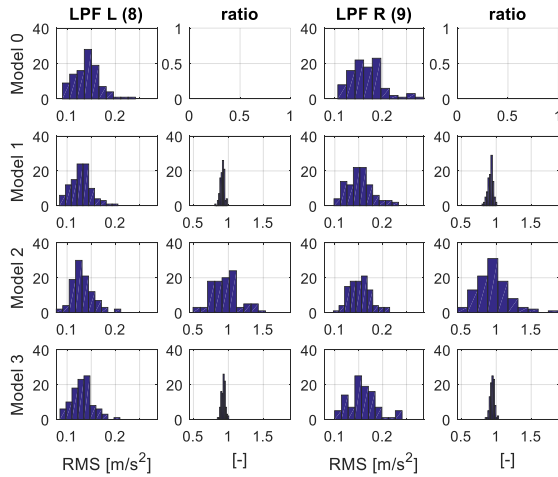


Fig. 191 Histograms of the Global RMS of acceleration and of the normalized by Model 0 ones; accelerometer 8 (left) and 9 (right); simulations made with the “heel” database; test number 9.

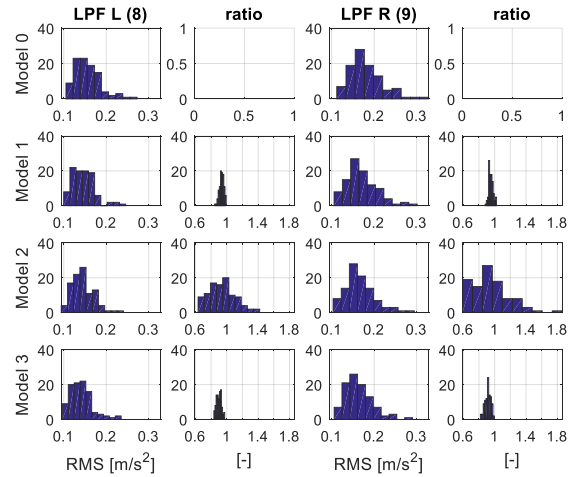


Fig. 192 Histograms of the Global RMS of acceleration and of the normalized by Model 0 ones; accelerometer 8 (left) and 9 (right); simulations made with the “tiptoe” database; test number 9.

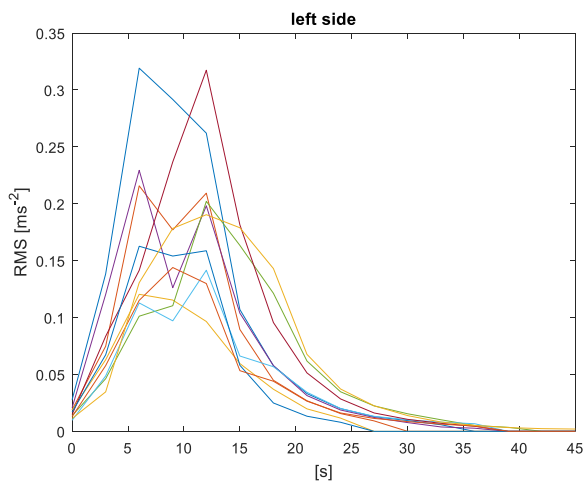


Fig. 193 Moving RMS of acceleration evaluated every 3 s; experimental data - accelerometer 8, test number 9.

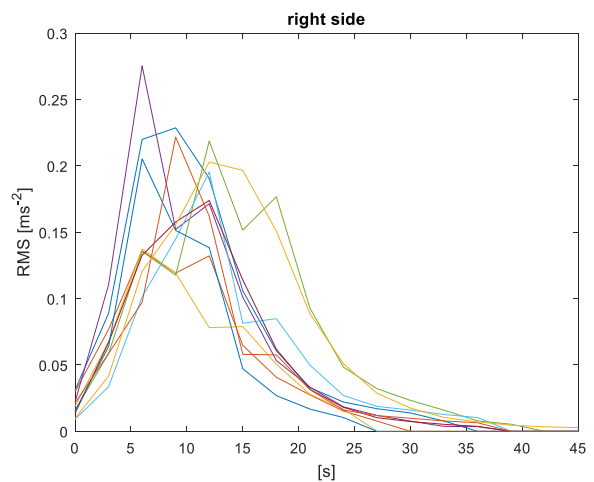


Fig. 194 Moving RMS of acceleration evaluated every 3 s; experimental data - accelerometer 9, test number 9.

Test number 10: 1 pedestrian (random) goes upstairs

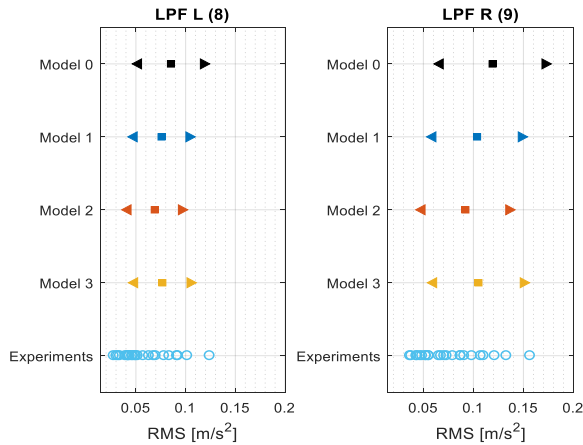


Fig. 201 Global RMS values of the acceleration; accelerometer 8 (left) and 9 (right); simulations made with the “heel” database; \square : mean value / $\triangleleft \triangleright$: confidence interval at 95 %; test number 10.

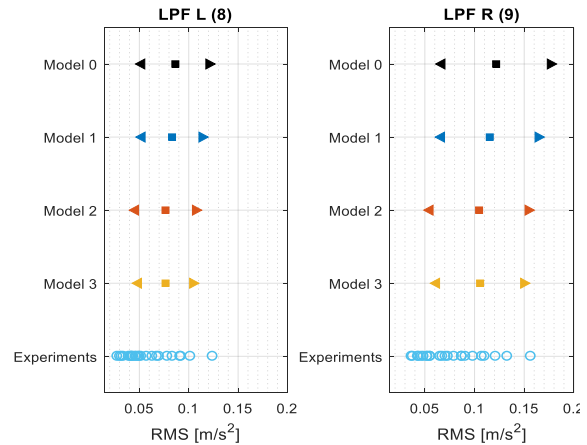


Fig. 202 Global RMS values of the acceleration; accelerometer 8 (left) and 9 (right); simulations made with the “heel” database; \square : mean value / $\triangleleft \triangleright$: confidence interval at 95 %; test number 10.

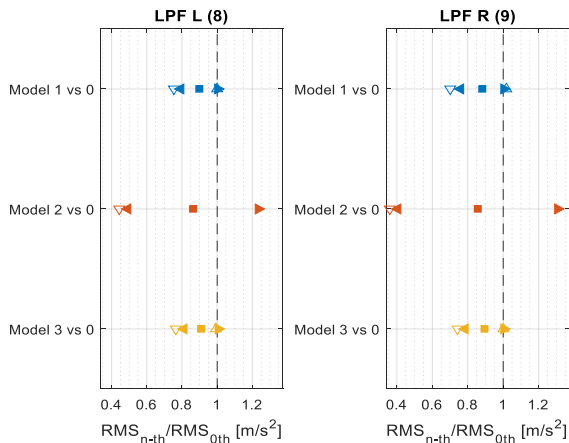


Fig. 203 Global RMS values of acceleration normalized by Model 0; accelerometer 8 (left) and 9 (right); simulations made with the “heel” database; \square : mean value / $\triangleleft \triangleright$: confidence interval at 95 % / \triangle : maximum ratio value / ∇ : minimum ratio value; test number 10.

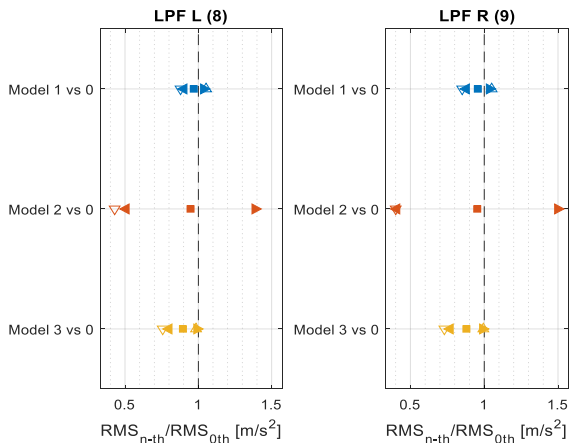


Fig. 204 Global RMS values of acceleration normalized by Model 0; accelerometer 8 (left) and 9 (right); simulations made with the “tiptoe” database; \square : mean value / $\triangleleft \triangleright$: confidence interval at 95 % / \triangle : maximum ratio value / ∇ : minimum ratio value; test number 10.

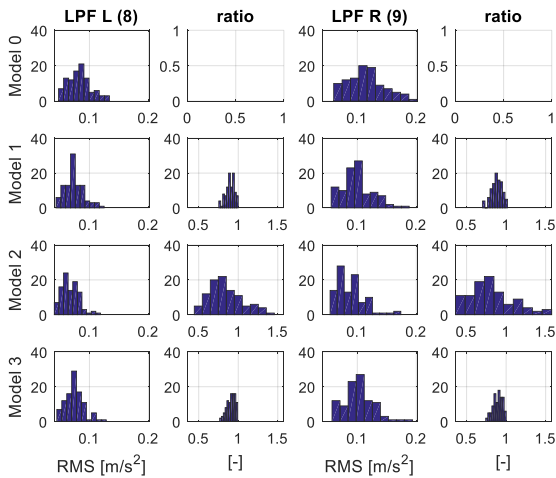


Fig. 205 Histograms of the Global RMS of acceleration and of the normalized by Model 0 ones; accelerometer 8 (left) and 9 (right); simulations made with the “heel” database; test number 10.

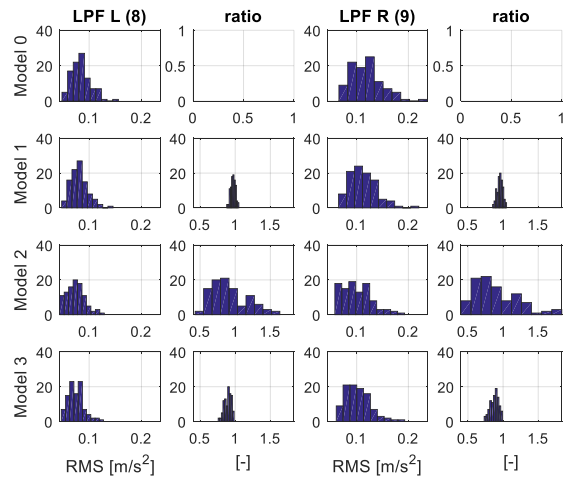


Fig. 206 Histograms of the Global RMS of acceleration and of the normalized by Model 0 ones; accelerometer 8 (left) and 9 (right); simulations made with the “tiptoe” database; test number 10.

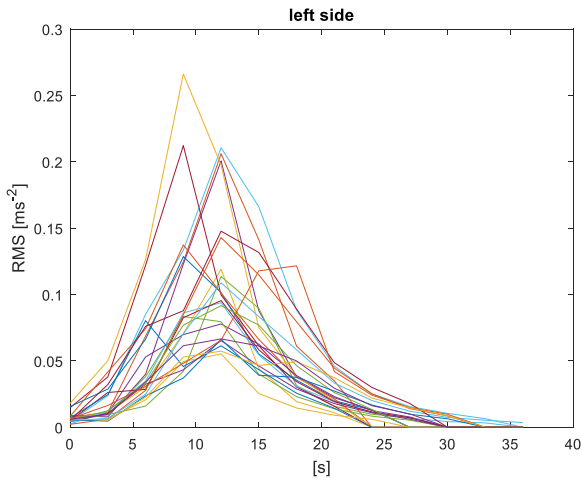


Fig. 207 Moving RMS of acceleration evaluated every 3 s; experimental data - accelerometer 8, test number 10.

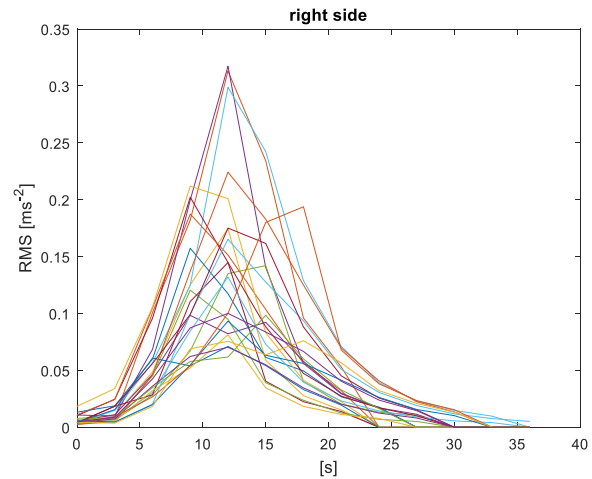


Fig. 208 Moving RMS of acceleration evaluated every 3 s; experimental data - accelerometer 9, test number 10.

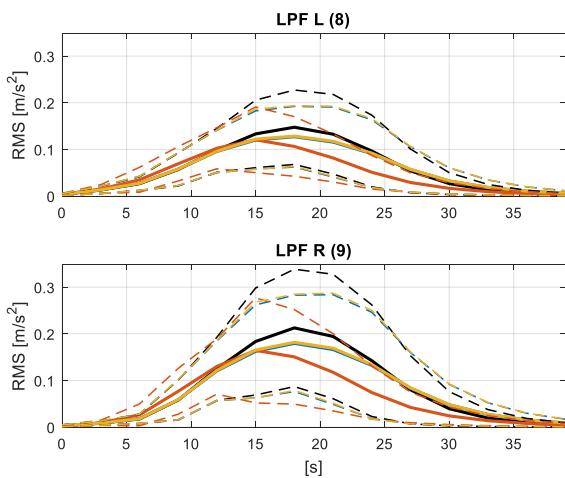


Fig. 209 Moving RMS of acceleration evaluated every 3 s; accelerometer 8 (up) and 9 (down); simulations made with the “heel” database; continuous line: mean value / dashed lines: confidence interval at 95 %; black curve: Model 0, blue curve: Model 1, red curve: Model 2, yellow curve: Model 3; test number 10.

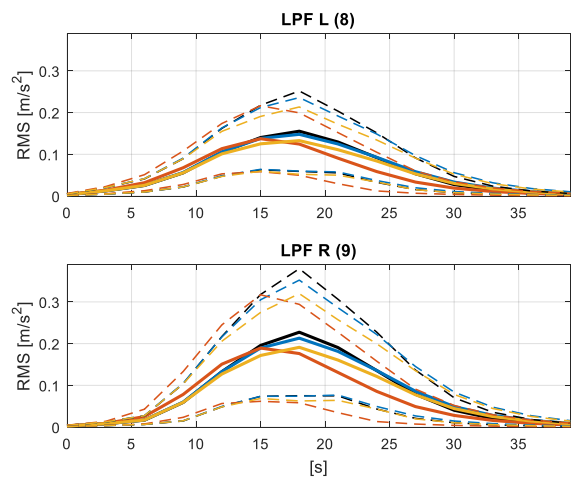


Fig. 210 Moving RMS of acceleration evaluated every 3 s; accelerometer 8 (up) and 9 (down); simulations made with the “tiptoe” database; continuous line: mean value / dashed lines: confidence interval at 95 %; black curve: Model 0, blue curve: Model 1, red curve: Model 2, yellow curve: Model 3; test number 10.

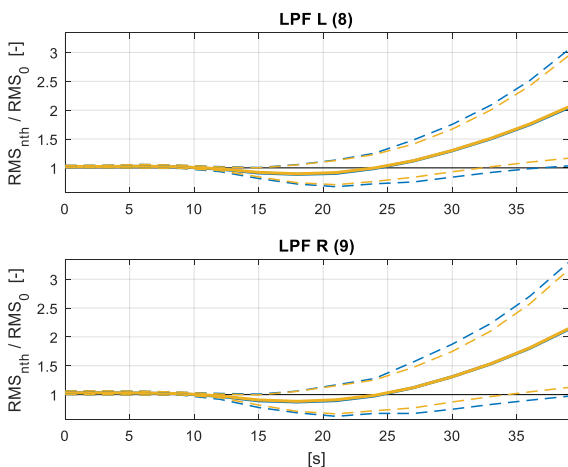


Fig. 211 Moving RMS of acceleration evaluated every 3 s normalized by Model 0; accelerometer 8 (up) and 9 (down); simulations made with the “heel” database; continuous line: mean value / dashed lines: confidence interval at 95 %; black curve: Model 0, blue curve: Model 1, yellow curve: Model 3; test number 10.

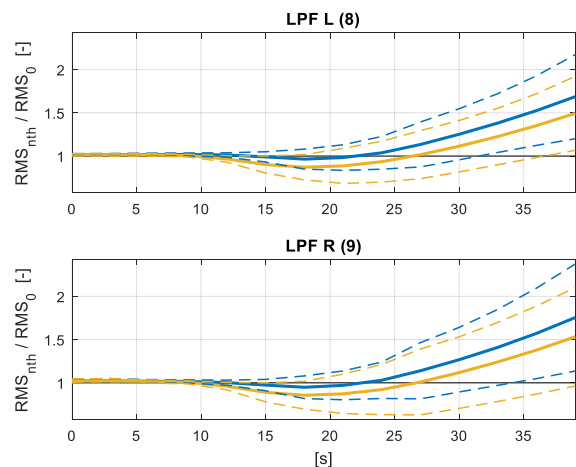


Fig. 212 Moving RMS of acceleration evaluated every 3 s normalized by Model 0; accelerometer 8 (up) and 9 (down); simulations made with the “tiptoe” database; continuous line: mean value / dashed lines: confidence interval at 95 %; black curve: Model 0, blue curve: Model 1, yellow curve: Model 3; test number 10.

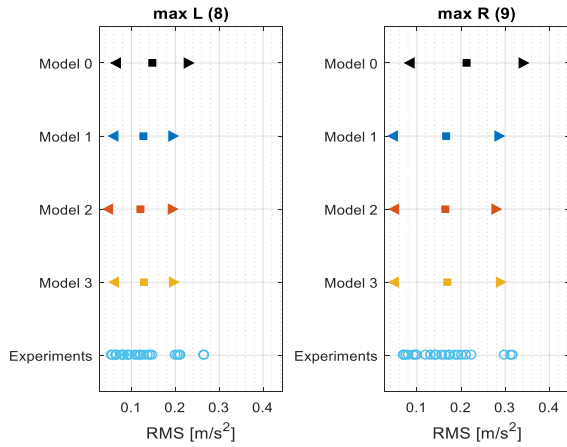


Fig. 213 Maximum Moving RMS values of acceleration evaluated by each Model; maximum of the experimental moving RMS; accelerometer 8 (up) and 9 (down); simulations made with the “heel” database; \square : mean value / $\triangleleft \triangleright$: confidence interval at 95 %; test number 10.

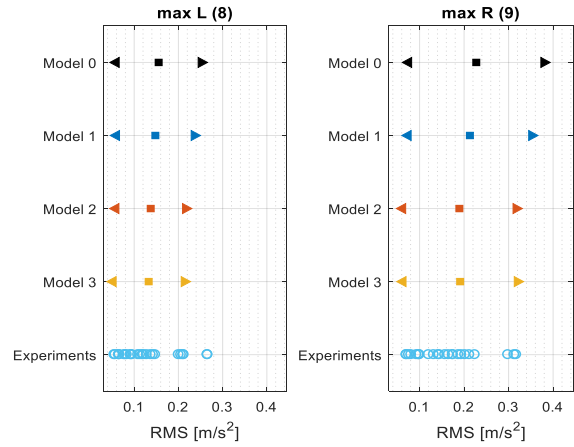


Fig. 214 Maximum Moving RMS values of acceleration evaluated by each Model; maximum of the experimental moving RMS; accelerometer 8 (up) and 9 (down); simulations made with the “heel” database; \square : mean value / $\triangleleft \triangleright$: confidence interval at 95 %; test number 10.

Test number 11: 1 pedestrian (random) goes downstairs

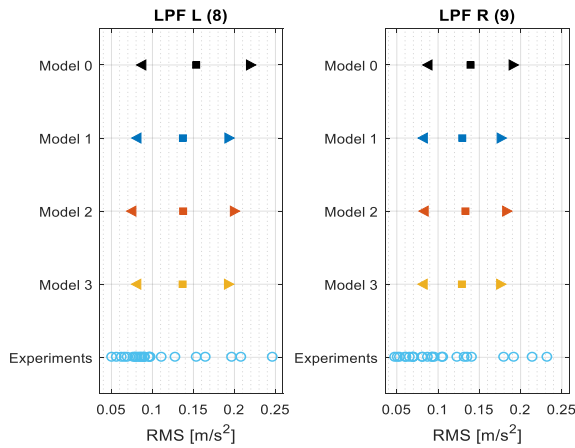


Fig. 215 Global RMS values of the acceleration; accelerometer 8 (left) and 9 (right); simulations made with the “heel” database; \square : mean value / $\triangleleft \triangleright$: confidence interval at 95 %; test number 11.

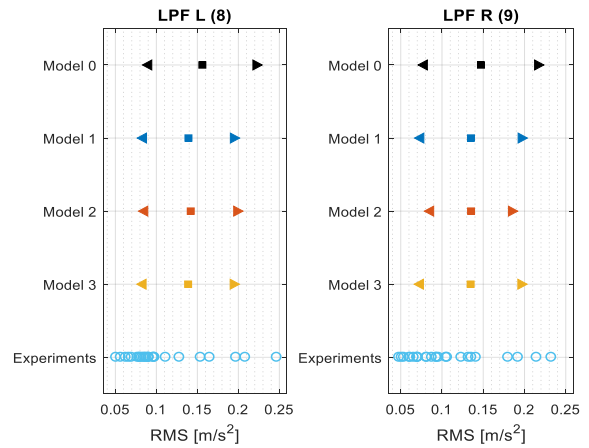


Fig. 216 Global RMS values of the acceleration; accelerometer 8 (left) and 9 (right); simulations made with the “tiptoe” database; \square : mean value / $\triangleleft \triangleright$: confidence interval at 95 %; test number 11.

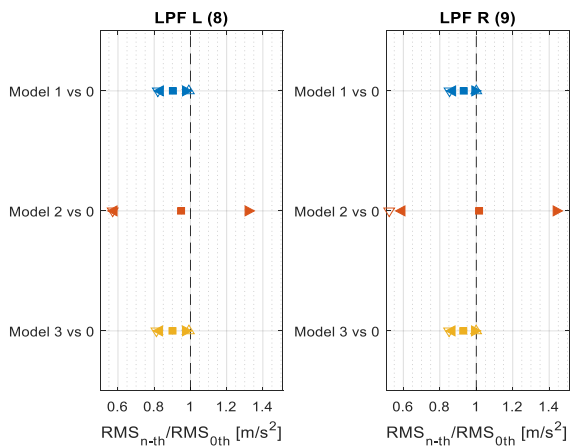


Fig. 217 Global RMS values of acceleration normalized by Model 0; accelerometer 8 (left) and 9 (right); simulations made with the “heel” database; \square : mean value / $\triangleleft \triangleright$: confidence interval at 95 % / Δ : maximum ratio value / ∇ : minimum ratio value; test number 11.

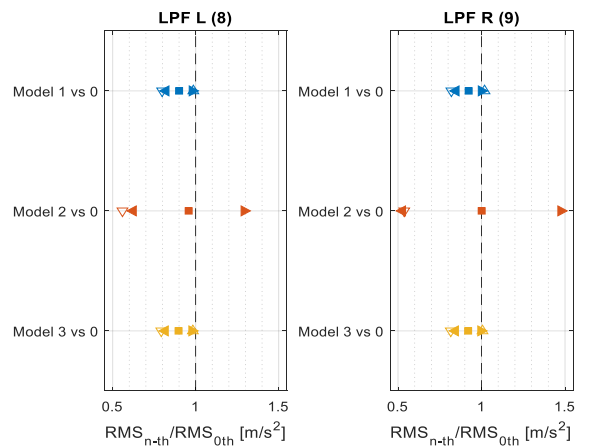


Fig. 218 Global RMS values of acceleration normalized by Model 0; accelerometer 8 (left) and 9 (right); simulations made with the “tiptoe” database; \square : mean value / $\triangleleft \triangleright$: confidence interval at 95 % / Δ : maximum ratio value / ∇ : minimum ratio value; test number 11.

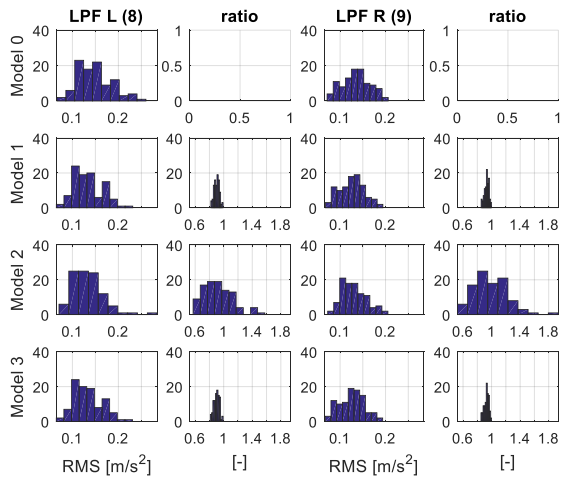


Fig. 219 Histograms of the Global RMS of acceleration and of the normalized by Model 0 ones; accelerometer 8 (left) and 9 (right); simulations made with the “heel” database; test number 11.

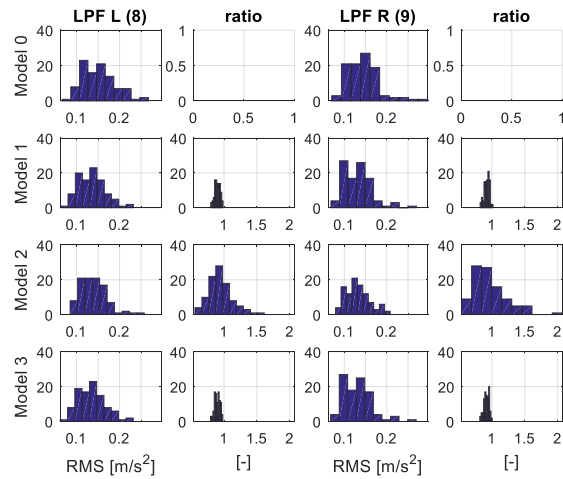


Fig. 220 Histograms of the Global RMS of acceleration and of the normalized by Model 0 ones; accelerometer 8 (left) and 9 (right); simulations made with the “tiptoe” database; test number 11.

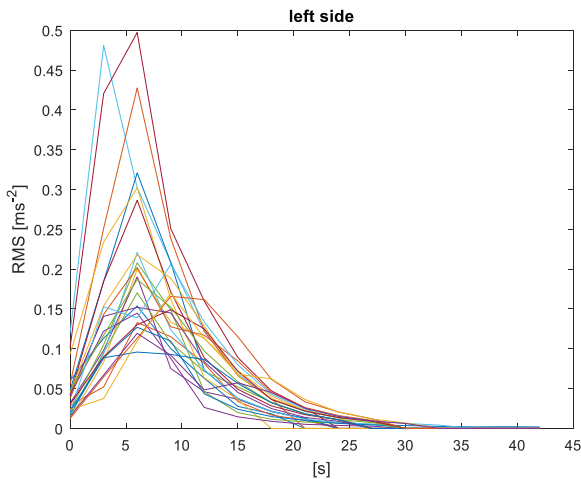


Fig. 221 Moving RMS of acceleration evaluated every 3 s; experimental data - accelerometer 8, test number 11.

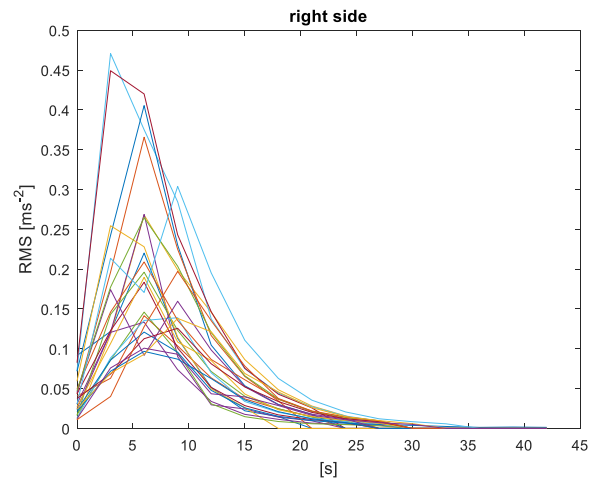


Fig. 222 Moving RMS of acceleration evaluated every 3 s; experimental data - accelerometer 9, test number 11.

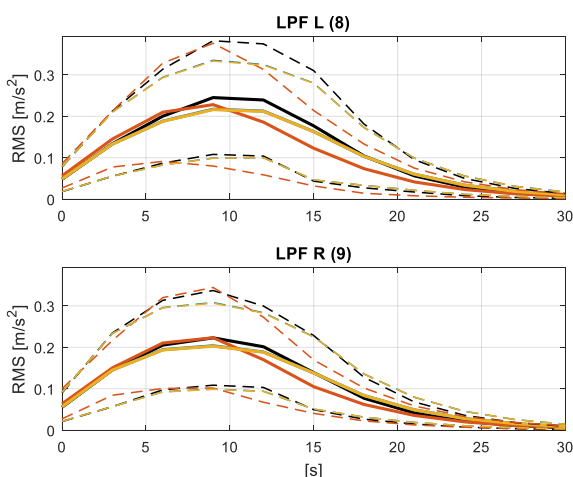


Fig. 223 Moving RMS of acceleration evaluated every 3 s; accelerometer 8 (up) and 9 (down); simulations made with the “heel” database; continuous line: mean value / dashed lines: confidence interval at 95 %; black curve: Model 0, blue curve: Model 1, red curve: Model 2, yellow curve: Model 3; test number 11.

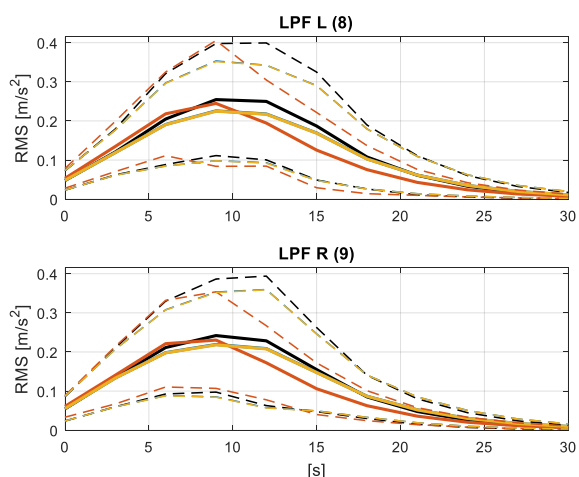


Fig. 224 Moving RMS of acceleration evaluated every 3 s; accelerometer 8 (up) and 9 (down); simulations made with the “tiptoe” database; continuous line: mean value / dashed lines: confidence interval at 95 %; black curve: Model 0, blue curve: Model 1, red curve: Model 2, yellow curve: Model 3; test number 11.

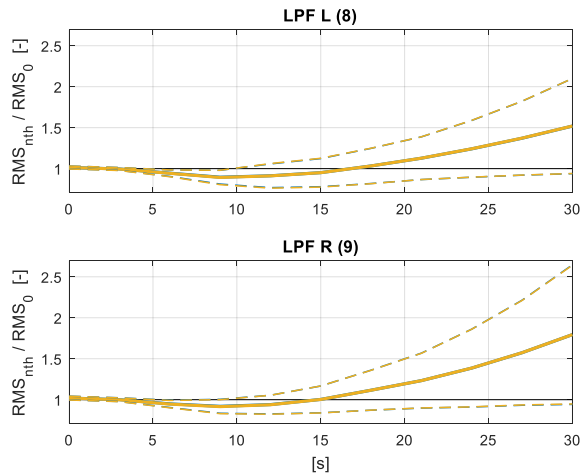


Fig. 225 Moving RMS of acceleration evaluated every 3 s normalized by Model 0; accelerometer 8 (up) and 9 (down); simulations made with the “heel” database; continuous line: mean value / dashed lines: confidence interval at 95 %; black curve: Model 0, blue curve: Model 1, yellow curve: Model 3; test number 11.

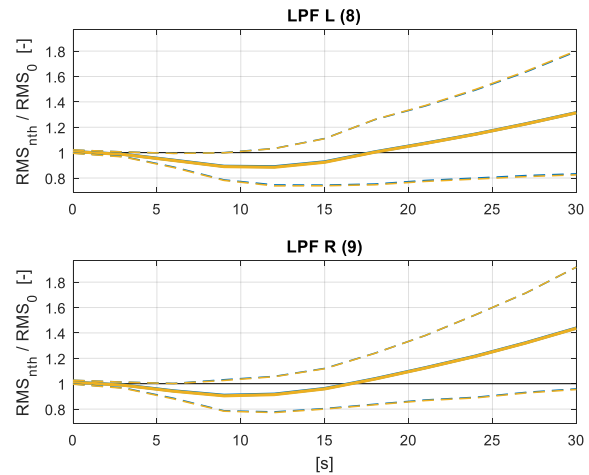


Fig. 226 Moving RMS of acceleration evaluated every 3 s normalized by Model 0; accelerometer 8 (up) and 9 (down); simulations made with the “tiptoe” database; continuous line: mean value / dashed lines: confidence interval at 95 %; black curve: Model 0, blue curve: Model 1, yellow curve: Model 3; test number 11.

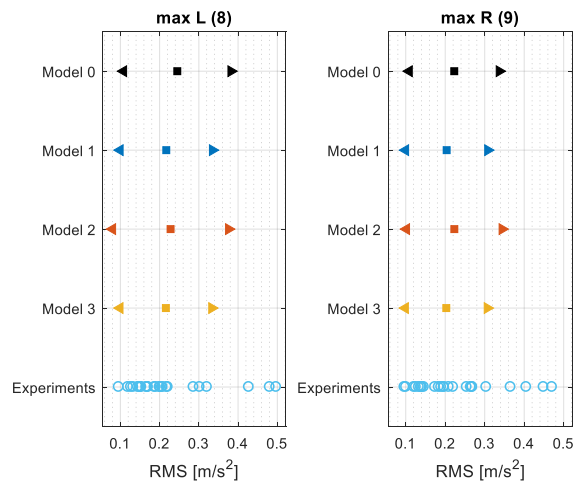


Fig. 227 Maximum Moving RMS values of acceleration evaluated by each Model; maximum of the experimental moving RMS; accelerometer 8 (up) and 9 (down); simulations made with the “heel” database; \square : mean value / $\langle \rangle$: confidence interval at 95 %; test number 11.

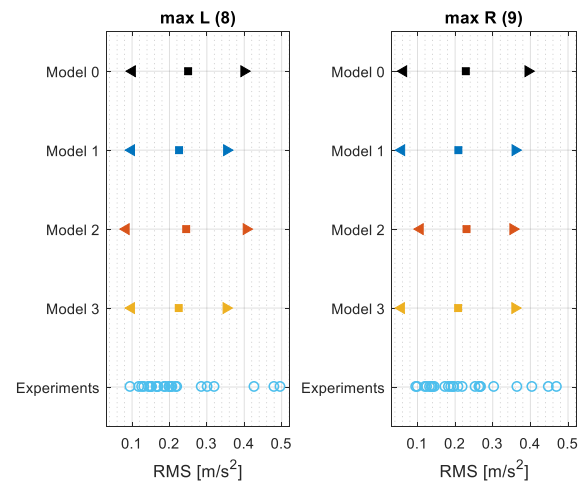


Fig. 228 Maximum Moving RMS values of acceleration evaluated by each Model; maximum of the experimental moving RMS; accelerometer 8 (up) and 9 (down); simulations made with the “heel” database; \square : mean value / $\langle \rangle$: confidence interval at 95 %; test number 11.

5.3 Other Tests

In the previous Section (5.2) have been reported the results of all the experimental and numerical tests performed. As explained, one of the most significant outcomes were the plots of the peak of the RMS values (e.g. Fig. 227 and Fig. 228). Indeed, in them, are reported the comparison between the numerical estimations of the peaks of acceleration, always in terms of RMS values. That is an important parameter, since it is the one used at the design stage of a new structure, for the serviceability check.

It is noted that in all the tested scenarios such values fell in the estimated range of peaks. The only cases in which there are some experimental RMS peaks that assume values higher than the

estimated intervals are in the pedestrian cases number 3, 10 and 11 of Table 5. All these tests involved one pedestrian who walk in loop for 5 min, who goes upstairs and goes down stairs, respectively.

It is also noted that to the individual active force database of each subject, active force time histories were added, coming from an already existing database, in order to have a greater variability of the active histories. In this way, the change of the active force time histories of the single subject, along the day, was accounted too (see Section 3.1).

In order to mitigate the mentioned cases in which some underestimations of the RMS peaks took place, such tests were numerically repeated for a subject (subject 3), using as database of the active force time histories the only ones measured in the experimental campaign of subject 3, without any addition of other pre-existing active force time histories.

The new numerical simulations show an optimal estimation of the specific subject considered, for what concerns the peaks of RMS of acceleration (Fig. 241 and Fig. 242 for the test number 3, Fig. 255 and Fig. 256 for the test number 10, Fig. 269 and Fig. 270 for the test number 11) with respect to the previous ones, which were based on a random selection of the subject involved (Fig. 115 and Fig. 116 for the test number 3, Fig. 213 and Fig. 214 for the test number 10, Fig. 227 and Fig. 228 for the test number 11).

Of course, this additional analysis was done only for the evaluation of the reliability of the Models, in the estimations of the vibration levels with specific subjects. In a design stage of a new structure, such an approach (i.e. consideration of specific subjects) would be unfeasible. Since mean parameters of the possible subject involved should be considered. Hence, the plots obtained with a random extraction of pedestrians should be taken in that case (Fig. 115 and Fig. 116 for the test number 3, Fig. 213 and Fig. 214 for the test number 10, Fig. 227 and Fig. 228 for the test number 11). It is to be pointed out that in them, the main experimental cloud of points fall in the estimated ranges, and only a low number of experimental observations assume values slightly higher with respect to the ones predicted.

Test number 3: 1 pedestrian (subject 3) walks in loop

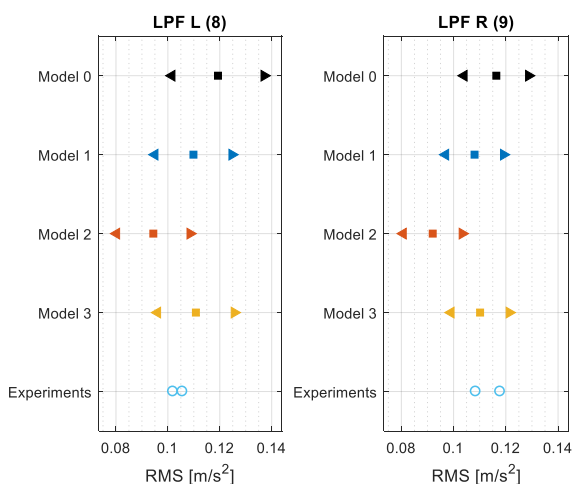


Fig. 229 Global RMS values of the acceleration; accelerometer 8 (left) and 9 (right); simulations made with the “heel” database; \square : mean value $\triangleleft \triangleright$: confidence interval at 95 %; test number 3.

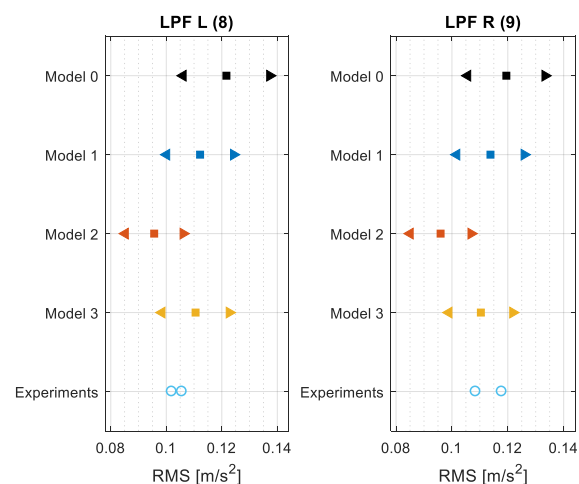


Fig. 230 Global RMS values of the acceleration; accelerometer 8 (left) and 9 (right); simulations made with the “tiptoe” database; \square : mean value $\triangleleft \triangleright$: confidence interval at 95 %; test number 3.

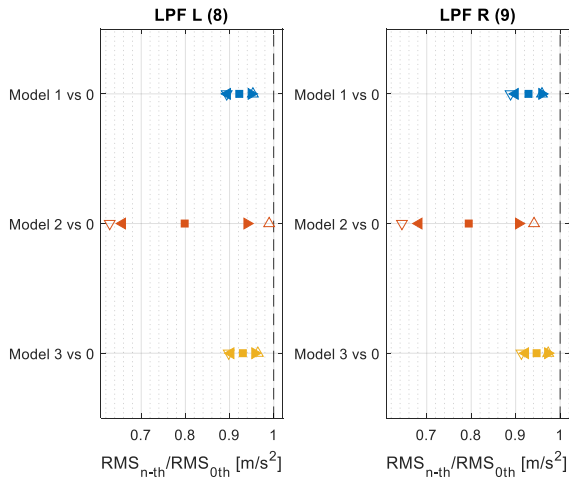


Fig. 231 Global RMS values of acceleration normalized by Model 0; accelerometer 8 (left) and 9 (right); simulations made with the “heel” database; \square : mean value / $\triangleleft \triangleright$: confidence interval at 95 % / \triangle : maximum ratio value / ∇ : minimum ratio value; test number 3.

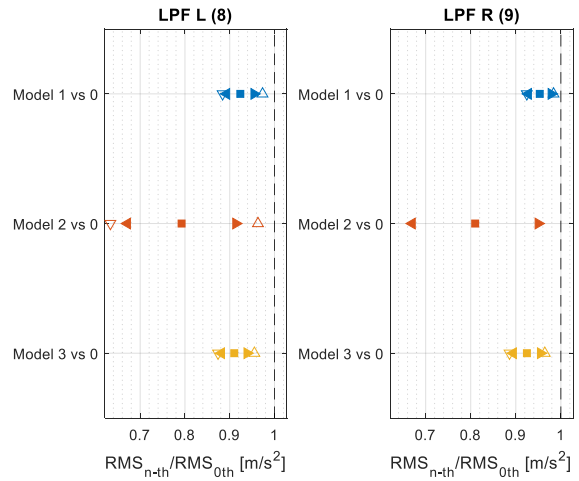


Fig. 232 Global RMS values of acceleration normalized by Model 0; accelerometer 8 (left) and 9 (right); simulations made with the “tiptoe” database; \square : mean value / $\triangleleft \triangleright$: confidence interval at 95 % / \triangle : maximum ratio value / ∇ : minimum ratio value; test number 3.

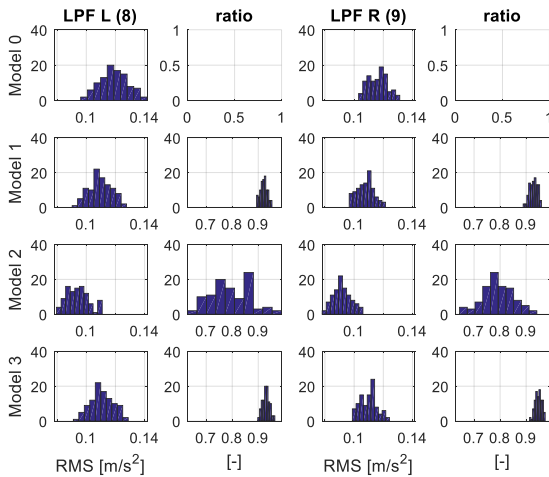


Fig. 233 Histograms of the Global RMS of acceleration and of the normalized by Model 0 ones; accelerometer 8 (left) and 9 (right); simulations made with the “heel” database; test number 3.

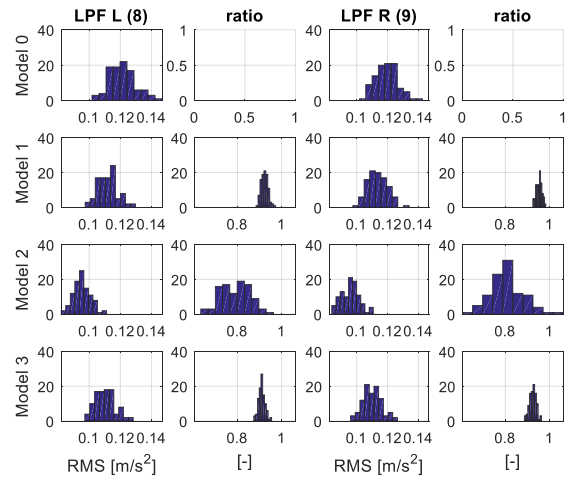


Fig. 234 Histograms of the Global RMS of acceleration and of the normalized by Model 0 ones; accelerometer 8 (left) and 9 (right); simulations made with the “tiptoe” database; test number 3.

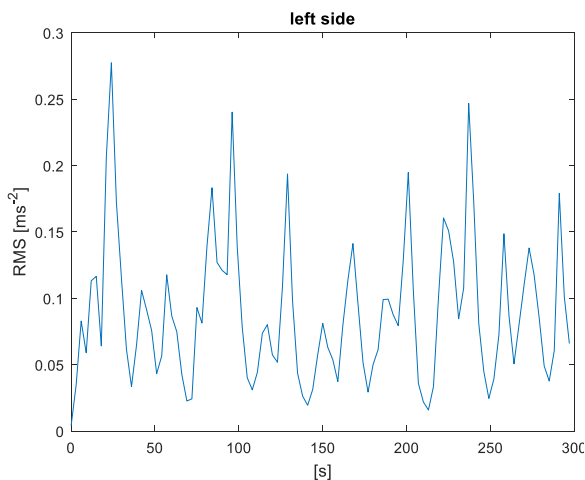


Fig. 235 Moving RMS of acceleration evaluated every 3 s; experimental data - accelerometer 8, test number 3.

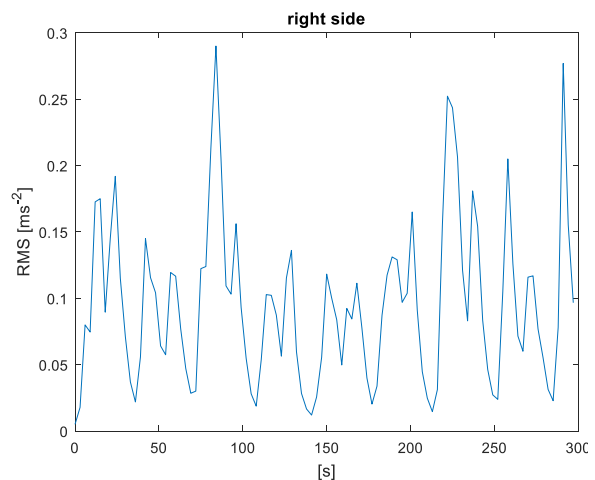


Fig. 236 Moving RMS of acceleration evaluated every 3 s; experimental data - accelerometer 9, test number 3.

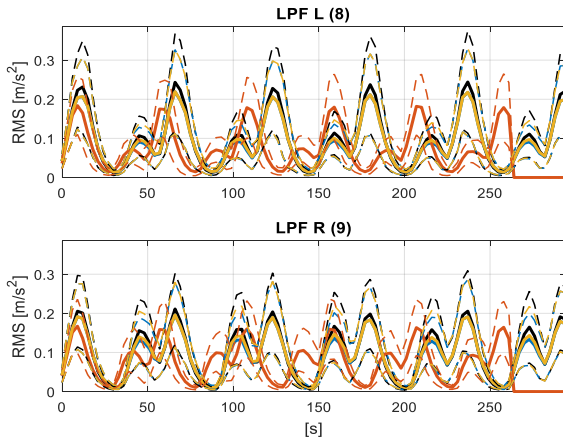


Fig. 237 Moving RMS of acceleration evaluated every 3 s; accelerometer 8 (up) and 9 (down); simulations made with the “heel” database; continuous line: mean value / dashed lines: confidence interval at 95 %; black curve: Model 0, blue curve: Model 1, red curve: Model 2, yellow curve: Model 3; test number 3.

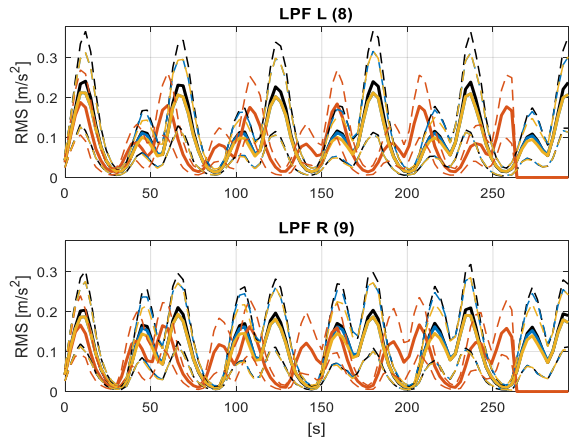


Fig. 238 Moving RMS of acceleration evaluated every 3 s; accelerometer 8 (up) and 9 (down); simulations made with the “tiptoe” database; continuous line: mean value / dashed lines: confidence interval at 95 %; black curve: Model 0, blue curve: Model 1, red curve: Model 2, yellow curve: Model 3; test number 3.

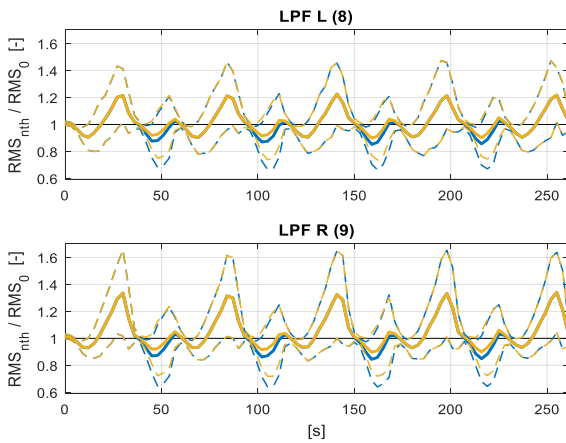


Fig. 239 Moving RMS of acceleration evaluated every 3 s normalized by Model 0; accelerometer 8 (up) and 9 (down); simulations made with the “heel” database; continuous line: mean value / dashed lines: confidence interval at 95 %; black curve: Model 0, blue curve: Model 1, yellow curve: Model 3; test number 3.

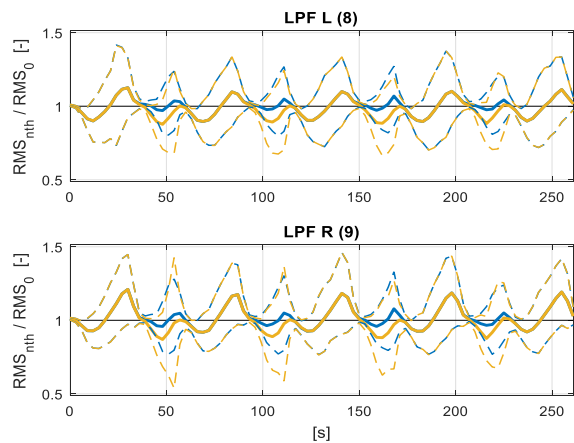


Fig. 240 Moving RMS of acceleration evaluated every 3 s normalized by Model 0; accelerometer 8 (up) and 9 (down); simulations made with the “tiptoe” database; continuous line: mean value / dashed lines: confidence interval at 95 %; black curve: Model 0, blue curve: Model 1, yellow curve: Model 3; test number 3.

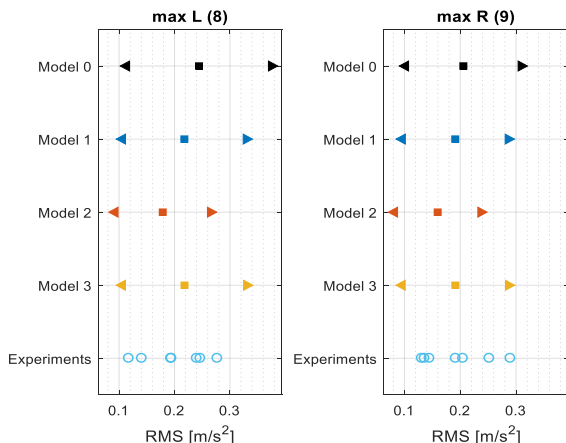


Fig. 241 Maximum Moving RMS values of acceleration evaluated by each Model; maximum of the experimental moving RMS evaluated every 40 s; accelerometer 8 (up) and 9 (down); simulations made with the “heel” database; \square : mean value / $\triangleleft \triangleright$: confidence interval at 95 %; test number 3.

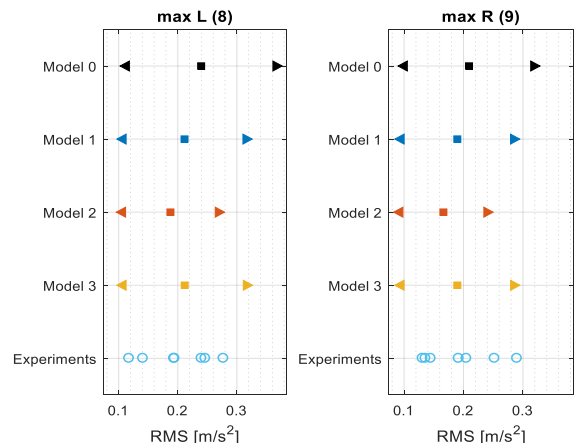


Fig. 242 Maximum Moving RMS values of acceleration evaluated by each Model; maximum of the experimental moving RMS evaluated every 40 s; accelerometer 8 (up) and 9 (down); simulations made with the “heel” database; \square : mean value / $\triangleleft \triangleright$: confidence interval at 95 %; test number 3.

Test number 10: 1 pedestrian (subject 3) goes upstairs

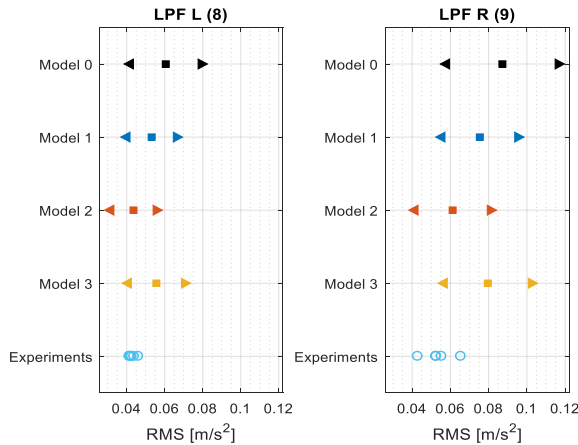


Fig. 243 Global RMS values of the acceleration; accelerometer 8 (left) and 9 (right); simulations made with the “heel” database; \square : mean value / $\triangleleft \triangleright$: confidence interval at 95 %; test number 10.

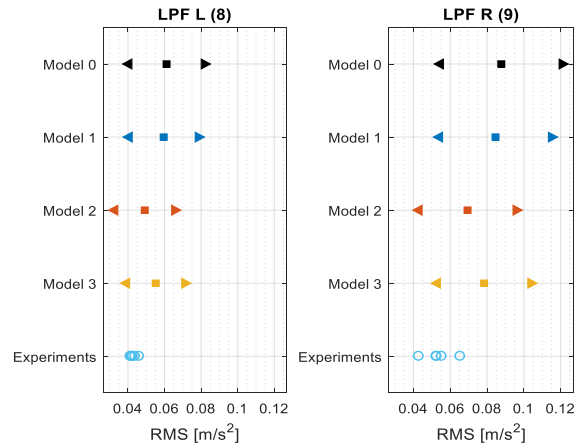


Fig. 244 Global RMS values of the acceleration; accelerometer 8 (left) and 9 (right); simulations made with the “heel” database; \square : mean value / $\triangleleft \triangleright$: confidence interval at 95 %; test number 10.

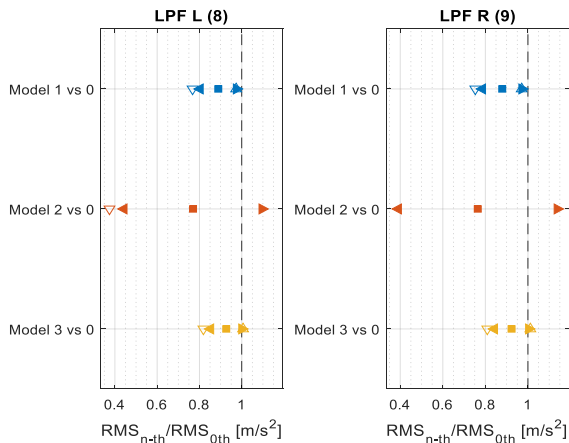


Fig. 245 Global RMS values of acceleration normalized by Model 0; accelerometer 8 (left) and 9 (right); simulations made with the “heel” database; \square : mean value / $\triangleleft \triangleright$: confidence interval at 95 % / \triangle : maximum ratio value / ∇ : minimum ratio value; test number 10.

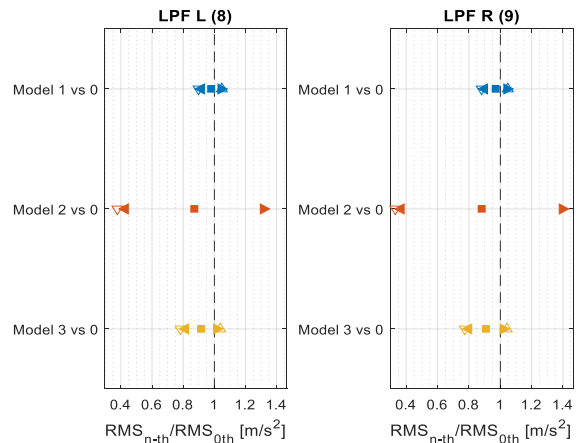


Fig. 246 Global RMS values of acceleration normalized by Model 0; accelerometer 8 (left) and 9 (right); simulations made with the “tiptoe” database; \square : mean value / $\triangleleft \triangleright$: confidence interval at 95 % / \triangle : maximum ratio value / ∇ : minimum ratio value; test number 10.

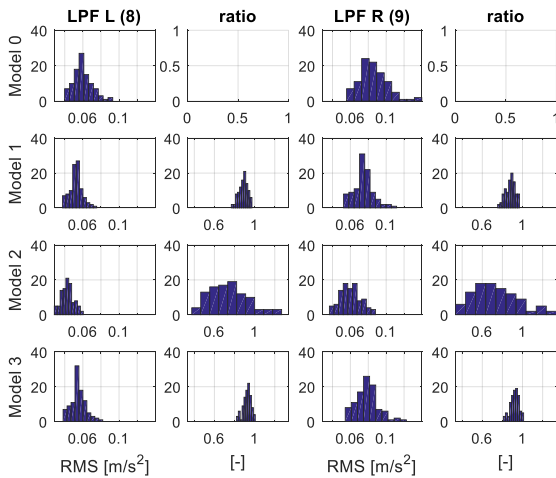


Fig. 247 Histograms of the Global RMS of acceleration and of the normalized by Model 0 ones; accelerometer 8 (left) and 9 (right); simulations made with the “heel” database; test number 10.

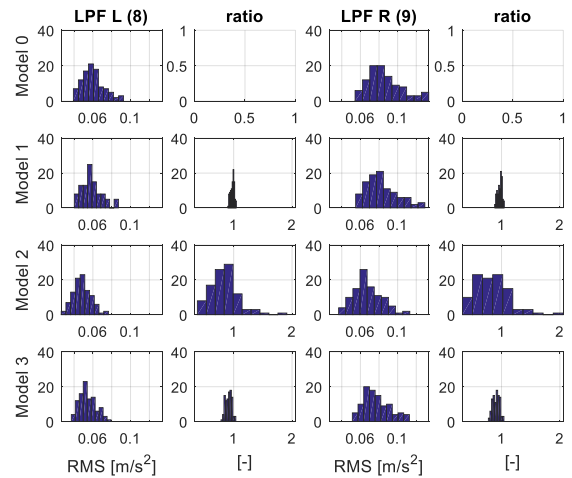


Fig. 248 Histograms of the Global RMS of acceleration and of the normalized by Model 0 ones; accelerometer 8 (left) and 9 (right); simulations made with the “tiptoe” database; test number 10.

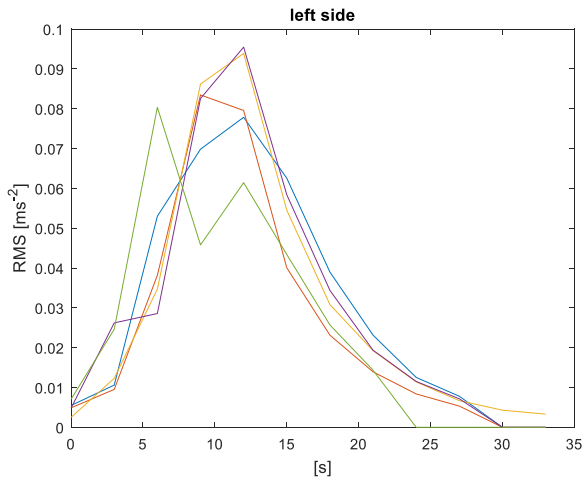


Fig. 249 Moving RMS of acceleration evaluated every 3 s; experimental data - accelerometer 8, test number 10.

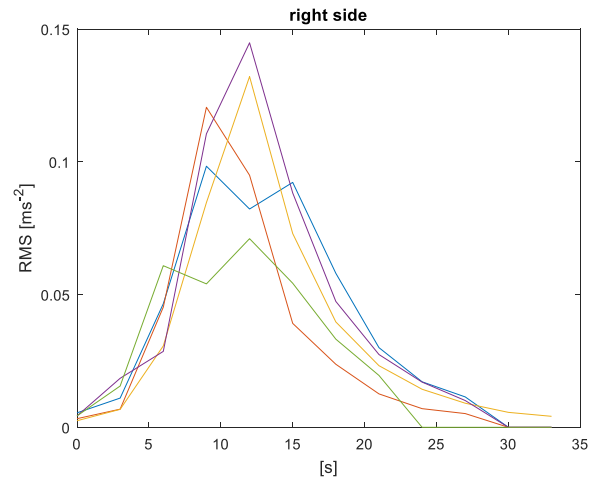


Fig. 250 Moving RMS of acceleration evaluated every 3 s; experimental data - accelerometer 9, test number 10.

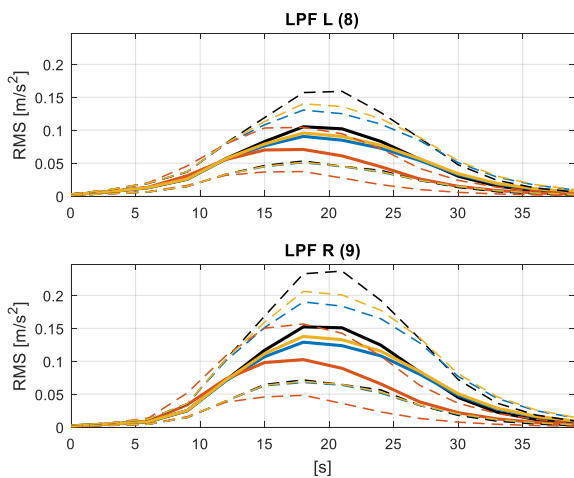


Fig. 251 Moving RMS of acceleration evaluated every 3 s; accelerometer 8 (up) and 9 (down); simulations made with the “heel” database; continuous line: mean value / dashed lines: confidence interval at 95 %; black curve: Model 0, blue curve: Model 1, red curve: Model 2, yellow curve: Model 3; test number 10.

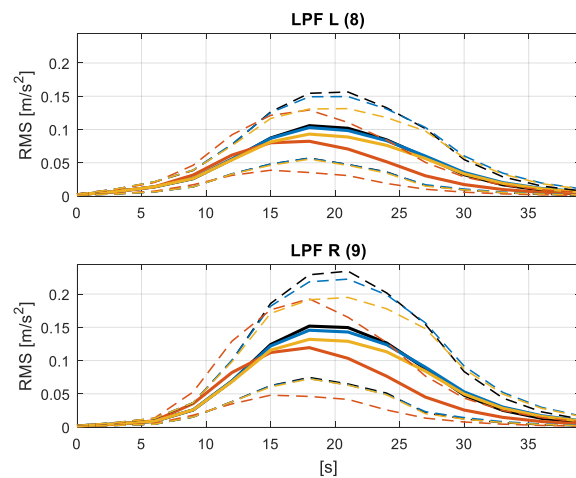


Fig. 252 Moving RMS of acceleration evaluated every 3 s; accelerometer 8 (up) and 9 (down); simulations made with the “tiptoe” database; continuous line: mean value / dashed lines: confidence interval at 95 %; black curve: Model 0, blue curve: Model 1, red curve: Model 2, yellow curve: Model 3; test number 10.

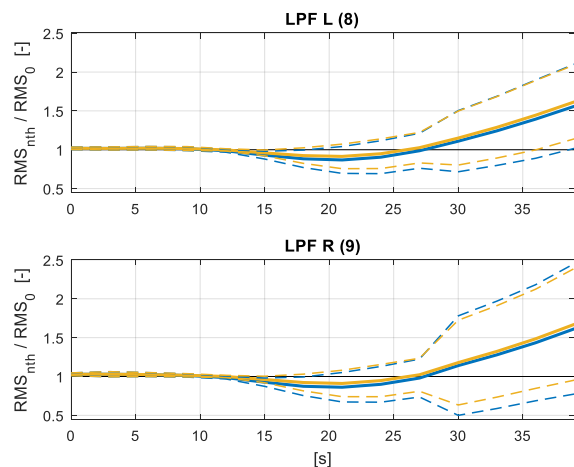


Fig. 253 Moving RMS of acceleration evaluated every 3 s normalized by Model 0; accelerometer 8 (up) and 9 (down); simulations made with the “heel” database; continuous line: mean value / dashed lines: confidence interval at 95 %; black curve: Model 0, blue curve: Model 1, yellow curve: Model 3; test number 10.

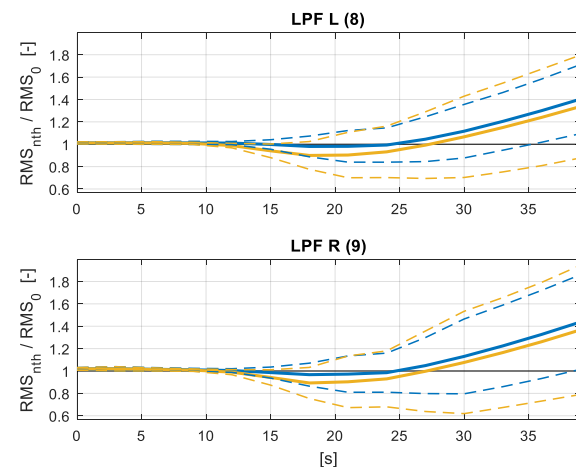


Fig. 254 Moving RMS of acceleration evaluated every 3 s normalized by Model 0; accelerometer 8 (up) and 9 (down); simulations made with the “tiptoe” database; continuous line: mean value / dashed lines: confidence interval at 95 %; black curve: Model 0, blue curve: Model 1, yellow curve: Model 3; test number 10.

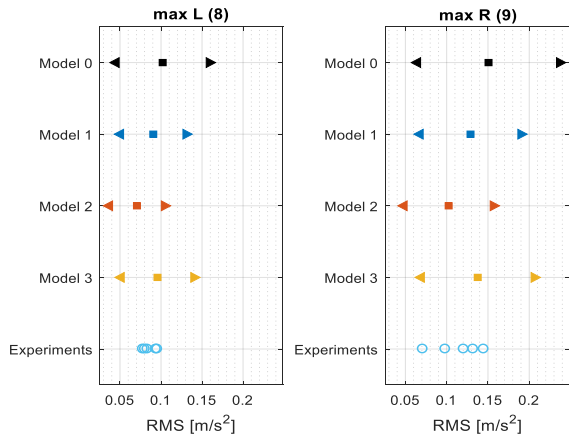


Fig. 255 Maximum Moving RMS values of acceleration evaluated by each Model; maximum of the experimental moving RMS; accelerometer 8 (up) and 9 (down); simulations made with the “heel” database; \square : mean value $\triangleleft\triangleright$: confidence interval at 95 %; test number 10.

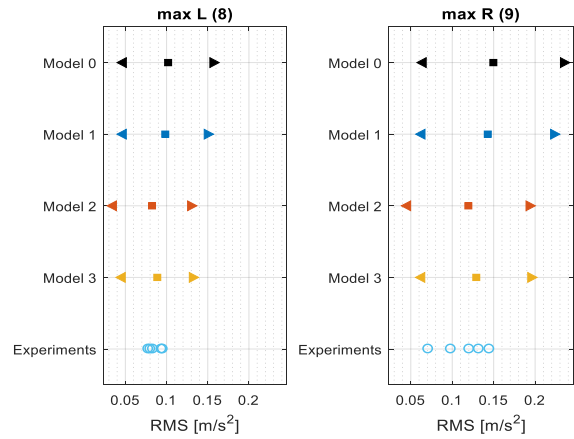


Fig. 256 Maximum Moving RMS values of acceleration evaluated by each Model; maximum of the experimental moving RMS; accelerometer 8 (up) and 9 (down); simulations made with the “heel” database; \square : mean value $\triangleleft\triangleright$: confidence interval at 95 %; test number 10.

Test number 11: 1 pedestrian (subject 3) goes downstairs

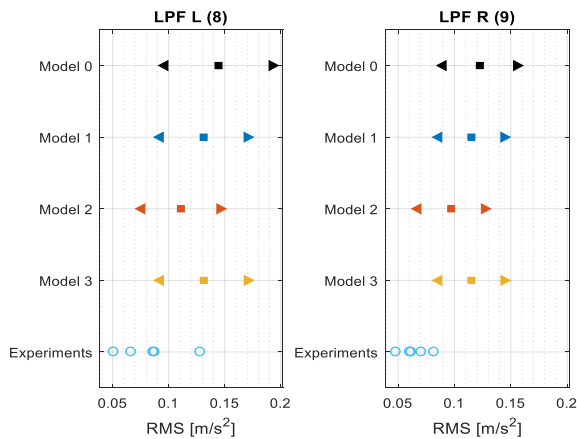


Fig. 257 Global RMS values of the acceleration; accelerometer 8 (left) and 9 (right); simulations made with the “heel” database; \square : mean value $\triangleleft\triangleright$: confidence interval at 95 %; test number 11.

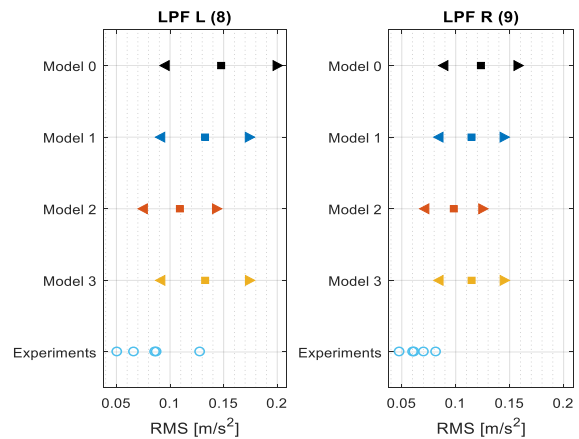


Fig. 258 Global RMS values of the acceleration; accelerometer 8 (left) and 9 (right); simulations made with the “tiptoe” database; \square : mean value $\triangleleft\triangleright$: confidence interval at 95 %; test number 11.

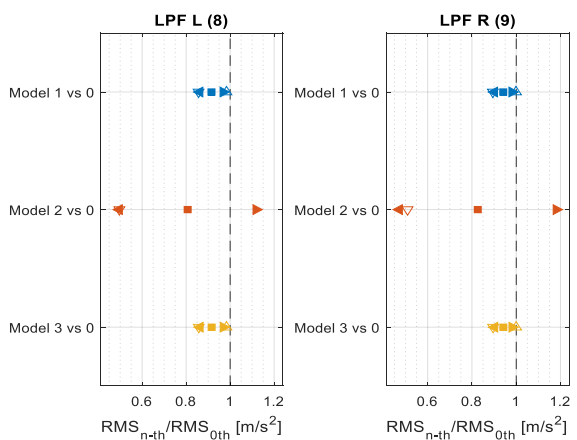


Fig. 259 Global RMS values of acceleration normalized by Model 0; accelerometer 8 (left) and 9 (right); simulations made with the “heel” database; \square : mean value $\triangleleft\triangleright$: confidence interval at 95 % \triangle : maximum ratio value ∇ : minimum ratio value; test number 11.

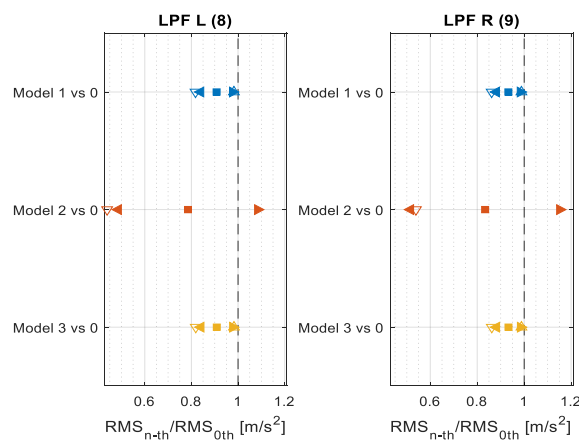


Fig. 260 Global RMS values of acceleration normalized by Model 0; accelerometer 8 (left) and 9 (right); simulations made with the “tiptoe” database; \square : mean value $\triangleleft\triangleright$: confidence interval at 95 % \triangle : maximum ratio value ∇ : minimum ratio value; test number 11.

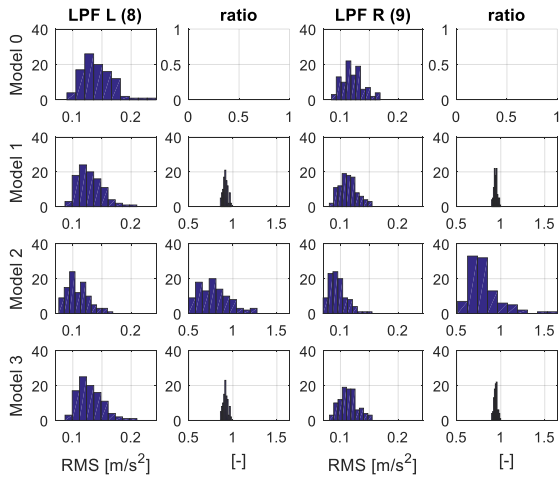


Fig. 261 Histograms of the Global RMS of acceleration and of the normalized by Model 0 ones; accelerometer 8 (left) and 9 (right); simulations made with the “heel” database; test number 11.

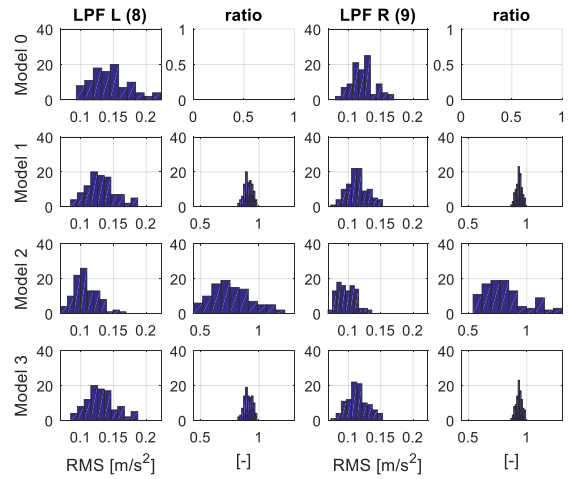


Fig. 262 Histograms of the Global RMS of acceleration and of the normalized by Model 0 ones; accelerometer 8 (left) and 9 (right); simulations made with the “tiptoe” database; test number 11.

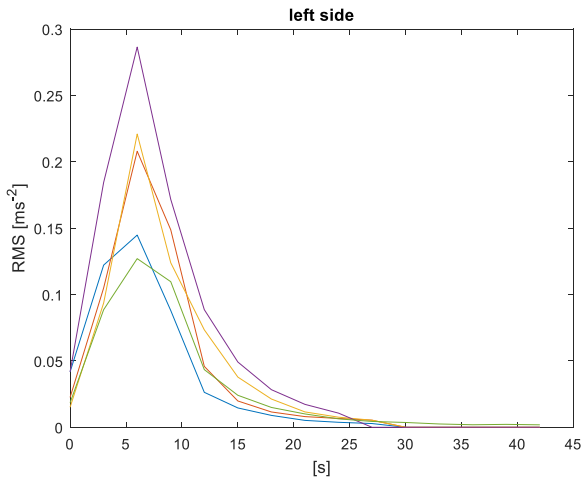


Fig. 263 Moving RMS of acceleration evaluated every 3 s; experimental data - accelerometer 8, test number 11.

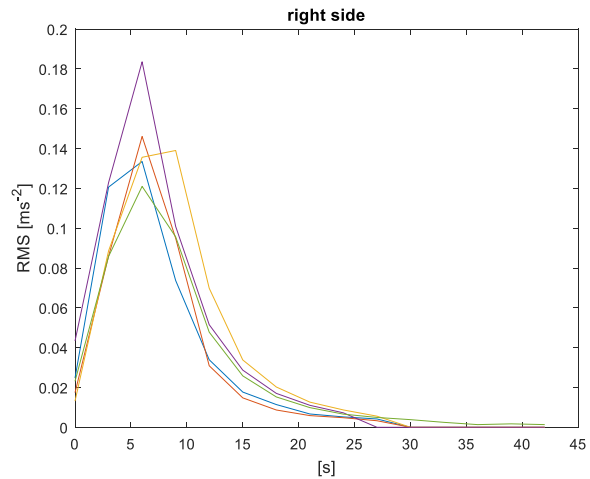


Fig. 264 Moving RMS of acceleration evaluated every 3 s; experimental data - accelerometer 9, test number 11.

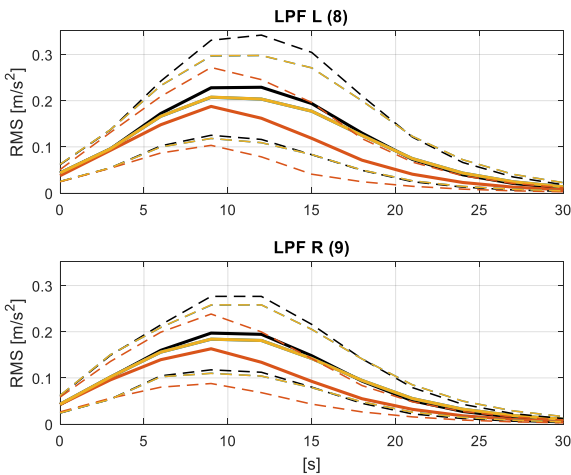


Fig. 265 Moving RMS of acceleration evaluated every 3 s; accelerometer 8 (up) and 9 (down); simulations made with the “heel” database; continuous line: mean value / dashed lines: confidence interval at 95 %; black curve: Model 0, blue curve: Model 1, red curve: Model 2, yellow curve: Model 3; test number 11.

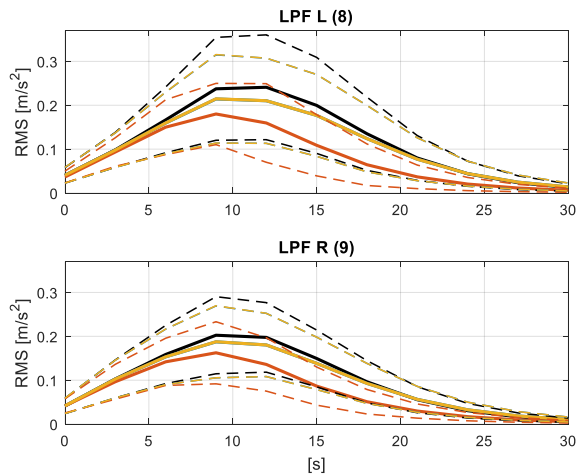


Fig. 266 Moving RMS of acceleration evaluated every 3 s; accelerometer 8 (up) and 9 (down); simulations made with the “tiptoe” database; continuous line: mean value / dashed lines: confidence interval at 95 %; black curve: Model 0, blue curve: Model 1, red curve: Model 2, yellow curve: Model 3; test number 11.

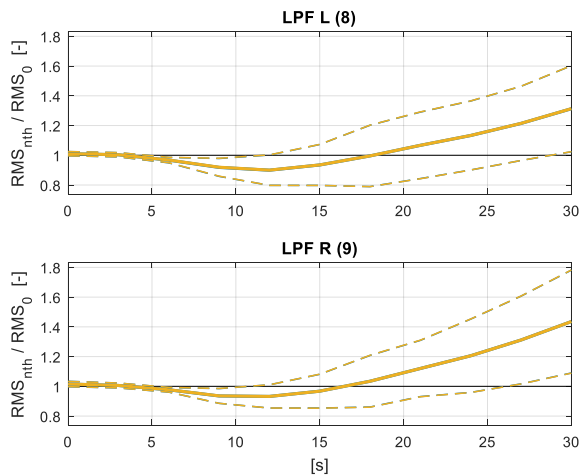


Fig. 267 Moving RMS of acceleration evaluated every 3 s normalized by Model 0; accelerometer 8 (up) and 9 (down); simulations made with the “heel” database; continuous line: mean value / dashed lines: confidence interval at 95 %; black curve: Model 0, blue curve: Model 1, yellow curve: Model 3; test number 11.

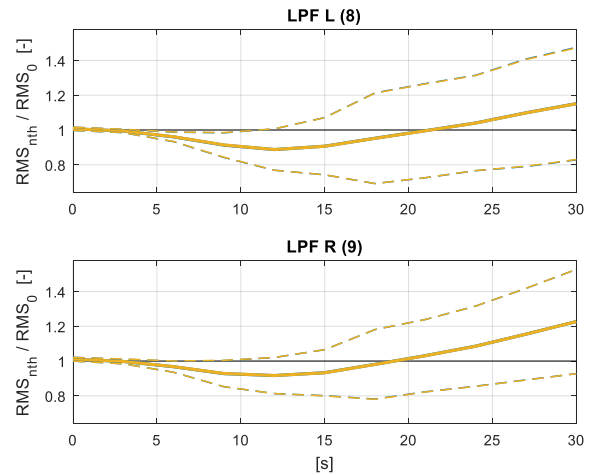


Fig. 268 Moving RMS of acceleration evaluated every 3 s normalized by Model 0; accelerometer 8 (up) and 9 (down); simulations made with the “tiptoe” database; continuous line: mean value / dashed lines: confidence interval at 95 %; black curve: Model 0, blue curve: Model 1, yellow curve: Model 3; test number 11.

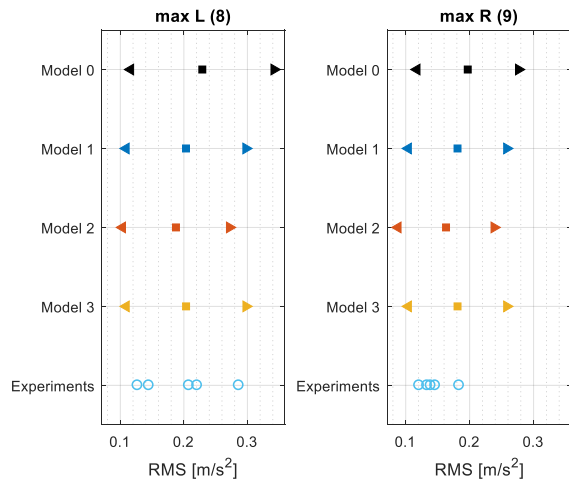


Fig. 269 Maximum Moving RMS values of acceleration evaluated by each Model; maximum of the experimental moving RMS; accelerometer 8 (up) and 9 (down); simulations made with the “heel” database; \square : mean value / $\langle \rangle$: confidence interval at 95 %; test number 11.

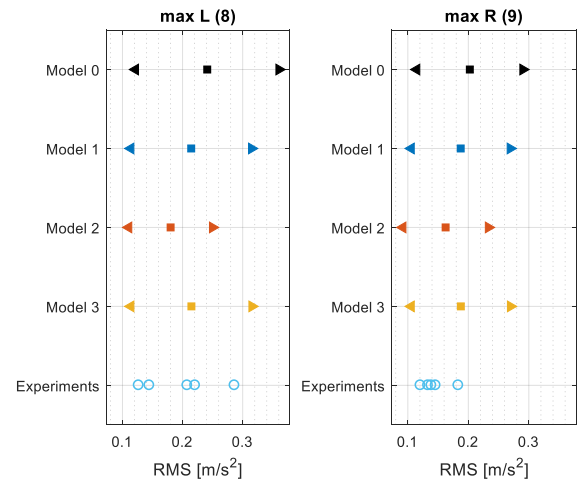


Fig. 270 Maximum Moving RMS values of acceleration evaluated by each Model; maximum of the experimental moving RMS; accelerometer 8 (up) and 9 (down); simulations made with the “heel” database; \square : mean value / $\langle \rangle$: confidence interval at 95 %; test number 11.

5.4 Summary Tables (Mode Filtered Results)

As was explained, the numerical results were Low Pass Filtered (LPF) and also Band Pass Filtered (BPF) around the two modes of the structure (i.e. $f_1 = 7.81$ Hz and $f_2 = 8.87$ Hz). Refer to Section 4.1.5 for details on the used filters. The filtering around the two modes was done in order to analyse the contribution of each mode of the structure to the global response in every tested pedestrian scenario. The results will not be reported extensively, as done for the ones of the Low Pass Filtered case, but summary tables, as the ones introduced at the beginning of the LPF case, are reported. Only the ones obtained with the heel database, as was done for the LPF tables, are shown. The tables are reported per pair of modes, with at first the one for the BPF around the first mode and then the one BPF around the second mode.

RMS [m/s ²]	1 person goes downstairs on the left side				1 person goes upstairs on the right side			
	Left side		Right side		Left side		Right side	
	μ	$\pm 2\sigma$	μ	$\pm 2\sigma$	μ	$\pm 2\sigma$	μ	$\pm 2\sigma$
model 0	0.086	0.036	0.129	0.055	0.085	0.039	0.130	0.060
model 1	0.082	0.034	0.122	0.051	0.073	0.033	0.112	0.051
model 2	0.086	0.035	0.127	0.054	0.064	0.033	0.099	0.051
model 3	0.082	0.033	0.122	0.051	0.074	0.033	0.114	0.052

Table 11 Estimations of the vibration levels by means of Global RMS acceleration values obtained with the four Models, BPF around the first mode, expressed in terms of mean value and confidence interval at 95 % with respect to the mean value. Left column: test number 11 of Table 5, right column: test number 10 of Table 5. Acceleration values read in correspondence of accelerometer 9, heel tests.

RMS [m/s ²]	1 person goes downstairs on the left side				1 person goes upstairs on the right side			
	Left side		Right side		Left side		Right side	
	μ	$\pm 2\sigma$	μ	$\pm 2\sigma$	μ	$\pm 2\sigma$	μ	$\pm 2\sigma$
model 0	0.135	0.068	0.083	0.040	0.042	0.016	0.031	0.009
model 1	0.118	0.057	0.074	0.034	0.041	0.016	0.030	0.009
model 2	0.117	0.066	0.074	0.039	0.040	0.020	0.029	0.011
model 3	0.118	0.057	0.073	0.034	0.041	0.016	0.030	0.009

Table 12 Estimations of the vibration levels by means of Global RMS acceleration values obtained with the four Models, BPF around the second mode, expressed in terms of mean value and confidence interval at 95 % with respect to the mean value. Left column: test number 11 of Table 5, right column: test number 10 of Table 5. Acceleration values read in correspondence of accelerometer 9, heel tests.

It is interesting to notice that, for the case of a pedestrian who goes downstairs (i.e. on the left side of the structure) (left macro columns of Table 11 and Table 12), the first mode (Table 11) produces higher global RMS values for the right side of the staircase. While an expected higher left side response is produced by the second mode (Table 12). Can be said that the contributions of the two modes are mirrored one to the other.

As for the ascending crossing (on the right side of the structure) (right macro columns of Table 11 and Table 12), only the second modes (Table 12) has the non-crossed side of the structure (the left one) with an higher response with respect to the crossed side. Instead, mode 1 (Table 11) has the crossed side with a higher response, in terms of global RMSs. Therefore, fore the ascending crossing, the first mode appears to have the higher contribution.

RMS [m/s ²]			Left side		Right side	
			μ	$\pm 2\sigma$	μ	$\pm 2\sigma$
5 min	1 person	model 0	0.095	0.022	0.143	0.033
		model 1	0.089	0.020	0.133	0.031
		model 2	0.087	0.019	0.131	0.029
		model 3	0.089	0.021	0.135	0.031
	3 persons	model 0	0.141	0.025	0.211	0.038
		model 1	0.135	0.023	0.201	0.035
		model 2	0.130	0.021	0.195	0.033
		model 3	0.137	0.023	0.205	0.035
	5 persons	model 0	0.156	0.013	0.232	0.020
		model 1	0.154	0.014	0.228	0.021
		model 2	0.150	0.014	0.224	0.022
		model 3	0.158	0.014	0.234	0.022

Table 13 Estimations of the vibration levels by means of Global RMS acceleration values obtained with the four Models, BPF around the first mode, expressed in terms of mean value and confidence interval at 95 % with respect to the mean value. The tests per rows are: third test of Table 5 in the first set of rows, second test of Table 5 in the second set of rows and first test of Table 5 in the third set of rows. Acceleration values read in correspondence of accelerometer 9, heel tests.

RMS [m/s ²]			Left side		Right side	
			μ	$\pm 2\sigma$	μ	$\pm 2\sigma$
5 min	1 person	model 0	0.108	0.034	0.068	0.020
		model 1	0.099	0.029	0.063	0.018
		model 2	0.107	0.031	0.068	0.019
		model 3	0.098	0.029	0.063	0.018
	3 persons	model 0	0.166	0.034	0.105	0.021
		model 1	0.155	0.032	0.100	0.020
		model 2	0.168	0.030	0.107	0.018
		model 3	0.156	0.032	0.100	0.020
	5 persons	model 0	0.192	0.022	0.123	0.012
		model 1	0.187	0.020	0.120	0.011
		model 2	0.201	0.021	0.129	0.013
		model 3	0.188	0.020	0.121	0.011

Table 14 Estimations of the vibration levels by means of Global RMS acceleration values obtained with the four Models, BPF around the second mode, expressed in terms of mean value and confidence interval at 95 % with respect to the mean value. The tests per rows are: third test of Table 5 in the first set of rows, second test of Table 5 in the second set of rows and first test of Table 5 in the third set of rows. Acceleration values read in correspondence of accelerometer 9, heel tests.

As for the loop BPF testes (tests number 1, 2 and 3), their values (in terms of global RMSs) are reported in Table 13 for the first mode and in Table 14 for the second mode. All the types of tests agree with the fact that in loop walking conditions, the second mode is more responsible for the response of the left side of the structure, while the first mode is the one more responsible for the response of the right side of the structure.

RMS n-th / RMS 0		fast test (one stroke)		long test (5 min)	
		μ	$\pm 2\sigma$	μ	$\pm 2\sigma$
1 person	model 1 / model 0	93.5%	32.0%	96.4%	21.1%
	model 3 / model 0	94.3%	30.3%	96.9%	20.4%
5 persons	model 1 / model 0	90.1%	33.6%	99.3%	17.4%
	model 3 / model 0	91.1%	33.5%	100.6%	18.2%

Table 15 Estimations of the vibration levels by means of Global RMS acceleration values obtained with the four Models, BPF around the first mode, expressed in terms of mean value and confidence interval at 95 % with respect to the mean value. The tests per rows are: third test of Table 5 in the first set of rows, second test of Table 5 in the second set of rows and first test of Table 5 in the third set of rows. Acceleration values read in correspondence of accelerometer 9, heel tests.

RMS n-th / RMS 0		fast test (one stroke)		long test (5 min)	
		μ	$\pm 2\sigma$	μ	$\pm 2\sigma$
1 person	model 1 / model 0	97.6%	18.0%	96.1%	18.0%
	model 3 / model 0	97.9%	17.6%	96.0%	18.2%
5 persons	model 1 / model 0	90.9%	29.8%	98.9%	15.4%
	model 3 / model 0	90.9%	30.0%	99.0%	15.5%

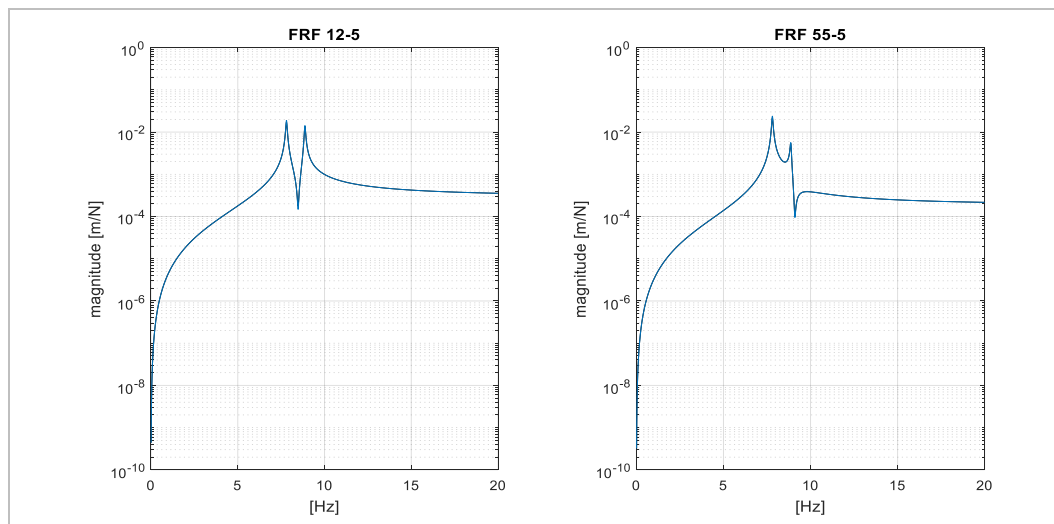
Table 16 Estimations of the vibration levels by means of Global RMS acceleration values obtained with the four Models, BPF around the second mode, expressed in terms of mean value and confidence interval at 95 % with respect to the mean value. The tests per rows are: third test of Table 5 in the first set of rows, second test of Table 5 in the second set of rows and first test of Table 5 in the third set of rows. Acceleration values read in correspondence of accelerometer 9, heel tests.

For what concern the most limit tested cases (i.e. low/high number of pedestrians vs short/long times), the Model 0 normalized global RMS values of acceleration appear to have the same trend in both the modes. That means that the differences among the Models are practically the same between the modes.

5.5 Frequency Response Functions (FRFs)

In this Section, an additional frequency analysis, with respect to the one performed for the identification of the modal parameters of the structure (Section 3.3), is reported. Indeed, in order to better analyse the different ways in which every Model treats the occupied structure (i.e. the one obtained by the empty structure plus the application of the passive contributions of the pedestrians), some FRFs of such structure were evaluated. The observation points are always kept in correspondence of the nodes 12 and 55 of the discretized structure (Fig. 70), in terms of displacements. While, as excitation points, are taken a point per side co-located (i.e. nodes 12 and 55 of Fig. 70) and two point per side far from them (i.e. non-co-located: nodes 29-38 and 5-62 of Fig. 70). Such points were selected since at the nodes 12 and 55 the modal components of the structure have their higher values, and so, are the points in which the pedestrian effects are higher. Therefore, both points in the higher modal components of the structure (i.e. nodes 12 and 55) and points where the modal components are lower (i.e. nodes 5-62 and 29-38) were taken. The simulated case is the one of a pedestrian who walk on the staircase. Therefore, the apparent mass involved is the one of a one pedestrian only. It is noticed that Model 0 is the only one that considers such passive contribution always spread over the structure, while the other Models consider it as applied at the position of the pedestrian (i.e. the excitation points here). For simplicity, Model 1 (blue line) is taken as reference to represent the moving passive contribution approaches (also because of Model 2 and 3 are based on Model 1) against Model 0 (black line) in a series of FRF comparisons.

At first, the FRFs for the left side excitations (nodes 5, 12, 29) are reported, followed by the ones for the right side excitations (nodes 38, 55, 62), keeping always the nodes 12 and 55 as the observation points (12 on the left side and 55 on right side of the plots). Zooms of the resonant peaks follow the original plots.



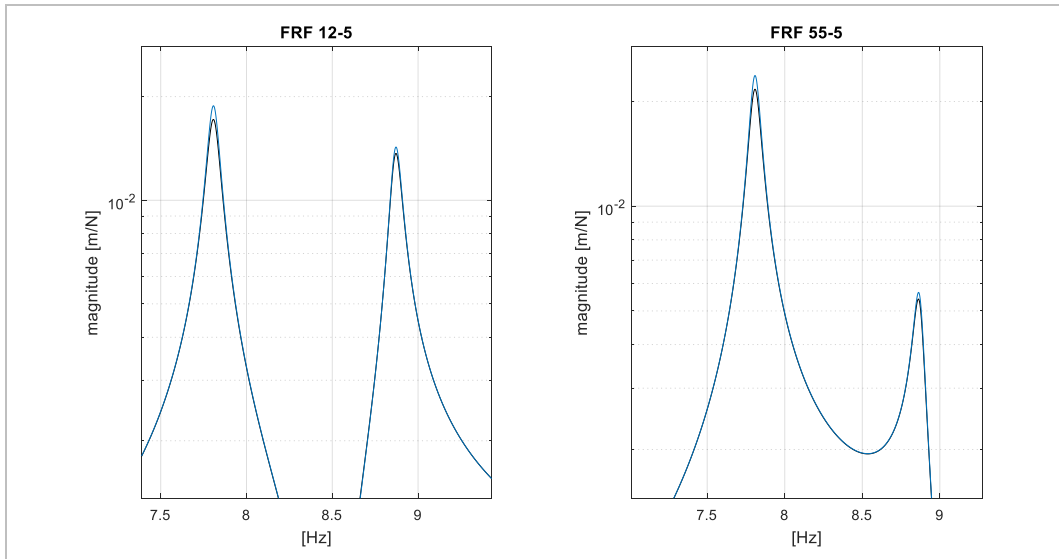


Fig. 271: FRFs with the pedestrian at node 5. Observation points: node 12 (left), node 55 (right).

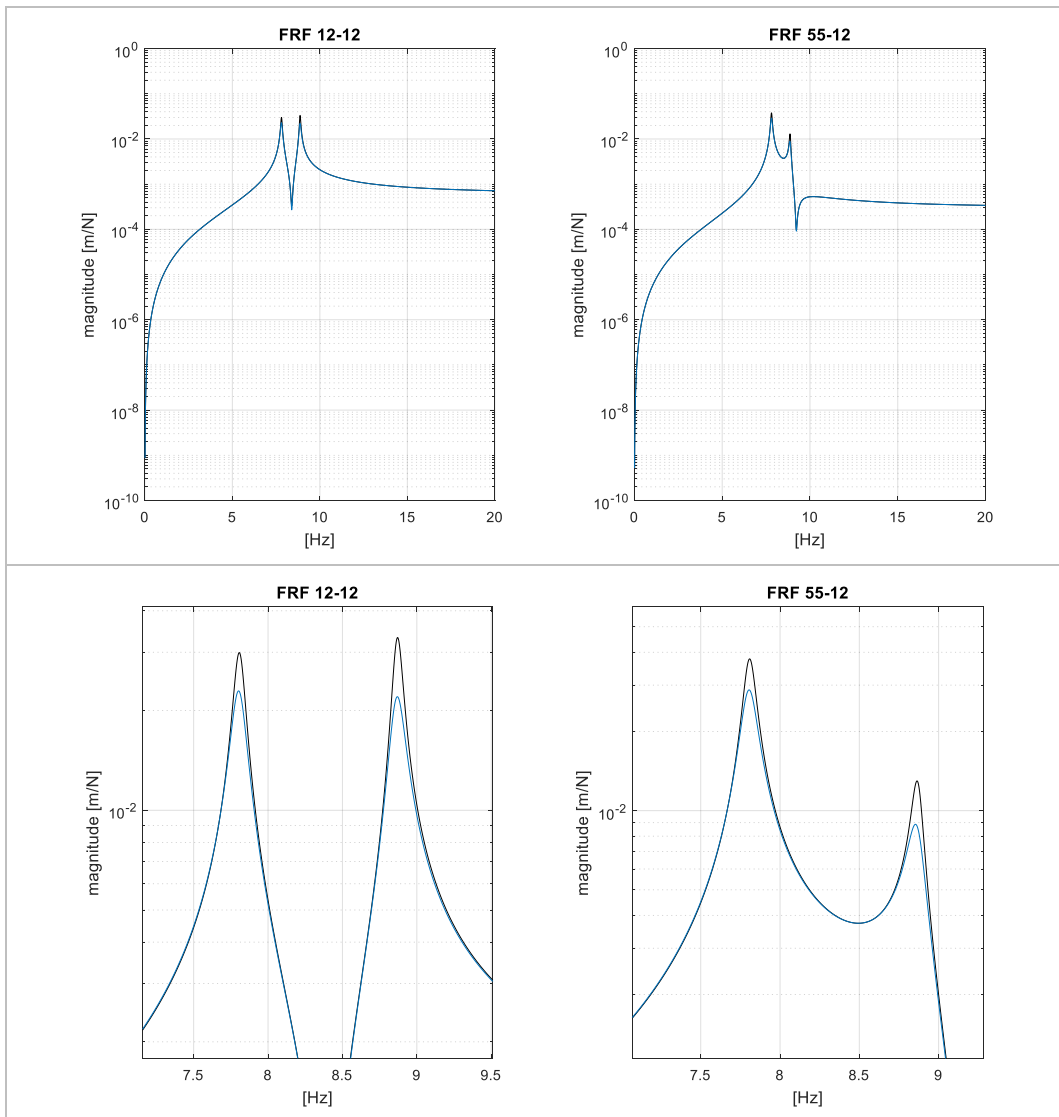


Fig. 272: FRFs with the pedestrian at node 12. Observation points: node 12 (left), node 55 (right).

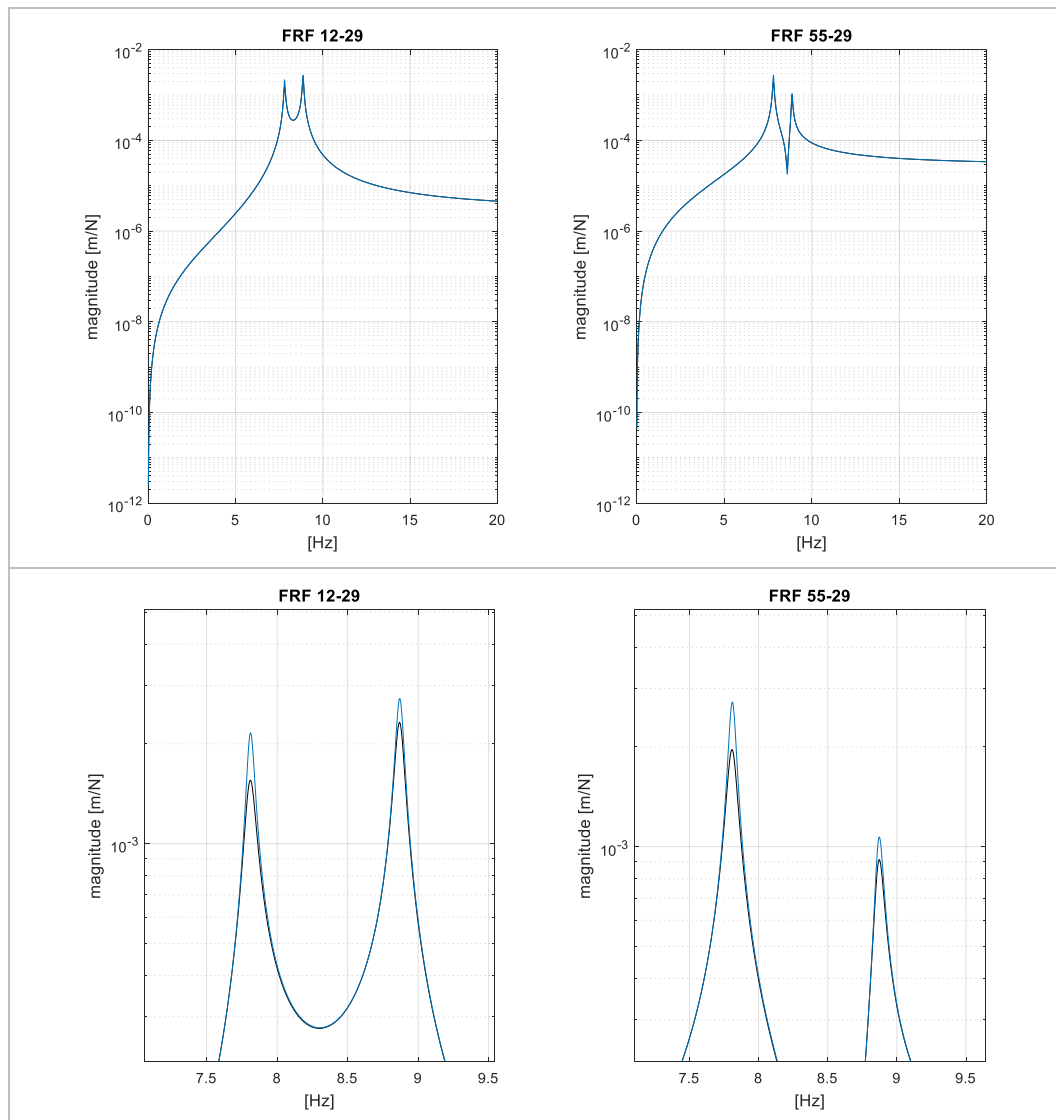
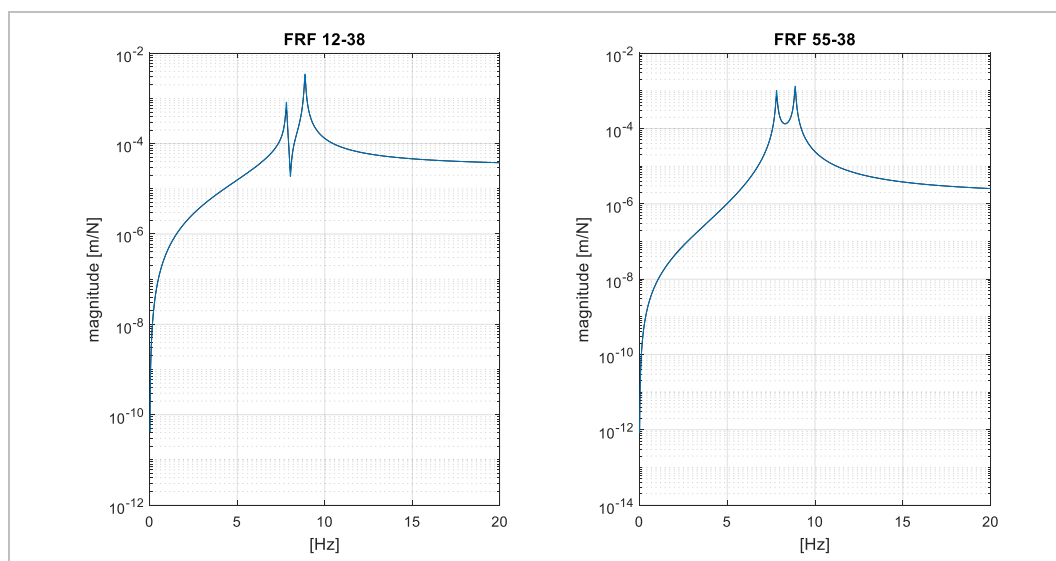


Fig. 273: FRFs with the pedestrian at node 29. Observation points: node 12 (left), node 55 (right).

While the FRFs for the pedestrian at the positions 38, 55 and 62 are:



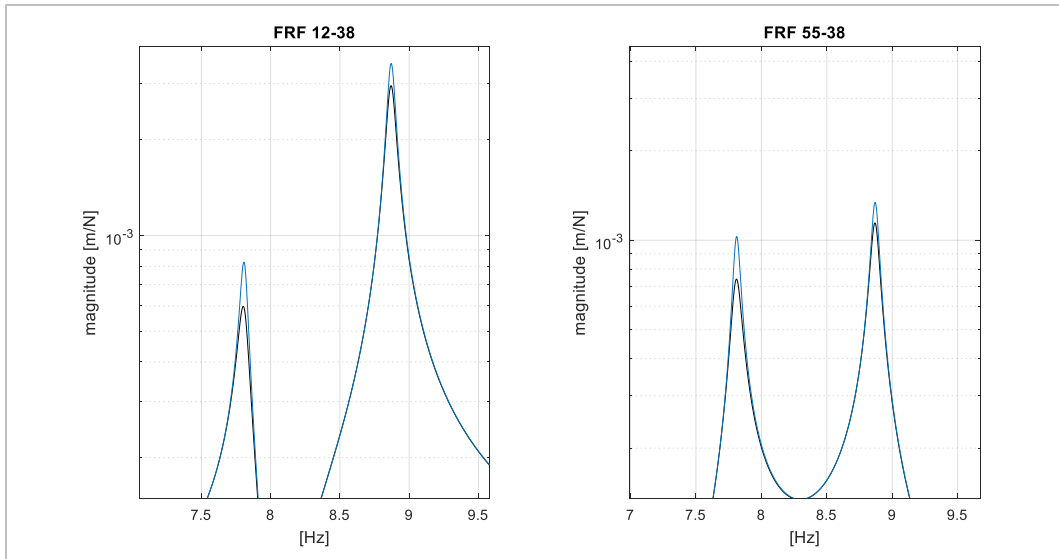


Fig. 274: FRFs with the pedestrian at node 38. Observation points: node 12 (left), node 55 (right).

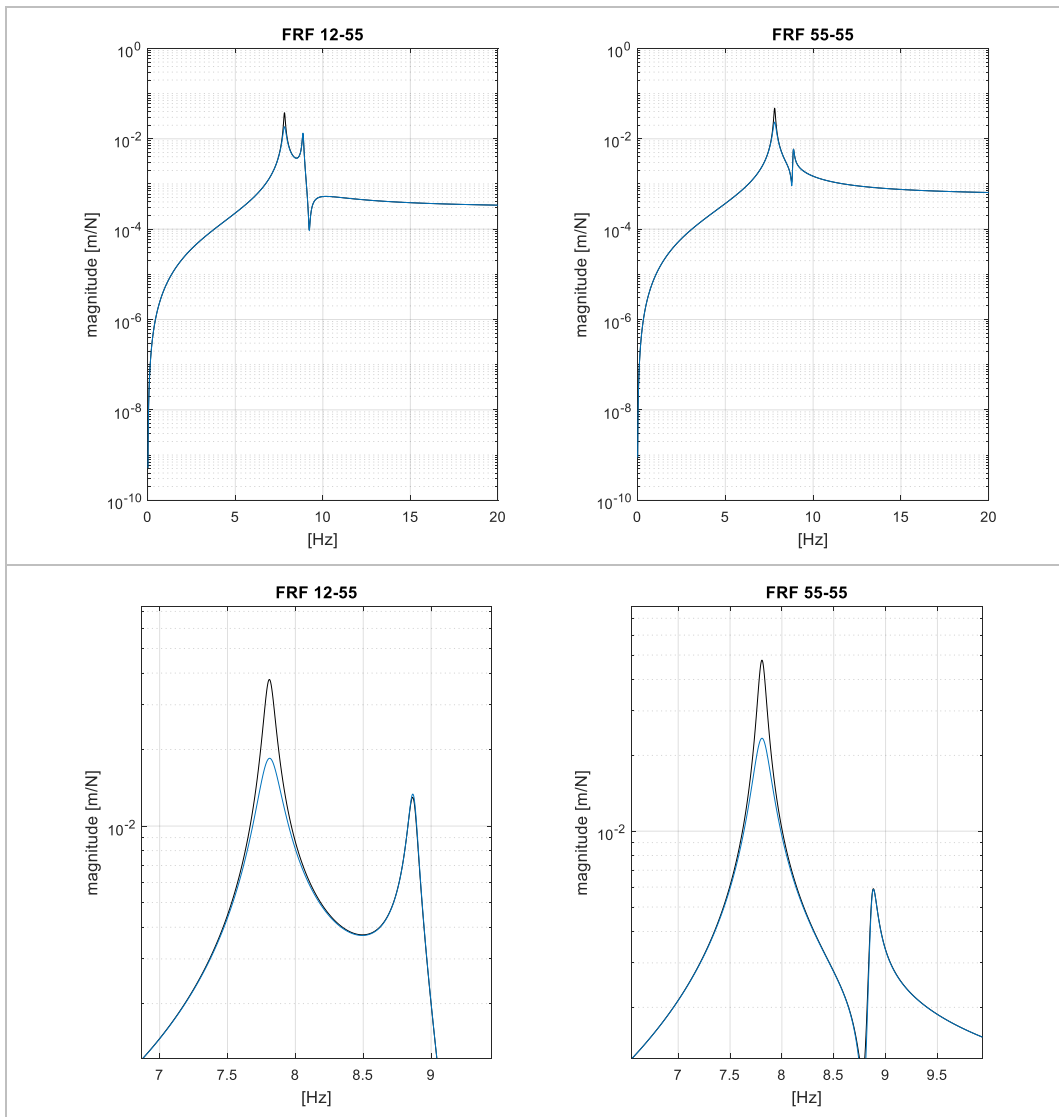


Fig. 275: FRFs with the pedestrian at node 55. Observation points: node 12 (left), node 55 (right).

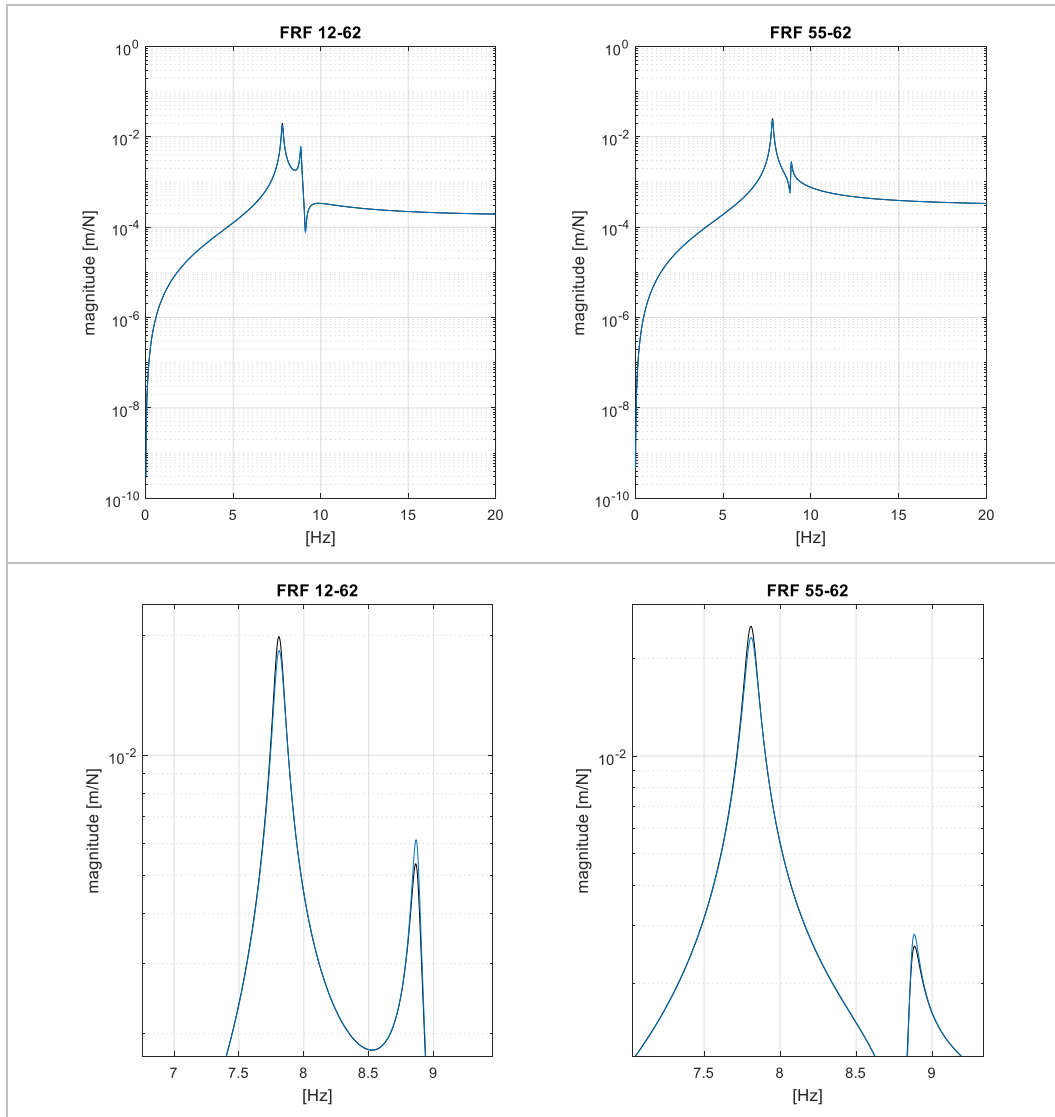
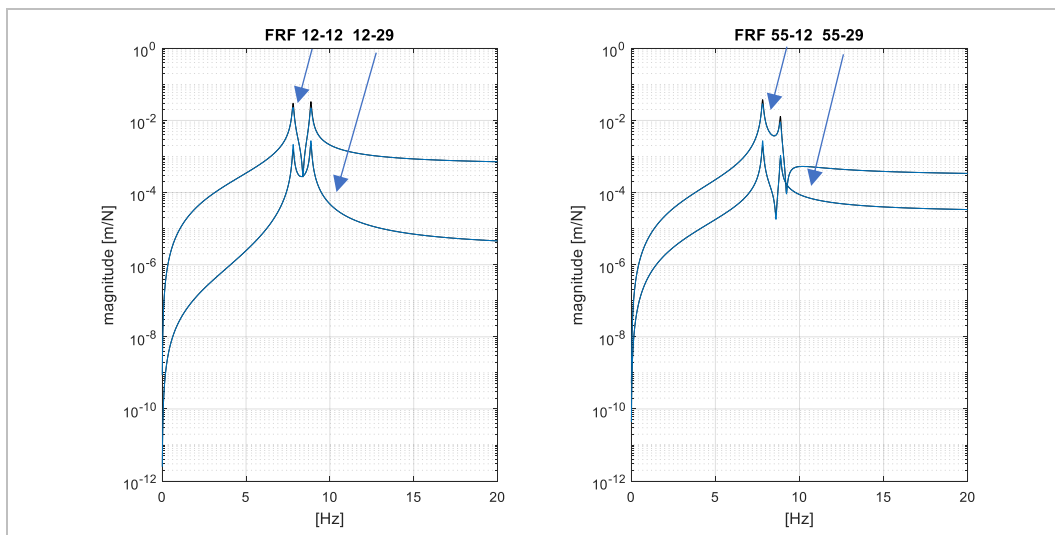


Fig. 276: FRFs with the pedestrian at node 62. Observation points: node 12 (left), node 55 (right).

In order to present a synthesis of the just showed FRFs, a comparison between the co-located FRFs (maximum pedestrian effect) and the FRFs with the farther from co-located exciting points (i.e. nodes 29 and 38) (minimum pedestrian effect) are below reported.



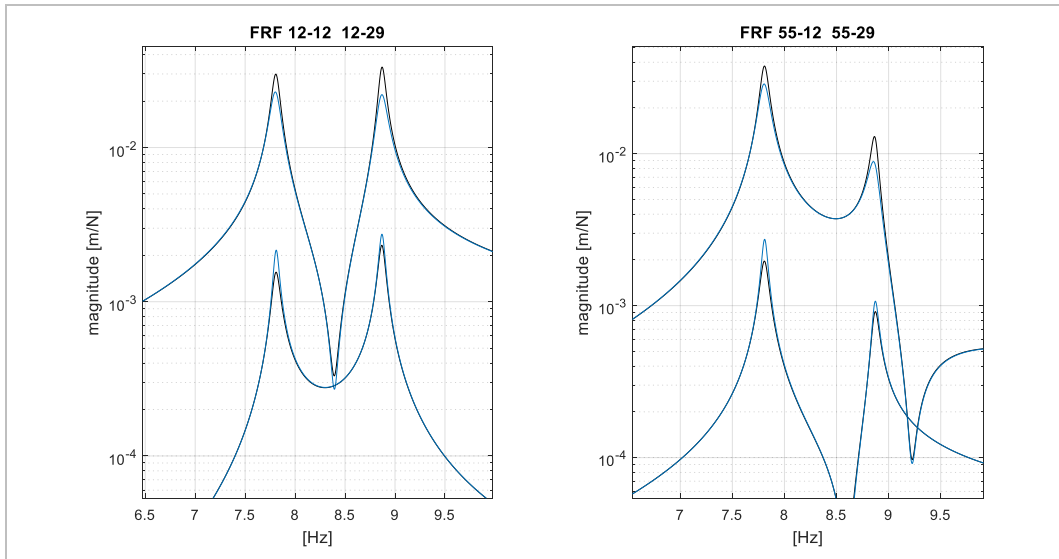


Fig. 277: Comparison between FRFs with the pedestrian at node 12 and node 29. Observation points: node 12 (left), node 55 (right).

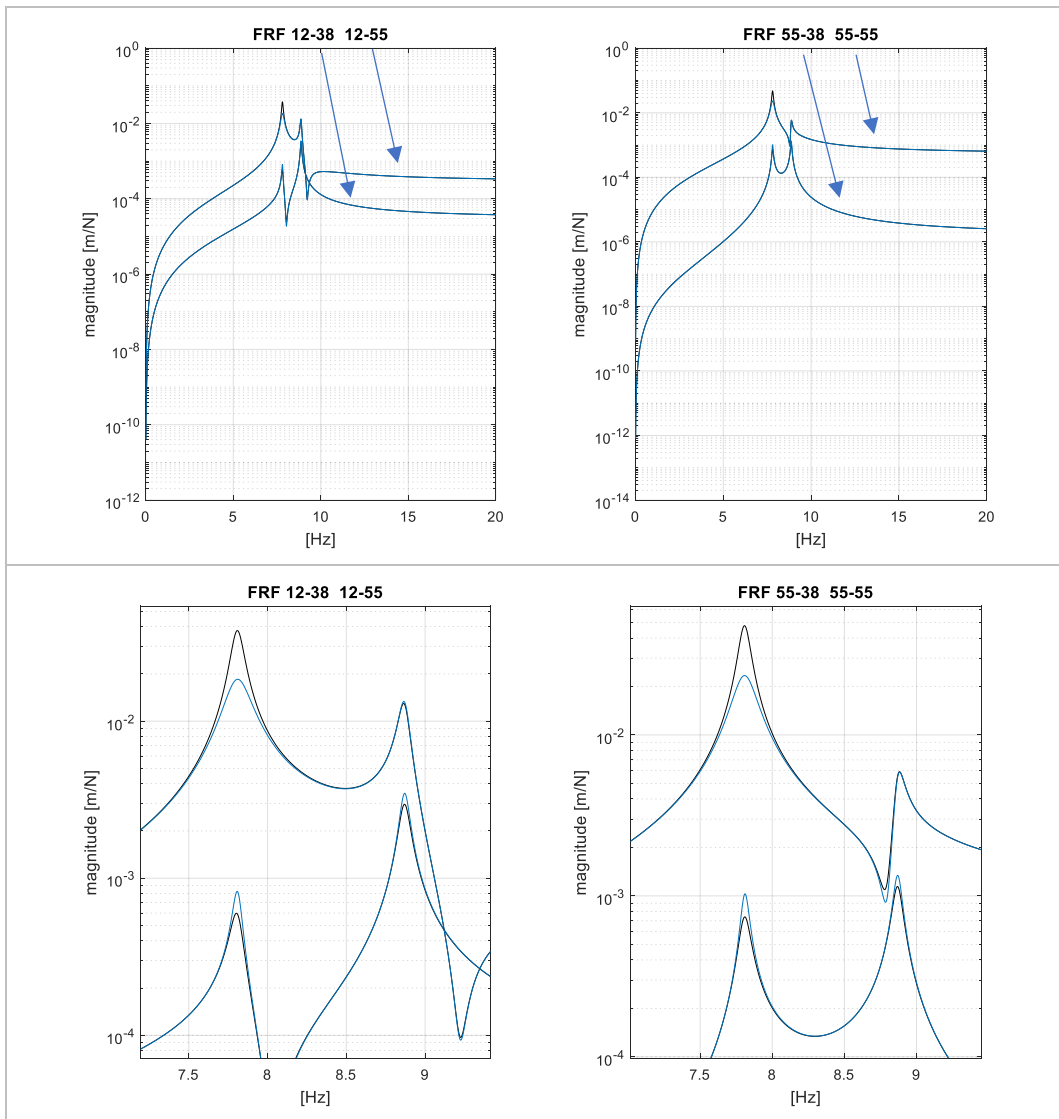


Fig. 278. Comparison between FRFs with the pedestrian at node 38 and node 55. Observation points: node 12 (left), node 55 (right).

With the left plot of Fig. 277 and the right one of Fig. 278, a comparison between the cases in which the pedestrian is placed in a position characterized by high modal components (once node 12 and once node 55) and the case in which he/she is in an area with lower modal components of the structure, the lower part of the staircase (nodes 29 and 38), is presented. From these figures, the inversion of the highest peaks can be observed between the Models. Indeed, while Model 0 spread the damping effect, due to the passive pedestrian contribution, over the structure, Model 1 keeps it concentrated at the node in which the pedestrian is applied. It is noted that both the Models locally apply the active pedestrian effect (i.e. the active force), hence in both the Models the structure is excited in the same way, independently from the effectiveness of the excitation (i.e. modal component magnitudes at the pedestrian point). As a consequence, the resonant peaks of Model 1 are lower than the ones of Model 0, if the pedestrian is placed in the points with the highest modal components (nodes 12 and 55), since all the damping effect of the passive pedestrian component is applied in the most effective positions. While Model 0 applies only the corresponding part of spread passive component on the most effective positions.

Conversely, higher resonant peaks are present for Model 1 with respect to Model 0, when the pedestrian is placed in positions with low modal components (i.e. nodes 29 and 38). That occurs because the effectiveness of the localized passive pedestrian component (Model 1) is lower. Instead, with Model 0, a fraction of the spread apparent mass is again present in the highest modal component area of the structure, leading to a greater damping of the vibrations.

Going forward, the observation points 12 and 55 are the ones in which the pedestrians were made converge during the simulated tests number 4, 5 and 6. Therefore, from the trends of these FRFs (Fig. 277 and Fig. 278, or directly from Fig. 271 - Fig. 276), the results of the just mentioned tests appear clearer (Fig. 117 - Fig. 158). Indeed, in each of them, a strong overestimation of the vibration levels is made by Model 0, which is due to its inability to localize the damping at the moment in which the pedestrians converge. This fact underline the applicability conditions of Model 0, which are not only high number of pedestrians, but also spread pedestrians. That is equivalent to ask for dense pedestrian conditions, where the word dense underline the homogeneity of the pedestrian positions over the structure.

Chapter 6

Conclusions

In this thesis, three Models to account for the Human-Structure Interaction were presented. At first, a recalling of a previous contribution was done (Section 1.2, [1,2]). In it, an approximated approach (named here Model 0) to account for the HSI was present. This method considers the presence of pedestrian as the sum of an active and a passive contribution. Then, it spreads the overall passive contribution of the pedestrians that occupy the structure over the structure itself. Starting from this point, the current work proposed a new approach, Model 1. This Model is not only able to locally consider the active pedestrian contributions, as Model 0 does, but to locally consider the passive contributions as well. In order to numerically compare these two approaches, an experimental campaign was performed to collect the active and passive contributions for a series of subjects (5 people).

The active contributions were acquired through a force plate (Section 3.1), and with them, a database of active force time histories was built up. It is to be pointed out that in this way, non-periodic active force profiles were applied to the structure, since each time history was unique. The database was broadened with an already existing database coming from the previous contribution [2]. Whereas, the passive contributions were obtained through the evaluation of the apparent mass curves of the involved subjects. They were evaluated by the frequency ratio (i.e. a transfer function) between the frequency response force released by the body to the ground and the input acceleration of the ground itself (Section 3.2). These curves were then fitted by a 2DOF model for their handling in the equations. Such apparent mass curves change with the body positions, leading to a Linear Time Variant problem. In order to have a more manageable problem to deal with, mean apparent mass curves, representative for the positions assumed during a single step, were evaluated and used in Model 1. In such a way, a series of Linear Time Invariant systems were obtained, leading to an easier integration of the HSI dynamical equations, by splitting the integration interval over the series of Linear Time Invariant systems.

Moving forward, another Model was introduced, by using Model 1 as background: Model 2. In this Model, the overlap that takes place between two subsequent footsteps was considered, both from an active and from a passive point of view (Section 2.4). One Model again was introduced, always keeping Model 1 as background for it. In Model 3, the variation of the apparent mass curves within the single footstep were accounted. Indeed, thanks to a body motion analysis, the main positions assumed during a single footstep were identified (3 positions) (Section 3.2). The dynamic equations of Model 2 and 3 were solved by integration, always through the splitting of the whole integration time over the series of Linear Time Invariant systems. The only difference with respect to Model 1 was a higher number of sub-integration intervals for Model 2, and an again greater

number of sub-integration intervals for Model 3, given the higher number of the series of Linear Time Invariant systems considered by Model 2 and 3 to reproduce the same HSI situation.

Two points have to be pointed out. First, since the considered structure was a staircase, the positions assumed by the human body during the ascending and descending crossing are different. Therefore, the apparent mass curves were identified for both the crossing directions. Second, differences were observed in the way in which different people, but even the same one, go upstairs. The issue involved the contribution or not of the heel of the feet during the ascent. No differences were observed for the descent. For this reason, the apparent masses of the subject were measured for both the configurations of the contact foot-step/ground. These configurations were named “heel” and “tiptoe” configurations, for the ascending positions with the contact of the heel on the step and with tip of the feet respectively.

A series of 11 tests were thought, which are reported in table 1 and 2, in order to test all the 4 Models (i.e. Model 0, 1, 2 and 3) in different pedestrian situations, ranging from few to many pedestrians involved. Not only, different ways to occupy the structure were considered: pedestrians who walk in loop over the staircase or pedestrians who cross the structure only one time and then leave it. Such tests were reproduced both numerically with the Models and experimentally on a real structure, the main staircase (Fig. 37) of building B12 of north Milan campus of Politecnico di Milano. An Experimental Modal Analysis of the structure was at first performed, in order to obtain its modal parameters. Indeed, they are the necessary information that the Models need to reproduce the structure. 100 simulations were numerically performed with the Models for each of the 11 scheduled pedestrian scenario, with both the apparent mass types (“heel” and “tiptoe” one).

The results were evaluated in terms of acceleration, more precisely by means of the RMS values of the entire time length of the simulations and the RMS values evaluated every 3 s of the time length of the simulations, global and moving RMS values respectively. Such indexes were provided in terms of mean value and the limit values for a confidence interval at 95 % (i.e. two times the standard deviation). Such indexes were evaluated for both the numerical and the experimental accelerations, evaluated in correspondence of the points in which the first two modes of the structure (that are the modes used in the numerical simulations to reproduce the structure) assume their higher modal components, that are the positions of accelerometer 8 and 9 (Fig. 70). The global and the moving RMS values of Model 1, 2 and 3 were further elaborated by normalizing them with respect to the ones of Model 0, in order to underline the differences among these Models. Since one of the significant parameters utilized at the design stage of a new structure, for the evaluation of the serviceability conditions of the structure itself, is the value of the peak of the expected accelerations, an analysis of the maximum values of moving RMS was performed too.

The numerical results showed an appreciable agreement with the experimental ones, both from a global and from a moving RMS point of view. However, sometimes the estimated ranges of global RMSs of the Models slightly overestimate the experimental values (a higher estimation of the RMS acceleration values is safer than an underestimation). For what concerns the peaks of the moving RMS values, they fall in the predicted RMS peak ranges. The few cases in which some experimental point was underestimated (case number 3, 10 and 11/ Fig. 115 - Fig. 116, Fig. 213 - Fig. 214 and Fig. 227 - Fig. 228 respectively), even if the cloud of the main experimental peak values fell in the predicted range, the numerical simulations were reperformed for them. This time, the specific active and passive parameters of a specific subject (subject 3) were used for all the 100 simulations, instead of a random extraction of the involved subject and so of his/her parameters. The results of the specific subject perfectly fell in the estimated intervals for the peaks of acceleration, always in RMS (Fig. 241 and Fig. 242 for case 3, Fig. 255 and Fig. 256 for case 10, Fig. 269 and Fig. 270 for case 11).

As for the Models, they showed different results as a function of the tested pedestrian scenario. In test number 1 (5 people that walk for 5 min in loop over the staircase) all the Models show a good agreement on the estimation of the ranges of acceleration. Indeed, the pedestrian were spread

over the entire structure before to start to walk. This is the applicability condition of the approximation introduced by Model 0: dense pedestrian occupied structure. Such condition is given by a high number of pedestrians and by their placement over the entire structure. For this reason, the predicted vibration values of Model 0 are in agreement with the ones of the other Models, even if they adopt a more precise description of the HSI.

Completely different results are instead obtained in the tested scenarios number 4, 5 and 6. They involved 5 (in test number 4 and 5) and 3 (in test number 6) pedestrians who converge in the position of the structure with the highest modal components of the first two modes (i.e. the second landing). In this way, the maximum excitation of the structure was obtained. This was reproduced with all the Models, since all of them locally consider the active force of each pedestrian. What changes between the new proposed Models (i.e. Models 1, 2, and 3) and the old one (i.e. Model 0), it is how the passive contributions of the pedestrians (i.e. apparent mass curves) are treated. In the new Models, both in case of use of an average apparent mass per step (as in Model 1 and 2) or multi-apparent masses per step (as in Model 3), the passive contributions are always applied at the pedestrian positions, along with the active forces. Conversely, in Model 0, the apparent mass of all the involved pedestrian is gathered and then equally spread over the structure. This is a good approximation of what really happens, in case of a high number of pedestrians that are spread over the structure. This is not a good representation of what really happens, in case of a high number of pedestrians gathered in a point of the structure, as these cases are (i.e. test number 4, 5 and 3). Because in the first case, the damping capability of the pedestrians is really spread over the structure. Brief note, the main effect of the passive component of a pedestrian is the addition of damping to the structure, while the main effect of the active component of a pedestrian is the excitation of the structure; end of the note. In the second example instead, the damping capability of the pedestrian is localized in the point in which the pedestrians converge. Therefore, Model 0 is unable to locally damp the vibrations, as the new Models can do, obtaining an estimation of the vibration levels higher with respect to the experimental one (e.g. Fig. 131 and Fig. 132 for case number 5, global RMS values). While the new Models estimate lower vibration ranges, closer to the experimental data. Their estimated ranges of RMS of acceleration differ from the ones of Model 0 up to 20 % in mean value and up to 30 % with the lower limit of the confidence interval at 95 % (Fig. 133 and Fig. 134 of case number 5). A Frequency Response analysis of the structure was also presented in Section 5.1.5, which further clarifies the concept of localized and spread passive contribution. The aim was to show the effects, from a FRF point of view, of the different way in which the occupied by pedestrian structure (i.e. empty structure + passive pedestrian contributions) is modeled by the advanced Models and by Model 0.

As for the remaining cases, in which 2 pedestrians cross the structure in queue and in cross (tests 7, 8 and 9) and in which 1 pedestrian crosses the staircase (test number 10 and 11), the differences among the new Models and Model 0 are again present but reduced. 10 % of difference in the global mean RMS values, for the case of two walking pedestrians (up to 15 % with the confidence interval), while up to 20 % with the confidence interval for the 1 crossing pedestrian cases. Considering that the variations for the first three tests (i.e. the ones with the pedestrians walking in loop over the staircase) barely reach 10 % as limit difference with the confidence intervals, the above results are pretty good.

Looking at the numerical results obtained with the use of both the databases of the apparent mass curves evaluated with a complete contact of the feet with the ground (“heel” configuration) and with only the tip of the feet in contact with the ground (“tiptoe” configuration), the ones obtained with the second database are higher with respect to the ones obtained with the heel database. This trend of the results was expected, since the apparent mass curves for the tiptoed configuration showed a lower damping capability (Section 3.2). Moreover, since sometimes the Models with the use of the heel database slightly overestimate the experimental results, under a global RMS point of view, the ranges estimated with the tiptoed configurations go farther.

As last, the comparison among the proposed Models. Less than the cases depicted by Fig. 75 (case 1: 5 pedestrian walk for 5 min in loop; “tiptoe” database) and Fig. 89 (case 2: 3 pedestrian walk for 5 min in loop; “tiptoe” database), Model 1, 2 and 3 always show similar estimated ranges of vibration levels. The purpose of the current work was the evaluation of the improvements in the estimation of the vibration levels obtained with a more detailed description of the Human-Structure Interaction. Improvements were observed with respect to the previous approach, Model 0, since a wider range of cases was found to be correctly predicted. Appreciable improvements in case of low number of pedestrians, great improvement in case of high number of pedestrians localized on the structure. It is therefore concluded that the implementation of Model 1 for the estimation of the vibration levels is worth, in order to properly account for the local effect produced by the pedestrian passive contribution. As for Model 2 and 3, been they upgrades of Model 1 for a more detailed description of the HSI, the modeling and the simulation complexity that accompanies them is not worth, since no appreciable improvements in the estimation of the vibration levels follow too.

References

- [1] G. Busca, A. Cappellini, S. Manzoni, M. Tarabini, M. Vanali, Quantification of changes in modal parameters due to the presence of passive people on a slender structure, *J. Sound Vib.* 333 (2014) 5641–5652. doi:10.1016/j.jsv.2014.06.003.
- [2] A. Cappellini, S. Manzoni, M. Vanali, A. Cigada, Evaluation of the dynamic behaviour of steel staircases damped by the presence of people, *Eng. Struct.* 115 (2016) 165–178. doi:10.1016/j.engstruct.2016.02.028.
- [3] Steel, Concrete and Composite Bridges—Part 2: Specification for Loads; Appendix C: Vibration Serviceability Requirements for Foot and Cycle Track Bridges, BS 5400. UK: British Standards Association, London, (1978).
- [4] SÉTRA, Technical guide Footbridges Assessment of vibrational behaviour of footbridges under pedestrian loading, (2006).
- [5] P. Dallard, A. Flint, S. Le Bourva, A. Low, R.M.R. Smith, M. Willford, The London Millenium Footbridge, *Struct. Eng.* 79 (2001) 17–35. doi:10.2749/101686699780481709.
- [6] P. Reynolds, A. Pavic, Changes of modal properties of a stadium structure occupied by a crowd, *Proc. IMAC 2004.* (2004) 1–10.
- [7] J. Caicedo, S. Pakzad, Dynamics of civil structures, volume 2: Proceedings of the 33rd IMAC, a conference and exposition on structural dynamics, Chapter 34, *Conf. Proc. Soc. Exp. Mech. Ser. 2* (2015) 319–330. doi:10.1007/978-3-319-15248-6.
- [8] R. Sachse, A. Pavic, P. Reynolds, Human – Structure Dynamic Interaction in Civil Engineering Dynamics : A Literature Review, 35 (2003) 1–53.
- [9] S. Zivanovic, A. Pavic, P. Reynolds, Vibration serviceability of footbridges under human-induced excitation: A literature review, 2005. doi:10.1016/j.jsv.2004.01.019.
- [10] V. Racic, A. Pavic, J.M.W. Brownjohn, Experimental identification and analytical modelling of human walking forces: Literature review, *J. Sound Vib.* 326 (2009) 1–49. doi:10.1016/j.jsv.2009.04.020.
- [11] F. Venuti, L. Bruno, N. Bellomo, Crowd dynamics on a moving platform: Mathematical modelling and application to lively footbridges, *Math. Comput. Model.* 45 (2007) 252–269. doi:10.1016/j.mcm.2006.04.007.
- [12] E.T. Ingólfsson, C.T. Georgakis, A stochastic load model for pedestrian-induced lateral forces on footbridges, *Eng. Struct.* 33 (2011) 3454–3470. doi:10.1016/j.engstruct.2011.07.009.
- [13] R. Sachse, A. Pavic, P. Reynolds, Parametric study of modal properties of damped two-degree-of-freedom crowd-structure dynamic systems, *J. Sound Vib.* 274 (2004) 461–480. doi:10.1016/j.jsv.2003.08.052.
- [14] N.A. Alexander, Theoretical treatment of crowd–structure interaction dynamics, *Proc. ICE - Struct. Build.* 159 (2006) 329–338. doi:10.1680/stbu.2006.159.6.329.
- [15] F.P. Figueiredo, J.G.S. da Silva, L.R.O. de Lima, P.C.G. da S. Vellasco, S.A.L. de Andrade, A parametric study of composite footbridges under pedestrian walking loads, *Eng. Struct.* 30 (2008) 605–615. doi:10.1016/j.engstruct.2007.04.021.
- [16] Murray TM, Allen DE, Ungar EE. Floor vibrations due to human activity. Steel design guide series, American Institute of Steel Construction, AISC, (1997).
- [17] International Standards Organisation/ISO 2631-2. Evaluation of human exposure to whole-body vibration. Part 2: Continuous and shock-induced vibration in buildings (1–80 Hz), (1989).
- [18] M. Setareh, D. Ph, M. Asce, Vibrations due to Walking in a Long-Cantilevered Office Building Structure, *J. Perform. Constr. Facil.* 26 (2012) 255–270. doi:10.1061/(ASCE)CF.1943-5509.0000188.
- [19] Bachmann, H. et al. Vibration problems in structures: Practical guidelines, Birkhäuser Verlag, Basel, Switzerland, (1995).
- [20] Smith, A. L., Hicks, S. J., and Devine, P. J. “Design of floors for vibration: A new approach.”

- SCI Publication P354, Steel Construction Institute, Ascot, Berkshire, U.K., (2007).
- [21] ISO. "Bases for design of structures-Serviceability of buildings and walkways against vibrations." ISO 10137, Geneva, (2007).
- [22] Khoncarly, M. M. "Dynamic response of floor systems to footfall-induced vibrations." Ph.D. thesis, Case Western Reserve Univ., Cleveland, OH, (1997).
- [23] E.S. Mashaly, T.M. Ebrahim, H. Abou-Elfath, O.A. Ebrahim, Evaluating the vertical vibration response of footbridges using a response spectrum approach, *Alexandria Eng. J.* 52 (2013) 419–424. doi:10.1016/j.aej.2013.06.003.
- [24] K. Van Nimmen, G. Lombaert, G. De Roeck, P. Van den Broeck, Vibration serviceability of footbridges: Evaluation of the current codes of practice, *Eng. Struct.* 59 (2014) 448–461. doi:10.1016/j.engstruct.2013.11.006.
- [25] Research Fund for Coal and Steel. HiVoSS: Design of footbridges, (2008).
- [26] M.A. Toso, H.M. Gomes, F.T. Da Silva, R.L. Pimentel, Experimentally fitted biodynamic models for pedestrian-structure interaction in walking situations, *Mech. Syst. Signal Process.* 72–73 (2016) 590–606. doi:10.1016/j.ymssp.2015.10.029.
- [27] ISO 10137 International Organization for Standardization. Bases for Design of Structures-Serviceability of Buildings and Walk ways against Vibrations, (2012).
- [28] P. Young, Improved Floor Vibration Prediction Methodologies, In: *Proceedings of the Arup Vibration Seminar on Engineering for Structural Vibration- Current Developments in Research and Practice*, (2001).
- [29] UK-NA to BS EN 1991-2:2003-British Standards Institute, UK National Annex to Eurocode 1: actions on structures – Part 2: Traffic loads on bridges. London: BSI, (2008).
- [30] F. Venuti, V. Racic, A. Corbetta, Modelling framework for dynamic interaction between multiple pedestrians and vertical vibrations of footbridges, *J. Sound Vib.* 379 (2016) 245–263. doi:10.1016/j.jsv.2016.05.047.
- [31] C.C. Caprani, E. Ahmadi, Formulation of human-structure interaction system models for vertical vibration, *J. Sound Vib.* 377 (2016) 346–367. doi:10.1016/j.jsv.2016.05.015.
- [32] Y. Matsumoto, M.J. Griffin, Dynamic Response of the Standing Human Body Exposed To Vertical Vibration: Influence of Posture and Vibration Magnitude, *J. Sound Vib.* 212 (1998) 85–107. doi:10.1006/jsvi.1997.1376.
- [33] Y. Matsumoto, M.J. Griffin, Mathematical models for the apparent masses of standing subjects exposed to vertical whole-body vibration, *J. Sound Vib.* 260 (2003) 431–451. doi:10.1016/S0022-460X(02)00941-0.
- [34] J. Sim, A. Blakeborough, M. Williams, Modelling effects of passive crowds on grandstand vibration, *Proc. Inst. Civ. Eng. Build.* 159 (2006) 261–272. doi:10.1680/stbu.2006.159.5.261.
- [35] J. Sim, A. Blakeborough, M. Williams, Modelling of joint crowd-structure system using equivalent reduced-DOF system, *Shock Vib.* 14 (2007) 261–270. <http://iospress.metapress.com/index/g1773n6268w14689.pdf>.
- [36] S.H. Kim, K.I. Cho, M.S. Choi, J.Y. Lim, Development of Human Body Model for the Dynamic Analysis of Footbridges under Pedestrian Induced Excitation, *Int. J. Steel Struct.* 8 (2008) 333–345.
- [37] G. Piccardo, F. Tubino, Equivalent spectral model and maximum dynamic response for the serviceability analysis of footbridges, *Eng. Struct.* 40 (2012) 445–456. doi:10.1016/j.engstruct.2012.03.005.
- [38] J. Caicedo, S. Pakzad, Dynamics of civil structures, volume 2: Proceedings of the 33rd IMAC, a conference and exposition on structural dynamics, Chapter 7, *Conf. Proc. Soc. Exp. Mech. Ser. 2* (2015). doi:10.1007/978-3-319-15248-6.
- [39] K. Van Nimmen, G. Lombaert, I. Jonkers, G. De Roeck, P. Van Den Broeck, Characterisation of walking loads by 3D inertial motion tracking, *J. Sound Vib.* 333 (2014) 5212–5226. doi:10.1016/j.jsv.2014.05.022.
- [40] S. Krenk, Lectures presented at "Semi-Active Vibration Suppression – The Best from Active and Passive Technologies", CISM, Udine, (2007).
- [41] D. J. Ewins, *Modal Testing: Theory, Practice and Application*, 2nd Ed. Taylor and Francis Group, London, (2001).

- [42] M. A. Woodbury, *Inverting Modified Matrices*, Statistical Research Group, Princeton University, Princeton, N. J, (1950).
- [43] F.W. Galbraith, M.V. Barton, Ground loading from footsteps, *Journal of Acoustic Society of America* 48 1288–1292, (1970).
- [44] T.P. Andriacchi, J.A. Ogle, J.O. Galante, Walking speed as a basis for normal and abnormal gait measurements, *Journal of Biomechanics* 10 261–268, (1977).
- [45] J. Hamill, S.L. McNiven, Reliability of selected ground reaction force parameters during walking, *Human Movement Science* 9 117–131, (1990).
- [46] T.S. Keller, A.M. Weisberger, J.L. Ray, S.S. Hasan, R.G. Shiavi, D.M. Spengler, Relationship between vertical ground reaction force and speed during walking, slow jogging, and running, *Clinical Biomechanics* 11 253–259, (1996).
- [47] T.A. McMahon, G. Valiant, E.C. Frederick, Groucho running, *Journal of Applied Physiology* 62 2326–23337, (1987).
- [48] J.E. Bertram, A. Ruina, Multiple walking speed-frequency relations are predicted by constrained optimization, *Journal of Theoretical Biology* 209 445–453, (2001).
- [49] A.D. Pizzimenti, F. Ricciardelli, Experimental evaluation of the dynamic lateral loading of footbridges by walking pedestrians, *Sixth European Conference on Structural Dynamics EUROLYN*, Paris, France, (2005).
- [50] A. Ronnquist, *Pedestrian Induced Lateral Vibrations of Slender Footbridges*, Norwegian University of Science and Technology, Trondheim, (2005).
- [51] H. Bachmann, W. Ammann, *Vibrations in Structures Induced by Man and Machines*, International Association of Bridge and Structural Engineering, Zurich, Switzerland, (1987).
- [52] a. Pavic, S. Živanović, P. Reynolds, Human–structure dynamic interaction in footbridges, *Proc. ICE - Bridg. Eng.* 158 (2005) 165–177. doi:10.1680/bren.2005.158.4.165.
- [53] T.A. McMahon, P.R. Greene, The influence of track compliance on running, *Journal of Biomechanics* 12 893–904, (1979).
- [54] S.V. Ohlsson, *Floor Vibrations and Human Discomfort*, Chalmers University of Technology, Goteborg, (1982).
- [55] Henry D'Angelo - *Linear Time-Varying Systems, Analysis and Synthesis.pdf*, (1970).
- [56] F. Cheli, G. Diana, *Advanced Dynamics of Mechanical Systems*, 2015.
- [57] A. Belli, P. Bui, A. Berger, J.R. Lacour, A treadmill for measurements of ground reaction forces during walking, *The XVth Congress of the International Society of Biomechanics, Jyva" skyla"*, Finland, July, pp. 100–101, (1995).
- [58] T.M. Owings, M.D. Grabiner, Measuring step kinematic variability on an instrumented treadmill: how many steps are enough?, *Journal of Biomechanics* 36 1215–1218, (2003).
- [59] B. Peeters, H. Van Der Auweraer, P. Guillaume, J. Leuridan, The PolyMAX frequency-domain method: a new standard for modal parameter estimation?, *Shock Vib.* 11 (2004) 395–409. doi:10.1155/2004/523692.
- [60] A. Quarteroni, F. Saleri, P. Gervasio, *Calcolo Scientifico Esercizi e problemi risolti con MATLAB e Octave*, 2012.

